UNIVERSITY of BRADFORD Library

University of Bradford eThesis

This thesis is hosted in Bradford Scholars – The University of Bradford Open Access repository. Visit the repository for full metadata or to contact the repository team

© University of Bradford. This work is licenced for reuse under a Creative Commons Licence.

Design and Linearization of Energy Efficiency Power Amplifier in Nonlinear OFDM Transmitter for LTE-5G Applications

Simulation and measurements of energy efficiency power amplifier in the presence of nonlinear OFDM transmitter system and digital predistortion based on Hammerstein-Wiener method

Buhari Abubakar MOHAMMED

MSc, MPhil

Submitted for the Degree of

Doctor of Philosophy

Faculty of Engineering and Informatics

University of Bradford

2019

Abstract

Buhari Abubakar Mohammed

Design and Linearization of Energy Efficiency Power Amplifier in Nonlinear OFDM Transmitter for LTE-5G Applications.

Simulation and Measurements of Energy Efficiency Power Amplifier in the Presence of Nonlinear OFDM Transmitter System and Adaptive Digital Predistortion Based on Hammerstein-Wiener Approach

Keywords

Energy efficiency, Linearity, Class AB power amplifier, Class F power amplifier, Radio frequency, Nonlinear OFDM transmitter, Adaptive digital predistortion, Wiener system, Hammerstein system and Long term evolution.

This research work has made an effort to understand a novel line of radio frequency power amplifiers (RFPAs) that address initiatives for efficiency enhancement and linearity compensation to harmonize the fifth generation (5G) campaign. The objective is to enhance the performance of an orthogonal frequency division multiplexing-long term evolution (OFDM-LTE) transmitter by reducing the nonlinear distortion of the RFPA.

The first part of this work explores the design and implementation of 15.5 W class AB RF power amplifier, adopting a balanced technique to stimulate efficiency enhancement and redeeming exhibition of excessive power in the transmitter. Consequently, this work goes beyond improving efficiency over a linear RF power amplifier design; in which a comprehensive investigation on the fundamental and harmonic components of class F RF power amplifier using a load-pull approach to realise an optimum load impedance and the matching network is presented. The frequency bandwidth for both amplifiers was allocated to operate in the 2.620-2.690 GHz of mobile LTE applications.

The second part explores the development of the behavioural model for the class AB power amplifier. A particular novel, Hammerstein-Wiener based model is proposed to describe the dynamic nonlinear behaviour of the power amplifier. The RF power amplifier nonlinear distortion is approximated using a new linear parameter approximation approach. The first and second-order Hammerstein-Wiener using the Normalised Least Mean Square Error (NLMSE) algorithm is used with the aim of easing the complexity of filtering process during linear memory cancellation. Moreover, an enhanced adaptive Wiener model is proposed to explore the nonlinear memory effect in the system. The proposed approach is able to balance between convergence speed and high-level accuracy when compared with behavioural modelling algorithms that are more complex in computation.

Finally, the adaptive predistorter technique is implemented and verified in the OFDM transceiver test-bed. The results were compared against the computed one from MATLAB simulation for OFDM and 5G modulation transmitters. The results have confirmed the reliability of the model and the effectiveness of the proposed predistorter.

Acknowledgement

First and foremost, I would like to thank Almighty God for giving me this opportunity to take on this task and make this breakthrough.

I wish to express my gratitude to my supervisor and mentor *Prof R. A. Abd-Alhameed* for his continuous support, guidance, encouragement and advice up to the last stage of my work. It will be impossible to accomplish this research work without help and support. He has always been a source of encouragement and inspiration. I would like to thank Dr Roger Clarke, Dr Abubakar Sadiq Hussaini and Dr Kelvin Anoh for their ideas, support, and guidance throughout this work.

Furthermore, I would like to thank all my colleagues in the Radio Frequency and antenna laboratory for their great support and help. They are always there to help in their best way. Thanks also to my co-authors who I have been enjoying their support in terms of paper review, help in design, simulations and their constructive criticism which improved my work and quality of my publications.

I wish to acknowledge Fundacão para a Ciência e a Tecnologia, Portugal under European Union's Horizon 2020 research and innovation programme which some of my publications sponsored on grant agreement H2020-MSCA-ITN- 2016 SECRET-722424. I also acknowledge the role of the National Space Research and Development Agency (NASRDA), Sokoto State Government and Petroleum Technology Trust Fund (PTDF) in this work.

Finally, special thanks to my wife, Ubaida Haruna Rasheed, my children, Nana Khadija, Nana Aisha, Nana Fatima, Muhammad Al-Amin, my mother, my brothers, my sisters and all members of my family. The support and encouragement you have given me throughout this period of time have been magnificent. My uncle, the Sultan of Sokoto, Alhaji Saad Sadiq Abubakar III, and his support has been a great source of energy.

Dedication

I would like to dedicate this work to my father, the late Sultan of Sokoto, Alhaji Muhammadu Maccido Abubakar III, may his soul rest in peace, Amin. My mother, my wife and my children.

Table of Contents

List of Figures

List of Tables

List of Abbreviations

ACI	Adjacent Channel Interference
ACPR	Adjacent Channel Power Ratio
ADC	Analogue to Digital Converter
ADS	Advanced Design System
AFB	Analysis Filter Bank
AM-AM	Amplitude to Amplitude
AM-PM	Amplitude to Phase
AWGN	Additive White Gaussian Noise
BER	Bit Error Rate
CAD	Computer Aided Design
CDF	Cumulative Distribution Functions
CDMA	Code Division Multiple Access
CP	Cyclic Prefix
CRN	Cognitive Radio Network
DAB	Digital Audio Broadcast
DAC	Digital to Analogue Converter
dB	Decibel
DEWMA	Dynamic Exponential Weighted Moving Average
DFT	Discrete Fourier Transform
DPSK	Deferential PSK
DSP	Digital Signal Processing
DUSTM	Differential Unitary Space Time Modulation
DUT	Device Under Test
DVB	Digital Video Broadcast
EDGE	Enhanced Date for Global Evolution
EER	Envelope Elimination and Restoration
ESM	Envelope Special Mask
EVM	Error Vector Magnitude
FBMC	Filter Bank Multicarrier
F-OFDM	Filtered-OFDM
FDM	Frequency Division Multiplex
FET	Field Effect Transistor
FFT	fast Fourier Transform
5G	Fifth-Generation
4G	Fourth-Generation
FIR	Finite Impulse Response
FQAM	Frequency Quadrature Amplitude Modulation
FS	Frequency Spreading
FSK	Frequency Shift Keying
G-OFDM	Generalized-OFDM
Gan HEMT	Gallium Nitride High Electron Mobility Transistor
GSF	Generalized Space and Frequency
GSM	Global System for Mobile Communications

IEEE	Institute of Electrical and Electronics Engineers
IDFT	Inverse Discrete Fourier Transform
IBO	Input Power Back-Off
ICI	Inter-carrier Interférence
ID	Drain Current
IDC	DC Current
IOUT	Output Current
IDQ	Quiescent Current
IF	Intermediate Frequency
IFFT	Inverse Fast Fourier Transform
IMAX	Peak Amplitude
IMD	Intermodulation Distorsion
IM	Index Modulation
IP3	Third-Order Intercept Point
IPK	Peak Current
I & Q	In phase and Quadrature
ISI	Inter-symbol Interférence
LD MOS	Laterally Diffused Metal Oxide Semiconductor
LINC	Linear Amplification with Nonlinear Components
LLR	Log Likelihood
LMS	Least Mean Square
LO	Local Oscillator
LTI	Linear Time-Invariant
LTE	Long Term Evolution
LUT	Look Up Table
MATLAB	Matrix Laboratory
MIMO	Multiple-Input Multiple-Output
MLD	Maximum Likelihood Decoding
MOSFET	Metal Oxide Semiconductor Field Effect transistor
MPSK	Multi-level Phase Shift Keying
MQAM	Multi quadrature Amplitude Modulation
NLMS	Normalized Least Mean Square
OFDM	Orthogonal Frequency Division Multiplexing
OOB	Out Of Bound
OQAM	Offset Quadrature Amplitude Modulation
OSTBC	Orthogonal Space-Time Block Coding
OTFS	Orthogonal Time Frequency and Spacing
PA	Power Amplifiers
PAE	Power Added Efficiency
PAPR	Peak to Average Power Ratio
P_{av}	Average Power
PDS	Predistortion System
Pin	Input Power
PL	Load Power
PLL	Phase-Locked Loop

PM	Phase Modulation
Pout	Output Power
PS	Parallel-to-Serial
PSD	Power Spectral Density
QPSK	Quadrature Phase Shift Keying
RB	Rate Bits
RCE	Received Constellation Error
RE	Real
RF	Radio Frequency
RL	Load Resistance
RMS	Root Means Square
SE	Spectral Efficiency
SFB	Synthesis Filter Bank
SGA	Stochastic Gradient Algorithm
SISO	Single Input Single Output
SM	Spatial Modulation
SMMT	Staggered Modulate Multi Tone
SNR	Signal to Noise Ratio
SP	Serial-to-Parallel
SR	Spectral Regrowth
SSPA	Solid State Power Amplifier
SVD	Singular Value Decomposition
TDMA	Time Division Multiple Access
3G	Third-Generation
TWTA	Travelling Wave Tube Amplifier
UFMC	Universal Filtered Multicarrier
UMTS	Universal Mobile Telecommunications System
USTM	Unitary Space Time Modulation
UWB	Ultra-Wideband
VCO	Voltage Control Oscillator
VDC	DC Voltage
VDD	Drain Voltage
V_{IN}	Input Voltage
VGS	Gate Source Voltage
V_{max}	Peak Voltage
V_{out}	Output Voltage
WAM	Wave Modulation
WCDMA	Wideband Code Division Multiple Access
WLAN	Wireless Local Area Network
Wi-MAX	Worldwide Interoperability for Microwave Access
Z_{in}	Source Impedance
Z_L	Load Impedance

CHAPTER 1

Introduction

1.1 Background and Motivation

Wireless mobile communication systems are becoming more dominant over the years. These systems continue to increase growth in providing diverse multimedia services for more wireless service users. The very fast growth of service users makes the system become more complex and however prompt efficient usage of limited available spectrum resource. New generation wireless communication systems are complex modulation base which involve high-speed data rate to support the demand for multimedia services. The recent wireless communication systems such as long term evolution (LTE) [1], wireless local area network (WLAN) [2, 3] and worldwide interoperability for microwave access (WiMAX) [4] support adaptation of energy-efficient transmitter for high capacity and transmission speed. The high transmission data rate demands the use of bandwidth with efficient modulation techniques such as orthogonal frequency division multiplex (OFDM) [5, 6] and quadrature phase shift keying (QPSK) [2, 7]. However, the spectral efficient modulation schemes require high power efficiency with maximum linearity from the power amplifier device [8].

Modulation schemes such as OFDM and wideband code division multiple access (WCDMA) [9, 10] are multiple access techniques which produce high constellation diagrams. These modulations are uncovered to nonlinear distortion due to the high peak to average power ratio (PAPR) [11, 12]. PAPR is caused by fluctuation of the modulation time-domain signals. The QPSK mapping technique is also a bandwidth-efficient modulation scheme which requires amplifier linearity for spectral efficiency. Linear amplifiers are traditionally poor efficient devices with

a high cost of operation and demand for a heat sick against excessive heat dissipation. Signals with high PAPR are derived in low efficiency. On the other hand, the nonlinear amplifiers distort the signal constellation based on high PAPR signal which led to increase in adjacent channel power ratio (ACPR) [13]. The ACPR is measured based on the system application and the magnitude of the PAPR. For instance, wideband CDMA and CDMA2000 [14, 15] exhibit up to 10 dB PAPR, while OFDM will have a PAPR of around 17 dB for WLAN IEEE 801.11a and less PAPR for the current WLAN IEEE 801.11ax system. The bandwidth can be up to 20 MHz and above, according to [13, 16].

Radio frequency power amplifiers (RFPAs) are basically fundamental components in communication system transmitters. The power amplifier nonlinearities generate nonlinear crosstalk which offset transmission process and cause spectral re-growth. These result to severe interference, in-band distortion and bit error ratio (BER) performance becomes low which also produces out-of-band emission (CO2 emission). Power amplifier nonlinear distortion according to [8, 17] can effectively be reduced by power back-off and PAPR reduction techniques, which in the end, result to low power efficiency. Thus, linear amplification is essential and can be obtained using a linear amplifier or using a nonlinear amplifier with the aid of the linearization technique. Furthermore, power amplifier efficiency can effectively increase depending on the adaptive design techniques [18, 19].

To achieve efficiency, linearity and high data rate for a modern energy-efficient wireless communication transmitter, a linearization scheme and a trade-off between linearity and efficiency power amplifier need to be considered in this

research. A class AB amplifier delivers higher linearity and acceptable efficiency. Another choice is a nonlinear class F power amplifier which can produce up to 85% power added efficiency (PAE). To linearize a nonlinear RF power amplifier, an adaptive predistortion system is suggested for the advancement of the research to obtain both efficiency and linearity at the same time. Consequently, there are futuristic energy-efficient amplifier design techniques such as balanced Configuration [20], Doherty Configuration [21], Chireix out-phase [22, 23], ET and Kahn EER [24]. The most common and useful compensation techniques are feedback, feedforward, linear amplification with nonlinear components (LINC) [25], envelope elimination and restoration technique (EER) and different types of pre-distortion techniques. The state-of-the-art among all linearization techniques appears to be the adaptive digital predistortion which can be cascaded at the baseband of the transmitter to linearize the output signal of a power amplifier. Similarly, a power amplifier can reach its saturation stage, maintaining excellent linearity to increase efficiency with the predistortion system. This process progressively changes the characteristics of the components and increases transistor thermal runaway, resulting to temperature drifting. Therefore, pre-distortion system will take account of the changes and adapt [26]. It is a system that is used in improving the linearity of a RFPA in a radio communication transmitter. Consequently, the basic idea of a predistortion system is adding a nonlinear element before the RF power amplifier so that the mutual transfer characteristic of both elements is linear. The Power amplifier exhibits nonlinearities which cause intermodulation distortion and spectral regrowth in the signal spectrum. The spectral regrowth results to out-of-band emissions, adjacent channel interference and in-band distortion. The in-band distortion also reduces the BER and throughput of the transmitter system. Therefore, the digital

baseband predistortion system is utilised to cancel these impairments by improving the linearity of the RFPA system in the linear region [27].

To implement an adaptive digital predistortion in this research work, there is a need to pay attention to a power amplifier for a perfect behavioural model. A proposed balanced configuration is designed and simulated for the mobile LTE frequency band. A one-tone simulation and other tests will be performed to achieve the best behavioural modelling of the balanced configuration [28]. The instantaneous behavioural modelling is characterized by the amplitude and phase response of the power amplifier. While the current input amplitude is the function of the amplitude and phase deviation of the power amplifier output. Hence, a static model for AM-AM and AM-PM functions can be driven for memoryless model [8, 29].

Multicarrier applications such as WCDMA and OFDM have a wider bandwidth with a time-varying envelope signal. The behavioural model of the power amplifier of these applications exhibit memory effects and are useful for base stations. The memory effect of such amplifier is caused by thermal runaway of the transistor device or components in the bias network with frequency-dependent behaviours. As a result, the power amplifier becomes a nonlinear system with memory effect and as such the static functions which is able to accurately model power amplifier. The digital predistortion of such power amplifier cannot fully accomplish linearization functions. Therefore, the digital predistorter perform effectively with memory formation. Intensive research has been performed on the evaluation of memory effect and in general, memory effects are significant in the differentiation of power amplifier characteristic tasks over the envelope frequency. Memory

effect supports nonlinear distortion while limiting predistortion performance [30-33]. In this regard, the research will consider a predistorter with memory effects that can suppress the nonlinear distortion.

1.2 Aim and Objectives

This work considers the RF system design and the energy efficiency of the wireless communication OFDM transmitter system. Highly integrated wireless transmitter system is the dominant source of power consumption, nonlinear crosstalk due to local oscillator sharing and linear crosstalk due to antennas mutual coupling. It is obvious that these are important metrics for today's transmitter circuits. Power amplifiers and multiple antennas are the major sources of these impairments. This research will focus on efforts to improve the spectral efficiency of an LTE OFDM wireless transmitter circuits through the objectives to address the aforementioned performance issues by:

- Conducting a comprehensive study on RF power amplifier characteristics, distortions, memory effects and parameters for characterizing the nonlinearities.
- Present the challenges of using OFDM over 5G modulations to overcome the adjacent channel interference (ACI).
- Understanding the nonlinear behaviour of the power amplifier and use the model to analyse the distortion behaviour.
- Comparative details summarizing the modelling techniques for PA nonlinear behaviour and memory effects, specifically, polynomial models, Hammerstein and Wiener.
- Investigating memory effects of power amplifiers that causes these effect and the influence memory effects have over intermodulation distortion and

frequency-dependent distortions. This follows with performing a one-tone measurement, two-tone measurement and digitally modulated signal measurements for the power amplifier memory effects.

- Designing and implementation of proposed linear 15.5 W balanced RF power amplifier with an N-channel Si-LDMOS transistor device and a nonlinear 10 W class F RF power amplifier using GaN-HEMT transistor device using 2.620-2.690 GHz operating frequency. Comparative overview of the amplifiers in terms of efficiency, linearity, output power and reliability.
- Providing a comprehensive literature review on the current advancement in the area of linearization schemes and make a comparative analysis with the existing linearization schemes.
- Modelling the predistorter over the IEEE-OFDM transceiver system to verify the distortion behaviour of the proposed balanced RF power amplifier and the performance metric of the proposed adaptive pre-distorter.
- Verifying the performance of the predistorter over the 5G f-OFDM modulation communication system with manipulating the extracted amplitude and phase of the RF power amplifier for signal processing.
- Setting a test bench to verify the polynomial model extracted from the operation of a fabricated power amplifier, R&S SMBV100A vector signal generator and R&S FSG 13 vector signal Analyser. This test is implemented through an adaptive digital predistorter taking into account the memory effects and memoryless compensation caused by the power amplifier.

1.3 Scope of the Research

The concept of this research is to proposed new design of balanced RF power amplifier at 2.620-2.690 GHz LTE band. The design is expected to improve in terms of efficiency and linearity. The RFPA design is to be simulated, fabricated and to be linearized in the proposed adaptive digital baseband predistortion system. First of all, the AM-AM and AM-PM transfer functions of the proposed RFPA are extracted using curve fitting in MATLAB. The extracted coefficients will be modelled using enhanced adaptive Wiener model with first and second order approach. The model will be used in the proposed adaptive digital baseband predistortion system to linearize the distortion of our proposed balanced RFPA model. The predistortion model is verified in OFDM and f-OFDM modulation to see how much the predistorter can cancel the distortion of the proposed amplifier. The main concern of this research is to increase the linearity and reduce the out of bound emission of the RF power amplifier.

1.4 Main Contributions to the Present Research

The significant contributions of this work are in the area of designing an improved energy-efficient balanced RF power amplifier and the linearization techniques developed to cancel the distortion within the OFDM wireless application families. Some of these contributions include:

- The design of more robust, low distortion OFDM using FFT is presented in a journal paper, J1. The OFDM technique was modified for more effective cancellation and improve system performance.
- Proposed an adaptive Wiener behavioural modelling for the proposed balanced RFPA. The concept is by using first and second order terms with normalised least means square algorithm to memoryless and memory

effect of the amplifier. The algorithm is considered based on simplicity, convergence speed, stability and capability to model RFPA memory effects.

- To improve the nonlinearity operation of power amplifier and to deal with the performance reduction experienced by the OFDM transceiver system, a linear 15.5 W balanced RF power amplifier with an N-channel Si-LDMOS transistor device using 90^0 offset line to improve the efficiency has been designed and implemented. This contribution is reported in the present author work through journal publications, J1, J2, J3, J4, J5 and conferences, C4, C5, C6 respectively (please refer to the Authors' publication record at the end of the thesis).
- To make a comparative analysis with the proposed balanced RF amplifier in terms of efficiency, linearity, output power and reliability, a nonlinear 10 W class F RF power amplifier using GaN-HEMT transistor device has been designed. Conference publications, C1, C2 and C3 are referenced as the closed-form solution using a load-pull approach to achieve an optimum load impedance and effective matching network. Spectral analysis and power flow study of a linear and nonlinear power amplifier are described. The optimisation process of deriving the optimum loads of two-port active nonlinear has been developed.
- The proposed adaptive Hammerstein-Wiener predistorter model with the indirect learning-based structure used for identification to compensate for nonlinear distortion of the nonlinear device. The predistorter models along with the nonlinear model of the power amplifier are presented. The predistorter is an effective structure for LTE-OFDM power amplifiers. It is developed with less implementation complexity by distributing the pre-

distorter task such that the transmitter compensates for the static nonlinearity and the receiver equalizes the power amplifier memory and gives low complexity solution. This research work is considered in journal publication J2.

1.5 Structure of the Thesis

The main goal of this research is to focus on improving the overall performance of OFDM wireless communication for effective signal transmission. The recent wireless communication systems require high data rate and advanced modulation schemes. The key challenge for this system is to achieve linearity and efficiency at the same time. There was major effort over the years to enhance the energy efficiency of transmitter circuits, particularly the power amplifier to shrink nonlinearities through effective linearization. We will evaluate the performance of this system through theoretical analysis, simulation and measurements. The description of each following chapter for this present work are detailed as follows:

Chapter 2 presents the general fundamental of RF power amplifiers including the class of amplification. Overview characteristics and characterization of PA nonlinearities are explained in this chapter. Moreover, nonlinear distortion, source of memory effects, different criteria for quantifying memory effects and frequency-dependent transfer function are discussed.

Chapter 3 presents OFDM as a multicarrier system, its basic principles, advantages and disadvantages. Discusses the nonlinear effects of power amplifier over OFDM modulated signal and how these nonlinear effects can be estimated. To prove how the nonlinear distortion affects the signal, a simple

application over the nonlinear OFDM transmitter with and without saturator is studied and simulated using MATLAB. The OFDM is also compared with 5G modulations such as FQAM-OFDM, FBMC, UFMC and other schemes.

Chapter 4 presents different techniques of power amplifier behavioural modelling, the memory, memoryless models, the effects and modelling procedures are considered. Several existing parameter estimation algorithms for two-box models such as Hammerstein and Wiener are carefully studied. These algorithms are analysed in terms of simplicity, convergence speed and modelling ability over a different kind of memory effect. Finally, the behavioural models based on the Wiener and improved Wiener approaches are modified with an optimal technique for system parameter estimation.

Chapter 5 presents the characterisation and design of a linear energy-efficient balanced RF power amplifier using two class AB designs. This design comprised several design steps for which the optimization is applied to each amplifier in order to obtain global high performance of the entire system. Initially, the design of first and second carrier amplifiers, the input signal 3 dB 90^0 hybrid coupler designs, output 90^0 offset line and impedance transformer designs is implemented to improve efficiency.

Chapter 6 presents a class F approach to optimise load impedance at the fundamental frequency for the application of the active antenna concept. The design method and procedure are demonstrated through source-load pull for high efficiency and optimal load impedance. To improve efficiency and suppress the

harmonics, a high pass filter was designed. The filter would have to match with output of the class F power amplifier and input of the load.

Chapter 7 investigates the linearization techniques which include power back-off, feedback linearization, EER, LINC, feedforward analogue predistortion and digital predistortion. Several features of the predistortion technique and methods such as look-up tables and polynomials are described. A comprehensive study on a different type of predistorters designed for OFDM applications are studied. Three modified methods of parameter estimation to evaluate the Hammerstein blocks as well as improved Hammerstein system are developed. The modified predistortion technique is verified through simulation in OFDM and f-OFDM 5G applications. Finally, the proposed modified predistortion model is tested to verify the validity and the overall performance of the model in comparison with the simulation.

Chapter 8 presents a summary of the study with some suggestions for future studies on topics related to this work.

CHAPTER 2

RF Power Amplifier Principles

2.1 Introduction

A power amplifier is an electronic device used commonly in wireless communication applications to upturn the level of radio frequency signal strength. In all applications including recent wireless communication transmitter systems, the amplifier is at the final stage of amplification. It supports the signal with essential power to transmit through the channel [34]. However, nonlinear amplifiers such as class F exhibits an extensive degree of nonlinearity. The nonlinear behaviour of the device increases the input amplitude of the amplifier with the expense of the output signal. The output signal which due to saturation will not linearly increase. Hence, this type of amplifier depends on the network configuration [13]. Unlike the other class of amplifiers which are linearly based on quiescent point. Such amplifiers are class A, B, AB and C. In addition, they are such type of amplifiers with bias capability. Moreover, in the case of the class AB amplifier, the challenge is how to achieve a trade-off between efficiency and linearity to avoid distortion. Therefore, in designing a power amplifier, there are basic requirements to consider such as frequency of operation, linearity, efficiency, output power, the transistor of interest and most importantly the temperature stability of the device. This chapter presents the commonly known classes of power amplifier, the mode of operations, features and parameters to characterize power amplifier nonlinearities [34-36].

2.2 Class of Amplification

Power amplifiers are grouped into different classes of operation such as class A, B, AB, C, D, E and F. These are based on the method of operation, circuit

configuration and conduction angle (360^0). The classes range from exclusively linear with low efficiency to nonlinear with high efficiency. The choice of conduction angle has an impact on efficiency, linearity and output power. It is the most common way to define the class of amplifier. Conduction angle is the region of the RF cycle where the amplifier remains operational. Therefore proper class of operation must be wisely chosen [34, 35]. Figure 2.1 has presented the choice of conduction angle for gate voltage and drain voltage for which the class of operation played a major role as shown below.

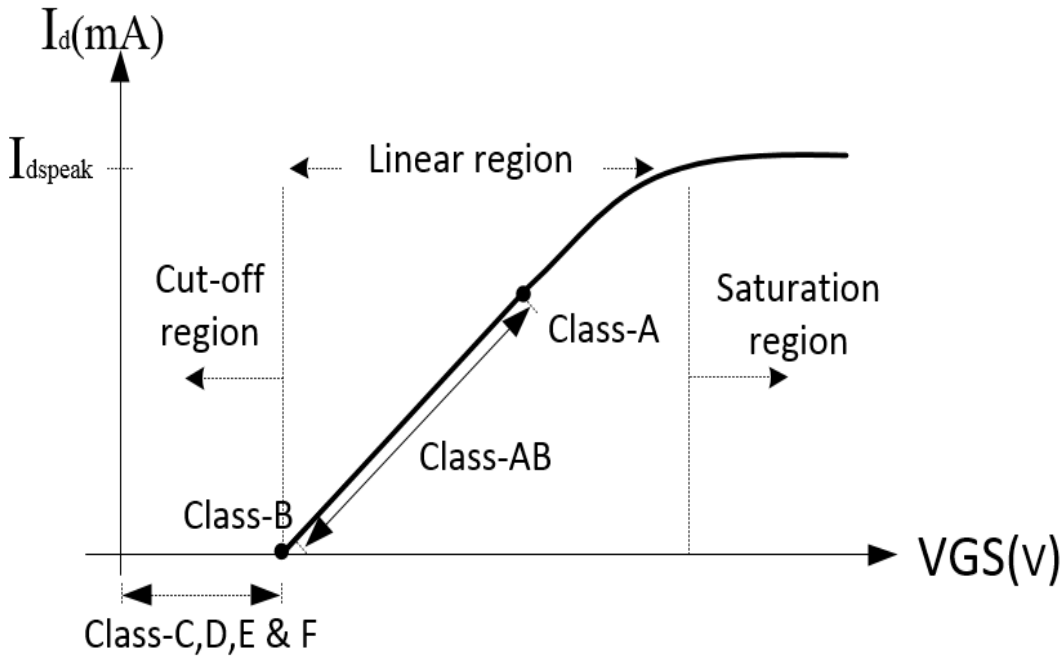

Figure 2.1: Quiescent point of linear amplifiers.

2.2.1 Class A

The class A amplifier has the highest linearity among other classes where it operates in the linear region of its active mode. The transistor is kept inactive region during the entire RF cycle. The current at the output flows throughout the conduction time and signal level remains small to avoid transistor cut-off point.

The active transistor device of the amplifier conducts for the full cycle of the input signal. This implies that the class A amplifier conduction angle is almost 360^0 ($2\theta_c$) as presented in Figure 2.2. Moreover, class A remains the most linear of all amplifiers [37].

However, to attain linearity of this magnitude, the drain and gate-source voltage of the amplifier must be chosen wisely. According to [38], linearity is just how close the output signal of the amplifier imitates the input signal. Linearity is a very important figure of merit for power amplification, specifically, when the signal contains amplitude and phase modulation [38, 39].

Apart from the linearity benefit, class A amplifier is also the least efficient system with less than 50% efficiency. It is not able to achieve high efficiency as the output capability is one out of eight and in the event consumes only a small fraction of the total DC power. However, class A amplifier, due to its low-level efficiency is only used as low-level drivers. Mobile base stations use class A power amplifier application as a starting point with harmonic control schemes. The efficiency can also be upgraded by changing the bias network configuration. However, temperature drifting depends on the bias network configuration. For an instant, a configuration where linearity of the amplifier is high cause for an increase in temperature which can result in clock drifting, while the entire device becomes extremely hot. To improve the performance of the device, the heat sink is applied to reduce the thermal runaway [39].

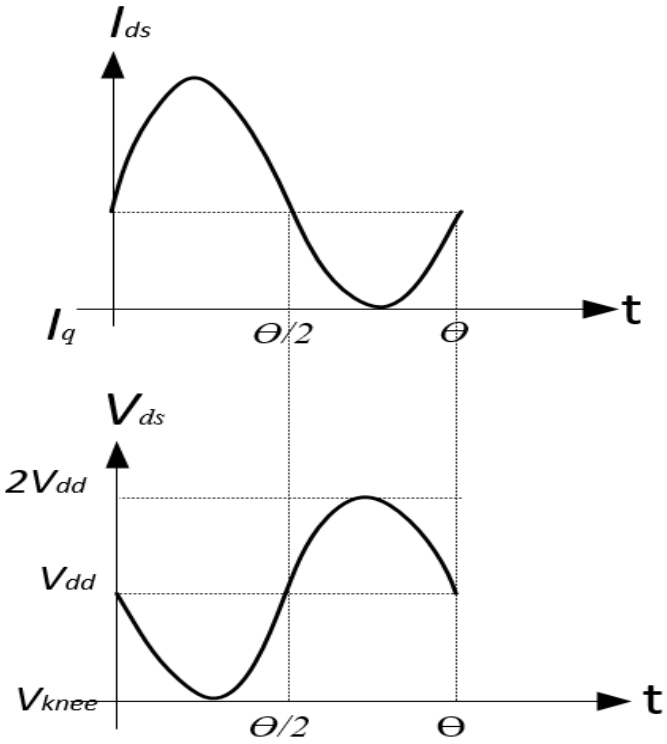

Figure 2.2: Voltage and current waveforms for a class A power amplifier.

The voltage and current waveforms of class A operation are shown in Figure 2.2. When the active device is biased within its linear region as presented in drain voltage (V_{DD}) and DC current (I_{DC}) waveform, the RF signal voltage is overlapped on the bias level [40]. The drain current (I_D) contains the RF current and the quiescent current (I_{DQ}), exhibited in (2.1) as:

$$I_D(t) = I_{DQ} - I_{\max}\sin(\omega t) \tag{2.1}$$

Where I_{max} is the peak amplitude of the RF drain current.

If coupling capacitor and a choke are used to block the DC and RF signals from specious passages, the current from the I_{DC} supply can be equal to the quiescent current (I_{DQ}) of the amplifier, while the RF output current ($i_{out}(t)$) equal the RF drain current (I_D):

$$I_{DC} = I_{DQ} \tag{2.2}$$

and

$$i_{out}(t) = I_{\max} \sin(\omega t) \tag{2.3}$$

So, the output voltage can be:

$$v_{out}(t) = i_{out}(t) R_L = I_{\max} R_L \sin(\omega t) \tag{2.4}$$

DC voltage (V_{DC}) and RF output voltage are the components of the drain voltage (V_{DD}) and are written as:

$$V_{DC}(t) = V_{DD} + v_{out} \tag{2.5}$$

$$V_{DC}(t) = V_{DD} + V_{\max} \sin(\omega t) \tag{2.6}$$

For the drain voltage ($V_{DC}(t)$), the equation (2.6) remains positive to keep the transistor active at all times. Therefore, the peak voltage magnitude of the RF signal will remain less than the DC voltage supply:

$$V_{\max} \leq V_{DD} \tag{2.7}$$

The power supply is written as:

$$P_S = V_{DD} I_{DC} = \frac{(V_{DD})^2}{R_L} \tag{2.8}$$

The RF output power is given as:

$$P_L = \frac{V_{\max} I_{\max}}{2} = \frac{(V_{\max})^2}{2R_L} \tag{2.9}$$

The output amplifier efficiency is defined:

$$\eta = \frac{P_L}{P_S} = \frac{(V_{\max})^2 R_L}{2R_L (V_{DD})^2} = \frac{(V_{\max})^2}{2(V_{DD})^2} \leq \frac{(V_{DD})^2}{2(V_{DD})} = \frac{1}{2} \quad (2.10)$$

Hence, from this expression above, the maximum class A amplifier efficiency cannot exceed 50%.

2.2.2 Class B

This amplifier is well known as a push-pull system, because of the two complementary or what is called matching transistors at the output stage. This amplifier is less linear but more power-efficient than class A amplifier. The conduction angle is operating over 180^0 during the entire cycle. This implies that the transistor conducts only half of the entire time on either positive or negative half cycle of the input signal. Hence, providing up to 78.5% ideal efficiency and 60% practical drain efficiency makes class B amplifier less heat dissipation than class A, which is also less efficient than class AB. Its deficiency is crossover distortion produced by the output signal. This is because 6 dB is required to drive the input power which leads to power gain reduction while impairing the amount of distortion in class B amplifier [39].

The voltage and current waveforms of class B operation have been presented in Figure 2.3. When the input signal (v_{in}) is at the positive half cycle, the bias voltage is greater than the threshold and the active device will conduct current and the drain current (I_D) appears in a form of half-sine pulse train. For the fundamental and DC components to appear, the drain voltage (I_D) at the RF part must be in a continuous sinusoid.

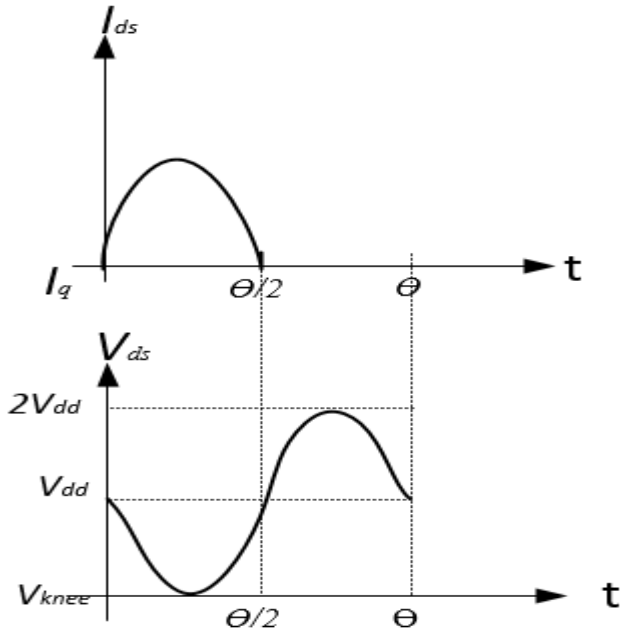

Figure 2.3: Voltage and current waveforms for a class B power amplifier.

Hence, the drain voltage is now equal to the output voltage (v_{out}) [19]. Similarly, the RF output current is equal to the drain current, which is a half-sine pulse train with maximum amplitude (I_{max}). This can be expressed in Fourier series as:

$$i_{out}(t) = I_D^{Fund}(t) = \frac{1}{2} I_D(t) = \frac{1}{2} I_{\max} \sin(\omega t) \tag{2.11}$$

The DC drain current (I_{DC}) is a half-sine pulse train the amplitude (I_{max}):

$$I_{DC} = \frac{1}{\pi} I_{\max} = \frac{I_{\max}}{\pi} \tag{2.12}$$

Hence, the power supply consumed can be written as:

$$p_S = V_{DD} I_{DC} = V_{DD} \frac{I_{\max}}{\pi} \tag{2.13}$$

The output power is:

$$p_L = \frac{(v_{out}(t))(i_{out}(t))}{2} = \frac{V_{\max} I_{\max}}{2 \times 2} = \frac{V_{\max} I_{\max}}{4} \quad (2.14)$$

Then the efficiency from DC to RF is given as:

$$\eta = \frac{P_L}{P_S} = \frac{\pi(V_{\max} I_{\max})}{4(V_{DD} I_{\max})} = \frac{\pi(V_{\max})}{4(V_{DD})} \leq \frac{\pi(V_{DD})}{4(V_{DD})} = \frac{\pi}{4} = 0.785 \quad (2.15)$$

Consequently, the overall efficiency of a class B amplifier is about 78.5%. The maximum achievable efficiency is within the range of 60 to 70%.

The greatest advantage class B has over class A is that it is more energy-efficient. No passage of DC current through the active device when there is zero input signal (v_{in}). Therefore, there is no power dissipation at the output of the device in the absence of an input signal. Furthermore, in the case of class A amplifier, the device remains active for a full cycle of the input signal which makes it to be more linear than the class B amplifier. In addition, the class B amplifier can be used for high power applications [19].

2.2.3 Class AB

This amplifier is also one of the most popular designs in power amplifiers. It is a system that is designed to deal with cross over distortion called the black zone effect in the class B amplifier. Class AB is the combination of class A and B configurations. It is also two transistors amplifier that is better than class A in terms of efficiency and more linear than class B amplifier. As a trade-off for efficiency and linearity, it becomes a compromise between the two classes of the amplifiers for superior performance [19, 34]. The biasing voltage at the input set

the transistor to conduct to acquiescent point to eliminate any crossover distortion in class B amplifier. The collector current at the input will flow to switch ON the transistor for more than a half a cycle, but less than a full cycle of the input signal to provide a conduction angle that is within 180 to 360^0 of the input signal. Moreover, the ideal efficiency ranges from 50 to 78.5% [19].

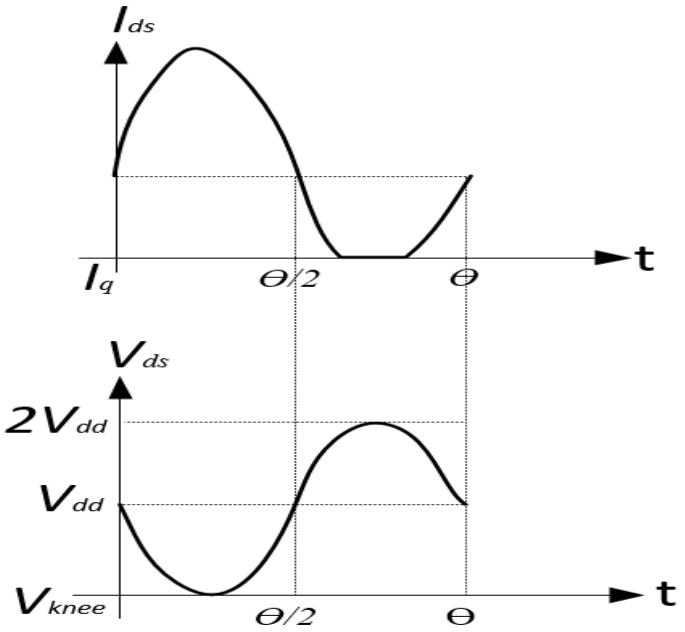

Figure 2.4: Voltage and current waveforms for a class AB power amplifier.

The voltage and current waveforms of class AB operation have been presented in Figure 2.4. When transistor conducts current, the drain current (I_D) appears in a form of more than half-sine pulse train. For the fundamental and DC component to appear, the drain voltage (V_D) at the RF part must be in a continuous sinusoid. Hence, the drain voltage is now equal to the output voltage (v_{out}) [19]. Similarly, the RF output current is equal to the drain current which is more than a half-sine pulse train with maximum amplitude (I_{max}). This can be expressed in Fourier series as:

$$i_{out}(t) = I_D{}^{Fund}(t) = \frac{2}{3} I_D(t) = \frac{2}{3} I_{\max} \sin(\omega t) \tag{2.16}$$

The DC drain current (I_{DC}) is a $\frac{2}{3}$ sine pulse train the amplitude (I_{max}):

$$I_{DC} = \frac{2}{3\pi} I_{\max} = \frac{2(I_{\max})}{3\pi} \tag{2.17}$$

Therefore the consumed power supply is given as:

$$P_S = V_{DD} I_{DC} = V_{DD} \frac{2(I_{\max})}{3\pi} \tag{2.18}$$

Now, the output power can be calculated as:

$$P_L = \frac{(v_{out}(t))(i_{out}(t))}{2} = \frac{V_{\max} I_{\max}}{2 \times 2} = \frac{V_{\max} I_{\max}}{4} \tag{2.19}$$

Similar, the efficiency, η can be expressed in terms of RF and DC supply terms as:

$$\eta = \frac{P_L}{P_S} = \frac{\pi(V_{\max} I_{\max})}{4(V_{DD} I_{\max})} = \frac{\pi(V_{\max})}{4(V_{DD})} \leq \frac{\pi(V_{DD})}{4(V_{DD})} = \frac{\pi}{4} \tag{2.20}$$

Hence, the overall efficiency of a class AB amplifier is 78.5% and less.

2.2.4 Class C

This amplifier is among the switching class and is based on network configuration. It is completely nonlinear and highly efficient with 100% ideal efficiency. The conduction angle of the transistor operates less than 180^0 of the input signal and is defined by gate bias and signal amplitude [34]. As a highly nonlinear class of amplifier, only a minor portion of the input signal is amplified to

produce very slight similarity at the output. Therefore the signal reproduction at the output is poor with high distortion. Class C amplifier, other than bad signal reproduction has other problems such as zero output power as the efficiency approaches 100% [34].

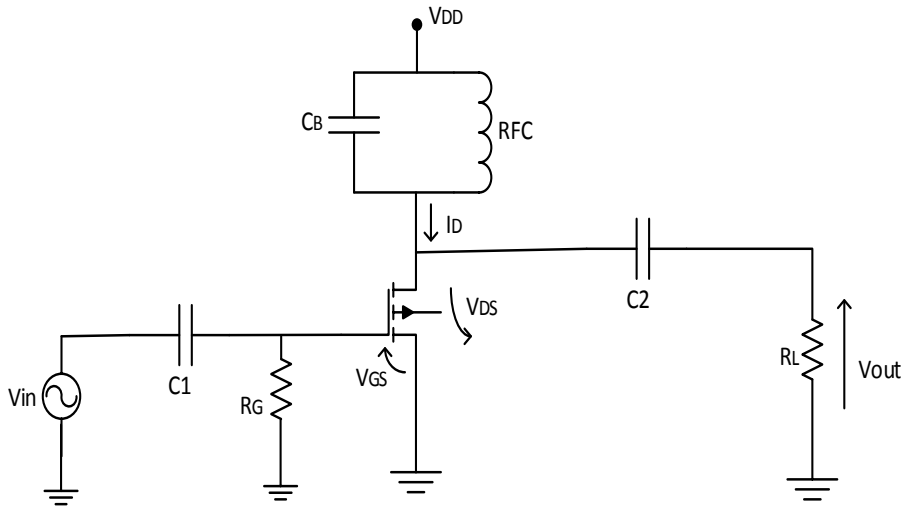

Figure 2.5: Basic class C amplifier circuit.

The class C amplifier can be used in applications where high linearity is acceptable with the linearization technique. A common application for class C amplifier is in RF transmitters where the distortion can be reduced using tuned load. The input signal (v_{in}) control the amplifier device switch. When the switch is turned ON, pulses of current flow through a tuned circuit [13, 34].

In the case of class C operation, it reduces the conduction angle even more than class B. However, DC power (P_{DC}) and output power (P_{out}) are affected in tumbling with power strength. Output power (P_{out}) approaches almost 100% efficiency. Introduction of a load resistor in the large signal system tolerates full drain voltage and current swing.

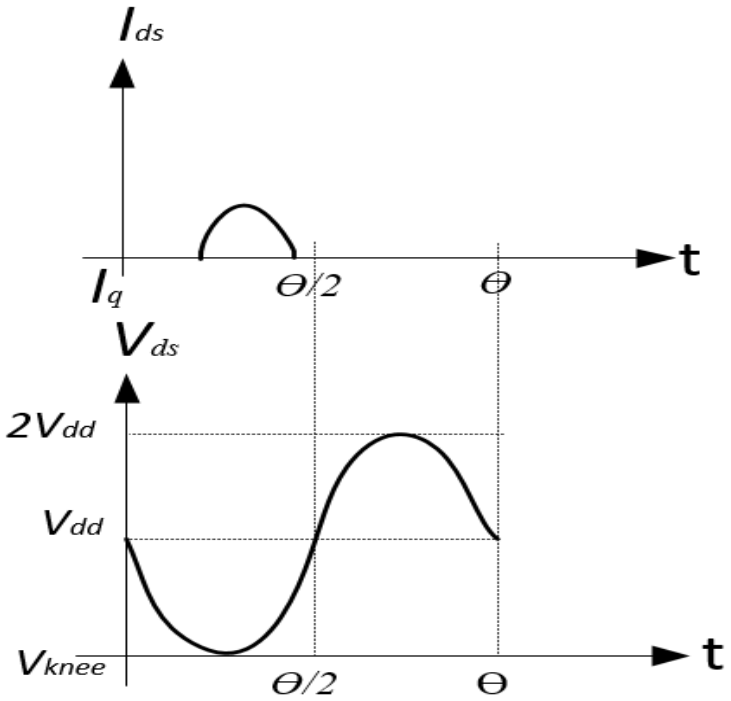

Figure 2.6: Voltage and current waveforms for a class C power amplifier.

To obtain a full voltage swing, the DC current is not proportional to load resistance [19], which is expressed as:

$$I_{DC} = \frac{V_{DD}}{R_L} \tag{2.21}$$

For load resistance,

$$R_L = \frac{V_{DD}}{I_{DC}} = \frac{2V_{DD}}{I_{\max}} \tag{2.22}$$

Hence, the power supply consumed is calculated as:

$$P_{DC} = \frac{V_{DD} I_{\max}}{\pi} = \frac{2(V_{DD})^2}{\pi R_L} \tag{2.23}$$

Then, the output power is written as:

$$P_L = \frac{1}{2} R_L (I_{DD})^2 = \frac{(I_{\max})^2 R_L}{8} = \frac{I_{DD}(V_{DD})^2}{2R_L} \quad (2.24)$$

The efficiency can be calculated from the DC to RF as:

$$\frac{P_L}{P_{DC}} = \frac{(V_{DD})^2 / 2R_L}{2(V_{DD})^2 / \pi R_L} = \frac{\pi}{4} \quad (2.25)$$

The overall efficiency of the class C amplifier is near 100%.

2.2.5 Class D

Class D amplifier is a voltage mode amplifier. It is a nonlinear amplifier with a switching circuit in the configuration that generates both half-sinusoidal and current waveform. It has two or more transistors acting as switches which are meant to generate a square drain-voltage waveform. Class D amplifier is difficult to realize especially at high frequency due to its multiple problems. That is why it cannot be used in base station applications [41]. Theoretically class D amplifier efficiency can rise up to 100%, because of non-periodicity where the current and voltage waveforms overlap as the current is drained only when any of the transistors is at the active region. It does not produce much heat and very small in size. It is used in mobile phones, powered speakers and in home theatre systems. This is due to its efficiency in preserving battery life and other numerous advantages [42].

2.2.6 Class E

Class E amplifier is a switching amplifier with an angle transistor. It achieves higher efficiency than class B or class C amplifier. The transistor operation is based on ON/OFF switch where in the circuit the load network shapes the voltage

and current waveforms to avoid simultaneous high voltage and current in the transistor. The transistor reduces power dissipation during switch transition. In low order class E circuit, a transistor performs well at frequencies of up to 70% of frequency of good class B operation. It operates with power losses of factors of 2.3 better than class B or class C amplifier using the same transistor at the same frequency and output power. The amplifier is also designed for narrow band operation or for fixed-tuned operation on frequency band between 225 to 400 MHz. The harmonic output is similar to that of class B amplifier. The zero overlap between voltage and current through transistor is due to the behaviour of class E amplifier as a compromise between class AB and switched mode power amplifier. This gives a theoretical efficiency of 100% and a robust performance [43, 44].

2.2.7 Class F

The class F power amplifier is a highly efficient amplifier based on switched-mode transistor circuit. Network configuration amplifier achieves better efficiency than the quiescent point-based amplifiers. Class F amplifier ideal efficiency capability is up to 100% with zero linearity. To achieve high efficiency the amplifier uses harmonic resonators to control the harmonics. The output power uses the harmonic resonators to shape the drain current and voltage waveform. The drain voltage wave-form comprises of one or more odd harmonics and in the order of a square wave, while the current waveform comprises even harmonics and in the order of a half sine wave [45].

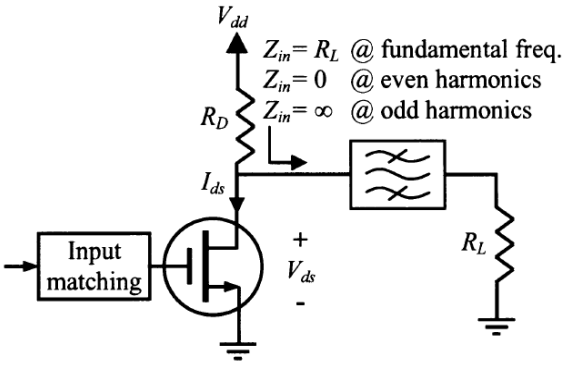

Figure 2.7: Class F power amplifier circuit.

Consequently, it is not easy to design a class F amplifier due to a complex circuit configuration of the output matching network. It has more output filters than other classes of amplifiers. Class F amplifier require more attention than other amplifiers due to complexity. Another significant hitch of class F amplifier is that harmonic is unachievable at high frequency, however limiting the maximum theoretical efficiency to 75% [45].

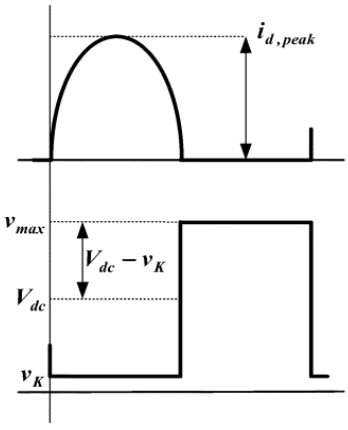

Figure 2.8: Ideal time-domain drain voltage and current waveforms for class F.

As illustrated in Figure 2.7 and 2.8 above, class F amplifier achieves higher efficiency with the adoption of proper harmonic terminations of the output. The odd harmonics are open to producing square wave as the voltage waveform,

even harmonics remain short to produce current wave. When $Z_{in} = R_L$, the first harmonic is totally delivered to the output of the power amplifier. The DC power is presented as:

$$P_{DC} = V_{DD} I_{DD} = \frac{V_{DD} I_{\max}}{\pi} \tag{2.26}$$

Where V_{DD} and I_{DD} are the magnitudes of the DC voltage and current. The RF output at the fundamental frequency is written as:

$$P_{out} = V_{DD} I_{DC} = \frac{4\left(V_{DD} I_{\max}\right)}{\pi\sqrt{2} \times 2\sqrt{2}} = \frac{V_{DD} I_{\max}}{\pi} \tag{2.27}$$

Hence the efficiency of class F is expressed as:

$$\eta = \frac{P_{out}}{P_{DC}} \tag{2.28}$$

and the power added efficiency can be expressed as:

$$PAE = \frac{P_{out} - P_{in}}{P_{DC}} \tag{2.29}$$

Therefore, the overall efficiency of the class F power amplifier is near 100%.

2.2.8 Summary of Power Amplifier Classes

The class of operation for a power amplifier is noteworthy for this research and is based on the amount of transistor bias require for operation as well as the amplitude for the input signal. Amplifier classification takes into account the input signal which the transistor conducts, the efficiency and the amount of power that

the switching transistor dissipates in the form of heat. Then we can make a comparison between the most common types of power amplifier classifications in the resulting table.

Table 1.1: Amplifier classes comparison

Class	Modes	Conduction Angle	Efficiency (%)	Linearity	Distortion
A	Biasing	2π	<45	Excellent	Zero
B		π	<78	$<\mathrm{AB}$	Dead Zone
AB		$3\pi/2$	>78	$>\mathrm{B}$	Low
C	Switching	$\pi/2$	100	Bad	High
D		Poor			
E					
F					

2.3 Characteristics of Power Amplifier

Characteristics of RF Power amplifier are one of the fundamental features to define the operations of the device. They are considered to be properties of the power amplifier. Task about power amplifier will not be accomplished until the parameter on which its performance can be evaluated are known [46]. In this research, the insight of power amplifier basic parameters such as linearity, efficiency and gain will also be deliberated.

2.3.1 Linearity

Linearity is one important figure of merit that evaluates the performance of a power amplifier. Nonlinearity is a looming source of obstruction and system performance deficiency. Nonlinearities of power amplifier cause distortion in signal transmission. The main part of the RF transmitter nonlinear impairment is caused by the nonlinear performance of the power amplifier device [39]. Therefore, the signal has to be amplified linearly for RF transmitter to perform effectively. Linearity is simply defined as how closely the output signal of a device is similar to the input signal. Moreover, one of the parameters that measure linearity is the 1 dB compression point which will be discussed in gain saturation topic below [8, 39].

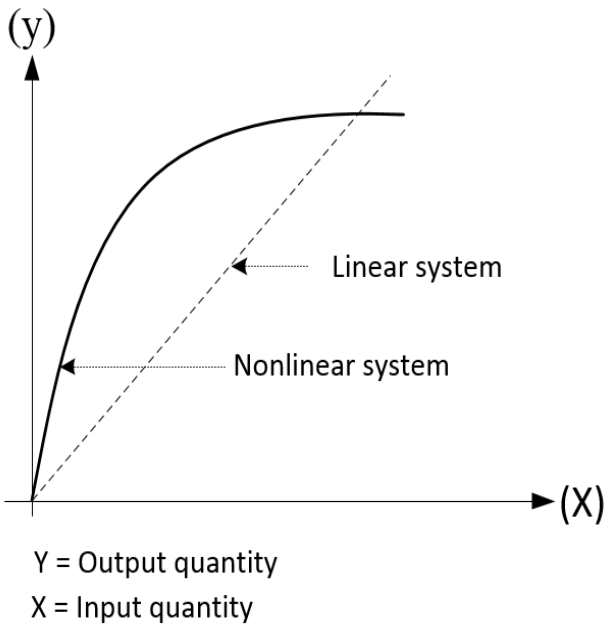

Figure 2.9: Linear and nonlinear system.

2.3.2 Efficiency

Efficiency is one of the effective attributions in the design of wireless system power amplifier. The power efficiency of the mobile station is one of the

characteristics that pilots the increase of battery lifetime and talk time. Efficiency at the mobile base station pilots reduction of power consumption and the need for active cooling. However, it is an important parameter of the power amplifier. It is measured by converting the DC power supply to the signal power delivered to the load. It is not defined by the standard, other than the two performance metrics which power amplifier efficiency can be measured as presented [8, 34, 39]:

- Power Added Efficiency (PAE): PAE recognizes the effect of regular usage of drive power at RF frequency which is a ratio of RF output power (P_{out}) delivered to the load minus RF input power (P_{in}), then to the DC power (P_{dc}).

$$\eta = \frac{P_{out} - P_{in}}{P_{dc}} \times 100\,\% \tag{2.30}$$

  Power added efficiency determines the power amplifier performance such as power consumption, power dissipation which are quantified in percentage.

- Drain efficiency: This is the ratio of the RF output power (P_{out}) delivered to the load of the power supply by the *DC* (P_{dc}).

$$\eta = \frac{P_{out}}{P_{dc}} \times 100\,\% \tag{2.31}$$

The drain efficiency is not the overall efficiency of the power amplifier, which in this case, the input power is not included to drive the signal to the output of the amplifier. These are the most common power efficiency performance metrics used in power amplifier design. Efficiency depends on the class of operation where the conductor experienced losses due to dielectric and heat effect as other

factors unfavourable to power amplifier overall efficiency. Therefore, proper design of PA has to be ensured by also taking account of thermal and mechanical standard requirement and the zero losses in the circuits [28, 34].

2.3.3 Power

In the RF transceiver system, the two concepts of power are available power and dissipated power. In RF systems, power is produced from the source and dissipate to the load. This concept is very vital in linear and nonlinear systems. It is more important in nonlinear systems, where a waveform will have components at different frequencies that may not be related [8, 36].

- Available power: This is maximum transferable power which is obtainable from the source as the input impedance (Z_{in}) of the amplifier is equivalent to the conjugate of the source impedance (Z^*_{in}). Hence, the maximum available power as a function of frequency is expressed as:

$$P_{av}(w) = \frac{\{V_s(w)\}^2}{8R_e\{Z_s(w)\}} \tag{2.32}$$

  $V_s(w)$ is the peak value of a sinusoidal voltage applied at the input, while $R_e\{Z_s(w)\}$ is the real part of the system source impedance.

- The power dissipated or obtainable from the source is the power dissipated to the load can be expressed as:

$$P_d(w) = \frac{\{V_s(w)\}^2}{2R_e\{Z_L(w)\}} \tag{2.33}$$

$V_L(w)$ is the peak value of a sinusoidal output voltage and $R_e\{Z_L(w)\}$ is the real segment of the load impedance.

2.3.4 Gain

This is one of the most trivial characteristics of RF power amplifier which is also a defined quantity in RF microwave circuits. It is used in the measurement of the degree of amplification. Gain can be defined as the difference between input and output signal. That is to say, the amount of input signal put forward to the output of the circuit. The power delivered to the load divided by the power available from the source [34].

$$G_t = \frac{P_d \ at \ the \ output}{P_{av} \ at \ the \ input} \tag{2.34}$$

This applies to both linear and nonlinear circuits, although more attention is given to nonlinear circuits due to nonlinear distortion. However, in wireless communication systems, transducer gain is an essential concept that can tell how much power a circuit deliver to a 50 Ω standard load. The acceptable standard gain ratio for today's wireless communication system power amplifiers starts from 9 dB [47].

2.4 Other Parameters for characterization of PA Nonlinearities

As stated before, the power amplifier is the fundamental consumer of the most generated power in the transmitter. However, it introduces a large number of impurities to the transmitted signal becomes a source of severe errors to the received data. These effects caused by power amplifier are described and quantified according to size, amount and severity. The most common nonlinearities are adjacent channel power ratio (ACPR), intermodulation

distortion products (IM), spectral regrowth, error vector magnitude, etc. This work will highlight some parameters for power amplifier nonlinearities characterization [48].

2.4.1 Gain Saturation

This is one of the fundamental parameters that define the ability of a power amplifier to reach its highest point of active operation [49]. The output power level of the power amplifier may cease to appreciate in direct proportion to the input signal of the system. For a power amplifier to reach the saturation point means a linear gain of the device is fully saturated. Linearity is not always certain in the power amplifier. However, 1 dB compression point is one of the critical tools in defining the linearity of power amplifier [49]. Moreover, 1 dB compression is useful in power amplifier operation. A voltage ($v_i(t)$) is a source to the input of power amplifier and response of the amplifier output voltage ($v_o(t)$) can be represented as:

$$v_o(t) = g_0 + g_1 v_i(t) + g_2 v_i^2(t) + g_3 v_i^3(t) + \cdots + g_n v_i^n(t) \tag{2.35}$$

A small input voltage allows power amplifier to operate linearly and can be shown at the output, presented as:

$$v_o(t) = g_1 v_i(t) \tag{2.36}$$

The output of the power amplifier is almost comparable to the input voltage as well as the voltage gain (g_1). Increase in input voltage increases the number of terms which cause the power amplifier to respond nonlinearly. The increased

term (g_2) becomes negative due to the increase in input voltage and caused power amplifier saturation at the 1 dB compression.

Therefore, 1 dB compression point is a region power amplifier gain declines by 1 dB less than the input power [34].

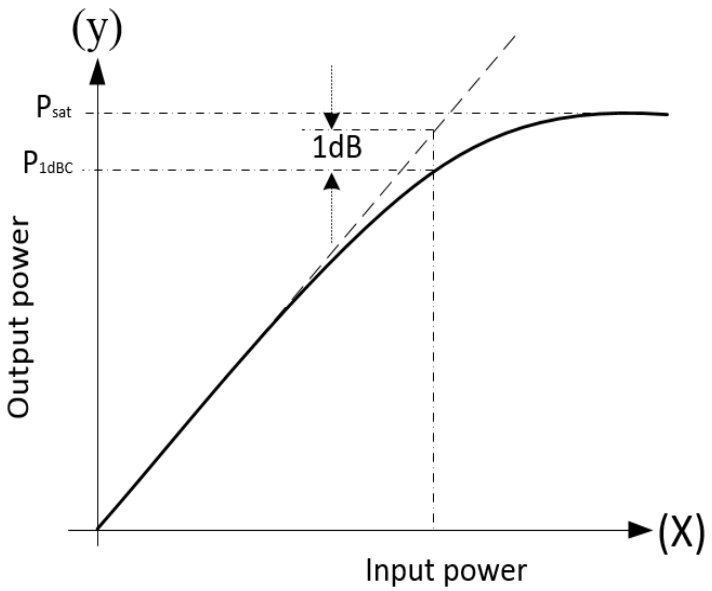

Figure 2.10: 1 dB compression point.

This is the maximum output power a power amplifier can reach, as illustrated in Figure 2.10. The maximum PA output power refers to a saturation power point (P_{sat}), beyond a 1 dB compression point [49].

2.4.2 AM-AM and AM-PM Characteristics

These are linear and nonlinear responses of a power amplifier system. A linear amplifier encloses a constant gain over the system bandwidth and does not respond to phase deviation. However, with the increase in amplitude, the output ceases to increase linearly, which cause saturation and this is called AM-AM distortion [39]. A nonlinear amplifier has a non-constant envelope. However, due

to the phase deviation, the gain equally decreases and the output signal clipped through saturation. When the input signal increases, the amplifier operates in a nonlinear region where nonlinear circuit causes a phase shift. This relation of input amplitude and the phase shift is the AM-PM characteristics of the amplifier and the distortion caused is called AM-PM distortion [8, 29].

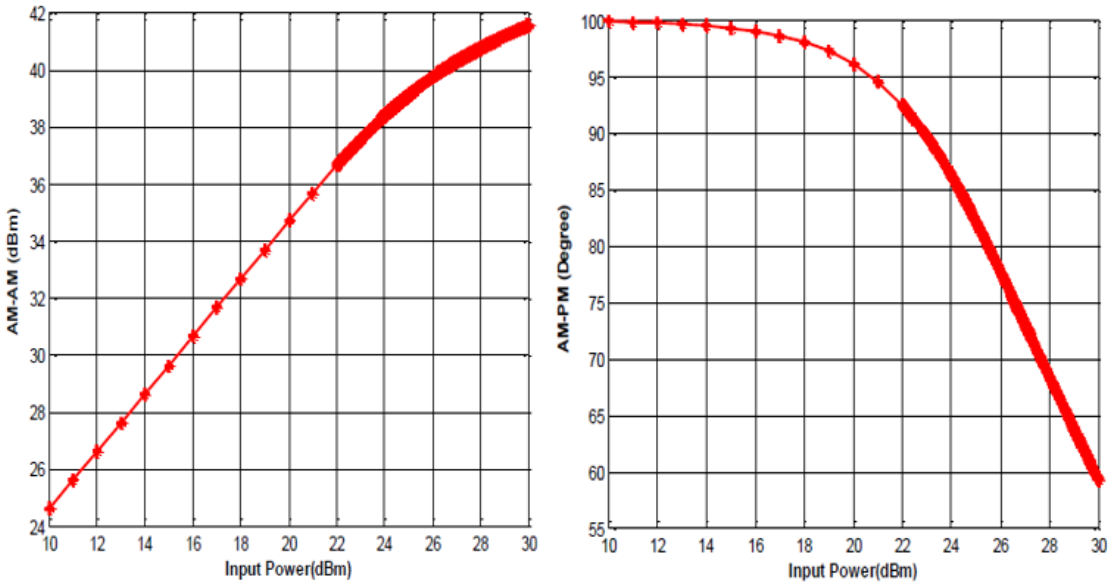

Figure 2.11: The AM-AM (a) and AM-PM (b) characteristics for a PA.

2.4.3 Intermodulation Distortion

This is the amplitude modulation of two or more signals, having different frequencies due to nonlinearities. Intermodulation distortion is as a result of nonlinearities from the power amplifier or the type of algorithms applied in the system. In addition, the amplifier, due to nonlinear behaviour generates harmonics of the input signal as well as mixing products when two or more input signals are fed into the system. These additional frequency products are called intermodulation products [29].

Two-tone of two equal amplitude frequencies, (f_1) and (f_2) can be applied to a nonlinear transmitter. The output of the transmitter consists of DC frequency components such as in-band distortion (f_1+f_2) and out-of-band distortion ($2f_1$, $2f_2$, $3f_1$) are the harmonic distortions and the intermodulation distortions (f_1-f_2, f_1+f_2, $2f_1-f_2$, $2f_2-f_1$, $2f_1+f_2$, $2f_2+f_1$) are collectively illustrated in Figure 2.12.

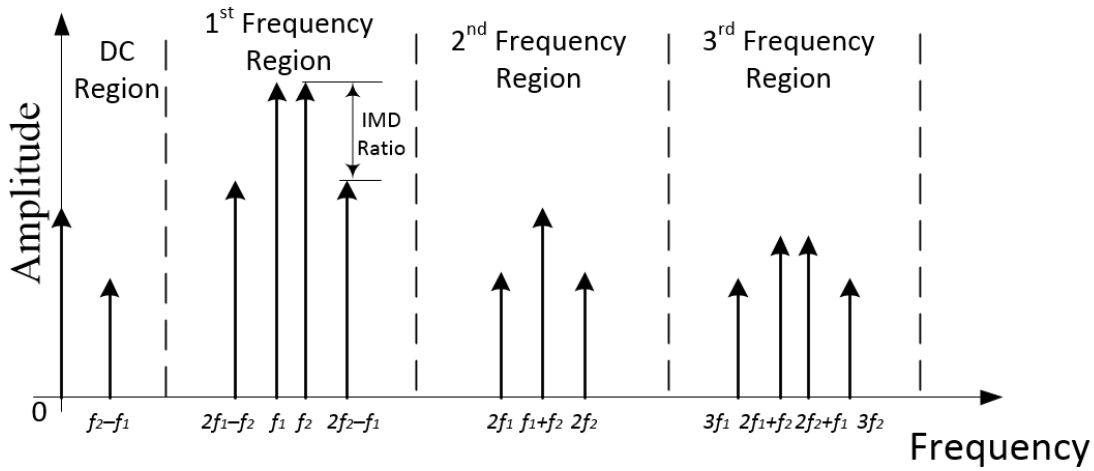

Figure 2.12: 3-IMD distortion with lower and higher intermodulation.

According to Aitchison, et el [50], the second and third harmonic products ($2f_1$, $2f_2$, $3f_1$) of the amplifier can be minimized by filtering. However, second-order intermodulation products ($2f_1-f_2$, f_1+f_2) can also be filtered as being far enough from the fundamental signal. The third order intermodulation product ($2f_1-f_2$, $2f_2-f_1$, $2f_1+f_2$, $2f_2+f_1$) appears so close to the fundamental. It is a very delicate product among all the distortion products, causing a critical effect on the signal during amplification and cannot be eliminated by filtering. Intermodulation products, specifically, third-order product can be avoided using linearization technique. Linearization technique can be used in this instance, to minimize these unwanted components that cannot be filtered through other common techniques. Another solution is to operate at a sufficiently low input power where the amplitude of third-order intermodulation products is very small [50].

2.4.4 Adjacent Channel Power Ratio (ACPR)

This is one of the most key figures of merit that express the degree of spectral re-growth into adjacent channel [51]. Adjacent channel power ratio as it is called is the ratio of the total power of the adjacent channels to the signal power in the main channel, measured over the signal band. ACPR is used mainly by frequency standard regulators to characterize signal interference with other adjacent channels and it can be used to describe the linearity of a communication system [52].

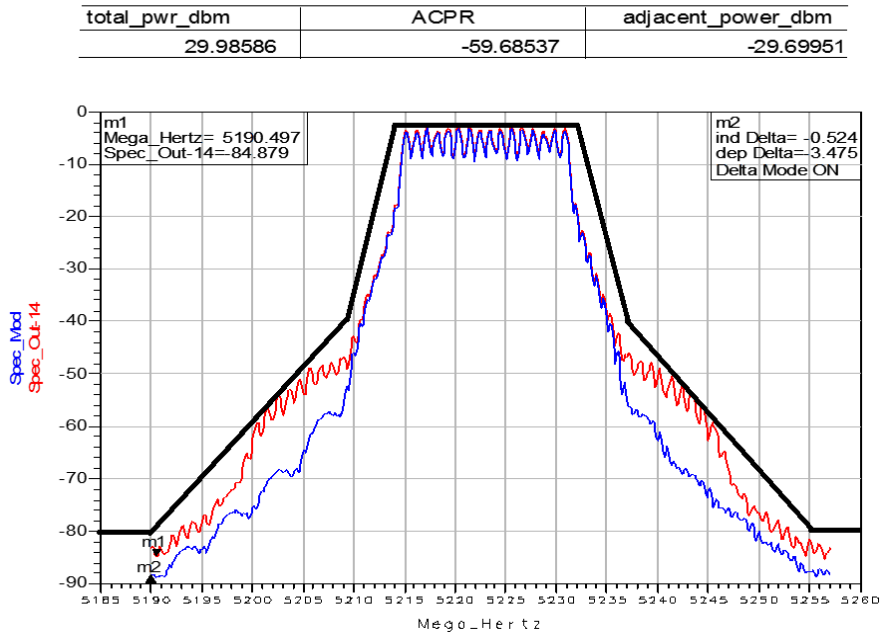

Figure 2.13: Upper and lower adjacent channel bands (constrain level, filtered and unfiltered OFDM).

Spectral re-growth is parallel to the intermodulation and can cause unwanted leakage of the adjacent channel due to interference. However, spectral re-growth can be examined when a modulated input signal passes through a nonlinear power amplifier. Its bandwidth is widened due to nonlinearities which is caused by the generation of the mixing products between the frequency components [51]. The Figure 2.13 has shown illustration of spectral mask for OFDM and 5G

modulations. The OFDM in the OFDM families shows worst performance to spectral regrowth. The 5G modulation systems such as the filter bank multicarrier (FBMC), generalized frequency division multiplexing (GFDM), universal filtered multicarrier (UFMC), filtered OFDM, and other waveform contenders have shown robustness to spectral regrowth. These are modulations that have resilience, compatibility and spectral containment. However, the 5G modulations at the same time suffer high PAPR and loss orthogonality due to phase distortion.

2.4.5 Error Vector Magnitude (EVM)

Error Vector Constellation is the modulation quality and error performance in complex wireless communication systems. It is used in computing the performance of a transmitter or receiver. A signal is transmitted or collected by a receiver to acquire all constellation points at the precise position called ideal symbol location. The EVM is sometimes called receive constellation error (RCE) as a performance metric to measure how far the points are from the ideal location. Different imperfections in the implementation can cause the actual constellation points to diverge from the ideal location. These imperfections include phase noise, carrier leakage, low image rejection ratio, distortions, spurious signals corrupt the EVM measurement [19, 39].

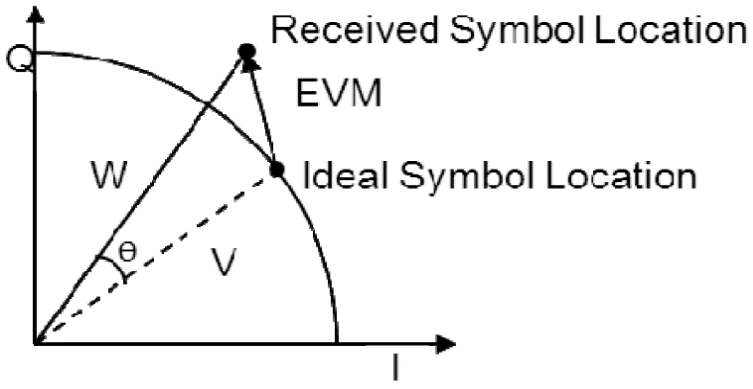

Figure 2.14: Error vector magnitude.

EVM is used in software-defined radio performance evaluation for both transmitters and receivers. It is also used as an alternative to BER measurements to validate impairments that affect signal reliability. Groe [53] assert that EVM measurements can be applied in methods and applications such as the multi-symbol methods which consist of multi-level phase-shift keying (MPSK), quadrature phase-shift keying (QPSK) and multi-quadrature amplitude modulation (MQAM). These methods are widely used in wireless local-area networks (WLANs), broadband wireless and 4G cellular radio systems like Long-Term Evolution (LTE) where MQAM is combined with orthogonal frequency division multiplexing (OFDM) modulation. One of the stages in a typical phase-shift keying demodulation process produces a stream of I-Q points which can be used as a reasonably reliable estimate for the ideal transmitted signal in EVM calculation [8, 13, 34, 54].

The error vector magnitude (EVM) also estimates the properties of deficiency in the communication system constellation. The error vector ($E(c)$) is the variation between the actual transmitted constellation point ($AT(c)$) and the ideal constellation point ($I(c)$). The EVM can be expressed in RMS form as:

$$EVM_{rms} = \sqrt{\frac{\frac{1}{N}\sum_{c=1}^{N}\left|E(c)\right|^2}{\frac{1}{N}\sum_{c=1}^{N}\left|I(c)\right|^2}} \tag{2.37}$$

Where N is the total number of constellation points defining the level of modulation. N is also used for *EVM* calculation. $I(c)$ is the c^{th} number of normalised constellation points and $E(c)$ can be expressed as:

$$E(c) = x(c) - y(c) \tag{2.38}$$

Where $x(c)$ is the measured normalised symbol which is equal to measured normalised point (W) and $y(c)$ is equal to $v(c)$ as the ideal reference point. The rms value of the error vector magnitude is calculated by taking the average value of all the frames. In the measurement, it is recommended by the IEEE 802.11a for WLAN standard to take a large number of transmitted frames of at least 20 frames [55]. The computation of error vector magnitude for the IEEE 802.11a, WLAN standard is expressed in [8, 55] as:

$$EVM_{rms} = \frac{\sum_{a=1}^{N_f} \left(\sqrt{\frac{\sum_{v=1}^{L_p} \left(\sum_{n=1}^{52} \left\{ (In - Io)^2 + (Qn - Qo)^2 \right\} \right)}{52 L_p P_a}} \right)}{N_f} \tag{2.39}$$

Where N_f is the frame number, L_p is the packet data length, P_a is the average power of the constellation diagram, a is the symbol index, v is the v^{th} symbol received and n is the OFDM symbol subcarrier. I_n and I_o are the in-phase of measured and referenced constellation point, while Q_n and Q_o are the quadrature of measured and referenced constellation point respectively. EVM can also be achieved in percentage by using the rms value. In the system level, it is very important for figure of merit to evaluate the precision of the OFDM signal. EVM% can be expressed as:

$$EVM_{\%} = \frac{\sqrt{\frac{1}{N} \sum_{a=0}^{N_f - 1} I_{er}(a)^2 + Q_{er}(a)^2}}{N_r} \times 100\% \tag{2.40}$$

Where *N* is the number of symbols. N_r is the normalized reference of *EVM* and *a,* is the symbol index. Then, I_{error} = $I_{reference}$ - $I_{measured}$, while Q_{error} = $Q_{reference}$ - $Q_{measured}$. Where I and Q are the in-phase and quadrature components. The EVM can also be measured in decibel (dB) which is expressed as:

$$EVM_{dB} = 10\log_{10}\left[\frac{P_{error}}{P_{reference}}\right] \tag{2.41}$$

Where P_{error} stands for the error vector power, and $P_{reference}$ is the reference constellation point power for both single and multiple carrier modulation. It is the average power of the reference constellation. In the IEEE 802.11 standard for LTE, the ACPR, envelope spectral mask (ESM) and EVM are needed as expressed in the existing standard.

2.5 Power Amplifier Nonlinear Distortions

2.5.1 Harmonic Generation

A nonlinear power amplifier can be characterized using an equation written as:

$$v_o(t) = g_0 + g_1 v_i(t) + g_2 v_i^{\,2}(t) + g_3 v_i^{\,3}(t) + \ldots + g_n v_i^{\,n}(t) \tag{2.42}$$

The single tone signal is expressed as:

$$v_i(t) = \cos(2\pi f t) \tag{2.43}$$

Where $v_i(t)$ is a harmonic frequency component to the input of the power amplifier. These harmonic components are the source of a harmonic generation which

cause distortion if they are not suppressed. The harmonic products are not a serious threat since they are far from the fundamental tone on the spectrum, they are easy to filter [56].

2.5.2 Intermodulation Distortion

The equation (2.43) shows the results of the nonlinear system. A two-tone sinusoidal signal is applied to the input of a power amplifier is expressed as:

$$v_i(t) = \cos(2\pi f_1 t) + \cos(2\pi f_2 t) \tag{2.44}$$

Where the frequency components at the output consist of second and third-order intermodulation products of the power amplifier. If these components are not suppressed enough, they cause distortion. Since second-order intermodulation products are not close to the fundamental components, it can easily be filtered. However, the third-order frequency of intermodulation components are close to the fundamentals and cannot be filtered out easily [29].

2.5.3 Cross Modulation Distortion

Cross modulation, in a nonlinear power amplifier system, is the transfer of amplitude modulation of one carrier frequency (f_1), to another carrier frequency (f_2). The amplitude modulation of one signal appears on the other carrier frequency signal when there is two-tone excitation where the amount of density for a given signal rely on the reoccurrence of the other signal. Therefore, the cross-modulation of the first carrier relies on the square magnitude of the other carrier [32].

Let assume that two carrier frequencies, wanted signal (f_1) and unwanted signal (f_2) are applied to the input of a power amplifier as expressed in equation (2.45):

$$v_i(t) = v_1 \cos(2\pi f_1 t) + (1 + m(t)) v_2 \cos(2\pi f_2 t) \tag{2.45}$$

Where $m(t)$ represents the modulating waveform. Let the power amplifier nonlinear model of 3^{rd} order be used from the equation (2.42). By replacing (2.45) in (2.42), only the first three terms are considered for simplicity where the output of the wanted signal will be:

$$v_o = \left(a_1 v_1 + \frac{3}{4} a_3 {v_1}^3 + \frac{3}{2} a_3 v_1 (1 + m(t))^2 \cos(2\pi f_1 t) \right) \tag{2.46}$$

This has shown that there is an occurrence of cross-modulation when the unwanted carrier of the frequency (f_2) of the input is transferred to the wanted carrier of frequency (f_1) after passing through the nonlinear power amplifier [32].

2.5.4 Spectral regrowth

Spectral regrowth is similar to intermodulation distortion caused by nonlinearity of a power amplifier at the presence of two-tone signal applied to the device. It occurs when a modulated signal is applied to the input of the nonlinear device. In the process, however, the bandwidth is widened by the nonlinearities. This is caused by the production of the various products from different frequency components of the spectrum [51].

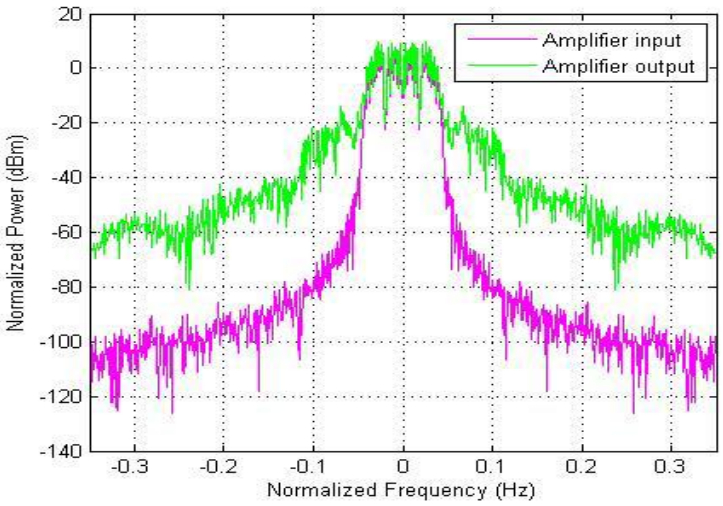

Figure 2.15: Spectral regrowth [57].

The Figure 2.15 has shown a typical example of spectral regrowth of a spectrum signal as explained in the paragraph. The unwanted leakage of the adjacent channel causes spectral regrowth which results to adjacent channel interference. The ACPR as discussed is kept low to avoid interference. It is a figure of merit for defining the degree of linearity in wireless communication systems. It can be calculated based on the definition as upper, lower or total ACPR [28], which can be expressed as:

$$ACPR_u = \left(\frac{P_{mch}}{P_{uadch}} \right) \tag{2.47}$$

$$ACPR_l = \left(\frac{P_{mch}}{P_{ladch}} \right) \tag{2.48}$$

and

$$ACPR_t = \left(\frac{P_{mch}}{P_{uadch} + P_{ladch}} \right) \tag{2.49}$$

Where P_{mch} stands as the main channel power, P_{uadch} is the upper adjacent channel power and P_{ladch} is the lower adjacent channel power respectively.

2.5.5 Desensitization

Strong unwanted signals of various frequencies from nonlinear power amplifier tent to block wanted weak signals [29]. Let the signals applied to the input of the nonlinear power amplifier be:

$$v_i(t) = v_1 \cos(2\pi f_1 t) + v_2 \cos(2\pi f_2 t) \tag{2.50}$$

If the wanted signal has a carrier (f_1), while unwanted signal carrier is called (f_2), then, $v_1 > v_2$. The equation (2.42) is assumed to be the power amplifier nonlinear model with up to 3^{rd} order component. Let introduce the equation (2.50) into (2.42), while considering simplicity only in the first three terms, the output of the wanted signal will be:

$$v_o = \left(a_1 v_1 \frac{3}{4} a_3 {v_1}^3 + \frac{3}{4} a_3 v_1 {v_2}^2 \right) \cos(2\pi f_1 t) \tag{2.51}$$

Here, a_1 gives the negative property of the amplifier saturation. And so, the (f_1) component is controlled by the (f_2) component. This is called desensitization [29].

2.6 Memory Effects of Power Amplifier

The investigation has revealed that most modern wireless communication transmitters use the non-constant envelope to improve the speed transmission rate and bandwidth. The power amplifier has remained the source of nonlinearities and hence, exhibit memory effects. The nonlinearity behaviour of the amplifier is potentially dependent not only on immediate input but also on the

preceding inputs. Memory effect is defined as changes in modulation frequency which leads to changes in amplitude and phase of distortion components such as power amplifier [39, 58]. Memory effect cause distortion products such as harmonic distortion, intermodulation, spectral regrowth, cross-modulation distortion product, desensitization, and so on. These products are produced by nonlinear power amplifier is variable and dependent on many conditions such as the input signal's magnitude, carrier frequency and bandwidth [29].

In the case of memoryless system, the output signal is an instantaneous function of the input signal without phase difference. In other words, a nonlinear power amplifier with memory effect has the output signal as the function of previous input signals. This, in turn, causes a delay in the transient signal before the output reaches the steady-state. However, in [33], input and output characteristics of a memoryless power amplifier can be defined using the equation (2.42).

However, two-tone signals are applied to a power amplifier device, resulting in a third-order intermodulation product. According to [33], the distortion product depends on the input amplitude, while the memoryless product component depends only on the input amplitude which is not the case in reality. For nonlinear power amplifier third-order intermodulation, the dependency is on the two-tone spacing. It is considered to be a memory effect for any non-constant distortion at various modulation frequencies. Consequently, memory effects produce frequency-dependent gain and phase difference through the power amplifier in nonlinear system. In other words, memory effects are dependants of magnitude and phase of the output signal on modulation frequency [59].

The memory effect of a power amplifier is considered as dynamic nonlinearity (weak nonlinearity). Dynamic nonlinearity is classified as the linear and nonlinear memory effect. The linear memory effect can be affected by the non-ideal fundamental frequency response and can be characterized by a linear filter. The nonlinear memory effect is considered to be more important than the linear memory effect. It is the dominant source of power amplifier dynamic nonlinearity. Moreover, it can be affected by trapping effects, matching condition at harmonic frequencies, bias circuit design condition and influence ionization. Moreover, it can be characterized by a nonlinear filter. According to [60] nonlinear memory effects are basically essential factors in RF power amplifier and are classified as electrical and electro-thermal memory effects which will be discussed in detail in the next section.

2.6.1 Electrical Memory Effects

The main cause of electrical memory effects is effective ionization, trapping effects, bias network design, impedance matching condition at harmonic frequencies and the envelope frequency. In other words, the electrical memory effects are influenced by the variable frequency response of the amplifier due to the presence of passive components in the circuit. The electrical memory effects depend on the power amplifier external node impedance and variation of the envelope impedance. Power amplifier external node impedance varies based on the input and frequency response. This, in turn, affects the voltage waveform and causing unavoidable electrical memory effects.

The varying envelope, fundamental impedance or harmonics at different modulation frequencies cause electrical memory. The varying envelope

experiences more fluctuation from DC to the highest modulation frequency. The electrical memory effects usually appear at higher frequencies in MHz range. The varying envelope impedance cannot be kept constant over different frequency bands due to the changes in output impedance. Consequently, the memory effects of the varying envelope impedance must be taken seriously. Moreover, the fundamental and harmonic impedance have negligible deviation, narrow and simple matching circuit. However, the memory effects have serious effect as well. To reduce electrical memory effects, the input impedance variations are maintained in the low region. Consequently, most wideband applications such as LTE, WCDMA and WiMAX are more sensitive to the effects [60, 61].

2.6.2 Thermal Memory Effects

These memory effects are principally traced in the power amplifier active component as a result of excessive heat. The thermal memory effects are ultimately caused by the dependence of electrical characteristics and dynamic variation of the active component of the power amplifier on temperature. Changes in junction temperature due to various electro-thermal factors result in changes in active component thermal impedance. This, in turn, transforms the whole power amplifier behaviour and creates further distortions [61].

The nonlinearity and the nature of thermal memory effects have impacted the appearance of the effect in the amplifier only during a longer period of time as against the electrical effects which spend a shorter time interval. However, due to this factor, thermal memory effects are best known as long-term memory effects. For this reason, thermal memory effects are subjected to as low modulation frequencies as up to 1 MHz. Therefore, the thermal memory of a

power amplifier affects narrow-band signals such as Global System for Mobile (GSM) communications or Enhanced Date for Global Evolution (EDGE) [62, 63].

2.6.3 Quantifying Memory Effect

Previous studies have shown that the electro-thermal memory effects are more significant for envelope frequencies below 1 MHz as the mass of the active device is remarkable to vary its temperature fast enough to keep up with high envelope frequency. With broadband signals, electrical memory effects play the most important role [33]. In contrast, with IMD components, the output power variation as a function of the input signal over the fundamental frequency is less than 0.5 dB. Thus, IMD components are more sensitive to these effects and most research quantifies the memory effect as IMD variations over the envelope frequency. In other words, memory effects can be related to the IMD component variations as well as to non-constant AM-AM and AM-PM distortions over the frequency bandwidth [33, 59].

In applications using non-constant modulation scheme, a variation of envelope frequency results in a great variation in bias network impedance which itself leads to nonlinear fluctuations in IMD components. To overcome this dependency, the bias network impedance should be zero (short circuit) at envelope frequency and infinite (open circuit) at RF. In order to bias an active device in a specific operation class, constant current and voltage should be applied to the gate-source. However, in non-constant envelope frequency applications, every single change in DC power supply leads to variation in the gate and drain source voltages. These effects can be considered as when a cascade of two nonlinearities are

connected and hence, can demonstrate the existence of memory effects in the RFPA [64].

Memory effects of power amplifiers result in additional distortions of the output signal even if operating in a linear model. These distortions can be reduced by implementing a sub-circuit compensating for memory effects. There are several methods aimed at measuring and quantifying memory effects. The main techniques which provide information about the dependence of memory-related distortions on power level and modulation frequency can be classified into the following three categories:

- A single tone test with analysis of the gain and phase dependence on frequency and power level.
- A two-tone test with analysis of the IM3 dependence on tone spacing and power level.
- A digitally-modulated signal test with analysis of the distorted constellation diagram in a linear model.

In summary, memory effects can be considered as the dependency of the RFPA on past events. Carrier frequency, envelope frequency and self-heating of the RFPA, play major roles in causing the memory effects. Some memory effects exhibit themselves by producing asymmetric IMD components. This asymmetry could be due to a delay between amplitude and phase modulation of PA bias voltage due to the bias network impedance at envelope frequency or the fact that the AM and PM modulation do not happen in synchronism [64].

2.6.4 One Tone Test

The first method used to quantify memory effects in power amplifiers is a single tone test using a power and frequency sweep. The main idea is excitation of a PA with RF carrier input signal having the frequency swept over the whole operation bandwidth and the power level swept over the whole operating power range. The measured characteristics include the dependence of AM-AM and AM-PM curves on the input signal's frequency and power. Alternatively, variations of the PA gain and phase versus input signal's frequency and power are measured and analysed [33].

The main advantages of the single-tone analysis are its simplicity and convenience of processing the measured results which can be directly used for calculating the pre-compensation circuit's parameters. As memory-compensating techniques are often based on constructing the inverse frequency-dependent gain and phase characteristics, the single-tone analysis provides the required data. However, the accuracy of memory effects quantification by this method is limited because the frequency-dependent distortions of AM-AM and AM-PM characteristics are very small comparing to the fundamental signal. This makes the measurement of memory effects practically difficult by a single-tone test. Another drawback of this method is its inability to analyse intermodulation distortions related to memory effects. This can be accomplished by a two-tone analysis [33, 60].

2.6.5 Two Tone Test

The second method used to quantify memory effects in power amplifiers is a two-tone test with variable tone-spacing and input power level. A RFPA is excited with

two RF carriers of equal magnitudes. Similarly to the previously described technique, the power of the input tones is swept in order to cover the whole dynamic range of the RFPA and the difference between the tone frequencies is swept over the whole RFPA operating bandwidth. Using this method, the dependence of the magnitude and phase of higher and lower third-order intermodulation products IM3-higher and IM3-lower on frequency and power are measured. To consider 12 dB gain and the 1 dB compression point at 25 dBm output power amplifier, for example is varying in the range of P_{OUT} = 0…15 dBm in order to quantify only memory effects but not the distortion caused by the RFPA transfer characteristic nonlinearity.

The ADS simulation test-bed is configured similar to the single-tone test. The unmodulated RF signals are placed around the centre frequency with the tone spacing varying in the lower frequency range such as 10, 20 kHz,…30, 40 MHz, etc. The IM3 magnitude and phase fluctuations caused by memory effects can be observed in different plots versus tone spacing and output power level of the considered PA. In a memoryless system, the IM3 magnitude is proportional to the third power of the input signal magnitude and does not vary with frequency [65].

The main advantages of the two-tone analysis are its ability to measure intermodulation distortions and relatively high accuracy due to the fact that memory effects cause significant variations in the IM3 magnitude and phase which can be easily measured. However, the method does not directly provide the AM-AM and AM-PM characteristics of the RFPA and hence is not very useful in calculating or optimizing parameters of the memory pre-compensation system. Consequently, it is often convenient to use both of the described methods [65].

2.7 Frequency-Dependent Transfer Function for Power Amplifier Device

A simple two-tone test signal can be used in the power amplifier device to estimate the transfer functions of amplitude and phase modulations on the envelope frequency. In general, a modern transmitter system with power amplifier nonlinearities, an OFDM system and digital PD are to be implemented at baseband frequency. In the front end of the transmitter, a discrete-time complex baseband power amplifier model needs to be developed.

The Figure 2.16 below has illustrated a modern RF transmitter and a power amplifier baseband equivalent model. The digital to analogue converter (DAC) receives a baseband modulated signal which is fed to up-converter before transmitting to the channel. The power amplifier at baseband is represented by the discrete-time signal $y(n)$ in Figure 2.16 (b) as an oversampled form of the continuous-time signal $x(t)$ [66] shown in Figure 2.16 (a). Let the input band pass signal towards the power amplifier be expressed as:

$$y(t) = \mathrm{Re}\left\{w(t)e^{j\omega t}\right\} = z(t)\cos\left(\omega_c t + \vartheta(t)\right) \tag{2.52}$$

Where $w(t)$ represents the complex envelope signal to the power amplifier, $w_c t$ is the carrier centre frequency, $z(t)$ and $\vartheta(t)$ are the respective time-varying amplitude and phase of the complex signal $y(t)$.

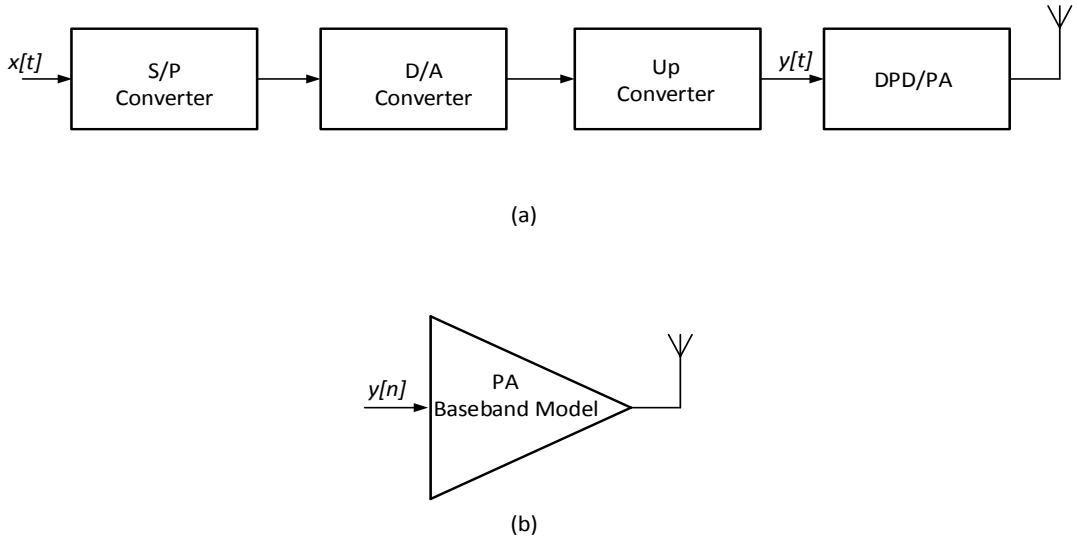

Figure 2.16: (a) RF transmitter and (b) baseband equivalent model.

Using polynomials, the equivalent baseband power amplifier model for a band pass memoryless nonlinearity can be defined by as:

$$r(t) = \mathrm{Re}\left\{ f(t) e^{j\omega t} \right\} \tag{2.53}$$

Where

$$f(t) = \sum_{k=1}^{n} b_{2k-1} |w(t)|^{2(k-1)} w(t) \tag{2.54}$$

The b_{2k-1} are complex coefficients. Let equation (2.52) be substituted in (2.54) to produce an odd-order complex power series which can be expressed as:

$$F(z(t)) = \sum_{k=1}^{n} b_{2k-1} z(t)^{2k-1} \tag{2.55}$$

Again,

$$r(t) = |F(z(t))| \cos(\omega t + \vartheta(t) + \angle F(z(t))) \tag{2.56}$$

Where $|F(z(t))|$ and $\angle F(z(t))$ represent the amplitude (AM-AM) and phase (AM-PM) modulations distortion respectively. The complex envelope signal $f(t)$ is applied in performing a two-tone test. In the test, $|F(z(t))|$ and $\angle F(z(t))$ of the power amplifier are achieved. These are the transfer functions of the power amplifier, linear or nonlinear system. The two single tone signals can be written as:

$$v_i(t) = (C/2)[\cos((\omega - \omega_n)t + \varphi(t)) + \cos((\omega + \omega_n)t + \varphi(t))] \quad (2.57)$$

Where $C/2$, φ and ω_n are the magnitudes, phase and tone spacing of the single tone signal [67, 68]. The signal can be summarized as:

$$v_i(t) = C\cos(\omega_n t)\cos(\omega_c t + \varphi(t)) \quad (2.58)$$

Hence, in the input signal envelope, the amplitude of the signal $z(t)$ is the complex signal $C\cos(w_n t)$. Thus, the output complex envelope signal $f(t)$ is expressed as:

$$f(t) = \sum_{k=1}^{n} b_{2k-1} C^{2k-1} \cos^{2k-1}(\omega_n t) e^{j\varphi(t)} \quad (2.59)$$

$$f(t) = \sum_{k=1}^{n} l_{2k-1} \cos((2k-1)\omega_n t) e^{j\varphi(t)} \quad (2.60)$$

And

$$l_{2k-1} = \sum_{i=k}^{n} \frac{1}{4^{i-1}} \binom{2i-1}{i-k} b_{2i-1} C^{2i-1} \quad (2.61)$$

The power amplifier transfer functions shown in (2.60) proves the RFPA dependency on two-tone signals spacing (w_n). Two-tone measurements can be conducted for the input amplitude and different tone spacing to derive the

coefficient (b_{2k-1}). Thus, the frequency-dependent complex power series with memory effects are expressed as:

$$f(z(t),\omega_n) = b_1(\omega_m)z(t) + b_3(\omega_n)z(t)^3 + ... + b_{2n-1}(\omega_n)z(t)^{2n-1} \quad (2.62)$$

$$f(z(t),\omega_n) = \sum_{k=1}^{k} b_{2k-1}(\omega_n)z(t)^{2k-1} \quad (2.63)$$

The power amplifier output signal with memory effects can be expressed as:

$$r(t) = \left| f(z(t),\omega_n) \right| \cos(\omega t + \vartheta(t) + \angle f(z(t),\omega_n)) \quad (2.64)$$

2.8 Summarized Conclusion

This chapter has illustrated in details the classes of RF power amplifier based on a bias network to amplifier based on network configuration. Class A, B and AB Amplifiers are well-thought-out to be linear devices and are used in various applications such as GSM, EDGE, WCDMA, AM broadcast, etc. Class C, D, E and F amplifiers are highly efficient with zero linearity and are configured based on switching network. Characterization of RF power amplifier nonlinearities has been discussed.

CHAPTER 3

Orthogonal Frequency Division Multiplexing and Beyond

3.1 Introduction

Orthogonal frequency division multiplexing (OFDM) is a special form of frequency division multiplexing (FDM) with better-qualities of sub-channels orthogonality. It is a technique that simply combines modulation and multiple access to split a wideband channel into narrowband channels. This offers an opportunity to a user in sharing channel resources with other users through the ability of the technique to multiplex a large amount of signal and enhance throughput in the system. It is an efficient multicarrier mapping system that is able to implement a high data rate to meet the ultimate demand for massive growth and the emergence of future technologies in the mobile communication industry.

However, for this reason, several wireless communication systems such as Long Term Evolution (LTE) [69-71], Long Term Evolution Advanced (LTE-A) [69, 70], World Interoperability for Microwave Access (Wi-MAX) [70, 72], Wireless Fidelity (Wi-Fi) [73-75], Wireless-LAN and beyond [76], Digital Audio Broadcast (DAB) [77], Digital Video Broadcast (DVB) [78], Third Generation (3G) [79, 80], Fourth Generation (4G) [80], Fifth Generation (5G) [71, 81], Cognitive Radio Networks (CRNs) [82, 83], Spatial Modulation [84] and other future technologies adopt OFDM system.

One of the significant motives for using the OFDM technique in the transceiver device is to improve system robustness and transmission speed. The robust system mitigates narrowband channel interference and frequency selective channel interference. The vulnerability of narrowband carrier is that a weak

interference in the channel can result to complete system failure. The multicarrier multiplexing system resists the effect of interference which affects only a few subcarriers. However, this means the multicarrier system will not experience complete link failure due to interference. The effect of interference has an impact only on a certain portion of the subcarriers. The OFDM provides reliability and spectral efficiency, protect systems against inter carrier interference (ICI) and inter-symbol interference (ISI). In the OFDM system, inter symbol interference increases when delay spread (τ_d) in the channel is larger than the symbol duration (T_s).

The larger the channel delay spread, the severe the inter symbol interference. However, at the same time, the longer the symbol duration over the channel delay spread, the freer inter-symbol interference channel is projected. Mobile communication networks such as LTE, LTE-Advanced and Wi-MAX are multipath systems. These systems are designed with the long-range capability to transmit multiple signals in line of sight and non-line of sight. Due to multipath fading of the signal, the delay spread (τ_d) becomes prominent. Hence, most of these mobile communication networks adopted OFDM technique because of its resilience against ICI and ISI [85-91].

3.2 Philosophy of OFDM Signalling and Current State-of-the-Art

To transmit OFDM signals, orthogonality of the carriers must be kept in place and the system must be interference free. OFDM orthogonality means signals are mutually kept free from each other and are transmitted accurately in a common channel without interference. However, the relationship between the carriers must be carefully managed and signals are produced in digital form rather than

analogue. Analogue makes it a complex system and difficult to process signal due to a large number of local oscillators that slow down the system. Therefore, OFDM signals are generally conveyed in digital form. Figure 3.1 has presented a typical OFDM transceiver system. In the baseband of the transceiver system, the OFDM signals are randomly generated in the frequency domain. The signals are mapped based on the mapping scheme such as QPSK, 16-QAM, 64-QAM, 256-QAM used in the modulation process.

The OFDM signals are transformed from serial-to-parallel (S/P) and using inverse fast Fourier transform process (IFFT) to modulate the signals in the time domain. At the receiver, fast Fourier transform process (FFT) is used to demodulate and recover the OFDM transmitted signals. The cyclic prefix is used as a copy of the last portion of the OFDM symbol before the parallel-to-serial transformation as a copy of the last slot of the OFDM symbol to prevent the signals from ISI. ISI occurs due to multipath fading, caused by time diffusion of the channel.

However, up to 25% of the cyclic prefix symbol length, being one-quarter (1/4) of the FFT size is required. The IFFT complex time-domain signal, having a cyclic prefix added is now transferred to a digital-to-analogue converter where the real and imaginary symbols of the OFDM are up-converted. AT the carrier frequency channel, in-phase and quadrature (I and Q) signals are produced to band-pass level. These real and imaginary complex signal are transmitted to the RF front-end of the OFDM channel through possibly a digital predistorter and a power amplifier system [85, 92-94].

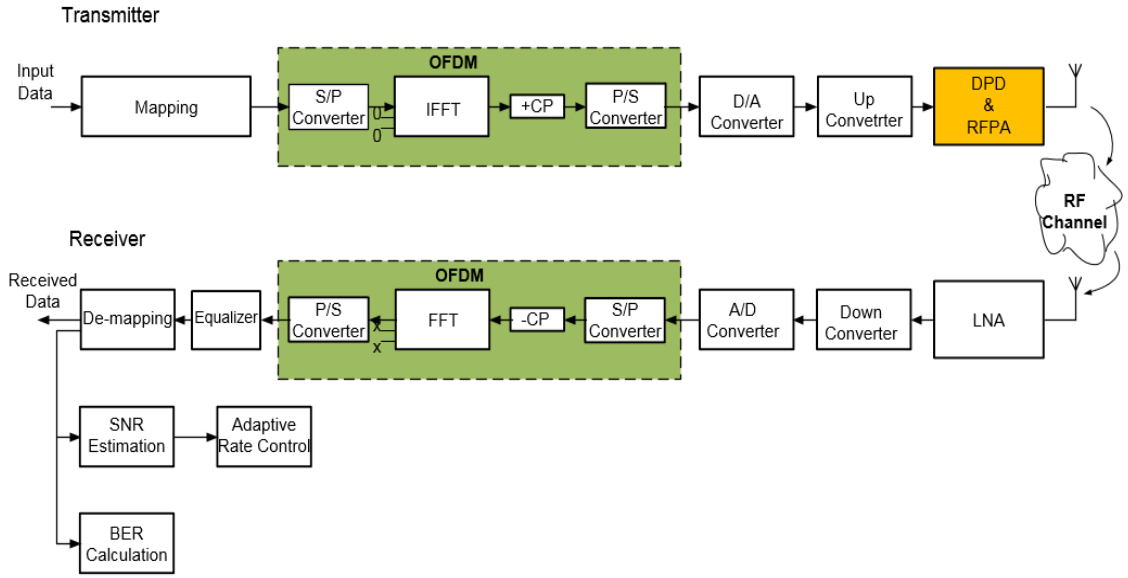

Figure 3.1: Advanced level architecture of an LTE-OFDM.

The OFDM system in Figure 3.1 illustrates the components that make up the transmitter and its receiver. Each component is explained vividly and it contributes toward the system as follows:

3.2.1 Modulation of Subcarrier Data

Mapping the subcarrier data means that the input serial data stream in the form of binary are plotted into amplitude and phase using any of the modulation techniques. The amplitude and phase are the complex vectors represented by in-phase (I) and quadrature (Q) of the modulation technique [92]. The constellation points depend on the number of bits from the modulation technique that will be mapped. If the data is transmitted in QPSK format, each symbol of the data is then mapped unto each point of the constellation represented in [90] as:

$$M_{bits} = \log_2(4) = 2\,bits \tag{3.1}$$

However, for higher modulation format such as 16-QAM is applied, the 4 x 4 bits are mapped unto the constellation base angle as represented in equation (3.2) as:

$$M_{bits} = \log_2(16) = 4 bits \quad (3.2)$$

This also applies to more sophisticated mapping schemes such as 64-QAM, 256-QAM etc. Thus, these schemes are in the form of very high mapping order, which is more complex and requires more transmit power in the process [86, 90, 95].

3.2.2 Demodulation of Subcarrier Data

In the case of de-mapping the subcarrier data back to the binary, the amplitude and phase of the signal experience random variation due to different reasons which includes time delay variation due to multipath effect, Doppler effect due to the movement of the receiver and additive white Gaussian noise in the channel. These and other variations have become main obstacles in the propagation channel, causing severe weakness to the received signal which can be mitigated by using receive channel equalization scheme to approximate the original signal vector at each constellation point which is transmitted to the propagation channel. There are other estimation schemes that can be applied for a reliable propagation channel and avoid severe channel propagation obstacles in wireless mobile communication systems [86, 90, 95].

3.2.3 Serial to Parallel Conversion

Serial to parallel conversion is done after mapping the input serial data stream. The input serial data stream is converted from a serial format into a parallel format. The parallel format consists of a number of subcarriers which each

subcarrier is then transmitted in parallel with assigned data information. The essence of transmitting the data stream in parallel format is to prevent the effect of ISI invading the data stream which results in distortion in the transmission process. Consequently, in the OFDM system, distortion in the channel has an effect on only a few subcarriers. Whereas, the data streams in other subcarriers will not experience any type of fading or distortion during the transmission. Therefore, it is easy to equalise the OFDM system for occupying slight ration of the bandwidth time slot than the FDM systems transmitting the whole serial data stream in a large portion of the bandwidth. As such, if the FDM carrier is infected with ISI, the whole information in the carrier is lost [90, 96].

3.2.4 Zero Padding

Zero paddings can be used as a guard band to reduce interference between symbols. It can be used in the middle of the symbol to overcome the DC offset in receivers. It can also be used to improve the power amplifier power ratio of the OFDM signal. OFDM system uses zero paddings in the frequency domain to avoid adjacent channel interference. Zero paddings can be used either in frequency or time domain, depending on the system requirements. It can transform the IFFT/FFT to a larger size. For instance, if the sampling frequency is given as 2048 kHz and the guards are 1 kHz apart, then 2048 point FFT must be implemented [85, 90]. It supports OFDM symbols against interfering with other active systems through the guard bands. Filter interpolation is used with the guard band after digital to analogue conversion and also implemented. This can be accomplished by modulating the subcarriers at the lower and upper side of the passband to zero. This provides the guard band against the adjacent system and simplifies the analogue anti-alias and abolish addition of more filters [97].

3.2.5 IFFT/FFT

After mapping the data stream at the subcarrier modulation point as shown in figure 3.1, each symbol in the subcarrier will be set to an amplitude and phase modulation responses according to the shown data. The OFDM system uses zero paddings to set the unused subcarriers to zero in the frequency domain. The signal is then transmitted in the time domain using IFFT. This implies that the Inverse-FFT converts the subcarrier data in the frequency domain to a corresponding discrete sample in the time domain. Hence, the inverse-FFT only generate time-domain discrete signal based on the modulation scheme used and a number of FFT points at the receiver side. This means that inverse-FFT shares the nominal bandwidth into several parallel channels of FFT points. In the same vein, the FFT at the receiver side is used to demodulate the discrete samples in the time domain to subcarrier symbols in the frequency domain. The unused subcarriers are set to null amplitude for frequency guard band before the FDE equalization [86, 98].

3.2.6 Cyclic Prefix

Wireless communication applications are researching for answers against time dispersion effect caused by the multipath effect. The multipath effect is as a result of non-line-of-sight transmission where the transmission signal reflects on objects in a multipath environment, such as high buildings, mountains, walls, etc. These signals are received at different times due to different transmission paths and distances. These cause channel delay in the propagation environment, spread borders of the symbol and causing energy outflows between the symbols. The cyclic prefix is used in preventing OFDM data stream against ISI. To achieve cyclic prefix in an OFDM system, an original copy of the data length is copied to

the front of the OFDM symbol. To solve the effect of inter-symbol interference, the OFDM channel maximum delay spread must be less or equivalent to the length of the cyclic prefix [97, 99]. The cyclic prefix inclusion in the OFDM symbol affects the linear time-invariant between the symbol and the channel impulse response, which is however transformed to a cyclic convolution [99]. Figure 3.2 shows the inclusion of cyclic prefix in the symbol.

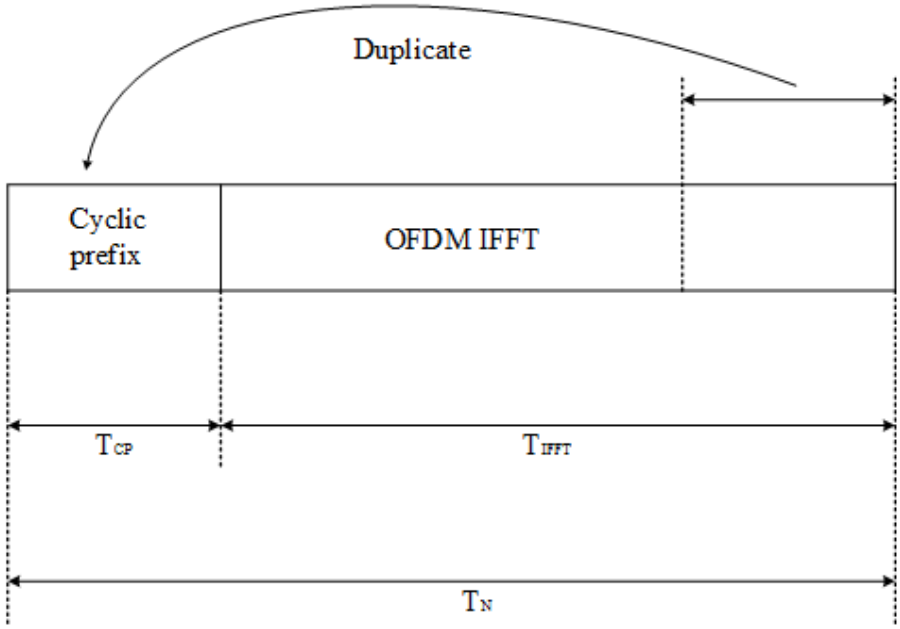

Figure 3.2: Addition of cyclic prefix to an OFDM signal.

The new length of OFDM symbol after adding cyclic prefix is represented as $T_N = T_{CP} + T_{IFFT}$, where T_N is the total length of OFDM symbol time, T_{CP} is the length of guard interval in sample time, T_{IFFT} is the useful data duration of IFFT for OFDM signal. Cyclic prefix protects the transmitted OFDM symbol against inter-symbol interference. OFDM data symbols travel on propagation paths are received at different times. The multipath delay spread effect caused by an obstacle in the propagation environment influences some of the OFDM symbols to arrive later than others. This effect, however, results in ISI. The cyclic prefix keeps the

symbol clean to arrive at the receiver without changes by adding T_{CP} to the transmitted signal [99].

3.2.7 Spectral Efficiency

Spectral efficiency is another name for bandwidth efficiency or spectrum efficiency. It refers to the amount of information that is able to be delivered per a given bandwidth in a particular communication system. It measures the information symbol in bits/s/Hz. Spectral efficiency determines the performance of a radio communication system. The higher the spectral efficiency, the excellent quality of service can be achieved for the subcarrier system. One of the ways spectral efficiency can decline in the OFDM system is by the used of cyclic prefix [100, 101]. The cyclic prefix is added to each OFDM symbol in the subcarrier for accurate inter-symbol interference reduction.

Like discussed previously, it was stated that for the cyclic prefix to be active in eliminating the inter-symbol interference, the cyclic prefix will have the same length or more than the maximum delay spread of the OFDM channel. However, the spectral efficiency in the OFDM system is higher than in the FDM system. If m is the number of OFDM carriers, while g is added as a cyclic prefix, then the spectral efficiency can be summarised as $\frac{m}{m+g}$. For a given OFDM that is band-limited, bandwidth (BW) is frequency spacing between the upper and lower channel index written as:

$$BW = \pm \frac{N_i}{2} \Delta f = \frac{N_i}{2} \Delta f - \left[-\frac{N_i}{2} \Delta f \right] = N_i \Delta f \tag{3.3}$$

Where $\pm N_i/2$ stands for the upper and lower bound of the channel index, while Δf is the frequency spacing in the OFDM channel. The frequency spacing (Δf) can be rewritten as $1/T_{IFFT}$, where T_{IFFT} stands for the useful duration of OFDM symbol [100, 101]. In this case, the spectral efficiency in relation to bits rate per given bandwidth can be expanded in this form as:

$$\eta = \frac{R_b}{BW} = \frac{R_b}{N_i \, \Delta f} = \frac{R_b}{N_i\left(\frac{1}{T_{IFFT}}\right)} = \frac{R_b \, T_{IFFT}}{N_i} \tag{3.4}$$

Where $N=R_bT_{IFFT}$ and R_b is the data bit rate in bits/s. Assuming that the OFDM system adopts a 16-QAM mapping technique to modulate the overall number of bits for N sub-channels are presented in [100] as:

$$N = N_i \log_2(m) \tag{3.5}$$

Hence, a total number of sub-carriers in the OFDM symbol (N_i) can be written as:

$$N_i = \frac{N}{\log_2(m)} = \frac{R_b T_{IFFT}}{\log_2(m)} \tag{3.6}$$

Substituting equation (3.6) into (3.4) can re-illustrate the spectral efficiency to be written as:

$$\eta = \frac{R_b T_{IFFT}}{1} \frac{1}{\left[\frac{R_b T_{IFFT}}{\log_2(m)}\right]} = \left(\frac{R_b T_{IFFT}}{R_b T_{IFFT}}\right) \log_2(m) = \log_2(m) \tag{3.7}$$

Adding cyclic prefix (T_{cp}) to the OFDM symbol guarantees prevention against ISI and to lengthen the size of the OFDM symbol shown in Figure 3.1 which is expressed as:

$$T_N = T_{CP} + T_{IFFT} \tag{3.8}$$

Where T_N is the overall OFDM symbol time, with an added cyclic prefix, while T_{CP} is cyclic prefix which is assumed to be slower than the poorest delay spread. To express spectral efficiency in terms of Δf and T_{IFFT}, we can recall equation (3.4) to give:

$$\eta = \frac{R_b}{N_i \Delta f} = \frac{R_b}{\left(\frac{N}{\log_2(m)}\right)\Delta f} = \frac{R_b}{\left(\frac{R_b T_{IFFT}}{\log_2(m)}\right)\Delta f} = \frac{\log_2(m)}{T_{IFFT}\ \Delta f} \tag{3.9}$$

By adding a cyclic prefix, the overall OFDM symbol shown in equation (3.8), T_N can be achieved when substituting T_{IFFT} in equation (3.9) is expressed as:

$$\eta = \frac{\log_2(m)}{T_N \Delta f} = \frac{\log_2(m)}{(T_{IFFT} + T_{CP})\Delta f} = \frac{Log_2(M)}{(T_{IFFT} + T_{CP})\left(\frac{1}{T_{IFFT}}\right)} = \frac{\log_2(m)}{1 + \left(\frac{T_{CP}}{T_{IFFT}}\right)} \tag{3.10}$$

Equation (3.10) illustrates the spectral efficiency of the overall OFDM symbol time when a cyclic prefix is added. However, including the prefix in the OFDM symbol to overcome inter-symbol interference has at the same time reduced the spectral efficiency. It is obvious that adopting a mapping scheme for the OFDM system depends on the size of the cyclic prefix. Application of more complex mapping scheme like the 16-QAM, 64-QAM, 256-QAM, results to the trade-off between the spectral efficiency and channel robustness against delay spread. The higher

the mapping scheme the higher the spectral efficiency. The bit-error-rate performance analysis will be poor and there will be a reduction in transmit power [101].

3.3 Orthogonality of Multicarrier in OFDM System

OFDM systems are spectrally efficient such that the signals are inherently orthogonal. Signals are mutually independent when they are orthogonal. The orthogonal system allows perfect multi-data transmission over a common carrier, without interference. Absence of orthogonality in a system causes distortion between the information data which can result in loss of communication [102, 103].

OFDM systems achieve orthogonality when a set of functions synchronize with each other such that the s^{th} basic function of the transmitter ($\psi_s(t)$) match with the r^{th} function of the receiver ($\psi_r(t)$). Hence, the set of functional carriers are orthogonal to each other if they equal the conditions in equation (3.11) which is expressed as:

$$\int_x^y \psi_s(t)\psi_r(t)\,dt = \begin{cases} (y-x) & for\ s=r \\ \\ 0 & for\ s\neq r\ \ and\ \ (y-x) = N\Delta t \end{cases} \tag{3.11}$$

The first case expresses that the two functions are orthogonal by satisfying the condition $\int_x^y \psi_s(t)\psi_r(t)\,dt = 0$. And if the two sets of functions lose their orthogonality such that the s^{th} basic functions of the transmitter ($\psi_s(t)$) mismatch the r^{th} functions of the receiver ($\psi_r(t)$), distortion occurs in the channel and results

to inter-channel interference. The OFDM set of transmitted carriers are defined as:

$$\psi_s(t) = e^{i2\pi\left(f_o + \frac{n}{N\Delta t}\right)t} \tag{3.12}$$

Where n = 0, 1, 2, …, N-1. While the OFDM received carriers are defined as:

$$\psi_r(t) = e^{i2\pi\left(f_o + \frac{n}{N\Delta t}\right)t} \tag{3.13}$$

Hence, the two sets of carriers are orthogonal to each other by setting condition expressed as:

$$\int_x^y \psi_s(t)\psi_r(t)\,dt = \int_x^y e^{i2\pi(s-r)\frac{n}{N\Delta t}dt} \qquad for\ n = s\ or\ r \tag{3.14}$$

There is a correlation between a transmitted or received a set of carriers. If s^{th} function matches with r^{th} function, then the two are orthogonal as expanded in (3.15) and (3.16):

$$\int_x^y \psi_s(t)\psi_r(t)\,dt = \frac{e^{i2\pi(s-r)\frac{y}{N\Delta t}} - e^{i2\pi(s-r)\frac{x}{N\Delta t}}}{i2\pi(s-r)/N\Delta t} \tag{3.15}$$

$$= \frac{e^{i2\pi(s-r)\frac{y}{N\Delta t}}\left(1 - e^{i2\pi(s-r)\frac{x-y}{N\Delta t}}\right)}{i2\pi(s-r)/N\Delta t} \tag{3.16}$$

Hence,

$$\int_x^y \psi_s(t)\psi_r(t)\,dt = 0 \qquad for\ s = r\ and\ (y-x) = N\Delta t \tag{3.17}$$

Finally, this has shown that every two carriers are orthogonal to each other until they prove otherwise. Inter-channel interference is no longer existing when two carriers are in the orthogonal state [103]. Hence, this can be used in OFDM signal mathematical expression.

3.4 Mathematical Description of an OFDM System

This part of the work presents a mathematical definition of the OFDM system. It is imperative to see how the OFDM signal can be transmitted and received in a transmission system. This allows us to understand the mathematical presentation, the operational function of each individual system and the effects of imperfections in the communication channel. The OFDM signal is transmitted in the frequency domain with a vast number of sub-carriers, closely spaced to one another. Fast Fourier Transform (FFT) is used as a modern digital communication and signal processing technique to substitute a large number of space and energy consuming components in the transceiver system.

The OFDM is a multicarrier structure which each narrowband carrier is modulated side-by-side in parallel with other narrowband carriers [2, 86, 90]. From the above expression which stated that $\{\psi_p(t)\}$ is the OFDM orthogonal signal set. An OFDM signal based on this arrangement can be expressed as:

$$y(t) = \sum_{k=-\infty}^{\infty} \sum_{p=0}^{N-1} x_{k,p} \psi_p(t - KT) \tag{3.18}$$

$\psi_p(t) = e^{i2\pi fpt}$ is also expressed as the sub-carrier in the equivalent baseband signal of the OFDM system. $f_p = f_0 + \frac{p}{T}$, f_p is the P^{th} sub-carrier frequency, equally spaced by $\Delta f = \frac{1}{T}$, $p = 1, 2, 3, ..., N-1$, $0 \le t \le T$. T is the OFDM symbol duration

and $x_{k,p}$ is the data transmitted on the p^{th} of the k^{th} symbol. Hence, the signal can be expanded as:

$$y(t)=\sum_{k=-\infty}^{\infty}\sum_{p=0}^{N-1}\left\{u_{k,p}\cos(2\pi f_p(t-KT))-v_{k,p}\sin(2\pi f_p(t-KT))\right\} \tag{3.19}$$

The OFDM symbol is represented as:

$$y(t)=\sum_{p=0}^{N-1}u_p\cos(2\pi f_p t)-v_p\sin(2\pi f_p t) \tag{3.20}$$

K is assumed to be *0*, while u_p is the p^{th} complex baseband symbol of the frequency domain. However, for multicarrier equivalent using Inverse Discrete Fourier Transform (IDFT) where a single carrier of the OFDM signal can be expressed as:

$$S_c(t)=Z_c(t)e^{i(2\pi f_c t+\varphi_c(t))} \tag{3.21}$$

In the OFDM signal, there is a number of N carriers, Z_c is the amplitude, while φ is the phase of the single carrier. The total OFDM complex signal can be described as:

$$S_s(t)=\frac{1}{N}\sum_{p=0}^{N-1}Z_p(t)e^{i(2\pi f_c t+\varphi_c(t))} \tag{3.22}$$

Where $f_p = f_i + p\Delta f$. $Z_p(t)$, $\varphi_p(t)$ and f_p represent the amplitude, phase and a carrier frequency of the p^{th} carrier. The OFDM complex waveform is a continuous signal. If the waveform of each component of the signal is taken into account over one period of OFDM symbol, the signal sampled at the sampling frequency $\left[\frac{1}{\Delta t}\right]$, $Z_p(t)$ and $\varphi_p(t)$ come to be Z_p and φ_p.

$$S_s(k\Delta t) = \frac{1}{N}\sum_{p=0}^{N-1} Z_p e^{i\left(2\pi(f_i + p\Delta f)k\Delta t + \varphi_p\right)} \tag{3.23}$$

Hence, the sampled signal can be described as:

$$S_s(k\Delta t) = \frac{1}{N}\sum_{p=0}^{N-1}\left(Z_p e^{i\left(2\pi(f_i k\Delta f) + \varphi_p\right)}\right)e^{i2\pi pk\Delta f\Delta t} \tag{3.24}$$

At this point, the signal has been sampled to N samples by means of sampling frequency $\left[\frac{1}{\Delta t}\right]$. It is worthy to take into account how much time is required to analyse the signal to a specific number of N samples. If we now assume $f_i = 0$, equation (3.24) can be simplified and the signal is given as:

$$S_s(k\Delta t) = \frac{1}{N}\left(Z_p e^{i\varphi_p}\right)\left(e^{i2\pi pk\Delta f\Delta t}\right) \tag{3.25}$$

If equation (3.25) is now compared with the IFFT which can be described as the following:

$$g(k\Delta t) = \frac{1}{N}\sum_{p=0}^{N-1} G(p\Delta f)e^{i2\pi pk/N} \tag{3.26}$$

The functions Z_p, e^j and φ_p in equation (3.25) are the sampled representation of the signal in the frequency domain. While $S_s(k\Delta t)$ represents the time domain signal. Hence, the time and frequency domain are the same if the condition is satisfied when:

$$\Delta f = \frac{1}{N\Delta t} \tag{3.27}$$

Where the OFDM signal consists of $S_s(k\Delta t)$ as the time domain signal, $Z_p e^{i\left(2\pi(f_i k\Delta f) + \varphi_p\right)}$ is the frequency domain signal, $N\Delta t$ is the symbol duration in each sub-channel and Δf is the spacing in each sub-channel, respectively. It has

proven that IDFT can generate an OFDM signal. Therefore, the OFDM signal can be described by a Fourier Transform.

3.5 Advantages and Disadvantages of OFDM System

Like any other technology, OFDM consists of advantages and disadvantages in wireless communication applications. These are itemised as follows:

Advantages

- Spectral efficiency is achieved through maintaining orthogonality between the subcarriers for easy symbol detection and separation at the receiver.
- The application of cyclic prefix is to prevent the unwanted signal in the channel such as inter-symbol interference, inter-carrier interference and inter-frequency interference.
- Provides more throughput.
- Solves the problem of design complexity by getting rid of oscillators and replaced with DFT.
- Interleaving and channel coding can be used in OFDM to recover a lost symbol caused by frequency selectivity of a channel.
- Simpler channel equalization due to frequency domain signal representations.
- Possible application of maximum likelihood decoding (MLD)
- Using IFFT/FFT techniques to easily and efficiently modulate/demodulate functionalities.
- OFDM has less sensitivity to sample timing offset than the FDM system.
- Immunity against impulsive parasitic noise and co-channel interference.

- Can be used for high-speed multimedia applications with the cost of service.

Disadvantages

- High peak to average power ratio due to large dynamic amplitude noise, reducing power amplifier efficiency and affecting the performance.
- OFDM is highly sensitive to carrier frequency offset and drift than FDM due to DFT leakages.
- In OFDM, the cyclic prefix is added to effect inter-symbol interference, at the same time a proportion of available bandwidth is wasted.
- Some part of transmit power is allocated to drive the cyclic prefix, such that the OFDM actual transmit power will drastically reduce.
- Addition of cyclic prefix increases the length of the normal symbol. This process increases the computational time.
- There is an increase in noise overhead.

3.6 The Effect of Nonlinear Power Amplifier Distortion and PAPR in Modulated Signal

Wireless communication systems that adapt OFDM technique suffers signal distortion by nonlinear devices such as nonlinear power amplifier. When an OFDM signal is passed through a nonlinear power amplifier device, imperfection occurs, resulting in spectral spreading and in-band noise. For an OFDM signal with sub-channels of multiple carriers, peak to average power can be as large as possible when compared with a single carrier system. The back-off position of the power amplifier is influenced by the crest factor. This, however, causes the reduction of power amplifier efficiency. There are several methods used in

reducing the OFDM signal high peak power caused by the nonlinear device [104-107]. In this work, a few of these approaches proposed in the literature are discussed as follows:

3.6.1 Active Constellation Extension

Active constellation extension is one of the PAPR reduction approaches that can be used in the OFDM system. Signal constellation is put into account based on the formation of any two or more constellation points. To extend signal constellation, minimum distance will not, in any case, be decreased. Reason for that is to avoid symbol moving more freely, except the space on the direction assign. This approach has its own advantage that the receiver decision region cannot be altered and coded side information remains not transported. This results in lossless throughput [108-111].

3.6.2 Tone Reservation

In tone reservation approach, numerous subcarriers with different orthogonality have been implemented. It is used in implementing the IEEE 802.16e standard. The subcarriers generate peak reduction signal for data transmission usage and few are kept for reduction purpose. The reserved subcarriers are used for anti-peak signals with the subcarriers orthogonal to each other exist no element of disturbance from the generated signal. The reserved tone generation signal only reduces the useful data rate without causing in-bound distortion or disturbing the data-carrying tones. Tone reservation technique experience some drawbacks. It losses spectral efficiency due to tone reservation and also reduces the BER performance due to the increase in the average energy per bit [112].

3.6.3 Clipping

Clipping is one of the simplest approaches used in high peak-to-average power ratio reduction. In this approach, peak amplitudes are simply reduced by clipping OFDM signal at the underline threshold. The signal is clipped at the output of the IFFT operation without sampling. This causes re-growth of the signal peak after interpolation. In order not to avoid re-growth, filtering is used to eliminate out-of-bound term of the signal peaks. The filters also cause distortion due to the complexity of the system. Peak window scheme can be an alternative of filtering to minimize the out-of-bound distortion using narrowband windows. Reducing the distortion increases performance in the system [113, 114].

3.7 OFDM System Modelling: Linear versus Nonlinear RFPAs and the Experimental Results

This model used an OFDM signal transmission over linear and nonlinear RF power amplifiers to determine the performance effect of each level of transmission with and without applying the amplifiers. The linear system represents the proposed balanced RF power amplifier and the nonlinear system represents class F RF power amplifier respectively. In the model, the OFDM transceiver system is furnished with functional devices and characteristics in different stages to sharpen the baseband signal. These include 128 number of OFDM subcarriers, a 25% cyclic prefix is used in the OFDM blocks to prevent inter symbol interference due to channel delay in the multipath transmission. A fast fading channel is used at 800 MHz carrier frequency with over 4×10^4 symbols at 20 kHz bandwidth per sub-carrier.

The OFDM subcarrier data was generated from the baseband and forwarded to the preferred modulation scheme where the serial data stream was mapped into binary form. The data was reshaped through the serial to parallel conversion. The IFFT was added to convert the subcarrier data from the frequency domain to corresponding discrete samples in the time domain. The data was converted back to serial after adding the prefix. The data passed through the RF power amplifier after the analogue to digital conversion. The level of signal distortion is based on the amplifier added to the OFDM system. The AWGN was added to the channel as illustrated in Figure 3.1.

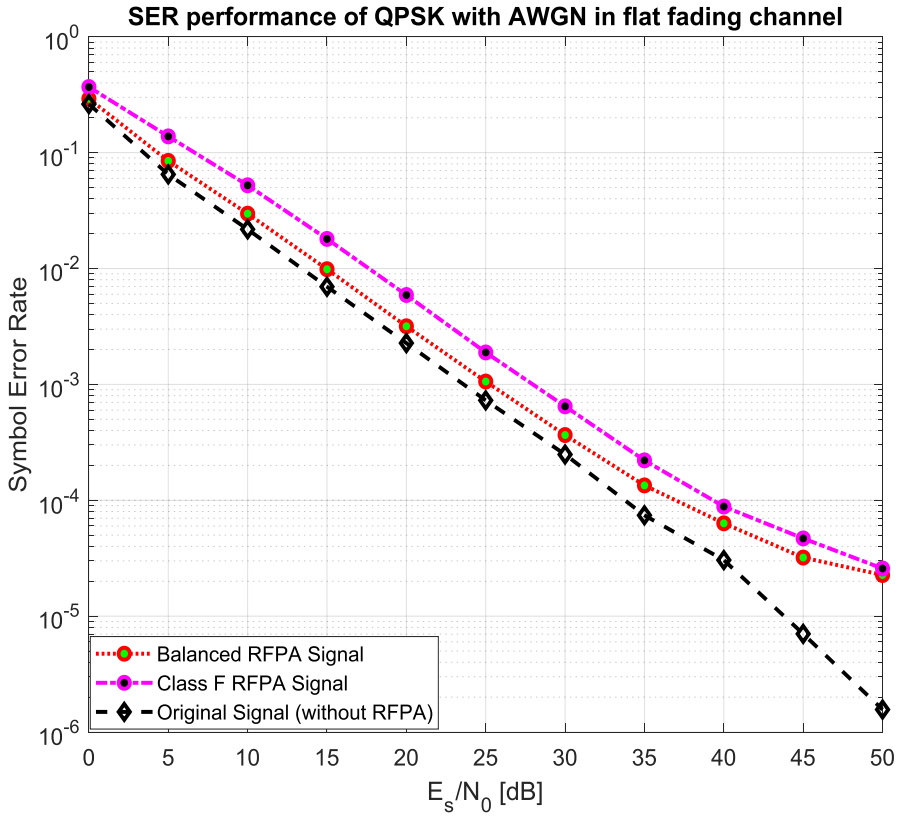

Figure 3.3: SER performance of the OFDM transceiver using QPSK.

At the OFDM receiver side, the signal was received by the low noise amplifier before down-conversion and analogue-digital signal conversion. The signal was reshaped through serial to parallel conversion, the cyclic prefix was removed, and

FFT was performed to generate frequency domain OFDM waveforms. To perform channel equalization and reshaping of the signal, parallel to serial conversion was performed. The data stream was mapped using different modulations and BER was computed for various systems of amplification.

Figure 3.3 has shown the OFDM system is simulation demonstrating the performance in terms of symbol error rate (SER) versus signal to noise ratio (SNR) in the presence of linear and nonlinear RFPA signal distortion. It can be seen that various systems for amplification play important role in SER performance in the OFDM transceiver system. Hence, in designing the OFDM system, the RF front end level of distortion must be controlled, otherwise, linearization is required to give adequate recovery at the receiver. The figure of the SER performance versus energy per symbol to noise density result has demonstrated various scenarios where the devices do not perform similarly. It can be seen that the OFDM system outperformed better than with the RF power amplifier. However, in the case of RFPAs, the linear RF power amplifier which is the proposed balanced RFPA is slightly better at the beginning in terms of SER performance. While increasing the energy per symbol to noise density, the nonlinear RF power amplifier which is the class F RFPA continued to bridge the gap and the performance of each system improves. We can presume that both amplifiers have been affected by the distortion. In this effect, a predistorter is required to linearize the nonlinear behaviour of the amplifiers.

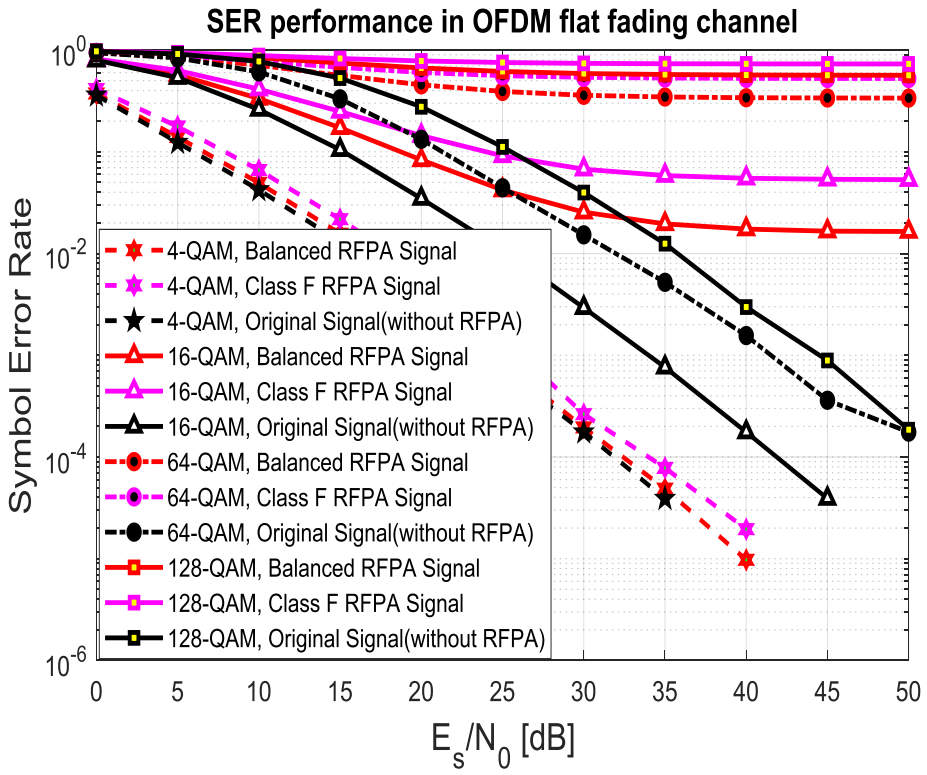

Figure 3.4: SER performance of the OFDM transceiver with QPSK, 16-QAM, 64-QAM and 128-QAM modulations.

The OFDM system is also used in simulating different M-ary modulation techniques such as QPSK, 16-QAM, 64-QAM and 128-QAM. The SER performance results of the different modulations is shown in figure 3.4. It can be noticed from the figure that the same scenario has been used which is the OFDM original signal, the balanced and the class F RFPAs simulated in without any means of distortion cancelation. It is also noticed that in the lower the modulation, the lower the SNR and the better performance. The best performance was achieved by QPSK which is the first modulation in the figure. The regular saturation level 1 was maintained for the simulation to observe the distortion signal of each device in use. Increase in the modulation reduces the strength of the signals and affect the SNR. In this case, the modulation level changes from QPSK level to a more higher-level modulation such as 16-QAM, 64-QAM and 128-QAM.

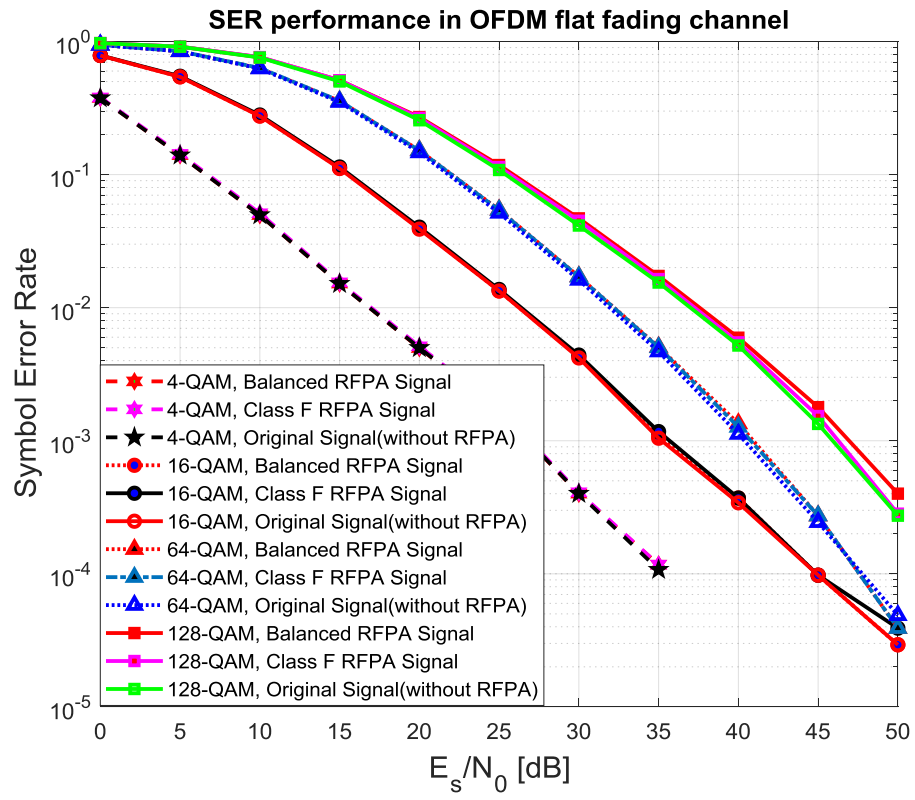
SER performance in OFDM flat fading channel
Symbol Error Rate
E_s/N_0 [dB]
4-QAM, Balanced RFPA Signal
4-QAM, Class F RFPA Signal
4-QAM, Original Signal(without RFPA)
16-QAM, Balanced RFPA Signal
16-QAM, Class F RFPA Signal
16-QAM, Original Signal(without RFPA)
64-QAM, Balanced RFPA Signal
64-QAM, Class F RFPA Signal
64-QAM, Original Signal(without RFPA)
128-QAM, Balanced RFPA Signal
128-QAM, Class F RFPA Signal
128-QAM, Original Signal(without RFPA)

(a)

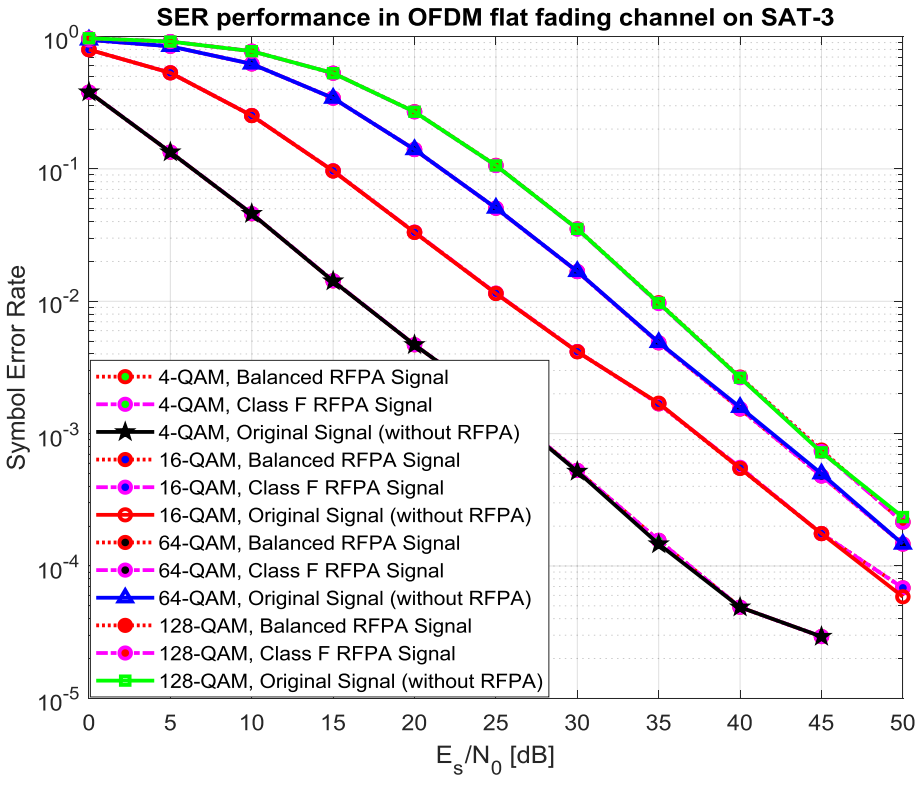
SER performance in OFDM flat fading channel on SAT-3
Symbol Error Rate
E_s/N_0 [dB]
4-QAM, Balanced RFPA Signal
4-QAM, Class F RFPA Signal
4-QAM, Original Signal (without RFPA)
16-QAM, Balanced RFPA Signal
16-QAM, Class F RFPA Signal
16-QAM, Original Signal (without RFPA)
64-QAM, Balanced RFPA Signal
64-QAM, Class F RFPA Signal
64-QAM, Original Signal (without RFPA)
128-QAM, Balanced RFPA Signal
128-QAM, Class F RFPA Signal
128-QAM, Original Signal (without RFPA)

(b)

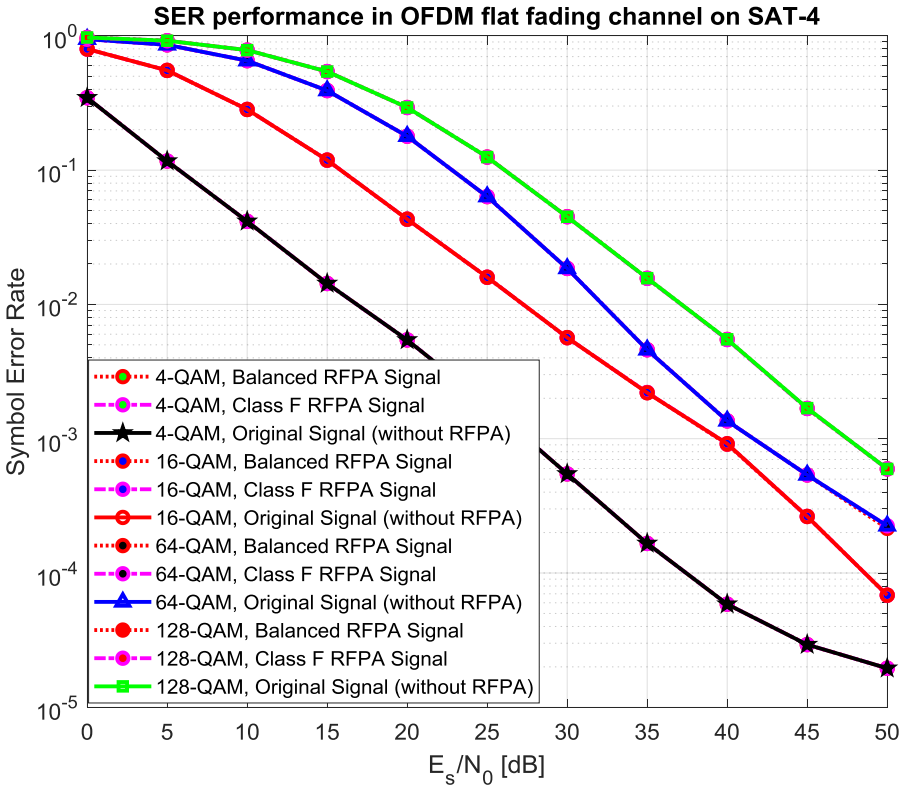

(c)

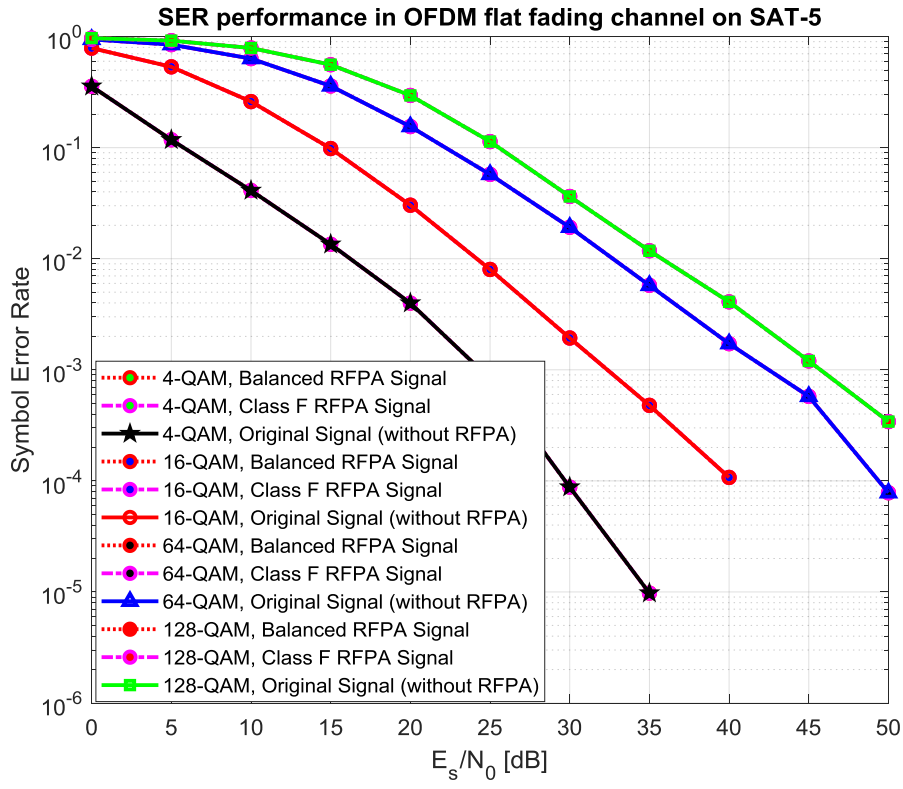

(d)

Figure 3.5: SER performance of the OFDM transceiver using QPSK, 16-QAM, 64-QAM and 128-QAM. (a) Saturation level 2. (b) Saturation level 3. (c) Saturation level 4. (d) Saturation level 5.

This work also compares the performance of different OFDM modulation techniques in terms of SER. Similarly, the OFDM system was simulated with different level of saturation to suppress the distortion of the amplifiers as shown in figure 3.5. The figure prior to this has shown the SER performance of different modulation techniques with a single saturation level. Furthermore, saturation level has been increased to 2, 3, 4 and 5 dBm as illustrated in Figure 3.5 (a), (b), (c) and (d). It is clearly seen that increasing the level of saturation sharpen the signal to significant accuracy. That is to say the more saturation in the OFDM system, the more signal pass through high power amplifiers with insignificants or no distortion. In addition, this results in better SER performance which also boosts the system efficiency. Likewise, decreasing the saturation level appreciate the probability of signal amplitude distortion resulting in poor SER performance. However, the simulation was maintained using the proposed linear balanced power amplifier and the nonlinear class F power amplifier. The simulation results confirm that using saturation level 5 yield better performance when compared to a lower saturation level for all the class of devices applied.

3.8 The New OFDM Modulation Techniques and Based Waveforms

OFDM has been considered the most successive multicarrier modulation and has many advantages. However, it cannot provide all of the anticipated advantages and demanding answers. A new adaptive OFDM modulation based techniques and waveforms have been found. Although, these modulations are from OFDM family with high data rate and multicarrier capability. These are considered as the candidate modulations and waveforms for 5G. As a result of the high-performance expectation towards the 5G modulations, the features of new generation OFDM candidate modulation techniques can be complemented with

higher spectral efficiency, lower complexity, asynchronous multiplexing ability, lower out of band emissions and lower power consumption. As a potential candidate for 5G systems, these challenges must be taken into account. And to succeed in achieving the potential features in 5G modulation techniques and waveforms, the requirement to be met include throughput, coverage, latency, reliability, reduce overhead signalling, support energy efficiency, multi-service support, flexibility for the use of the wide range of frequencies and multi-service support. Hence, some of the new modulation techniques that have demonstrated an interest in 5G are chosen due to the resilience and important advantages are to be discussed in details [115, 116].

3.8.1 Frequency Quadrature Amplitude Modulation (FQAM)

The frequency quadrature amplitude modulation known as FQAM is one of the new modern modulation techniques that are main candidates for 5G applications. FQAM is considered to be a great potential candidate in-terms of improving the transmission rates for cell-edge users [117-119]. It consists of frequency shift keying (FSK) and quadrature amplitude modulation (QAM) to attain the significant advantage of reducing inter-channel interference (ICI) in the network. The amalgamation of FSK and QAM result in high power and bandwidth efficiency in FQAM modulation which also has demonstrated a significant performance in terms of gain, particularly for the cell edge users.

The idea of FQAM operation is that during each transmission period, a frequency component is activated in order to transmit the QAM symbol. The data is transported both by the active frequency component index and QAM symbol [118]. The statistical distribution of the FQAM inter-cell interference for the cell

edge user and other possible applications is likely to be non-Gaussian. The Gaussian distribution of the worst-case additive noise depends on the channel capacity. Increase in channel capacity by the FQAM technique makes the inter-cell interference non-Gaussian. The FQAM activates only small numbers of subcarriers to improve energy efficiency with low PAPR [120]. In addition, using FQAM in the downlink of OFDMA can deviate the distribution of ICI from the Gaussian distribution and produce a superior performance better than QAM [121, 122].

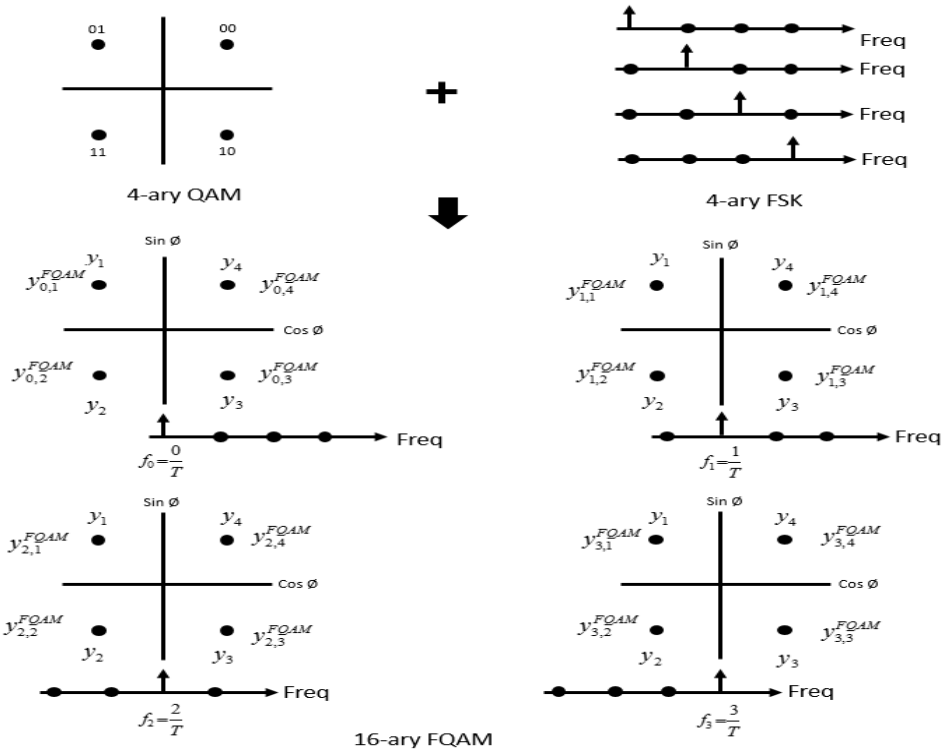

Figure 3.6: The 16-ary FQAM signal constellation that is a combination of 4-ary FSK and 4-ary QAM.

The signal constellation has shown FQAM symbols which are formed through a combination of frequency shift keying (FSK) and QAM modulation. It is well cited from [117] that the transmitted FQAM symbols as a result of M_f-ary bits and M_q-ary bits are mapped using grey mapping to form one FQAM symbol. The M_f-ary bits represents the frequency index and M_q-ary bits is the QAM index. Figure 3.6

shows the FQAM signal constellation, where the symbol carries $N = log_2 M$ information bits by choosing an active frequency tone among the FSK modulation bits and mapping the tone with an M_q-ary QAM signal constellation. Consequently, the resulting FQAM modulation order is given as $M = M_f M_q$ [117, 118, 121, 123].

The FQAM works with single and multicarrier applications such as the generalized space and frequency (GSF), Spatial Modulation (SM), generalized Orthogonal Frequency Division Multiplexing (G-OFDM) Index Modulation (IM), etc. For instance, when FQAM is used with the multi-carrier application such as OFDM, the same QAM-OFDM transceiver structure as shown in Figure 3.7 can be adopted. The figure demonstrates an FQAM-OFDM transceiver block diagram with turbo code at the baseband, FQAM modulation at the transmitter and the log-likelihood (LLR) at the receiver side respectively [117, 118, 121].

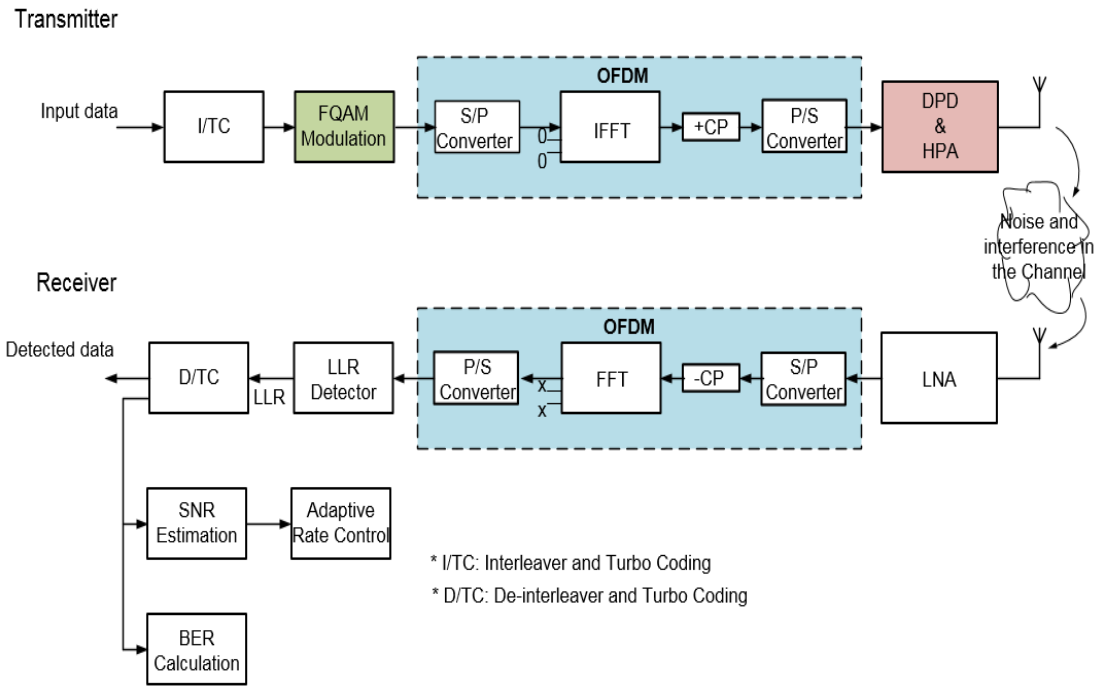

Figure 3.7: An FQAM-OFDM Advanced level structure.

The FQAM-OFDM transceiver as shown in the figure is similar to the QAM system where the features and operational process are nearly performed in the same manner. The FQAM-OFDM sequence of transmission bits are modulated as symbols and also processed with the use of IFFT. The cyclic prefix is added after IFFT to produce and transmit an OFDM symbol through the HPA to the channel. The symbols are transmitted through the fading channels between the base station and the mobile station. Noise and interference are added in AWGN of the OFDM channel. Consequently, the cyclic prefix is removed and FFT is performed at the receiver side. Instead of the QAM demodulation, a soft decoding metric called Log Likelihood is added with a subsequent turbo decoder to detect and de-interleave the receiver bits [118, 119].

In the LLR computation, the FQAM computation depends on the transmitted symbols. When the FQAM symbol is transmitted and is interfered by the base stations (BSs), it presented a complex generalised Gaussian (CGG) distribution at the edge of the cell. This creates a difference in LLR computation for the FQAM detector due to the distribution of combined ICI. While for QAM, the ICI presented a normal Gaussian distribution in the detector. This means that using FQAM increases the user speed rate located specifically at the cell-edge when compared with QAM modulation. For instance, a 3-cell structure is used as a frame error rate (FER) of 0.01, the rate at which the speed of cell-edge user improves approximately from 4-ary to 32-ary FQAM.

3.8.2 Filter Bank Multicarrier Based Modulation (FBMC)

This is a pulse shaping based modulation scheme used as one of the key candidates for the future 5G air interface. Filter bank multicarrier modulation

(FBMC) is a multicarrier transmission modulation technique with filter bank for each transmitted signal where the individual subcarrier receives efficient pulse shaping. FBMC, as it is called, is an enabling technology that can exhibit excellent spectrum shape, improves mobility and increase the spectral efficiency. The bank of filters used is band pass filters to separate the input signal to a multiple sub-carrier with each one carrying a single frequency sub-band of the baseband signal.

To meet the spectrum mask requirement, the pulse shaping filter adopted localises frequency and time traits to reduce the overhead of the guard band, needed to fit in the spectrum bandwidth. The frequency and time filter localization improves significantly the performance level as well as the structure of the system. FBMC is designed carefully to improve robustness against channel impairment. This makes it meet the 5G requirement and constraints imposed by numerous setups. The benefits of using FBMC are realized by increasing the number of prototype filters, expanding the pulse and symbol duration above *K* symbol intervals. This process is done in the time domain which results to pulse overlapped with duration KT in a specific T symbol intervals. FBMC comprises of Inverse Discrete Fourier Transform (IDFT) at the transmit side, Discrete Fourier Transform (DFT) at the receive side, synthesis and analysis poly-phase filter banks [119, 120, 124, 125].

There are numerous determining factors that sharpen FBMC modulation to be more effective in 5G applications. Several effective approaches have been proposed in the literature to achieve significant spectral efficiency. The FBMC considers alternative methods such as off-QAM, frequency spread (FS) and time-

frequency packed signalling (TFS) to reduce the frequency side lobes, reduce latency, increase robustness against channel impairment, improve robustness against timing offset, improve robustness against multipath impairment, etc. As a vibrant filtered modulation, FBMC has originally been proposed in [126], also called OFDM/OQAM in [127] and staggered modulated multi-tone (SMT) in [128]. FBMC adopted OQAM to provide optimum spectral efficiency and low access bandwidth without even using the cyclic prefix.

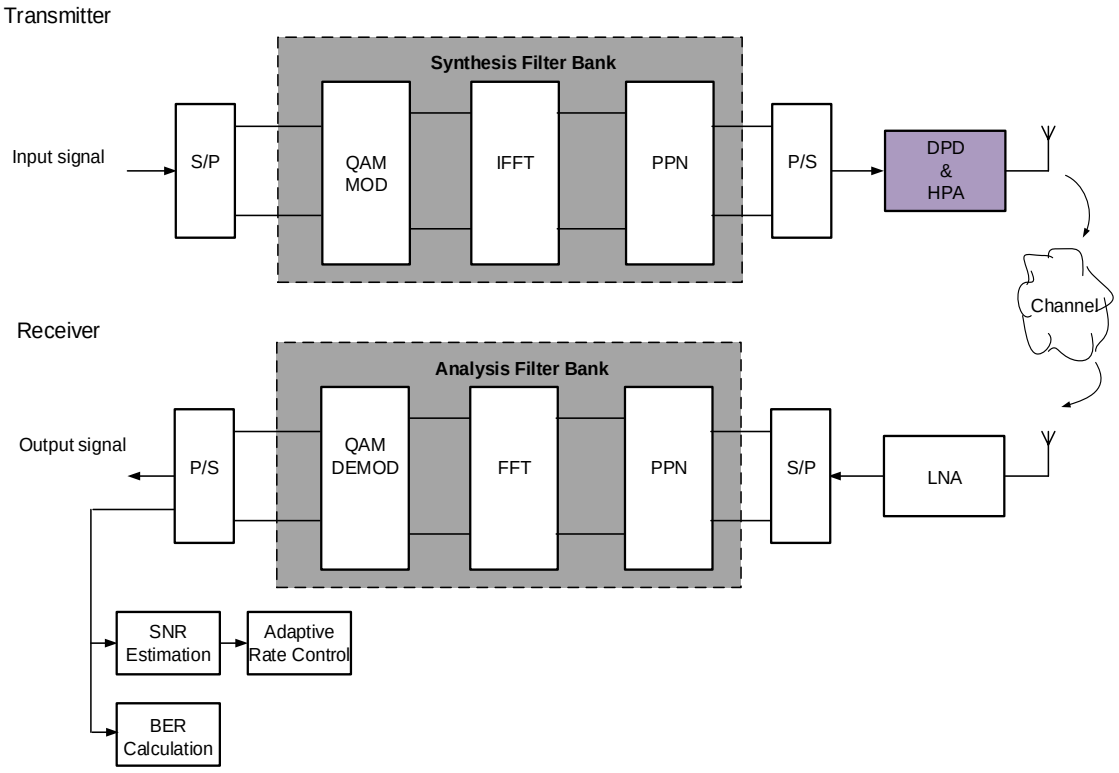

Figure 3.8: An advanced level block diagram of proposed FBMC-PPN transceiver system.

However, OFDM/OQAM is known with poor performance in high mobility situation, have burst transmission overhead, and capability constraint in all kinds of Multiple Input Multiple Output (MIMO) systems [129]. In that regard, [130] proposed QAM-FBMC approach to convey the QAM symbols for higher spectral efficiency without increasing complexity in signal processing. It is also capable of eliminating any inherent interference, implement channel estimation and easy to

adopt a massive MIMO system. It adapts different prototype filters for even and odd to uphold complex domain orthogonality [117, 118, 120, 127, 130].

Figure 3.8 has shown a block diagram of a multicarrier filter bank based modulation system (FBMC) with a few fundamental components of OFDM. The FBMC configuration is consist of synthesis filter bank (SFB) at the transmitter side and analysis filter bank (AFB) at the receiver side. The filter banks on the respective synthesis and analysis side contain an array of filters that process the input signal for the equivalent output signal.

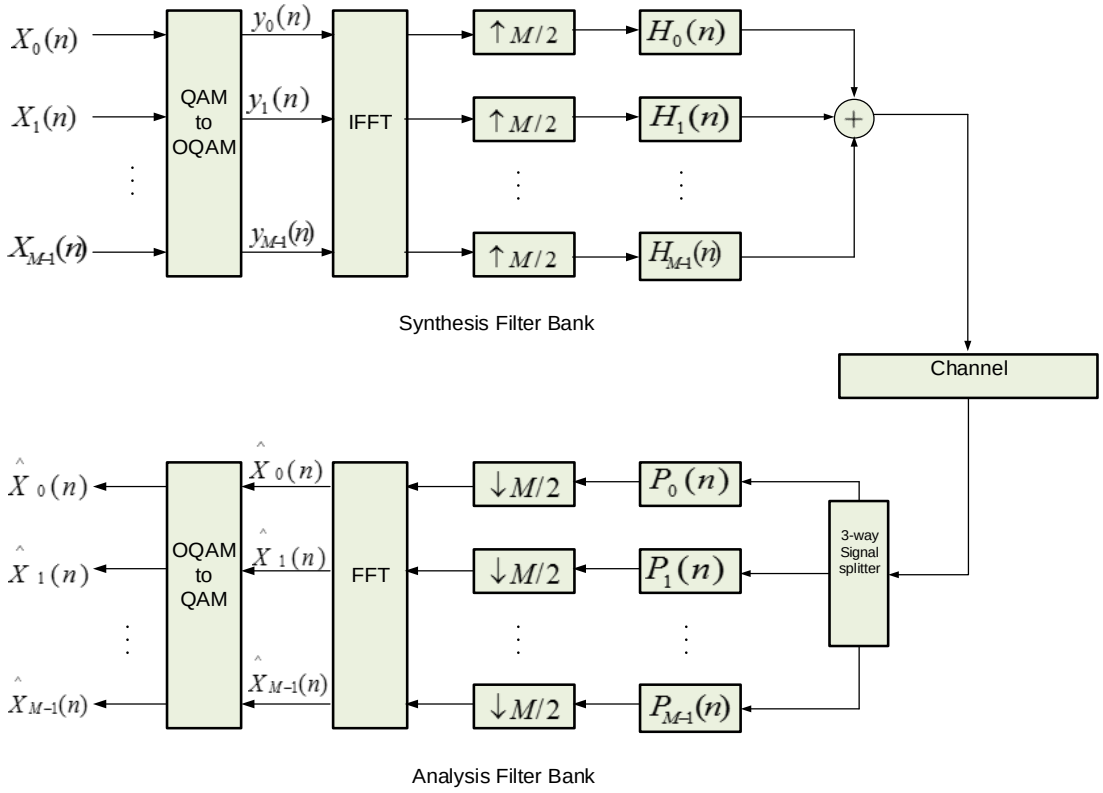

Figure 3.9: FBMC trans-multiplexing configuration diagram.

If the input of the filters is correlated together, the system is considered as an analogue type which can be measured as an analyser to the input signal based on the characteristics of each filter. At the baseband of the transmitter, an S/P block is used to convert the input signal from serial to parallel form. The signal

will pass through synthesis filter bank (SFB) and then convert again from parallel to serial form before the signal is transmitted to the channel. After reception from the channel, the signal is converted from serial to parallel form, then passed through analysis filter bank (AFB) and finally converting the signal from parallel to serial form. However, the synthesis-analysis which is called the trans-multiplexer can be explained in details by using the operating principle [124, 125].

Figure 3.9 has presented the trans-multiplexing configuration as the core of the FBMC system. The figure consists of the QAM to OQAM processing block and synthesis filter bank block in the transmitting system, while analysis filter bank and OQAM to QAM in the receiving system. The FBMC system orthogonality is needed for only adjacent sub channels, not for all the subcarriers. Hence, OQAM modulation exploits the full channel bandwidth where full capacity can be achieved. The symbols passed through complex to the real conversion process. The real and imaginary parts of a complex data symbol are transmitted separately, as the imaginary part of the data suffers delay by half period the symbol. The most significant components in this system are the synthesis and the analysis filter banks. The OQAM modulated signal will pass through the IFFT block and multiply by the FBMC filters which takes the form of an SFB at the transmitter and at the receive the signal passed through the AFB. In the multicarrier system, FBMC filters each modulated signal within the subcarrier. The prototype filter is the root for the other subcarrier filters and also used for the zero frequency carrier. The filters are considered by the overlapping factor (K) which is the number of multicarrier symbols that are overlapped in the time domain. The prototype filter order can be selected to be 3, 5 or 7 when filter order

equal to as 2×K-1 where K can be 2, 3, or 4 based on PHYDYAS project [129, 131].

Frequency spreading is useful to the current FBMC implementation. It adopts an M*K length of IFFT with symbols overlapped with a delay of M/2, where M is the number of subcarriers. The QAM-FBMC system which transmits the QAM symbols help to achieve fundamental spectral efficiency enhancement while ensuring low signal processing complexity and simplifying the compatibility with the OFDM system [131]. The signal processing for FBMC transceiver system was performed and the response plotting power spectral density to highlight the low out-of-band leakage [131].

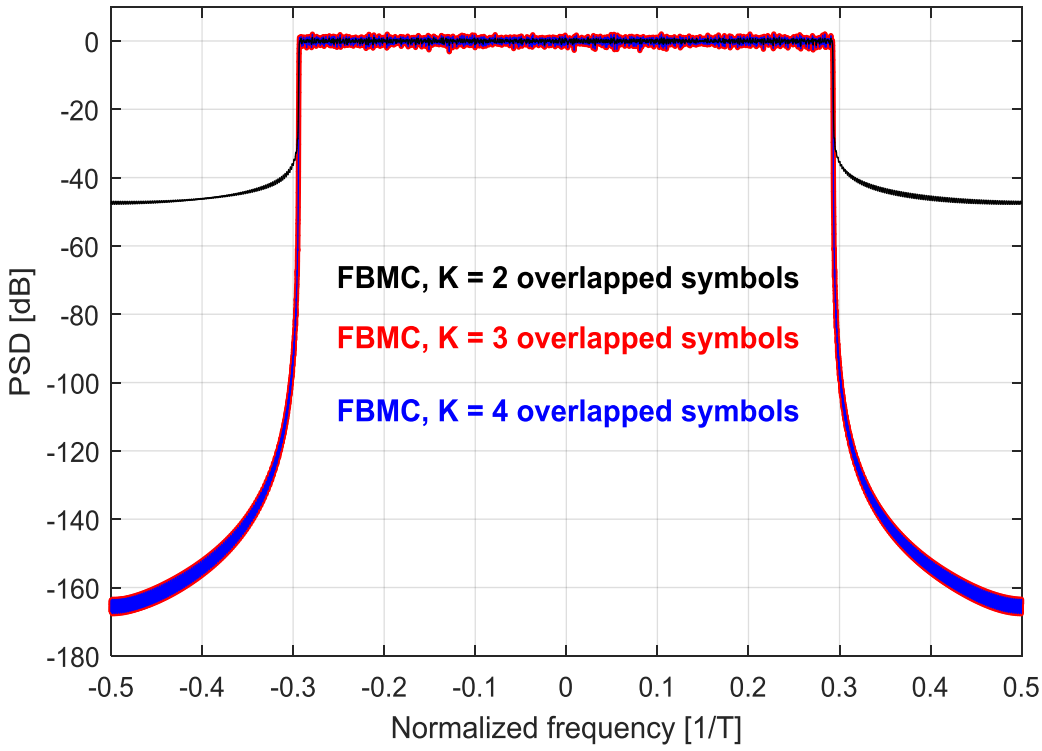

Figure 3.10: The PSD of FBMC in the different overlapped symbol for the different out-of-band omission.

FBMC modulation with corresponding parameters has been reviewed using the fully occupied band. Figure 3.10 has shown the plotted power spectral density (PSD) overall subcarriers FBMC in different overlapped symbols while increasing the modulation. FBMC has lower side lobes. The filtered spectrum enjoys a reduction of side lobes and smaller guard bands to minimise out-of-band emission in the FBMC system. This ensures greater exploitation of the allocated spectrum, increasing the number of subcarriers and improving the spectral efficiency [131].

3.8.3 Universal Filtered Multicarrier Based Modulation (UFMC)

UFMC is a multiple filter multicarrier modulation technique which is widely accepted by 5G applications such as Wi-Fi and LTE. Among several advantages of UFMC to these communication systems is that its efficiency application is robust to channel delay and single-tap frequency domain equalization. Its cost-effectiveness is quite clear such that spectral efficiency improves due to lower side lobes and moderate synchronization requirements [132]. These are some of the requirements in new modulations technique such as the UFMC being considered for 5G applications. The filters of subcarriers modulations such as UFMC-OFDM and T-OFDM are new 5G-OFDM communication applications. Like the UFMC which has blocks of filters as subcarriers.

Each subcarrier consists of sub-band to remove out-of-band emission as shown in Figure 3.11. Furthermore, UFMC uses several frame structure and the numerical calculation at each operating sub-band for adjustable and wider bandwidth. These can allow adaptive deployment and link types. To allow extra

protection on delay spread, UFMC allows adaptation of zero tail Discrete Fourier Transform (DFT) spreading to a specific sub-band [119, 133, 134].

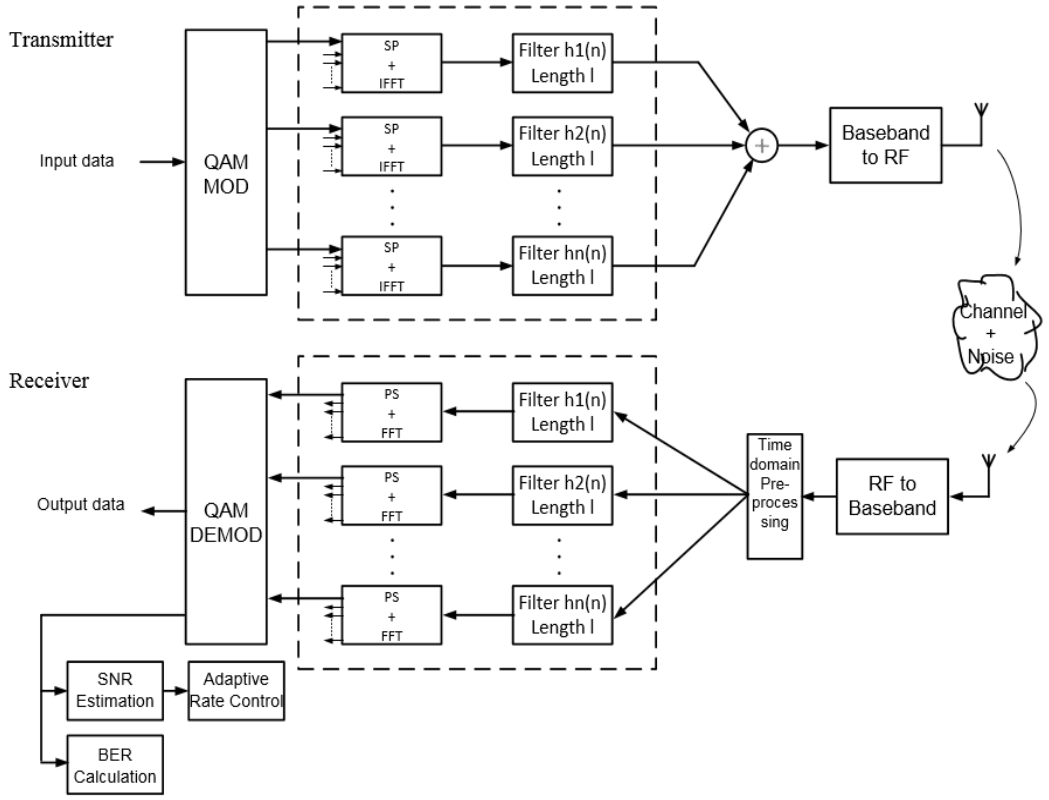

Figure 3.11: The proposed UFMC-OFDM transceiver system-level structure.

Figure 3.11 shows a proposed UFMC-OFDM transceiver system with blocks of subcarriers. The UFMC is considered as a generalised OFDM and FBMC multi-filters modulation system. This means that the whole band is filtered in OFDM filter and every subcarrier is filtered in FBMC filter, while the collection of sub-bands are filtered in UFMC. The grouping of subcarrier decreases the length of the filter. In addition to UFMC advantage, it is compatible with existing MIMO schemes due to a sustainable relationship with QAM to keep the complex orthogonality.

As depicted in the figure above, the whole sub-carrier band (N) is divided into several sub-bands. Each sub-band contain a specific number of sub-carriers in

which not all sub-bands will be used at once or for a given transmission. An N IFFT is allocated to each sub-band with zeros for the yet allocated carriers. The filter length L filtered each sub-band and the results from each sub-band. The IFFT converts the frequency domain sub-band signal into the time domain signal. After IFFT operation in each sub-band, FIR filter with length L is used to filter the output signal. The filtering is performed to improve robustness against out-of-band spectral emission. The summed up all filtered sub-band signals are now transmitted at the output of the UFMC transmit system [133, 135-137].

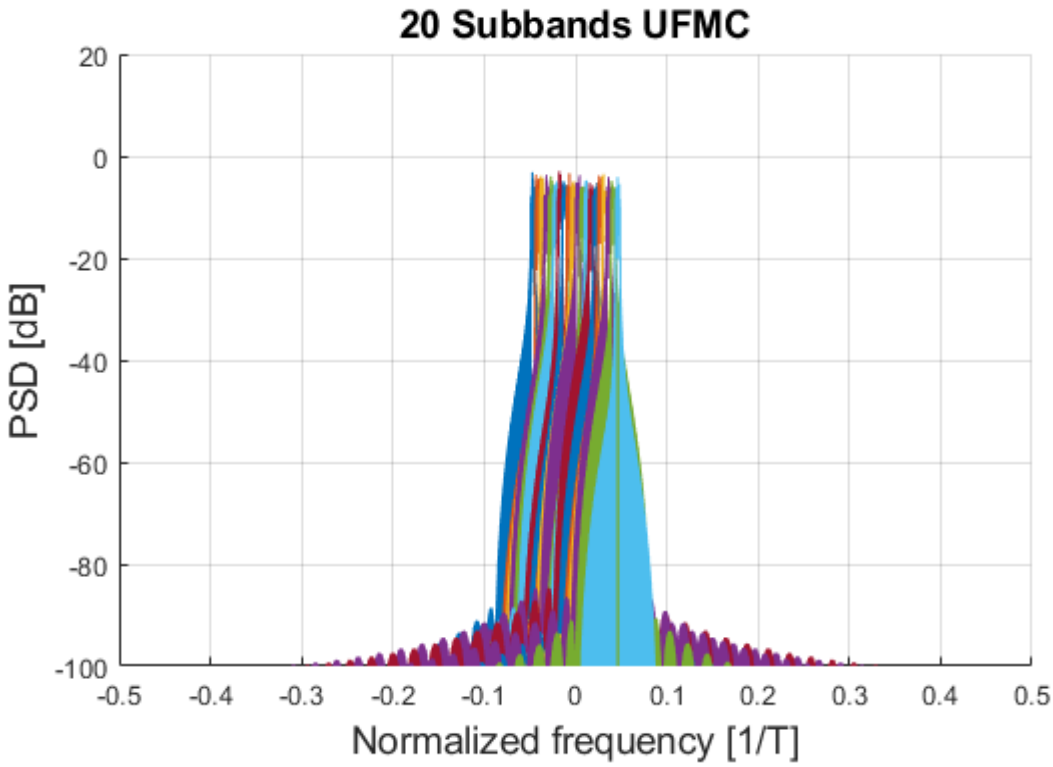

Figure 3.12: The UFMC-OFDM transceiver system-level structure.

Figure 3.12 shows the power spectral density versus normalised frequency of UFMC-OFDM transceiver system. The figure presented the simulation result of UFMC-OFDM different system characteristics for the number of sub-bands, a number of subcarriers in a sub-band, length of the filter used, attenuation on the side-lobes and signal-noise-ratio. As highlighted in the figure, the PSD consists

of 20 sub-band with 20 sub-carriers each in UFMC and 400 subcarriers equivalent in OFDM system. This result has shown how UFMC is considered to have an advantage over other modulations by providing excellent spectral efficiency. The spectral efficiency improves due to lower side-lobes of the UFMC modulation and utilization of the allocated spectrum. UFMC also illustrates a better PAPR than other schemes. As you can see, an increase in sub-band increases system complexity, sub-carriers and reduces the side lobe levels. What makes UFMC more attractive compared to other schemes is the reduction of filter length and the guards between the sub-bands by the sub-band filtering. It overcomes the ICI problem and improves the performance of the system by using the filtering operation to the subcarriers which also reduces the out-of-band effect. It results in excellent ICI robustness and better suitability for fragmented spectrum operation compared to OFDM. UFMC outperforms in both perfect and non-perfect frequency synchronization between the transmitter and receiver [138].

3.8.4 Other Modulation Techniques

There are other 5G modulation candidates we need to discuss in addition to the previous once which are also part of pulse shaping, sub-band filtering and other techniques that can help to suppress the out-of-band leakages. They are included among modulation techniques with respective advantages and meet the pre-requisite under the context of 5G networks. These modulation techniques are briefly discussed in order to have a performance comparison of different modulations. Among the pulse shaping (subcarrier based filtering) based modulations are the generalised frequency division multiplexing (GFDM). GFDM is one of the pulse shaping modulations that can reduce the effect of out-of-band leakages. Like the FBMC, the waveform is non-orthogonal in frequency and time

domain to produce high spectral efficiency. GFDM is a combination of single carrier frequency division multiplexing (SC-FDM) and orthogonal frequency division multiplexing (OFDM). To perform pulse shaping, unlike FBMC that uses the linear filter, the unique features of GFDM adopts circular shift filters to reduce the OOB leakages even without orthogonality. The circular shift filter adopted GFDM is suitable for sporadic transmission which allows compatibility with MIMO systems [139-141]. Other modulations based on pulse shaping has been proposed for 5G networks such as pulse-shaped OFDM and QAM-OFDM. For other modulations from sub-band filtering family are proposed and considered to be flexible in the frequency multiplexing and can be used in different applications with different parameters. In the following, the modulations to be introduced include filtered-OFDM having a cyclic prefix with same transmitter structure as UFMC, the windowed-OFDM with time-domain non-rectangular pulses to flatten the alteration at the edge of the symbol for OOB leakage reduction. The unique word-OFDM also replace the CP-OFDM to provide extra training to increase channel accuracy and synchronization [119, 133]. Another modulation technique suitable for 5G networks is Amplitude and Phase Shift Keying technique (APSK). It is the combination of Amplitude Shift Keying (ASK) and Phase Shift Keying (PSK) which makes it similar to QAM. It has a constellation that is more of the co-centric ring in the amplitude distribution nearly similar to Gaussian capacity than the QAM. To improve the channel capacity close to Shannon's capacity, a new constellation with channel coding in advanced demodulation algorithms can be developed. In fact, when the constellation appreciates to infinity, APSK can be similar channel capacity to that of Gaussian, while for conventional QAM constellation is estimated to 1.56 dB less Gaussian capacity [119, 133]. However, there are several proposed algorithms to improve channel capacity of APSK

constellation. Another high spectrally efficient modulation family that is considered to be extremely beneficial to the 5G network studied in the literature is the Unitary-space time modulation (USTM) technique. This type of modulation has been proposed for massive MIMO applications which can produce high throughput without using the channel state information (CSI) in any stage of the transceiver system. Algorithms have been proposed base on Differential USTM which generalised the Differential Phase Shift Keying (DPSK) to increase the transmit antennas. The DUSTM can produce very small Bit-Error-Rate (BER) and moderate signal to noise ratio (SNR) of less than 0 dB. And lastly, another interesting technology is the spatial modulation (SM) technique proposed as one of the potentials for 5G services. The SM is where only one antenna is active at each transmission time and the antenna indices are used to transmit the information. This modulation can reduce the inter channel interference, simplifies synchronization between antennas and reduce complexity on radio chain design as well. Other modulation techniques such as the Orthogonal Time-Frequency and Space (OTFS) and Wave Modulation (WAM) techniques are also reported to be among the highly important modulations for 5G applications in terms of improving the throughput and reducing the OOB leakages [119, 133]. These modulation techniques will be further analysed or compared with other modulation techniques in future work.

3.9 Summarized Conclusions

OFDM has been described in this work. It features, functionality, advantages and disadvantages, the effect of PAPR and reduction techniques were presented. This also presented the influence and importance of high data rate in the communication system. In addition, the effect and avoidance of ISI in the channel

have been discussed. The application of IFFT and FFT technology provide effective modulation and demodulation for easy implementation of OFDM in a transceiver system. OFDM has been established to be appropriate multicarrier modulation technique to avert multipath distortions and robust in multicarrier signalling. It was tested using linear and nonlinear RF power amplifiers over different digital modulation systems. The results show that due to RFPA distortion in the RF front end, the modulation schemes deteriorate in terms of BER. However, the OFDM signalling was affected significantly and ICI reduces the performance of an OFDM system. Due to these effects, other modulations are developed to harmonise the OFDM for the modern future applications and beyond such as the 5G systems. Few of the 5G modulation techniques have been discussed such as the FQAM-OFDM, FBMC, UFMC-OFDM, F-OFDM, spatial modulation and other candidates for potential 5G applications. Comparative analysis was also presented to determine the performance of the 5G modulations candidates with OFDM modulation. The study concluded that the 5G modulations reduce OBO, increases throughput and offer more spectral efficiency than the OFDM modulation.

CHAPTER 4

RF Power Amplifier Modelling

4.1 Introduction

Modern wireless transceiver design considers modelling the memory and nonlinear effects of the power amplifier and other nonlinear components as important factors that require more attention. Intensive research in the modelling of nonlinear components has been reported in the literature. However, there is no adequate state of the art knowledge respect to power amplifier baseband modelling approach for the calculation of the mathematical equation and optimization of the predistortion coefficients [31, 142]. These include developing a descriptive method of analysing the output signal distortion of the power amplifier and the transfer function of it nonlinearities. Modelling evaluates the transceiver performance and develop a linearizer suitable for the memory effect [31, 142]. There are two general methods according to [142, 143] which power amplifier can be model;

- Physical model: is an approach that requires physical information of the device internal composition or by the pragmatic way of observing the input as well as the output. In addition, the information on the device inner structure has to be specified. The precision increases the accuracy of the model as well as the simulation time. However, the drawback of this model is the lack of continues information [144-146].
- Behavioural model: this model is the most effective technique where the power amplifier is modelled using a black box. The behavioural model is different, where input-output relations of the device will be maintained without physical or circuit analysis [147-149].

This chapter will focus more on behavioural modelling methods as an effective approach to model nonlinear behaviour and memory effect of a power amplifier using a black box. The methods to be presented include memory and memoryless modelling methods, which elaborate both the fundamental and harmonics frequency model for any extent of nonlinearity in the system.

4.2 Behavioural Modelling

Behavioural modelling of nonlinear devices known as systematic modelling is important in the design of linearization techniques for nonlinear distortion effect caused by the nonlinear devices which in effect becomes detrimental to the overall performance of the communication system. This implies that behavioural modelling can be used for the evaluation of a system using the power amplifier characteristics as the model parameters [150]. Like mentioned in the introduction above, the power amplifier can be modelled either in circuit diagram method using values of the devices or with the help of black-box model where power amplifier characteristics are extracted, input-output measured and the system is optimized [142, 151].

The power amplifier can be model based on the existence or composition of nonlinear distortion in the system. However, various behavioural modelling approaches in the existing literature are identified and used for modelling nonlinear systems [150]. The most common are classified into three nonlinear systems;

- A memoryless nonlinear system is an instantaneous system where the AM-AM conversion function is slowly verified. The memoryless system is referred to as the absolute absence of memory effects in the system.

This model is developed for band pass nonlinearity model where the input consists of finite bandwidth around the modulated signal, while the output of the device with the same bandwidth is band-limited by the zonal filter [152, 153].

- Quasi memoryless nonlinear system: A nonlinear system that is determined by AM-AM and AM-PM functions. This means that it has a short term memory effect capable of modelling narrowband systems. Quasi-memory system use complex polynomials where AM-AM and AM/PM of the nonlinear device are measured while takes into account of the input-output complex envelope relation [67, 143, 154].
- Nonlinear memory system: A nonlinear system takes account of long term memory effects. The output complex envelope response depends on the input complex envelope and the frequency. In another word, the output of the device relies on past inputs and the current input of the device. The memory effect is originated from the thermal effects of the active component as well as the electrical effects from the DC bias circuits of the device. Unlike the quasi-memoryless system which takes account of short term memory effect and limited to model for the narrowband application. This system is a special case of high band applications and can model wideband systems such as WCDMA, OFDM and LTE [143, 154].

Behavioural modelling considers memoryless, quasi memoryless and the nonlinear memory system model in the literature. However, both the memory and memoryless effects are important, especially in the predistortion system. In this

chapter, the subsections will present the most common models for both memory and memoryless model.

4.2.1 Lookup Table Model

The look up table (LUT) model is one of the basic behavioural models for memoryless AM-AM and AM-PM nonlinearities. AM-AM and AM-PM characteristics represent magnitude and phase information for the input and output of a device under test. The AM-AM and AM-PM characteristics as a complex of the DUT are kept in two LUT [155, 156] and is written as:

$$v_o(n) = v_i(n)G(|v_i(n)|) \tag{4.1}$$

Where $v_o(n)$ is the output, $v_i(n)$ is the input, while $G(|v_i(n)|)$ is the instantaneous complex gain of the DUT. The AM-AM and AM-PM characteristics of the DUT are coefficients of the predistorter, derived from the raw measured data using polynomial curve fitting or averaging methods [157]. The block diagram of the look up table is given in Figure 4.1.

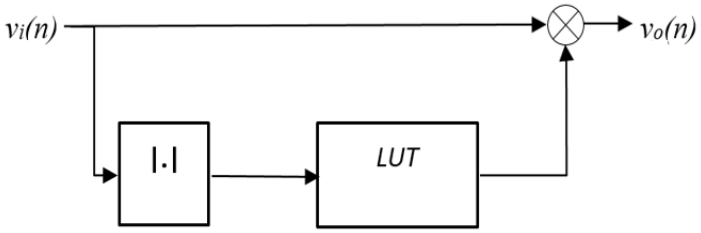

Figure 4.1: Block diagram of the lookup table model.

The general example of lookup table network behaves as a model for the static nonlinearity model in two or three-box-based model and digital predistorter which will be discussed in the next chapter.

4.2.2 Nested Lookup Table Model

This model is based on a nested lookup table as an extension to the conventional memoryless lookup table model. In the case of nested lookup model with added memory effects, the DUT estimated output signal is computed with respect to the actual input sample, $v_i(n)$ and the proceeding samples [142]. The nested look-up-table output sine wave can be expressed as:

$$v_o(n) = v_i(n)G(|v_i(n)|) \tag{4.2}$$

Where $v_o(n)$ is the output, $v_i(n)$ is the input vector with the $M\text{-}1$ proceeding samples, while $G(|v_i(n)|)$ stands for the instantaneous complex gain of the DUT. The output vector $v_o(n)$ is expressed as:

$$v_o(n) = [v_i(n), v_i(n-1), ..., v_i(n-M)] \tag{4.3}$$

The instantaneous complex gain of the DUT is a function of the actual input sample $v_i(n)$ and the $M\text{-}1$ as proceeding samples [$v_i(n)$, $v_i(n\text{-}1)$,…, $v_i(n\text{-}M)$].The M is the memory length of the DUT. K^{M+1} is the look up table size, and K is the number of bins required for the memoryless look-up-table model.

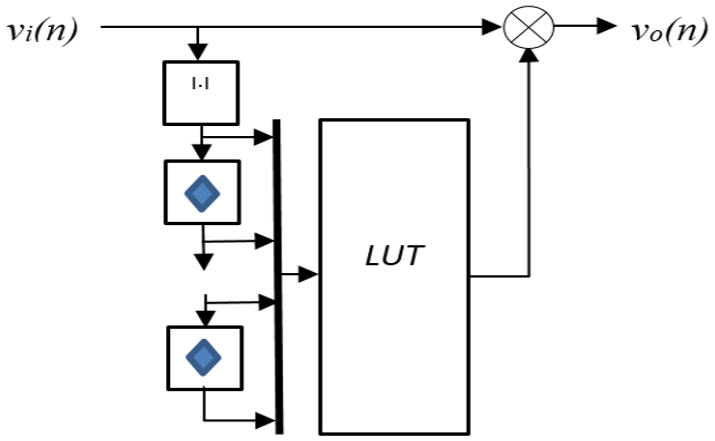

Figure 4.2: Block diagram of nested LUT model.

Nested look-up-table model is similar to the conventional look-up-table model, the AM-AM and AM-PM characteristics of the DUT have derived a complex gain from the raw measured data after accurate time delay alignment. In this case, the curve fitting of the measured data has not been used by the model [158].

4.2.3 Volterra Series Model

Volterra model is the most comprehensive polynomial functional model for representing and identifying memory effects of nonlinear systems. The model consists of linear convolution of input and a nonlinear power series. Most nonlinear analytical models use Volterra analysis to model finite memory of the nonlinear systems [31, 158, 159]. In Volterra series analysis, however, the frequency is selected based on the finite bandwidth of the linear and nonlinear filters in the nonlinear system model. The linear and nonlinear filters in the time domain are represented by their impulse response (kernel functions) where the kernel represents the memory of the system. This, in turn, is the input-output relation of a nonlinear and time-invariant system with fading memory. For the time-invariant system, the memory effects of a nonlinear power amplifier can be approximated by means of Volterra series approach [160] which is expressed in equation (4.4) as:

$$v_o(n) = \sum_{k=1}^{K} \sum_{i_1=0}^{M} \cdots \sum_{i_p=0}^{M} h_p(i_1,\ldots,i_p) \prod_{j=1}^{k} v_i(n-1), \tag{4.4}$$

Where $h_p(i_1,\ldots,i_p)$ is the Volterra series p^{th} order of the Volterra kernel, K is the nonlinearity order of the model, and M is the memory length. The Volterra series model of a nonlinear system can be defined by using the functional expansion of continuous functions:

$$y(t) = F_p(x(t)) = \int_{-\alpha}^{\alpha} \ldots \int_{-\alpha}^{\alpha} h_p(t;\lambda_1,\ldots,\lambda_p) \prod_{i=1}^{n} x(\lambda) d\lambda_i \quad (4.5)$$

Where $F_p(x(t))$ is a nonlinear function of the continuous function $x(t)$ and $h_p(t; \lambda_1,\ldots,\lambda_p)$ is the symmetric n-dimensional of Volterra kernel. However, in the Volterra series function, the Volterra kernel describes the memory of the system with the time interval defined to maintain the input-output relations of the system [28, 161, 162]. The Volterra series analysis characterises a generalised approach similar to the Taylor series for the analytical function. The number of coefficients rises up to an unwanted level when the memory length and the nonlinear order increases to a certain level [161].

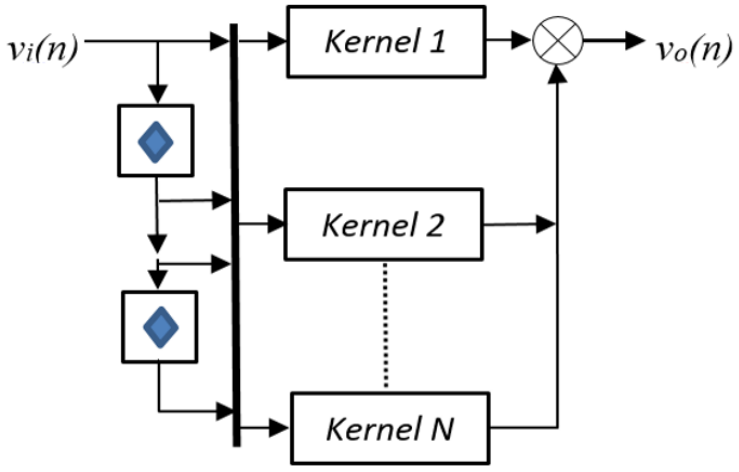

Figure 4.3: Block diagram of a volterra series model.

Volterra series, has become ineffective for systems with strong nonlinearity due to deficiency. Nonlinear systems of these magnitude experience difficulties in real-time implementation due to the complexity of the system which can only be used for weakly nonlinear systems. There are other special cases of the Volterra series such as pruning [159, 163], dynamic reduction deviation and Wiener-Bose model [164] which have high real-time implementation capability and at the same time simplify the original Volterra approach. Although these techniques are not

complex as Volterra series, they require a large number of parameters and time for estimation [165]. Figure 4.3 illustrates the Volterra model for weakly nonlinear power amplifier device.

4.2.4 Memory Polynomial Model

The memory polynomial model is one of the promising model, widely used for memory effects behavioural modelling and predistortion of the power amplifier. It is similar to the Volterra series model where the diagonal terms of both models are kept [166]. This implies that the coefficients of the former remain diagonal to that of the latter. The memory polynomial model is express in the output waveform as:

$$v_o(n) = \sum_{j=0}^{M} \sum_{i=1}^{N} a_{ji} v_i(n-j) \, | v_i(n-j) |^{i-1} \tag{4.6}$$

Where a_{ji} are the coefficients, M and N are the memory depth and nonlinearity order of the power amplifier device (DUT).

This model is easy to use in predistorters, is not very complex, takes account of the memory effects and the performance is satisfactory. To improve the conventional memory polynomial model, several variations of models have been proposed in the literature such as orthogonal memory polynomial model, generalized memory polynomial model known as cross-term memory polynomial model [165, 167].

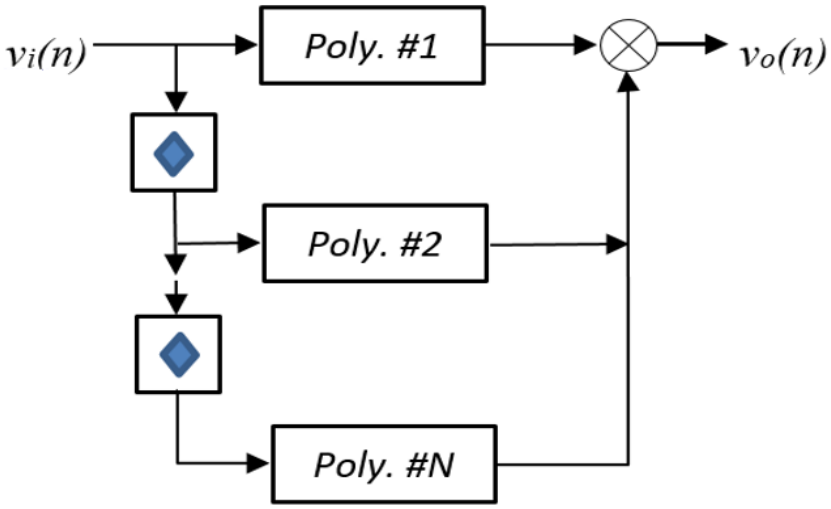

Figure 4.4: Block diagram of a conventional memory polynomial model.

4.2.5 Envelope Memory Polynomial Model

The envelope memory polynomial model was proposed to combine the conventional memory polynomial model and the nested look up table based complex multiplier model [167, 168]. The envelope memory polynomial predistortion model is implemented in a complex gain based structure and exploit the dependency of the weakly power amplifier nonlinearity as the function of the only magnitude of the input signal, against the inconsistency of its complex value. In the case of memory effects, it is easy and straightforward to model and linearize the weakly nonlinear power amplifiers [169]. The output waveform response of the envelope memory polynomial model can be described as:

$$v_o(n) = \sum_{j=0}^{M} \sum_{i=1}^{N} a_{ji} v_i(n) \, | v_i(n-j) |^{i-1} \tag{4.7}$$

Where a_{ji} represent the model coefficients, N is the nonlinearity order and M is the memory length of the power amplifier. The waveform response of the two polynomials are seen to be exactly the same, except the magnitude input signal of the two terms [$v_i(n)$, $v_i(n\text{-}1)$,…, $v_i(n\text{-}M)$] are required. The diagram in Figure 4.5

illustrates the envelope memory polynomial model for weakly nonlinear power amplifier systems.

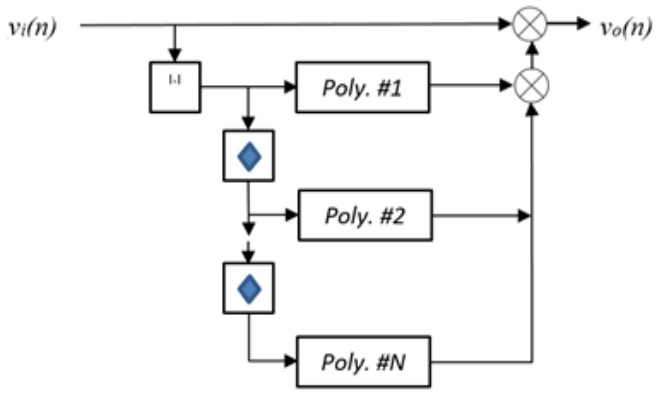

Figure 4.5: Block diagram of an envelope memory polynomial model.

In the diagram, complex gain value at the first level are computed with the help of the input samples [$v_i(n)$,…, $v_i(n\text{-}M)$] magnitude. The complex gain is forwarded to the baseband complex input signal $v_i(n)$ for output $v_o(n)$ sample. Envelope memory polynomial is more complex and less performed than the conventional memory polynomial model [169].

4.2.6 Wiener Model

The Wiener model is simply a two-box model that comprises linear finite impulse response (FIR) filter with a memoryless nonlinear function [142]. It is similar to a simple version of Volterra series expansion. Wiener series can be interpreted as an alternative way to systematically characterize a dynamic nonlinear system simpler than Volterra series [170]. The equation (4.8) and (4.9) have expressed the relationship between the output and the intermediate transfer function of the wiener series:

$$v_o(n) = v_1(n)G(|v_1(n)|) \tag{4.8}$$

Where $v_o(n)$ is the output of FIR filter, $G(|v_1(n)|)$ is the memoryless nonlinear instantaneous gain function of the P^{th} order of the look-up-table model. The output of the linear finite impulse response (FIR) filter is defined as:

$$v_1(n) = \sum_{j=0}^{M} h(j) v_i(n-j) \tag{4.9}$$

Where $h(j)$ are the coefficients of the filter impulse response which defined the memoryless nonlinearity, v_i is the input and M is the memory depth of the RFPA. In the Wiener model, as illustrated in Figure 4.6, the linear finite impulse response (FIR) filter and memoryless nonlinear function (look-up-table) are clearly identified.

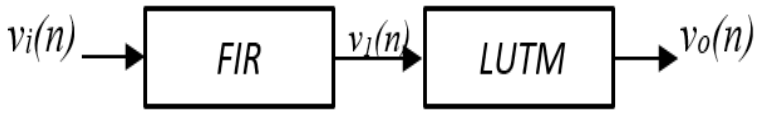

Figure 4.6: Block diagram of the Wiener model.

In the FIR filter, it is illustrated that the input and output waveforms are de-embedded, but the coefficients are identified. However, this model avoids the identification of a nonlinear system of equations. To compare with other models, this model performs better than memoryless polynomial and look-up-table models [164]. Clark et al [143] used it to represent modelling structure and simplicity of wiener model.

4.2.7 Hammerstein Model

The Hammerstein model is also a two-box model composed of first a memoryless static nonlinear function (look up table) and a linear finite impulse response (FIR)

filter [171]. Hammerstein model can be interpreted as an alternative way of improving modelling edifice of a dynamic nonlinear device under test. Consequently, the polynomial of the look up table is expressed in (4.10) as:

$$v_1(n) = v_i(n)G(|(v_i)|) \tag{4.10}$$

Where $v_1(n)$ is the output of FIR filter, while $v_i(n)$ is the input signal. $G(|(v_i)|)$ is the memoryless nonlinear instantaneous gain function of the P^{th} order of the look-up-table model. The output of the linear FIR filter is defined as:

$$v_o(n) = \sum_{j=0}^{M} h(j)v_1(n-j) \tag{4.11}$$

Where $h(j)$ are the coefficients of the filter impulse response which defined the memoryless nonlinearity, v_i is the input and M is the memory depth of the DUT. In the Wiener model, as illustrated in Figure 4.7, the linear FIR filter and memory-less nonlinear function (look up table) are clearly identified.

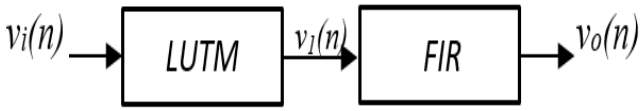

Figure 4.7: Block diagram of the Hammerstein model.

In the FIR filter, it is illustrated that the input and output waveforms are de-embedded, but the coefficients are identified. However, this model identification process of nonlinear system parameters is identical to that of wiener model. To

compare with other models, this model performs even better than wiener, memoryless polynomial and look up table models. It is simple like Wiener approach and not very effective for predistortion [171, 172].

The Hammerstein model can improve accuracy in modelling the nonlinear power amplifier by converting the single-stage Hammerstein to a parallel one. By adding more blocks in parallel can increase the performance, however, the complexity increase as well [173]. Figure 4.8 illustrates a parallel Hammerstein model.

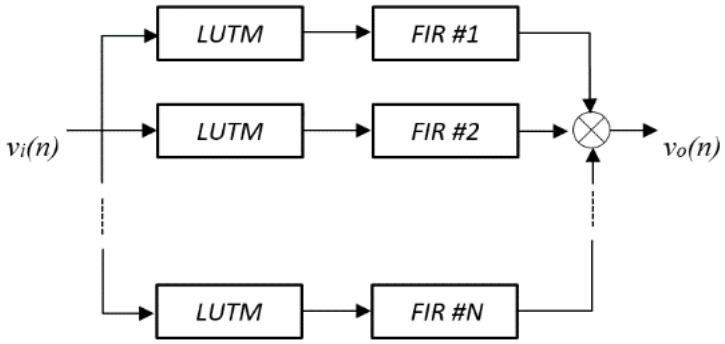

Figure 4.8: Block diagram of parallel Hammerstein approach.

4.2.8 Augmented Wiener Model

The augmented Wiener model is a twofold augmented Hammerstein model where the cascade is made of a slightly nonlinear dynamic function (filters) and a robustly nonlinear static model (LUT). The robustly nonlinear static model is composed of AM-AM and AM-PM characteristics of the power amplifier which can be implemented by the use of look up table [171]. The output signal $v_o(n)$ of the augmented Wiener model expressed by (4.11), while the intermediate signal $v_i(n)$ is defined in equation (4.12)

$$v_1 = \sum_{j_1=0}^{M_1} h_1(j_1) v_i(n-j_1) + \sum_{j_2=0}^{M_2} h_2(j_2) v_i(n-j_2) \,|\, v_i(n-j_2) \,| \qquad (4.12)$$

Where $h_1(j_1)$ and $h_2(j_2)$ are the impulse response filter FIR1 and FIR2, M_1 and M_2 are the memory depth of filter *1* and *2*. However, the block diagram in Figure 4.9 is illustrated as:

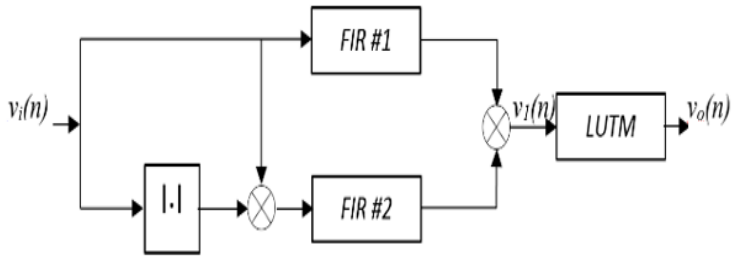

Figure 4.9: Block diagram of the augmented Wiener model.

4.2.9 Augmented Hammerstein

The augmented Hammerstein model is a dual case of two steps Hammerstein model where the cascade is made of a robustly nonlinear static model (LUT) and a slightly nonlinear dynamic function (filters). The robustly nonlinear static model is composed of AM-AM and AM-PM characteristics of the power amplifier which can be implemented by the use of look up table [171]. The intermediate signal $v_1(n)$ of the augmented Hammerstein model is shown in Figure 4.10, while the output signal $v_o(n)$ is defined in equation (4.13)*:*

$$v_o(n) = \sum_{j_1=0}^{M_1} h_1(j_1) v_1(n-j_1) + \sum_{j_2=0}^{M_2} h_2(j_2) v_1(n-j_2)\,|\,v_1(n-j_2)\,| \qquad (4.13)$$

Where $h_1(j_1)$ and $h_2(j_2)$ are the impulse response filter FIR1 and FIR2, M_1 and M_2 are the memory depth of filter *1* and *2,* while $v_i(n)$ is the output of the look-up-table box. However, the block diagram in Figure 4.10 is illustrated as:

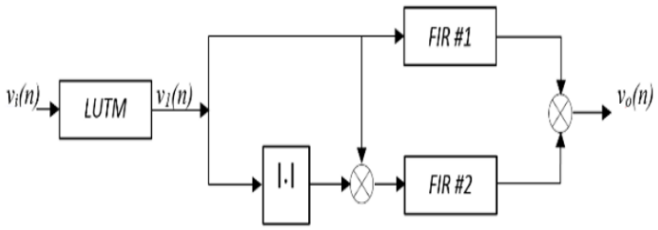

Figure 4.10: Block diagram of the augmented Hammerstein model.

Since the conventional Hammerstein model takes into account of linear filter, correcting the electrical memory effect caused by the frequency response of the power amplifier around the carrier frequency, in the same vein, negate the impedance variation of the bias network and matching circuits. This reason, however, called for the second branch with an additional linear filter (FIR) applied to the second-order nonlinearity to improve the performance of the model towards modelling of nonlinear systems [174].

4.2.10 Twin Nonlinear Two-Box Models

The twin nonlinear two-box models are generally two-box model that compose a static look-up-table nonlinear model and dynamically nonlinear memory polynomial model [175]. In this respect, there are three different sets of configurations of twin nonlinear two-box models such as:

- The forward twin nonlinear two-box model: As discussed in [176, 177], which the static look up table nonlinear model is placed before the memory polynomial model box as illustrated in Figure 4.11 and the forward twin nonlinear two-box model configuration is also expressed in equation (4.14) and (4.15).

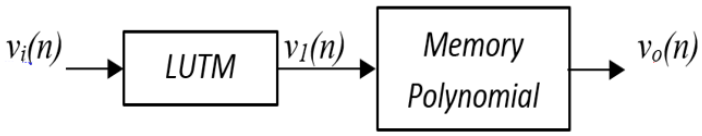

Figure 4.11: Block diagram of the forward twin nonlinear two-box model.

$$v_1(n) = v_i(n)G(|(n)|) \tag{4.14}$$

Where $v_i(n)$ is the input, $G(|(n)|)$ is the instantaneous complex gain of the DUT and $v_1(n)$ is the output of the look-up-table function.

$$v_o(n) = \sum_{j=0}^{M}\sum_{i=1}^{N} a_{ji} v_1(n-j)\,|\,v_1(n-j)\,|^{i-1} \tag{4.15}$$

Where a_{ji}, M, N and v_o are the coefficients of the time-aligned signal, memory depth, nonlinear order and the output of the memory polynomial function.

- The reversed twin nonlinear two-box model: Where the look up table model box is applied after the memory polynomial model box [178]. This model as illustrated in Figure 4.12 and the reversed twin nonlinear two-box model configuration is also expressed in equation (4.16) and (4.17).

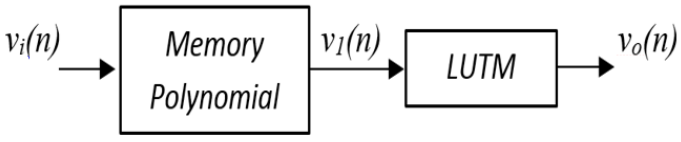

Figure 4.12: Block diagram of a reversed twin nonlinear two-box model.

$$v_1(n) = \sum_{j=0}^{M} \sum_{i=1}^{N} a_{ji} v_i(n-j) \,|\, v_i(n-j) \,|^{i-1} \tag{4.16}$$

Where a_{ji}, M, N and v_1 are the coefficients of the time-aligned signal, memory depth, nonlinear order and the output of the memory polynomial function:

$$v_o(n) = v_1(n)(G \,|\, (v_1) \,|) \tag{4.17}$$

Where $v_1(n)$ is the input, $(G|(v_1)|)$ is the instantaneous complex gain of the DUT and $v_o(n)$ is the output of the look up table function.

- The parallel-twin nonlinear two-box model is different from forward and reversed, where both look-up-table function and memory polynomial function are directly applied to the input [176]. This model as illustrated in Figure 4.13 is also expressed in equation (4.18), (4.19), (4.20) and (4.21).

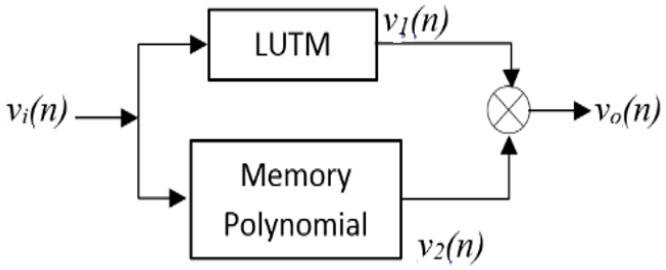

Figure 4.13: Block diagram of the parallel-twin nonlinear two-box model.

$$v_1(n) = v_i(n) G(|\, v_i(n) \,|) \tag{4.18}$$

Where $(|v_i(n)|)$ is the instantaneous complex gain of the DUT and $v_1(n)$ is the output of the look up table function.

$$v_2(n) = \sum_{j=0}^{M} \sum_{i=1}^{N} a_{ji} v_i(n-j) \,|\, v_i(n-j) \,|^{i-1} \tag{4.19}$$

Where a_{ji}, M, N and v_2 are the coefficients of the time-aligned signal, memory depth, nonlinear order and the output of the memory polynomial function. The overall output of the parallel-twin nonlinear two-box model is the composition of the static nonlinear look up table function versus the dynamic nonlinear memory polynomial function.

$$v_o(n) = v_1(n) + v_2(n) \tag{4.20}$$

Finding the sum of equation (4.18) and (4.19) will expand equation (4.20) to express the overall output as illustrated in equation (4.21)*:*

$$v_o(n) = v_i(n) G(|\, v_i(n) \,|) + \sum_{j=0}^{M} \sum_{i=1}^{N} a_{ji} v_i(n-j) \,|\, v_i(n-j) \,|^{i-1} \tag{4.21}$$

Where $v_o(n)$ is the overall output of the parallel-twin nonlinear two-box model. Consequently, each of these twin nonlinear two-box models can be used for the modelling of any device under test that is exhibiting nonlinear distortion. It can be recalled that the output response can be derived as a function of the input signal through a suitable combination of (4.2) and (4.5). The three models are classified into three in which each model can fall into a trend that in turn leads to a new model. These are the three possible new models:

- Memory polynomial based models: Conventional memory polynomial models augmented by adding more specific terms or reducing the model to improve performance and ease complexity [179].

- Volterra based models: The Volterra is composed of other techniques that can be applied to the original based model and keep the terms that can improve the power amplifier nonlinear behaviour [31].
- Wiener and Hammerstein based models: These two models can be combined together in two or three boxes and include weakly nonlinearities in the dynamic box. The combination can either be Wiener-Hammerstein models in three box or Hammerstein-Wiener models [171, 172].

4.2.11 Saleh Model and Simple Analytical SSP Model

The Saleh model [30] is the most commonly memoryless nonlinear function that can characterize the AM-AM and AM-PM parameters of the nonlinear power amplifier. The device of interest was originally a travelled wave tube amplifiers (TWT). However, this model has also been applied to model solid-state power amplifiers (STPA). The Saleh model characteristic functions of the amplifier can be expressed as:

$$A(z(n)) = \frac{\alpha_a \mid z(n) \mid}{1+\beta_a \mid z(n) \mid^2} \tag{4.22}$$

and

$$\Phi(z(n)) = \frac{\alpha_\Phi \mid z(n) \mid^2}{1+\beta_\Phi \mid z(n) \mid^2} \tag{4.23}$$

Where α_a, β_a, α_Φ, β_Φ are constant frequency-dependent parameters of the model used for the characterization of the power amplifier. They define the stability of the nonlinear characteristics and be modified to provide a desired nonlinear characteristics. The larger r becomes, $A(n)$ will be proportional to $1/r$ and $\Phi(n)$ will approach a constant level. In memoryless instance, the Saleh model decreases

when the parameters are frequency dependent. In this case, the output envelope of the power amplifier is given by [30] as:

$$\tilde{z}(t) = \frac{\alpha_a \,|\, \tilde{x}(t) \,|}{1 + \beta_a \,|\, \tilde{x}(t) \,|^2} \tag{4.24}$$

$$\tilde{y}(t) = \frac{\alpha_\Phi \,|\, \tilde{x}(t) \,|^2}{1 + \beta_\Phi \,|\, \tilde{x}(t) \,|^2} \tag{4.25}$$

V.J. Mathews and D. Falconer also underlined that the equation as given in (4.25) is used for solid-state power amplifier nonlinear characterization, is defined as:

$$A\big(z(n)\big) = \frac{|\, z(n) \,|}{\sqrt{1 + \left(\dfrac{|\, z(n) \,|}{A_0} \right)^2}}, \quad \Phi\big(z(n)\big) = 0 \tag{4.26}$$

Where A_o is used for the fitting of the measured data.

4.3 Power Amplifier Nonlinear Memory Effect Modelling for the Purpose of Predistortion

In recent years, digital predictive linearizing techniques are developed to achieve RF power amplifier linearity and efficiency enhancement. These techniques, due to the nature of the operation, sort for prior knowledge of the power amplifier nonlinear behaviour in order to specify a convenient characterization technique. The Volterra series amongst other techniques for this application appears to be malfunctioned in the modern predistortion systems due to its shortcomings such as practical difficulty in implementation and measurement of the Volterra kernels, high computational complexity and limited performance to weakly nonlinear

systems. It also exhibit dramatic performance degradation under strongly nonlinear conditions. Wiener-based modelling systems were implemented due to the weaknesses of the Volterra modelling approach [31, 180].

In the Wiener model, memory effect and nonlinear behaviour of an RF power amplifier can be corrected by the use of linear filter and a standalone polynomial model. It is easy and convenient to use these models to practically implement both the characteristics of the linear dynamic system and the static nonlinear function through estimation. These also include extracting and optimising coefficients of the amplifier without much computational complexity. Many approaches in the literature identify the Wiener model as a favourable system for modelling nonlinear power amplifiers. On the other hand, Wiener-based model is weak in identification where the nonlinearities are versatile and difficult to identify a suitable representation of the nonlinearity static function. The intermediate variables cannot be measured due to applications of this method are restricted by imposing a limitation. Hence, the nonlinear static function is not invertible to recover the intermediate variables from the output data stream which if done can results in potential measurement disorder during amplification. Among other drawbacks of this approach is accuracy in modelling the power amplifier. The low modelling accuracy of the power amplifier depends on the independence of the nonlinear behaviour and memory effects. However, the dependent memory effects and nonlinear behaviour can be modelled by numerous linear filters and independent polynomial blocks, which interface by either three-block series connection or a feedback loop [181].

The nonlinear behaviour and memory effects are fully discussed in this work. Several methods have been established to provide linearization and compensating for memory effects. This can be shared into system models poised of either interacting or independent memory in nonlinear blocks. For high effective memoryless adaptive digital predistorter, an excellent method is essential to extract and optimize coefficients of the predistorter. The characterisation of RF power amplifier parameters and extraction of digital predistorter have been explained for 3^{rd} and 5^{th} order polynomial models of the weakly nonlinear systems. Nevertheless, there is no adequate information regarding the higher degree of nonlinearity [182]. The generalized fundamental frequency modelling technique has been developed for any amount of nonlinearity. The different methods proposed for logical illustration of the fundamental frequency signal and the in-band distortion components for any order of the Wiener model. These methods are fast, suitable and perfect for extraction of the predistorter coefficients for a given order of nonlinearity using compact formulas [183].

Several techniques have been proposed for parameter estimation of the Wiener and Hammerstein models. The improved adaptive version of Kalman filter blocks has been used to identify the linear identification of the nonlinearity, the Wiener and Hammerstein two-box models. The final design is a linear system based on the modified state parameters. An iterative algorithm is applied in the final design which is a linear system with regards to improved state parameters. The algorithm consists of the consecutive decomposition of a compound mapping approach. Bai [172] presented in his work, an optimal two-stage method for estimation of the Wiener and Hammerstein parameters. Firstly, least-square (LS) estimation has been used to approximate the parameters and singular value decomposition

(SVD) in the second stage for extraction. The same method has also been on a smooth nonlinear function. The identification method has been verified in terms of robustness by using with and without white noise. In addition, [183] also identified nonlinearity using a decomposition method. The first stage was to use real data to identify memoryless nonlinearity. A classic linear identification algorithm was used for the estimation of the remaining linear system parameters, after removal of the memoryless nonlinearity [184-186].

In modelling nonlinear RF power amplifier, several structures of the memoryless nonlinear model are recommendable for Wiener or Hammerstein system. The Wiener-based model was proposed by Clark in [143] for RF power amplifier with memory effect. The first block is a static linear based on an ARMA filter for the memory effect. Second is the static nonlinearity where the conventional Bessel series model is used in this case to model the memoryless nonlinearity. However, the identification method represented by the author is hard to implement, while in the small-signal system, the ARMA filter parameters require the first estimation through a frequency domain measurement. In order to accurately model the memoryless static nonlinearity, a dynamic exponential weighted moving average (DEWMA) algorithm was employed to the raw measured signal sampled at the input and output region of the transmitter. Then, a linear FIR filter simulates the memory effect [187, 188].

Few robust algorithms have been proposed for memory effect. In Volterra series, the parallel Wiener and parallel Hammerstein models are considered to be special cases. The parallel Hammerstein is similar to the memory polynomial model. Numerical stability is one of the major disadvantages of the memory

polynomial model based on nonlinear behaviour. Lack of stability occurs when higher-order polynomials are required and this is due to the matrix inversion to detect the coefficients of the model. However, the memory polynomial methods are seen as not accurate due to the shortcoming. As a substitute, a more robust algorithm such as the QR-decomposition can be used to implement the least mean algorithms in place of matrix inversion. To improve the modelling algorithm with more accuracy, a spare delay tap structure is applied to the memory polynomial model. Another method that can resolve the numerical instability problem when high order is by using an effective orthogonal polynomial model [160, 189, 190].

In case of the strong dynamic nonlinear behaviour of the RF power amplifier, the orthogonal polynomial model is not sufficient to model the memory effect with a linear filter. Consequently, the augmented Wiener model was developed for this strong dynamic nonlinear behaviour of RF power amplifier. A dynamic exponentially-weighted moving average algorithm is used to model the memoryless nonlinearity. The new algorithm can get rid of spreading of the modulated signal. An improved algorithm for filtering was also proposed to characterize both linear and nonlinear memory effects. In addition, a weak nonlinear dynamic FIR filter was proposed to replace the single LTI block [191, 192].

This work has made a contribution to design a robust algorithm to model the wideband RF power amplifier. This contribution covers nonlinearities as well as short and long term memory effects. The first model was proposed based on the Wiener system, while the second algorithm is developed according to the

enhanced adaptive Wiener system. The first model was developed with a new accurate algorithm for parameter approximation using Hilbert space. The enhanced adaptive Wiener system considered a weak nonlinear dynamic FIR filter instead of an LTI filter.

4.3.1 Wiener by Parameter Estimation Algorithms

A linear parameter estimation algorithm is developed for a behavioural model based on Wiener approach. In the system, the characteristics of the nonlinear static function are unknown while the structure is known. The RF power amplifier frequency-dependent transfer function is used in many applications. Hence, the frequency-dependent transfer function of an RF power amplifier can be written as:

$$z(t) = \left|F(s(t)\omega_n)\right| \cos(\omega t + \vartheta(t) + \angle(s(t)\,\omega_n)) \tag{4.27}$$

And the base-band OFDM signal can be expressed as:

$$r(t) = \sum_{k=-S/2}^{S/2-1} J_k e^{jk\Delta\omega t}, \quad \Delta\omega = \frac{2\pi}{T}\ 0 < t < T \tag{4.28}$$

Where J_k is modulation data symbols per carrier S is the total number of subcarriers, and T is the OFDM transmitted symbol. The OFDM transmitted signal expressed in (4.29) has been modulated to a frequency domain with up conversion to the carrier frequency (ω_c). This signal can be represented as:

$$y(t) = \mathrm{Re}\left\{r(t)e^{j\omega t}\right\} \tag{4.29}$$

Then, $y(t)$ can be extended as:

$$y(t) = \sum_{k=-\frac{N}{2}}^{\frac{N}{2}-1} |J_k| \cos((\omega + K\Delta\omega)t + \angle J_k) \quad (4.30)$$

Figure 4.14 has shown a Wiener system based model adjusted to fit the complex frequency-dependent polynomial in (4.27). It is the frequency-dependent transfer function of an RF power amplifier. There is a significant relationship between (4.27) and (4.30), such that (4.27) produces an exact illustration of the RF power amplifier once (4.30) is applied to it.

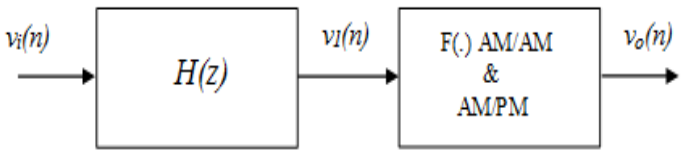

Figure 4.14: Wiener model for the power amplifier.

In the model, the OFDM input signal ($v_i(n)$) is sampled and the amplitude and phase modulation signal responses derived from single tone tests are used in the nonlinear block ($F(.)$) where the signals are described. The linear system (*H(z)*) represents the finite impulse response (FIR) filter. To identify the linear memory effect of the FIR filter, it is essential to know the information about the time history of the FIR filter input and output. It is, however, not easy or almost impossible to hold this information in a real transmitting system. So, to achieve the dynamic linear filter, the inverse of the static nonlinear system has to be identified before the measured output signal. The linear system (*H(z)*) which is the FIR filter can attain N number of unit delay sections using the cost function represented as:

$$C(n)=\sum_{k=1}^{K}\left|v_o(n)-v_m(n)\right|^2=\sum_{k=1}^{K}\left|e(n)\right|^2 \tag{4.31}$$

Where $v_o(n)$ is the output of the model $v_m(n)$ is the result obtained from the measurement and K is the number of respective sampled data. The cost function as expressed in (4.31) is the squared magnitude of the error between the output of the model and measured signal. The cost function can be minimized by adjusting the coefficients of *H(z)* in the least mean square (LMS) presentation. The modelled output of the Wiener system $v_o(n)$ can be expressed as:

$$v_o(n)=\sum_{p=1}^{P}c_{2p-1}v_1(n)^{2p-1}=F(v_1(n)) \tag{4.32}$$

Let the output of the linear block which is the intermediate variable be:

$$v_1(n)=\sum_{m=0}^{M}\mathrm{M}_m v_i(m-n) \tag{4.33}$$

Hence

$$v_o(n)=F\left(\sum_{m=0}^{M}\mathrm{M}_m v_i(m-n)\right)=\sum_{p=1}^{P}c_{2p-1}\left(\sum_{m=0}^{M}\mathrm{M}_m v_i(m-n)\right)^{2p-1} \tag{4.34}$$

Where c_{2p-1} is the amplitude and phase modulation responses which was been obtained from single-tone measurements. This is a place in the static nonlinear block representing the nonlinear power amplifier. M is the coefficients of the FIR filter, representing the dynamic linear system. M can be acquired by the adaptive LMS approach presented as follows:

$$\hat{\mathrm{M}}_m^{(n+1)} = \hat{\mathrm{M}}_m^{(n)} + \mu e(n)\left(\frac{\partial F(v_1(n))}{\partial \mathrm{M}_m}\right) \quad m = 1,\ldots,M \tag{4.35}$$

Where $e(n)$ is the mean square error expressed in (4.31). The source of the function ($F(.)$) with respect to the coefficients of the FIR filter, M is nonlinear. To estimate the intermediate variable, a linear approach using Hilbert space is used. The linear approach using the Hilbert space is an excellent way to provide an optimum estimation. In several approaches presented in the body of knowledge, developed a method in which F^{-1} and F are modelled by power series. To estimate $v_1(n)$, the inverse of F must be achieved. Hence, the estimated $v_1(n)$ can be expressed as:

$$\hat{v}_1(n) = F^{-1}(v_o(n)) = \sum_{l=1}^{L} \xi_{2l-1}(v_o(n))^{2l-1} \tag{4.36}$$

$\xi 2l\text{-}1$ is the coefficients of the inverse function of the nonlinear system ($F(.)$). To estimate the intermediate variable ($v_1(n)$), the few significant assumptions are made as follows:

- the nonlinear function must be invertible
- if the data is noiseless, the $v_1(n)$ must be utilized. In this case, the unknown FIR filter parameter M can be acquired from the normalized least mean square error method. The linear time-invariant (LTI) in terms of the unknown parameters is expressed as:

$$\hat{\mathrm{M}}_{m}^{(n+1)} = \hat{\mathrm{M}}_{m}^{(n)} + \mu \frac{(v_1(n) - \hat{v}_1(n)) v_i^*(n-m)}{\varepsilon + \left\| v_i(n-m) \right\|^2} \tag{4.37}$$

$\hat{v}_1(n)$ is defined by equation (4.36) and $v_1(n)$ is the intermediate variable expressed in (4.33). The μ represents the normalized step-size which is responsible for controlling the convergence speed and the stability of the algorithm. The OFDM signal ($y(t)$) must be kept small to avoid the problem in the least mean square algorithm caused by gradient noise amplification. The larger the $y(t)$, the convergence speed and stability of the algorithm cannot be controlled. Another method to keep the problem controlled is to adopt the NLMSE algorithm. The algorithm stabilises the LMS step size by $\|v_i(n)\|^2$ and introduces ε as a small positive number to ensure a similar problem does not occur when $\|v_i(n)\|$ becomes lesser.

Hilbert space is one of the pragmatic concepts of approximation. It is used in this case to approximate F^{-1} by finite-length polynomials. Using power series to approximate F, the independent sequence of vectors be expressed as $\{z^{2i-1}\}_{i=1}^{N}$, where z is the RF power amplifier input complex envelope signal expressed as:

$$\hat{F} = \sum_{i-1}^{N} \rho_i z^{2i-1} \tag{4.38}$$

ρ_i is the coefficients of the power series to define the RF power amplifier model. This can be explained as:

$$\begin{bmatrix} \langle z, z \rangle & \dots & \langle z^{2N-1}, z \rangle \\ \langle z, z^3 \rangle & \dots & \langle z^{2N-1,}, z^3 \rangle \\ \vdots & \vdots & \vdots \\ \langle z, z^{2N-1} \rangle & \dots & \langle z^{2N-1}, z^{2N-1} \rangle \end{bmatrix} \begin{bmatrix} \rho_1 \\ \vdots \\ \rho_N \end{bmatrix} = \begin{bmatrix} \langle F, z \rangle \\ \vdots \\ \langle f, z^{2N-1} \rangle \end{bmatrix} \quad (4.39)$$

The equation in (4.39) is expressed in matrix inversion, where the ρ_i coefficients are derived in the polynomial expression of F. The complex envelope ($F(.)$) has the transfer functions of the RF power amplifier in amplitude and phase modulation responses (AM-AM and AM-PM) which also represent the static nonlinearity in the nonlinear block. To expand the polynomials of the inverse F^{-1}, a new approach has been proposed by [193] to cope with the issue of numerical difficulties while using $\langle F^{-1}(z), z^{2i-1} \rangle = \int_{0}^{1} \xi_{2l-1} \; F^{-1}(\xi) d\,\xi$. In addition to the reason for this approach is the fact that there is no information in the body of knowledge where the inverse function F^{-1} is analysed. Hence, this approach can be used to estimate the matrix in equation (4.39). According to [193], the expression $\langle F^{-1}(z), z^{2i-1} \rangle$ can be written in this form as:

$$\langle F^{-1}(z), z^{2i-1} \rangle = \int_a^b z^{2i-1} F^{-1}(z)\, dz \quad (4.40)$$

Adjusting the variable in the form of $F^{-1}(z) = u$ or $F(u) = z$ expands the expression as:

$$\langle F^{-1}(z), z^{2i-1} \rangle = \int_{F^{-1}(a)}^{F^{-1}(b)} [F(u)]^{2i-1} u\, F'(u)\, du \quad (4.41)$$

This can be expressed further as:

$$\left\langle F^{-1}(z), z^{2i-1} \right\rangle = \frac{u}{2i}\left[F(u)\right]^{2i}\Big|_{F^{-1}(a)}^{F^{-1}(b)} - \frac{\int_{F^{-1}(a)}^{F^{-1}(b)} [F(u)]^{2i}\ du}{2i} \tag{4.42}$$

Equation (4.38) and (4.42) used to derive the polynomial representation of $F^{-1}(z)$ to the number of L order which can be expressed by:

$$F^{-1}(Z) = \sum_{l=1}^{\hat{L}} \xi_{2l-1} z^{2l-1} \tag{4.43}$$

$\xi 2l\text{-}1$ are the coefficients of power series expressing the inverse function. Unlike the approach used in [194] and [55] in which all the linear and nonlinear parameters of the two-box model are derived simultaneously. This implies that this proposed approach is more accurate and has no complexity.

4.3.2 Proposed Enhanced Adaptive Wiener Model

The concept of memory effects is generally discussed to explore the different classes which include linear and nonlinear memory effects [195]. The main sources of these memory effects are largely the wideband RF power amplifiers due to non-constant frequency response in the carrier frequency, the harmonic loading, bias circuit impedance variation at the envelope frequency and etc. The linear memory effects are mainly due to time delays or phase shift in the RF power amplifier matching network. The effects can also come from non-ideal frequency response which can be simulated using a linear filter. While the nonlinear memory effects are usually due to the bias network and trapping effects of RF power amplifier. A poor bias network design can cause impedance matching condition at the envelope frequency, matching condition at the harmonic components, impact ionization and trapping effects [195].

This research discussion is based on nonlinear memory effects caused by nonlinear RF power amplifier. The linear memory effects were model using the Wiener model as illustrated in Figure 4.14 above. This system can be improved in order to model the nonlinear memory effects by introducing the truncated Volterra filter before the static nonlinearity in the system as illustrated in Figure 4.15. Note that, the nonlinear memory effects and cross-terms are not acknowledged by LTI filter due to the interface between the earlier samples. As shown in Figure 4.15 the strength of the truncated Volterra filter towards the weak nonlinear system. The transfer functions extracted from the dynamic memory effect model has demonstrated a weak nonlinear behaviour. The truncated Volterra filter is used to represent the weak nonlinearity. The filter is also adequately represented for the cross-terms in the model [196].

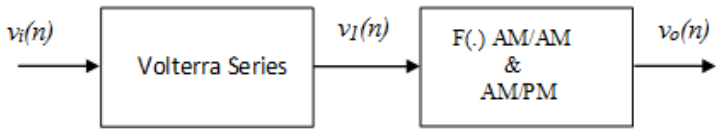

Figure 4.15 Enhanced adaptive Wiener model for PA.

Equation (4.44) expressed in discrete time for second-order Volterra series with finite memory systems:

$$v_1(n) = \sum_{i=0}^{M_1-1} q_1(i)\, v_i(n-i) + \sum_{i=0}^{M_1-1} \sum_{j=0}^{M_2-1} q_2(i,j) v_i(n-i) \left| v_i(n-j) \right| \qquad (4.44)$$

M_1 and M_2 represent the memory durations of the first and second-order terms. $v_i(n)$ and $v_1(n)$ are the complex input and output of the Volterra series block. $q_1(i)$ and $q_2(i, j)$ are the complex Volterra kernels of the nonlinear order 1 and 2. If the Volterra filter is required for a weak nonlinearity as well as cross-terms. To reduce

the complexity of the algorithm, a second-order term nonlinearity chosen. The series can be expressed in matrix form a follows:

$$v_1(n) = H^T Y = H^* Y \tag{4.45}$$

Where $M_1 = M_2 = M$ and

$$H = [q_1(0),..,q_1(M-1),q_2(0,0),..,q_2(0,M-1),q_2(1,0,..,q_2(1,M-1),.., \\ q_2(M-1,M-1)] \tag{4.46}$$

Then

$$Y = [v_i(n),\cdots,v_i(n-M+1),v_i(n)|v_i(n)|,\cdots,v_i(n)|v_i(n-M+1)|,\cdots, \\ v_i(n-1)|v_i(n-M+1)|,\cdots,v_i(n-M+1)|v_i(n-M+1)|] \tag{4.47}$$

It can be seen from expressions (4.46) and (4.46) that the Volterra series coefficients are linear. When the NLMSE algorithm is incorporated, the filter coefficients are acquired by:

$$H^{(n+1)} = H^{(n)} + \mu \frac{e(n)^* Y}{\varepsilon + \|Y\|^2} \tag{4.48}$$

Then, $e(n)$ is expressed as:

$$e(n) = v_1(n) - \hat{v}_1(n) \tag{4.49}$$

Where $v_1(n)$ and $\hat{v}_1(n)$ are previously expressed in (4.36) and (4.46).

6.3.2.1 Summary of the Most Used Algorithms for Characterization of RF Power Amplifiers Nonlinear Behaviour.

- Amplitude and phase modulation (AM-AM and AM-PM) measurements using multiple tone signals: This test involves test equipment, not suitable for digital predistortion and amplitude measurement errors reduce the calculated phase accuracy.
- Dynamic AM-AM and AM-PM measurement: This test involves test equipment, not suitable for digital predistortion.
- Application of power series in nonlinear gain modelling: Involves static measurements and not suitable for digital predistortion.
- Polynomial model: The model not adequate for transmitters with memory effects.
- Memory polynomials: Cross terms between the previous time samples not considered. However, considers the linear and nonlinear memory effects.
- RBFNN (neural networks): Not applicable for the signal with non-constant envelope signal.
- Volterra series: Too many parameters are to be identified for practical purposes when models of high nonlinear order and with in-depth memory length are involved.
- Hammerstein: Not effective on nonlinear memory.
- Parallel Hammerstein: Cross terms between the previous time's samples not considered. However, considers the linear and nonlinear memory effects.
- Wiener: Not effective on nonlinear memory.

- Augmented Wiener model: Cross terms between the previous time's samples not considered. However, considers the linear and nonlinear memory effects.
- Enhanced Adaptive Wiener model (including the truncated Volterra series): Involves the cross-terms as well as linear and nonlinear memory effects.
- Twin Nonlinear Two-Box Models: Involves the cross-terms as well as linear and nonlinear memory effects.

4.4 Summarized Conclusion

A new algorithm to identify parameters of the Wiener model has been presented. This contribution covers nonlinearities as well as short and long term memory effects. The first model was proposed based on the Wiener system, while the second algorithm is developed according to the adaptive enhanced Wiener system. The first model was developed with a new accurate algorithm for parameter approximation using Hilbert space. The adaptive enhanced Wiener system considered a weak nonlinear dynamic FIR filter instead of an LTI filter.

It was assumed that the static nonlinearity is identified where the parameters of the linear dynamic block and the nonlinear system are approximated. The benefit of the proposed techniques is that the parameters of the linear dynamic block and the static nonlinear system can be known concurrently without any information about the transitional signals.

CHAPTER 5

Improving Efficiency in the Design of Linear RF Power Amplifiers

5.1 Introduction

RF power amplifier is an important device not only in wireless communication systems, but also in TV transmission, radar systems and RF heating. The amplitude of the radio frequency signal is increased to a certain level of amplification [197, 198]. Spectral efficiency and linearity are the main elements driving the design of the power amplifier. The most challenging aspect of power amplifier concept is achieving an excellent efficiency with high linearity [40]. However, the design has to be accomplished in accordance with the system specifications, such as operating frequency, bandwidth, output power, gain, linearity, efficiency and return loss [135]. According to [199], linearity is required to sustain information for error-free transmission. Efficiency reduces power consumption and improves battery life span at the mobile station [200].

The effect of spectral regrowth in the power amplifier has become a major concern in communication systems engineering [201]. This effect causes evident existence of nonlinearity on the frequency band which can lead to transmission power loss and adjacent channel interference. To reduce the effect of nonlinearity and achieve state-of-the-art system, the power amplifier must be designed carefully to give a high data rate and spectral efficiency. A healthier design of power amplifier is a suitable application for technologies such as Orthogonal Frequency Division Multiplexing (OFDM), Multiple-Input-Multiple-Output (MIMO) and the recent technology on research called spatial modulation system, 5^{th} Generation systems and many more applications. The goods of these technologies include higher data rate and higher spectral efficiency in 20 MHz

signal bandwidth. The downlink data rate of 100 MB/S and the uplink rate of 50 MB/S are obtainable [198, 202].

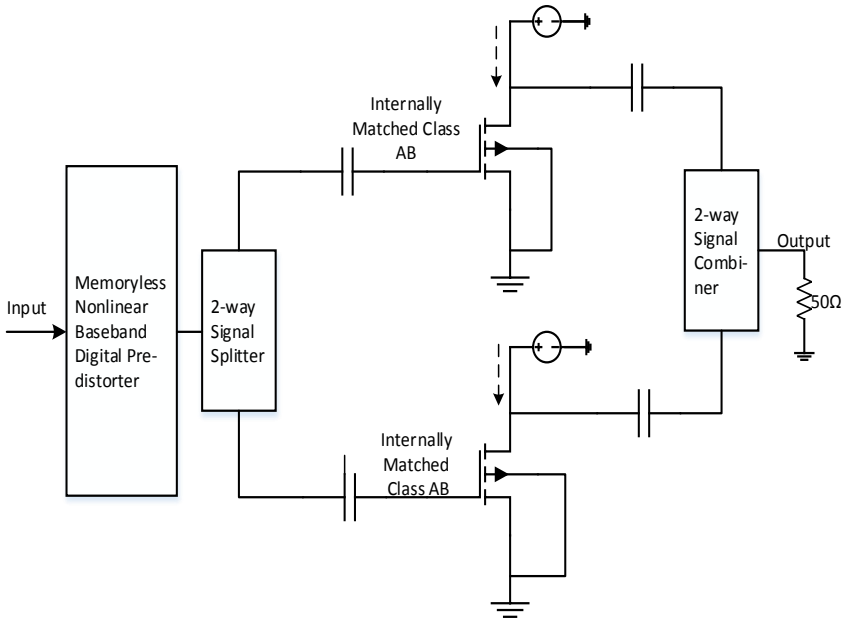

Figure 5.1: The schematic diagram for the double stage RF power amplifier.

This chapter discusses balanced RF power amplifier design, simulation and implementation. A lateral MOSFET transistor model is used for the design of the amplifier. Having cited that balanced RF power amplifier as a suitable candidate for LTE base station, it also provides high efficiency with a dynamic range of linearity to meet the even characteristics of 5^{th} generation applications. The balanced RF power amplifier acquires high power density factor and robustness, which for that reason has been chosen to work for LTE application [3, 8, 203].

5.2 A Proposed Balanced RF Power Amplifier Design Architecture

Figure 5.1 illustrates the typical schematic diagram of the balanced RF power amplifier. The amplifier is a cascaded system with two transistors opposite to each other. The two amplifiers share the same input and output. They have parallel output power capability, but different in the biasing circuit. The two

amplifiers are operating in class AB with the first one in the first carrier stage and the second one in the second carrier stage respectively. At this point, the first carrier stage is referred to the first amplifier, while the second carrier stage refers to the second amplifier. The signal from the input is divided equally using a 3 dB signal splitter. The splitter is designed with 90^0 phase difference and same amplitude, to drive the two cascaded class AB amplifiers. The outputs of both amplifiers are connected to a combiner which collects the amplifiers signals to the final stage of amplification [8, 204].

The balanced RF power amplifier attains high efficiency as a result of output power back-off over the traditional single-stage amplifier. Hence, the multicarrier applications are affected by nonlinear distortion due to PAPR which the efficiency of the power amplifier can be enhanced by the used of efficiency enhancement and linearization techniques.

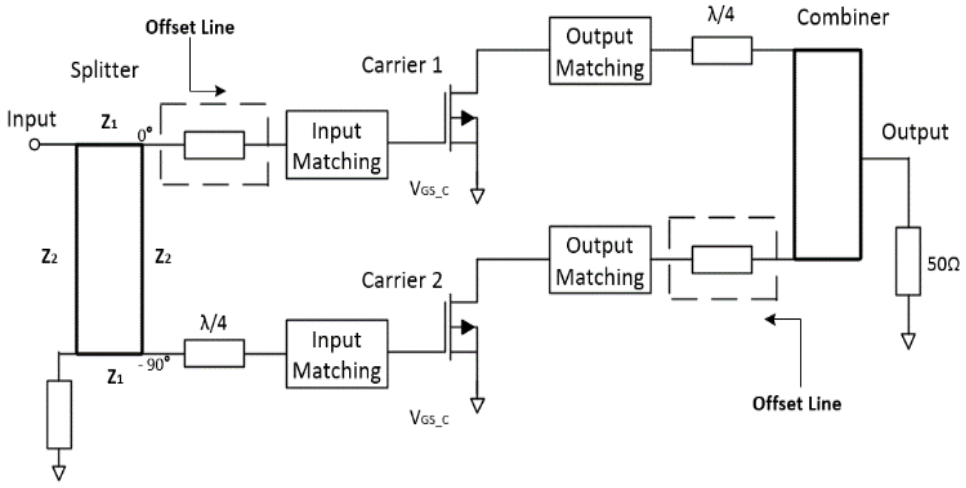

Figure 5.2: Proposed schematic diagram of the balanced RF power amplifier with offset lines.

Figure 5.2 has shown a proposed balanced RF power amplifier with two amplifiers parallel to each other, while having equal output power capability. The

two amplifiers have the same bias point which means they are both carrier amplifier stage operating in class AB mode. The phase difference between the two amplifiers is a 90^0 phase shift. A special signal splitter was separately designed for the input. A coupler was also designed for the output. Independent measurements were taken in term of operational bandwidth and frequency response for both the splitter and the output coupler. In the design, no mode was chosen to behave as the carrier amplifier. Both amplifiers operate at a similar time and capable of improving efficiency. Resonator circuits are applied to the input of the first carrier and output of the second carrier. These acts as the summing circuits which act as a phase difference signal compensator. The circuits constructively supplement the signal from the two amplifiers to the output load. The quarter-wave transmission line is similarly applied to the input of the second carrier and the output of the first carrier [203, 205, 206]. According to the study, the proposed balanced RFPA design complexity increases and equally improves the efficiency with a wide range of linearity which will be discussed in the next section [8].

5.2.1 Circuit Design Analysis

This circuit design derives and demonstrates the equation that runs the relationship between input current (I_i) and input voltage (V_i) to the output current (I_o) and output voltage (V_o) in the transmission line, showing how the frequency-dependent impedance of the material presents the attenuation and distortion of the high-frequency signal as presented in matrix form [19, 207].

$$\begin{bmatrix} V_i \\ I_i \end{bmatrix} = \begin{bmatrix} \cosh \pi/2 & z_o \sinh \pi/2 \\ 1/z_o \sinh \pi/2 & \cosh \pi/2 \end{bmatrix} \begin{bmatrix} V_o \\ I_o \end{bmatrix} \quad (5.1)$$

The source impedance $Z_i = V_i/I_i$, Z_o is the characteristic impedance of the transmission line, while Z_L is the load impedance given as $Z_o = V_i/I_i$. Hence, the source impedance Z_i can be expressed as:

$$Z_i = \frac{Z_L \cos \pi/2 + jZ_o \sin \pi/2}{j(Z_L/Z_o)\sin \pi/2 + \cos \pi/2} \tag{5.2}$$

From the wave equation to the relationship between voltage and current, quarter-wave transmission line source, Z_i can be defined by:

$$Z_i = \frac{V(-l)}{I(-l)} = Z_o \left[\frac{V_o^+ (e^{j\beta l} + \Pi e^{-j\beta l})}{V_o^+ (e^{j\beta l} - \Pi e^{-j\beta l})} \right] \tag{5.3}$$

This can be expressed by impedance function in:

$$Z_i = Z_o \left[\frac{\left[e^{j\beta l} + \left(\frac{Z_L - Z_o}{Z_L + Z_o} \right) e^{-j\beta l} \right]}{e^{j\beta l} - \left(\frac{Z_L - Z_o}{Z_L + Z_o} \right) e^{-j\beta l}} \right] \tag{5.4}$$

This equation can be expanded by:

$$Z_i = Z_o \left[\frac{Z_L \left(e^{j\beta l} + e^{-j\beta l} \right) + Z_o \left(e^{j\beta l} - e^{-j\beta l} \right)}{Z_o \left(e^{j\beta l} + e^{-j\beta l} \right) + Z_o \left(e^{j\beta l} - e^{-j\beta l} \right)} \right] \tag{5.5}$$

and this can be extended in sine waveform as:

$$Z_i = Z_o \left[\frac{Z_L (\cos \beta l) + jZ_o (\sin \beta l)}{Z_o (\cos \beta l) + Z_L (\sin \beta l)} \right] \tag{5.6}$$

Finally, the impedance, Z_i looking into the transmission line is given by:

$$Z_i = Z_o \left[\frac{Z_L + jZ_o \tan(\beta l)}{Z_o + jZ_L \tan(\beta l)} \right] \tag{5.7}$$

Figure 5.2 has shown the two-stage balanced RF power amplifier with a quarter wavelength at the output of the first carrier and the input of the second carrier amplifier respectively. These act as the basis for the impedance to stay low when the two carriers are on the active stage [8].

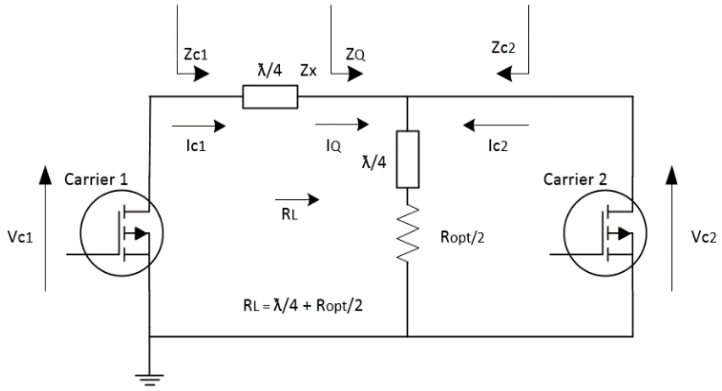

Figure 5.3: Current and voltage analysis diagram for balanced RF power amplifier.

Figure 5.3 shows a balanced RF power amplifier analysis diagram which will be used for the current and voltage analysis. The phase output current of the first carrier (I_{c1}) leads the phase output current of the second carrier (I_{c2}) by 90^0. This implies that the phase difference of the splitter is separating the two amplifiers by 90^0 phase shift. Nevertheless, the operating principle of the balanced amplifier two-stage load modulation can be derived by splitting the level of the input signal to high-level drive. In this mode, first carrier (I_{c1}) and second carrier (I_{c2}) are set to be turned on and there will be current flow through the circuit. When the balanced amplifier is in on-state, the current envelope can be expressed as:

$$I_{c1} = \frac{I_{\max}}{6}(1+x). \tag{5.8}$$

$$I_{c2} = \frac{I_{\max}}{3} x \tag{5.9}$$

At the passband drive, the x component will have a value of 1, where the two carrier amplifiers will turn on. The effective impedance (Z_Q) has a pulling influence on both carriers at the load as expressed below:

$$Z_Q = R_L \left[1 + \frac{I_{c2}}{I_Q} \right] \tag{5.10}$$

and

$$Z_{c2} = R_L \left[1 + \frac{I_Q}{I_{c1}} \right] \tag{5.11}$$

Where the resistive impedance of the quarter wavelength increases, the two carrier amplifiers act as load modulation. The quarter wavelength transmission line input, output transformation and the characteristic impedance can be expressed by:

$$Z_{c1} = \frac{Z_x^2}{Z_Q} \tag{5.12}$$

The output impedance can be substituted to effective impedance (Z_Q) with the quarter wavelength transmission line (Z_x) and can be seen by both amplifiers. The output impedance is written as:

$$Z_{c1} = \frac{Z_x^2}{\left[R_L \left(1 + \frac{I_{c2}}{I_Q} \right) \right]} \tag{5.13}$$

The effective output voltage V_{c1} of first carrier amplifier is expressed by:

$$V_{c1} = Z_{c1} I_{c1} = I_{c1} \left[\frac{Z_x^2}{R_L \left(1 + \frac{I_{c2}}{I_Q} \right)} \right] \tag{5.14}$$

Since $I_Q = V_{c1}/Z_x$ then output voltage becomes:

$$V_{c1} = \frac{I_{c1} Z_x^2}{R_L \left(1 + \frac{I_{c2} Z_x}{V_{c1}} \right)} \tag{5.15}$$

I_{c1} and I_{c2} have been substituted into Z_{c1} to become:

$$V_{c1} = \left(\frac{Z_x}{2R_L} \right) (I_{\max}) \left(Z_x (1 + x) - 2R_L x^2 + R_L x \right) \tag{5.16}$$

But $R_L = R_{opt}/2$. Hence the output voltage will be:

$$V_{c1} = \left(\frac{Z_x}{R_{opt}} \right) (I_{\max}) \left(Z_x (1 + x) - 2 \frac{R_{opt}}{2} x^2 + \frac{R_{opt}}{2} x \right) \tag{5.17}$$

Then $Z_x = R_{opt}$

$$V_{c1} = R_{opt} I_{\max} \left(-x^2 + \frac{x}{2} \right) \tag{5.18}$$

Finally, the mathematical illustration has shown that the output voltage maintains the stability at a high stage when the two carriers remain in the active stage. The output voltage increases significantly.

5.2.2 Circuit Design

This section describes step by step the design of proposed balanced RFPA using the commercial software Agilent Advanced Design System. The complete design flow presents two cascaded class AB connected opposite each other as shown

in the Figure 5.1. It is very essential before the design to observe the amplifier requirements, thermal and electrical specifications with regards to application the amplifier is to be designed. Next is to properly select the active device of interest which is the type of transistor to use for the design. The outline of the design steps of the proposed balanced RFPA include:

- Designing and simulating the DC I/V characteristics.
- DC bias point selection.
- Design the bias network.
- Design and simulate S-parameter for linear-nonlinear situation for stability.
- Considering the impedance matching which covers input and output of the amplifier.
- Use micro strip transmission lines in the design in the first design which is the class AB RFPA.
- Simulate the design and evaluate the return loss, gain and power added efficiency of the first design.
- Design and simulate the 3 dB 2-way 90^0 hybrid coupler.
- Combine and simulate the two class AB RFPAs to provide the proposed balanced power amplifier.
- Design the layout of the balanced power amplifier and fabricate the prototype.

Consequently, in this work, a proposed balanced RFPA is designed within 2.620-2.690 GHz frequency range and discussed by the use of two transistor models for LTE base station to provide efficiency with a dynamic range of linearity. Dynamic load adaptation is provided by the use of transmission line impedance

inverter of 50 Ω quarter wavelength. In the design of balanced RF power amplifier, there are stages that are necessary to adhere to, for the high-level performance of the entire system [8, 208, 209].

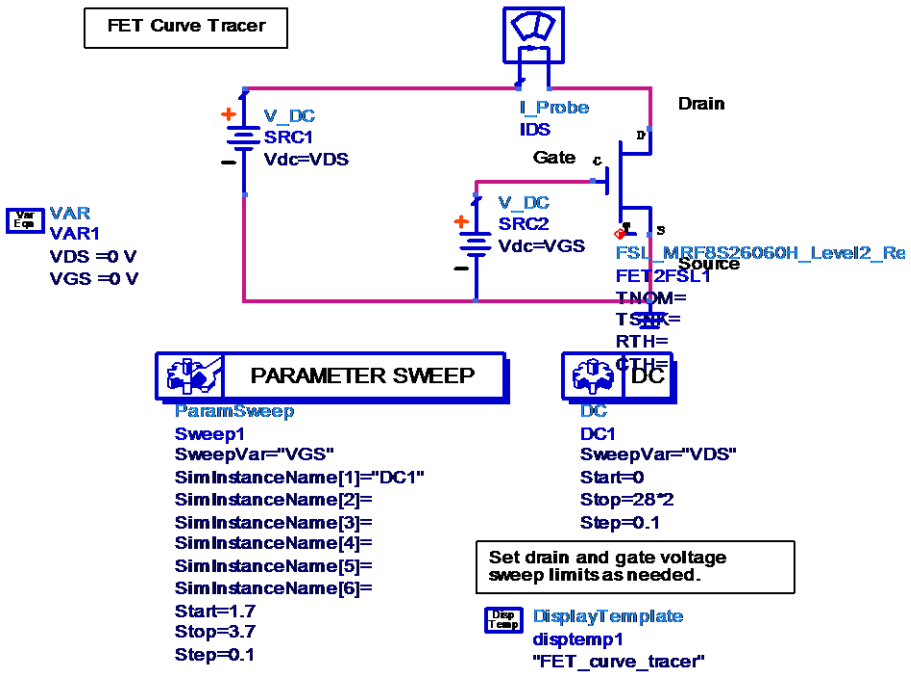

Figure 5.4: DC IV simulation circuit.

The first thing to do in the design steps is to design the DC simulation circuit as illustrated in Figure 5.4. Simulation of the DC circuit is to determine the bias point and bias network. This is according to the class of operation and power requirement.

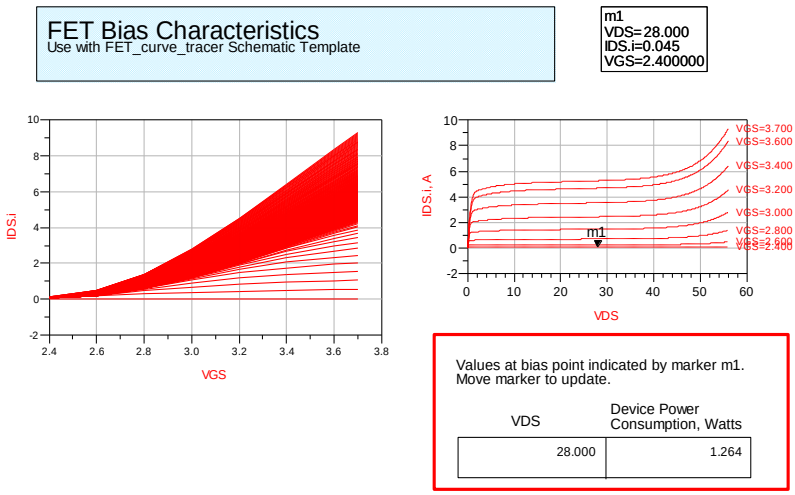

Figure 5.5: DC IV simulation results.

The bias condition set drain-source voltage (V_{ds}) = 28 V, gate-source voltage (V_{gs}) = 2.4 V and drain-source current (I_{ds}) = 45 mA shown in Figure 5.5.

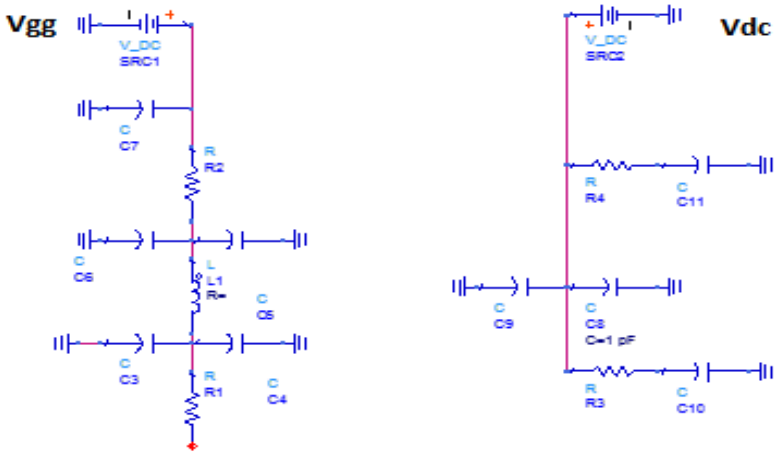

Figure 5.6: Bias selection circuit.

The bias network as shown in Figure 5.6 is designed based on class AB carrier. The DC simulation results specify the class of operation. The main purpose of good biasing is to prevent signal reflection. The DC quiescent current is obtained to prevent signal distortion.

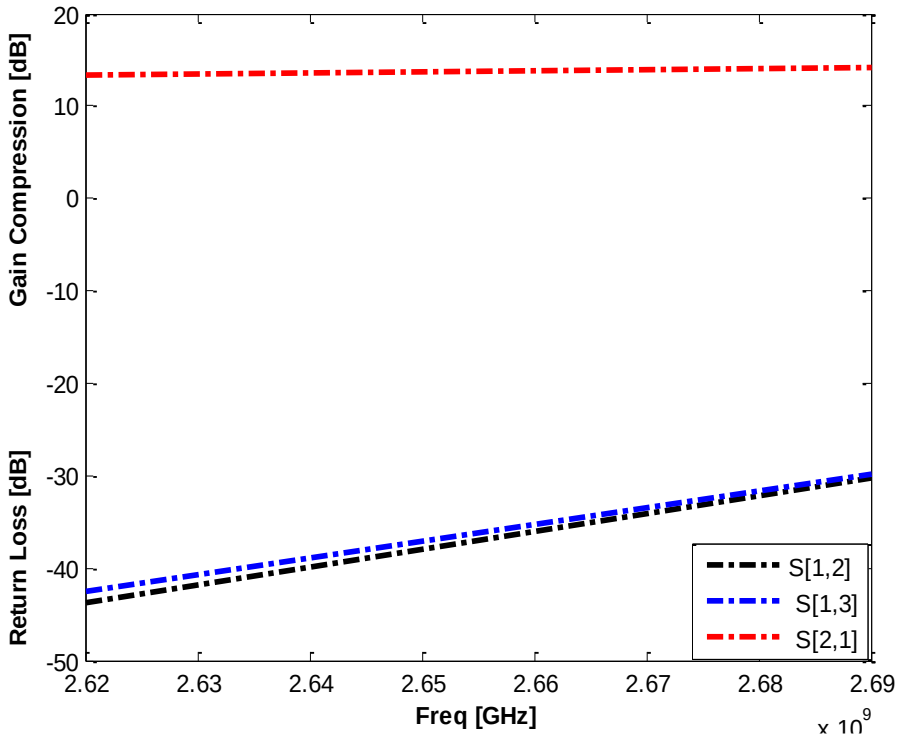

Figure 5.7: Linear simulation of return loss and gain of a balanced RF power amplifier.

The radio frequency is prevented from going back to the DC source. Regards to the matching network, this transistor requires no matching process, as the input and output impedance are internally matched. The 21 mm length of micro strip line are connected using line calc from ADS simulator with RT 5880 substrates, parameters; Er = 2.2, H = 0.508 mm, zo = ohms, T = 3 µm and Tan d = 0.017. The 50 Ω impedance of the 90^0 open and short circuit is incorporated to the right angle of the RF blocking transmission lines. A class AB power amplifier elements values have been positioned using tune tool of the Agilent advanced design simulator for best performance of the proposed system.

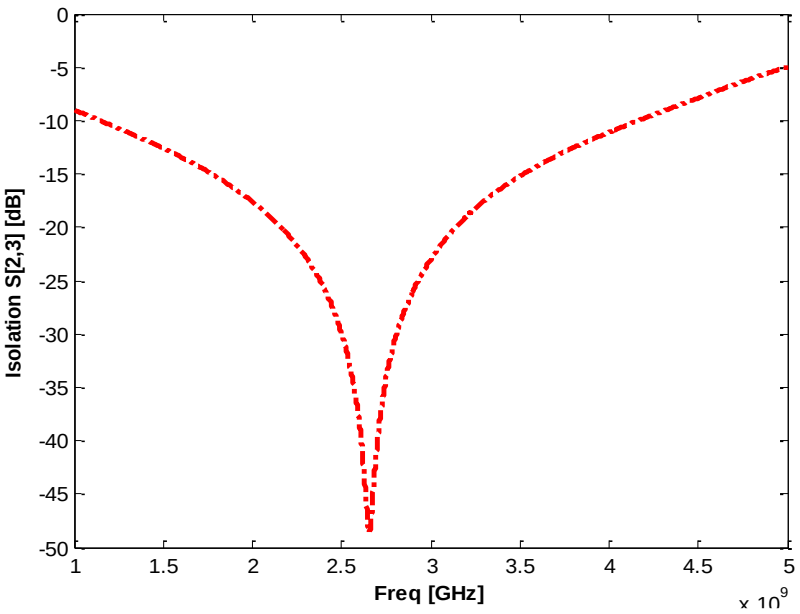

Figure 5.8: Isolation response over the operating bandwidth.

In order to choose the best model, single tone and two-tone tests have been conducted in terms of efficiency, power and linearity [8, 210].

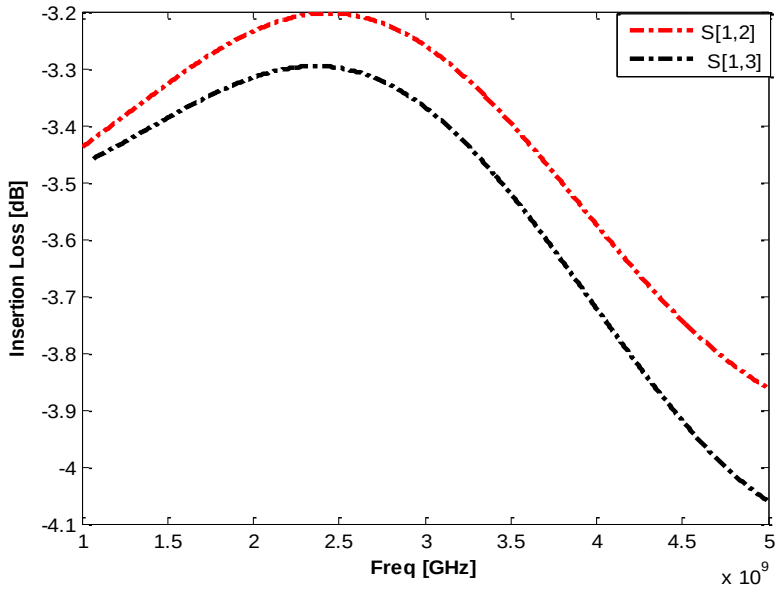

Figure 5.9: Insertion loss response of the coupler.

Linear and nonlinear simulation result were obtained from class AB design. The linear response is shown in Figure 5.7 where flat gain, s(2, 1) is almost 14 dB, the return loss, s(1, 1) and s(2, 2) also obtained at 1 dB compression point [8].

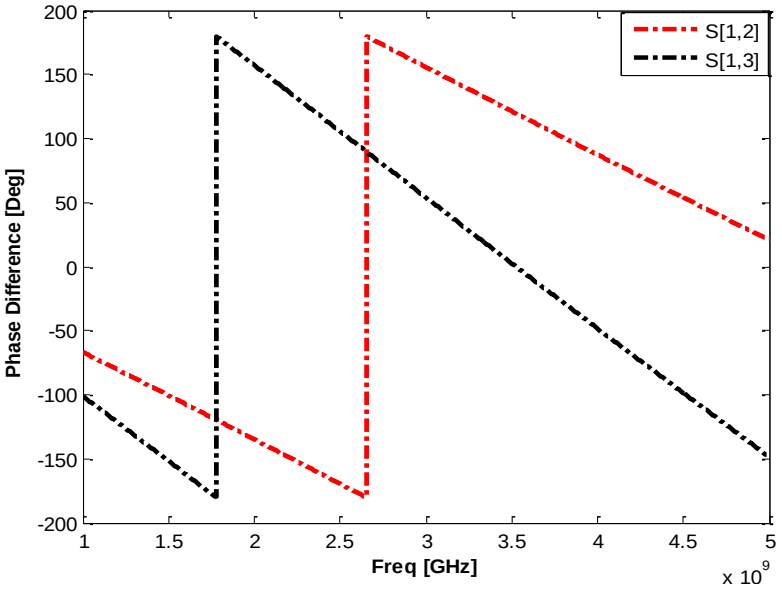

Figure 5.10: Phase difference across port 1-2 and 1-3.

The nonlinear single tone simulation result of class AB amplifier was realised. The output power is up to 39 dBm, while efficiency is up to 29% respectively. A 3 dB 2-ways 90^0 hybrid coupler was designed to split the input signal into two equal part, using 100 Ω impedance for optimum resistance to achieve 90^0 phase difference between the first and the second carrier amplifier. Since the carriers biases are in the same mode, the output impedance of the two amplifiers are similar, the input and output matching circuitry are also similar [211].

To couple a balanced RF power amplifier, impedance transformer is used as a coupler at the output of the two amplifiers. The 2-ways coupler was designed based on the series of tests carried out, while significant results seen in Figure 5.8, 5.9, and 5.10 have been achieved. However, in the design of the balanced RF amplifier, a good coupler can contribute to the overall efficiency of the system [211].

5.3 Implementation

The balanced power amplifier was designed and implemented using ADS software with RF field-effect Si-LDMOS 15.5 W transistor at 2.620-2.690 GHz frequency band. The final stage balanced RF power amplifier circuit is fabricated with RT 5880 substrates, H=0.5 mm and relative permittivity of 2.2. Figure 5.11 shows the layout of the proposed amplifier. In order to experimentally verify the amplifier circuit topology, the Agilent advanced design system-generated micro strip layout was used. The layout was exported as Gerber files from ADS and it was milled on a printed circuit board known as PCB. Note that metal pads have been added in the layout as ground plane and power supply connection in the layout [8]. Furthermore, the amplifier has been subjected to following mechanical engineering:

- The length of the cooling ribs was cut to fit the card
- Holes for the transistor was milled out
- A total number of 44 screw holes were threaded into the board
- 4 for the transistors
- 36 for in and outsides of the board
- 4 for each SMA connectors

The screws were positioned to have minimal impact on the scattering field from the lines. At the same time, it was necessary to place multiple screws relatively close to the transistor in order to provide good signal ground at this point. The same procedure was done with screws at each SMA connector. The components were fitted on the finished circuit board.

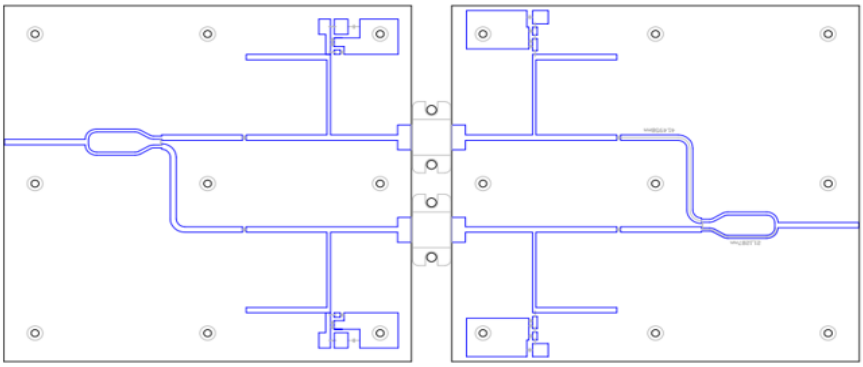

Figure 5.11: Layout.

The complete conventional balanced RF power amplifier circuit is fabricated with RT 5880 substrates, H=0.5 mm and relative permittivity of 2.2. The RT/duroid 5880 high-frequency laminate from Rogers-corporation is used. The substrate material is good for micro strip and strip-line applications. Because of the uniform dielectric constant over a wide range of frequency and the low dissipation factor of RT/duroid 5880, it extends its usefulness compared to FR-4 substrate in high-frequency Ku-band and above. The line calc application from ADS is able to calculate the width and the length of the micro strip line given the characteristics impedance and electrical distance or vice versa at 2.655 GHz. Some important characteristics of RT/duroid 5880 such as dielectric constant, the height of board and conductivity are defined in ADS line-calc [8].

After verifying the impedances in schematic and layout, the Gerber files are created from the layout and the circuit is milled on the RT/duroid 5880 board. During the RF operation, heat generation of the transistor would be one of the biggest problems causing performance degradation. Therefore, the transistor has to be mounted right on a heat sink in order to diffuse generated heat. In this project, a large piece of the aluminum plate will be used as a heat sink and the skeleton to support the RFPA.

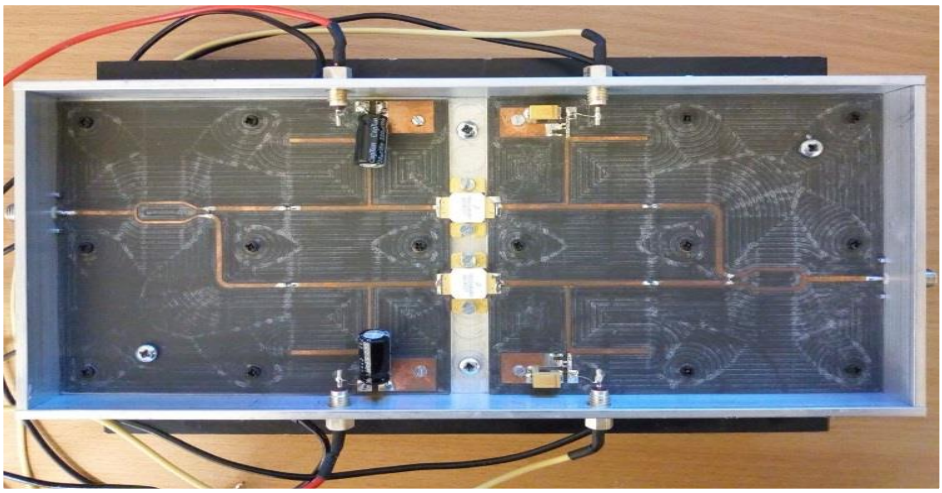

Figure 5.12: Implemented prototype of proposed balanced RF power efficient power amplifier.

The transistor is mounted on the aluminum plate with thermal paste glued in between in order to maximize heat transfer. The RFPA consists of two parts, the input board and the output board. SMA connectors are inserted at the input and output terminals. Banana plugs must be used for power connection as required by the competition rules. Vias are created by putting the wire through drilled holes or inserting long copper tape through cut slits as connection bridges between the top and bottom ground planes. Is to cover as much area as possible on the amplifier in order to provide the same reference level between the top and bottom ground planes. Components are then soldered on the board. 300 pF capacitors are used as coupling capacitors at the input and output board. 1/1000/33 pF capacitors are used as a decoupling capacitor in the gate bias. 1/1000/33 pF capacitors are put in parallel and used as decoupling capacitors in drain bias [8].

5.3.1 Results and Discussion

The proposed balanced RF power amplifier consisting of two similar class AB amplifiers have been measured. The results have shown quite a few kinds of

signal waveforms to characterize the best of performance and the best choice for LTE base station applications. Figure 5.13 has shown the efficiency results of the balanced RF power amplifier in comparison with a conventional class AB power amplifier. The performance results of amplifier response to 52% PAE, 41 dBm output power and 14 dB gain. The result of the conventional class AB amplifier is low with 29% PAE, 39 dBm P_{out} and 15 dB gain shown in Figure 5.13.

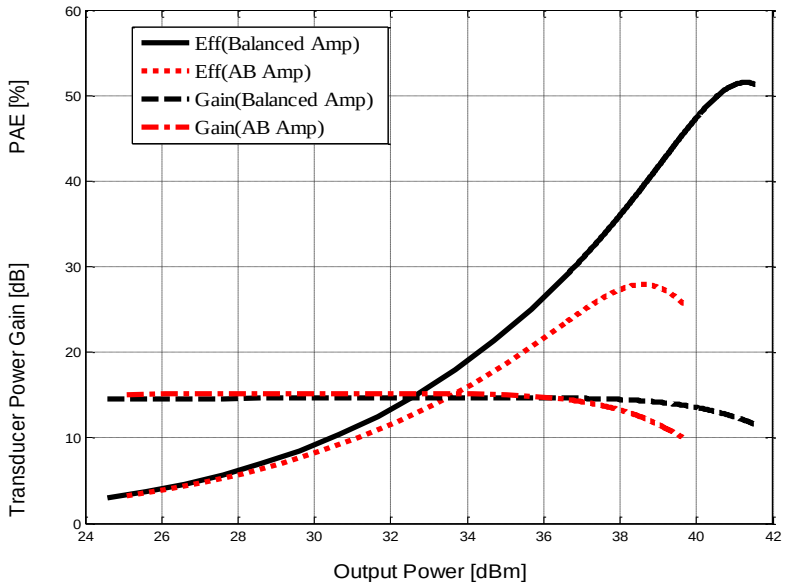

Figure 5.13: Simulated PAE and gain characterization for class AB and the proposed balanced power amplifier.

A linear simulation for the balanced RF power amplifier was performed using ADS and results obtained over the centre frequency of 2.655 GHz band. The gain is flat, excellent input and output return loss were achieved as well. The nonlinear simulation of a balanced power amplifier was performed. The following results are based on a single tone test and are characterized as AM-AM and AM-PM responses, transducer power gain, output power and efficiency as well [203]. The performance comparisons between the amplifier and class AB amplifier have been shown. The output power of the class AB amplifier design was 39 dBm, while the output power was increased to 41 dBm for the balanced amplifier. The

PAE for both class AB and balanced amplifier is 29% and 52%. Results of the simulation have demonstrated considerable improvement from the design of the balanced RF power amplifier [203].

Figure 5.14 shows the results of AM-AM and AM-PM curve from the amplifier. AM-AM and AM-PM are very important parameters which can be loaded onto a pre-distorter. A typical example is a WLAN IEEE 802.16 OFDM transceiver system. AM-AM and AM-PM coefficients, extracted from one tone test can be used in MATLAB. Curve fitting tool in MATLAB converts the AM-AM and AM-PM coefficients into polynomials to generate a memoryless model, and this signal was applied for linear and nonlinear digital predistortion [8].

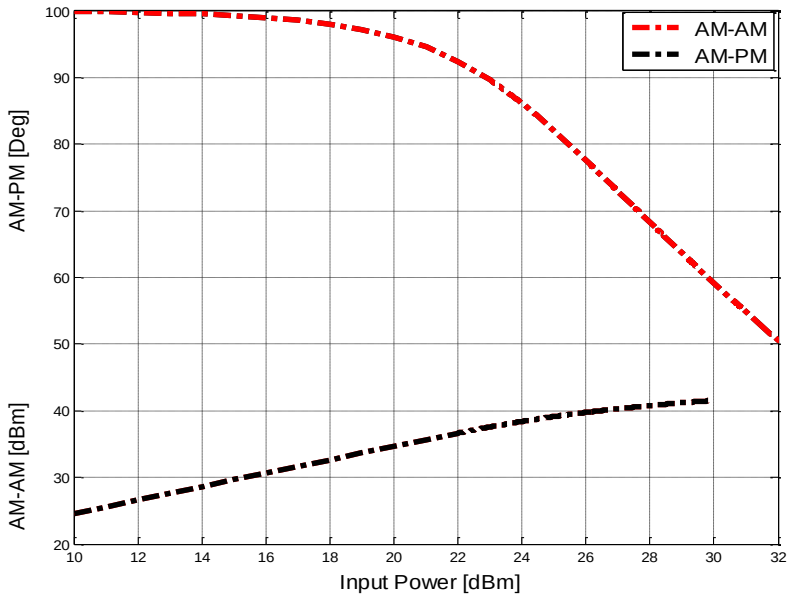

Figure 5.14: AM-AM and AM-PM characterization of balanced RF power amplifier.

The proposed amplifier has undergone a simulation test on the design circuit and measurement on the fabricated circuit. The phase variation of the power amplifier using various frequencies to report the differences at some points. The

measurement includes PAE, gain and linearity of the amplifier is to be observed by means of looking at the power from the input to the power at the output.

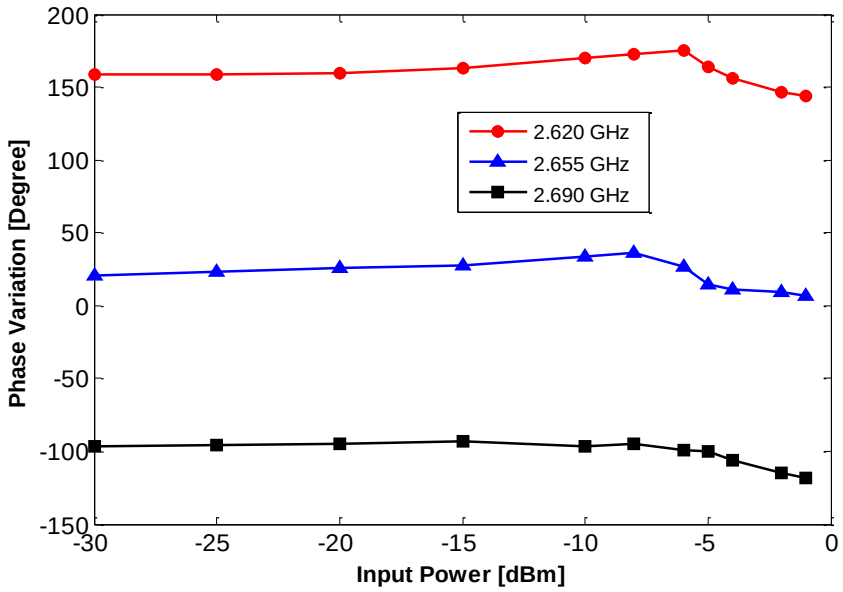

Figure 5.15: Phase variation of the proposed balanced RF power amplifier.

Figure 5.15 shows the phase variation of the amplifier which was derived as a function of the input power level. The result shows a range of frequency band used which is within the LTE mobile frequency level. The phases of the amplifier path are almost fixed along with bias condition throughout the range of the power used in the amplifier. There is no record of phase variation between the first carrier and second carrier in the low or high power region. The reason behind this development is because the amplifier consists of similar systems in both carriers. Nevertheless, the result shows power derive has increased at the output level when compared with that of input as the phase variation through both carriers path is almost close. It is assumed that a small drop at the full drive and both signals will look equal and disappear.

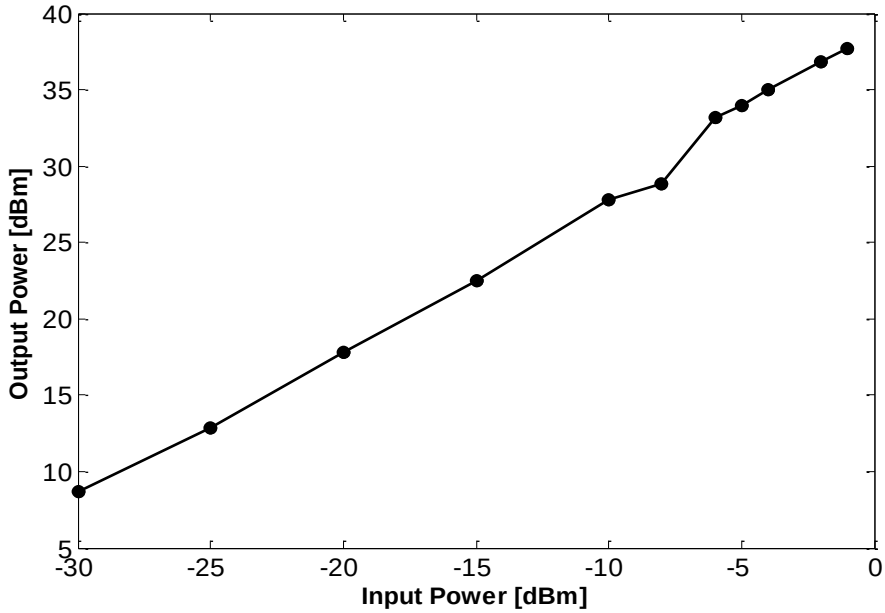

Figure 5.16: Output versus the input power of the balanced RF power amplifier.

The power that has been used between the input and the output of the amplifier is shown in Figure 5.16. It represents the evaluation of the phase variation of the signal. And this clearly shows how much power has been derived through the amplifier. Up to 37 dBm output power has been accomplished at the linear region of the amplifier.

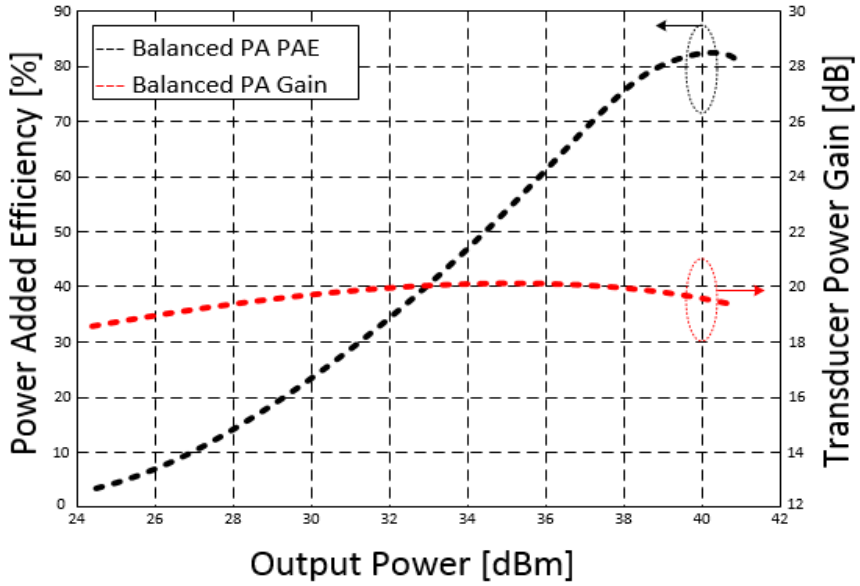

Figure 5.17: Measured results of the proposed balanced RF power amplifier with improved power added efficiency and gain.

Figure 5.17 shows the performance of the amplifier through measured PAE and gain. The same frequency range of 2.620-2.690 GHz has been used for the simulation as well as the measurement. 1 dB compression point of the amplifier was used to obtain up to 40 dBm of the output power, because of the two cascaded class AB amplifiers working actively at the same time. However, the balanced amplifier output saturation power (P_{sat}) point reached up to 40.90 dBm. The power added efficiency of the balanced amplifier at 40 dBm and 40.90 dBm were 83% and 81.5% respectively. While the gain of the amplifier reached up to 20 dB which was reduced to 19.5 dB before the saturation point. Increase in gain and PAE improves the linearity of the amplifier. This is attributed to the input and output offset lines used in the design and fabrication. This performance shows that the design and fabrication of the proposed balanced RF power amplifier have achieved a substantial improvement in this class of power amplifiers.

Table 1 shows the performance of present work in comparison with few selected PA's reported in the literature, taking account of operating frequency, output power, efficiency and gain. In [197, 212] a power amplifier consists of up to 54% PAE at 2.14 GHz operating frequency is presented. The design presented a two-stage line-up Doherty amplifiers consisting of a High Voltage HBT Doherty final design is cascaded with a 20 W LDMOS Doherty driver, exhibiting up to 325 W (55 dBm) power to improve the gain to 30 dB. In the case of [200, 213], a high power hybrid envelop elimination and restoration transmitter were designed using GaN High Electron Mobility Transistor at 2.655 GHz operating frequency. The design introduced a conventional hybrid switching amplifier with up to 71.2% PAE. However, the efficiency of H-EER transmitter reduced down to 37.04% at 41.18 dBm P_{out}. In [201, 214], a conventional balanced amplifier with 90^0 Branch

Line Hybrid Coupler (BLHC) was used to achieve power matching rather than maximum high gain. The impedance matching is not excellent and there is an inherent out-of-phase characteristic cause from the properties of 90^0 BLHC. To improve the performance and correct the high signal reflection, an auxiliary amplifier was added to the conventional balanced amplifier design, only to increase the PAE to 33.4%. The design for [208, 215] uses up to 250 W output power at saturation to achieve drain efficiency of 60%. The final 40 W GaN-HEMT Doherty power amplifier design used a digital predistorter to investigate the linearity as a result experienced a reduction in PAE to 48%. Finally, in [208, 209, 216] a 10 W, Si-LDMOS transistor power amplifier was presented with 50% PAE, 14.5 dB gain achieved at 41.8 dBm saturation within 1.8 to 2.0 GHz operating frequency. The drawback of [216] is that heat sink is used due to excessive heating produced by the amplifier, which extensively affects the general performance of the system.

However, this work presents a simplified balanced amplifier using Si-LDMOS transistor while achieving up to 53% PAE, 41 dBm output power with 14.6 dB gain at 1 dB compression point for the simulation. For the measurement, the amplifier PAE and gain improve to 83% at 40 dBm and 20 dB respectively. The operating frequency used for this design is between 2.62-2.69 GHz. This design is matched perfectly due to the internal input and output matching network in the transistor device. No evidence of leakage or signal reflection from the first stage of the design to the design of a balanced amplifier. Another advantage of this design is for its simplicity, requires no auxiliary amplifier or additional cascade Doherty device to improve the efficiency. Additional circuit accounts for extra

power consumption and resulting in a negligible impact on the overall efficiency of the amplifier.

Table 5.1: Performance comparison with similar various power amplifiers.

Device	f_c [MHz]	PAE [%]	P_{out} [dBm]	Gain [dB]	Reference
LDMOS	2655	53	41	14.6	Balanced
LDMOS	2655	29	39	15	Class AB
LDMOS	2140	54	48.77	30	[212]
GaN-HEMT	2655	37.14	41.18	12.78	[213]
GaN-HEMT	2125	33.4	34.9	7.7	[214]
GaN-HEMT	2500	48	46	13.4	[215]
Si-LDMOS	1900	50	40	14.5	[216]

5.4 Summarized Conclusion

A balanced RF power amplifier was presented with a two class AB amplifier. The design used Freescale N-Channel Enhancement Mode Lateral MOSFET transistor. The linear and nonlinear simulation were achieved with ADS simulator and on the performance metric result is presented with considerable improvement. A comparison was made between the conventional design, which is a class AB amplifier and the double stage symmetric balanced RF power amplifier. The balanced amplifier exhibited an acceptable improvement in terms of power added efficiency by 22%, output power, 2 dBm, while the gain decreases by 1 dB. A relative comparison was made with power amplifiers of various types and the present work has proven a good choice of device for LTE, W-CDMA applications and beyond 4G systems. The final fabrication of a balanced power amplifier was also implemented using RF field-effect Si-LDMOS 15.5 W transistor at 2.620-2.690 GHz frequency band. Further, the prototype was completed,

measured and results were analyzed. In order to experimentally verify the performance of the proposed amplifier, single and multiple tone measurements will be conducted. The measured characteristics include the dependence of AM-AM and AM-PM curves on the input signal's frequency and power. Alternatively, variations of the RFPA gain and phase versus input signal's frequency and power was measured [8].

CHAPTER 6

Class F RF Power Amplifier Design by Load-Pull Approach

6.1 Introduction

In all the diverse classes of RF power amplifiers, the class F power amplifier is recognized as the most efficient. It achieves 100% efficiency by harmonic resonators in the output network to shape the drain/collector waveforms such that the load appears to be short at even harmonics and an open at odd harmonics. The drain/collector voltage waveform includes one or more odd harmonics to approximate a square wave, whereas the drain/collector current waveform includes one or more even harmonics to approximate a half a sine wave [217, 218].

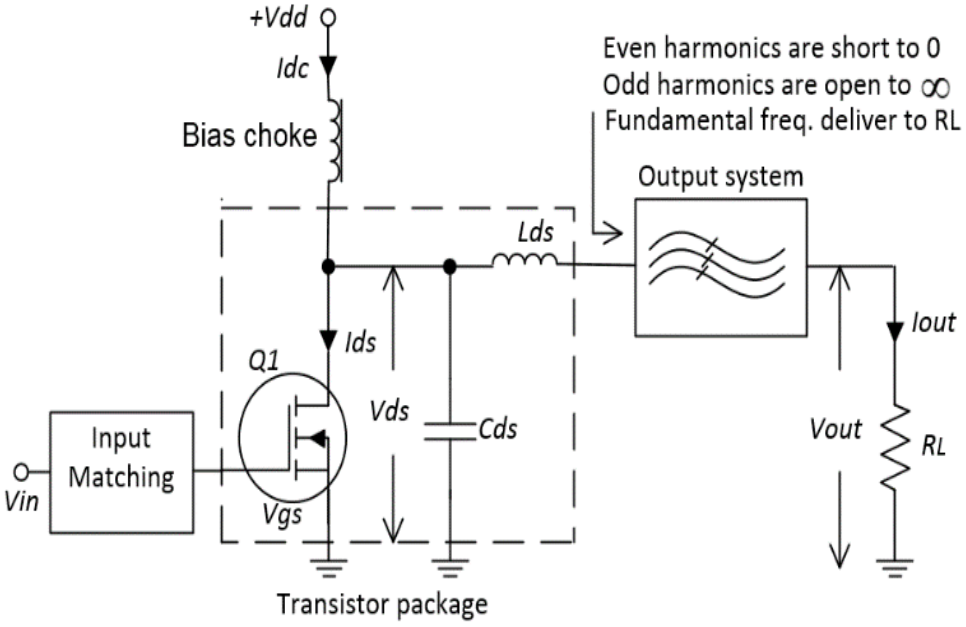

Figure 6.1: Generic nonlinear RF Power amplifier circuit.

This chapter presents a design of class F RFPA using load-pull approach to achieve high efficiency. Input matching circuits are designed with an active integrated antenna to obtain optimal fundamental load impedance. The 2.620

GHz frequency is used in this study to confirm the design principle and to achieve class F operation with an alternative type of power transistor.

The class F operation is a well-known technique for improving power added efficiency and the drain efficiency of RF power amplifiers [218]. It uses a multi-resonator to control harmonic waveforms so that the drain voltage waveform (ideally) becomes rectangular and the drain current waveform becomes half sinusoidal, thereby reducing DC power dissipation and increasing efficiency. This requires optimised impedance at the fundamental, low impedance at even harmonics and very high impedance at odd harmonics. A simple method is to interpose a quarter-wave line between the drain and the final load and to design the latter to have the lowest possible impedance at all harmonics above the fundamental [219].

It is suitable to use an active integrated antenna approach in the lumped element class F RF power amplifier operational device, where the second and third harmonics are shaped through the input resistance of the antenna. This, in turn, can allow the harmonic resistances to be almost zero at twice and three times the designed frequency, so that harmonic power is efficiently suppressed from radiation by the antenna. The input impedance of the antenna at the fundamental frequency should be equivalent to the optimum load impedance at the fundamental frequency of the amplifier for high efficiency and output power. In this design approach, an output matching circuit is eliminated because the antenna impedance is directly transformed to the Z_{opt} for maximum efficiency, thus decreasing the circuit complexity and power losses [220].

6.2 Proposed Class F RF Power Amplifier Design

The class F power amplifier was designed and optimised at 2.620 GHz using Agilent Technologies' Advanced Design System (ADS). Following the selection of suitable output power and operating frequency range, the active device selected was the Cree 10 W, RF Power GaN-HEMT large-signal transistor model. For a simple design, it is desirable to use a device like this which does not include built-in matching circuits, other than unavoidable parasitic within the package. Even with CAD tools, it is a very difficult problem to optimise all aspects of the design in one pass. No exact synthesis approach is known for shaping a patch antenna to achieve prescribed impedances at a set of harmonically related frequencies. However it is feasible to use the method of [221, 222], where the fundamental impedance can be kept reasonably close to optimum, higher resonances of the antenna can be separated as much as possible from harmonics of the operating frequency, so that the input resistance of the patch remains low at the harmonics. This may be a realistic target only for the first few harmonics, which auspiciously dominate the efficiency optimisation. Feedback effects on input impedance at harmonic frequencies will be a complex issue. However, in this study, the fundamental load impedance was initially optimised, so that the value is used in optimising the input match again while avoiding harmonic frequency feedback [222].

6.2.1 Circuit Design Theory

The schematic diagram of a generic amplifier shown in Figure 6.1 is a typical example of a class F RF power amplifier circuit architecture. The system uses an active GaN-HEMT transistor device which is controlled by its input source (V_{in}) and the bias network as the dc current source. The dc voltage source from the

drain ($+V_{DD}$) supplied the dc drain current (I_{dc}). The output system which represents the load impedance network provides the even harmonic frequencies shorted to zero, odd harmonic frequencies open to infinity and fundamental frequency delivered to the load (R_L) [223].

Figure 6.2 demonstrates the ideal time-domain voltage and current waveforms of a class F RF power amplifier. The amplifier achieves high efficiency with the adoption of proper harmonic frequency terminations at the output.

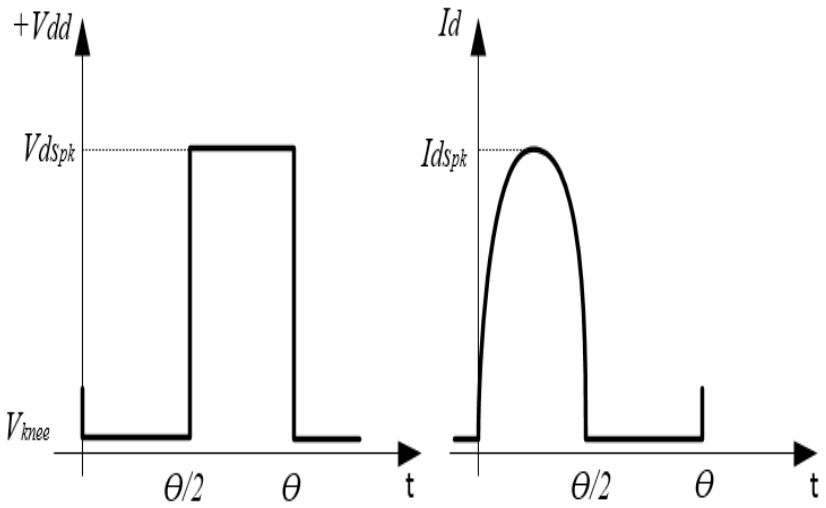

Figure 6.2: Class F PA ideal time-domain drain voltage and current waveforms.

The odd harmonics are open to producing square wave and even harmonics remain shorted to produce current wave respectively. The drain current and voltage ideal waveforms of the class F RF power amplifier are analytically discussed and expressed by the form:

$$V(\beta) = +V_{dd} + CV_1 \cos\beta - DV_1 \sin\beta + ... + ... \quad (6.1)$$

and

$$I(\beta) = I_{dc} + CI_1 \cos\beta - DI_1 \sin\beta + ... + ... \quad (6.2)$$

Where β equals to the first harmonic frequency (ω) of the waveform at a period of time (t). The first harmonic frequency remains as $sin(\beta)$ when $CV_1 = 0$ and $DV_1 = 1$. The amplifier output current (I_o) is the half-sine wave with maximum amplitude expressed as:

$$I_o = \frac{1}{\pi} I_{pk} \tag{6.3}$$

Where I_{pk} is the peak current. Thus, the dc power supply from the drain is presented as:

$$P_{dc} = V_{dd} I_{dc} = \frac{V_{dd} I_{pk}}{\pi} \tag{6.4}$$

Where V_{dd} and I_{dc} are the magnitudes of the dc voltage and current. The RF output power at the first harmonic frequency is expressed as:

$$P_{out} = V_{dd} I_{dc} = \frac{4 V_{dd} I_{pk}}{\pi\sqrt{2} \times 2\sqrt{2}} = \frac{V_{dd} I_{dc}}{\pi} \tag{6.5}$$

Thus, the maximum efficiency is achieved using (6.4) and (6.5) as expressed in (6.6):

$$\eta = \frac{P_{out}}{P_{dc}} = \frac{\frac{V_{dd} I_{dc}}{\pi}}{\frac{V_{dd} I_{pk}}{\pi}} \tag{6.6}$$

And then, the power added efficiency can be written as:

$$PAE = \frac{P_{out} - P_{in}}{P_{dc}} \tag{6.7}$$

If power added efficiency increases, power dissipation and harmonic power will be drastically reduced. Hence, the cause of power dissipation and harmonic

power is due to heat from the transistor device. The transistor makes the harmonic power larger than zero when the intersection between the drain voltage and current occur. This action reduces the class F amplifier power added efficiency from 100% to less than 90%. Furthermore, the efficiency of this grade can only be achieved based on the number of harmonics controlled in the network [224].

6.2.2 Bias Point Selection and S-parameter

The nonlinear model of this device (which was provided by the device manufacturer), and harmonic balance simulation including the first five harmonics were used in the simulation. The drain bias voltage (V_{ds}) was 28 V, while the gate bias voltage (V_{gs}) was set to be –3.0 V so that DC drain current is 68 mA [225]. Figure 6.3 shows the DC characteristics of the device and the selected quiescent bias point [225].

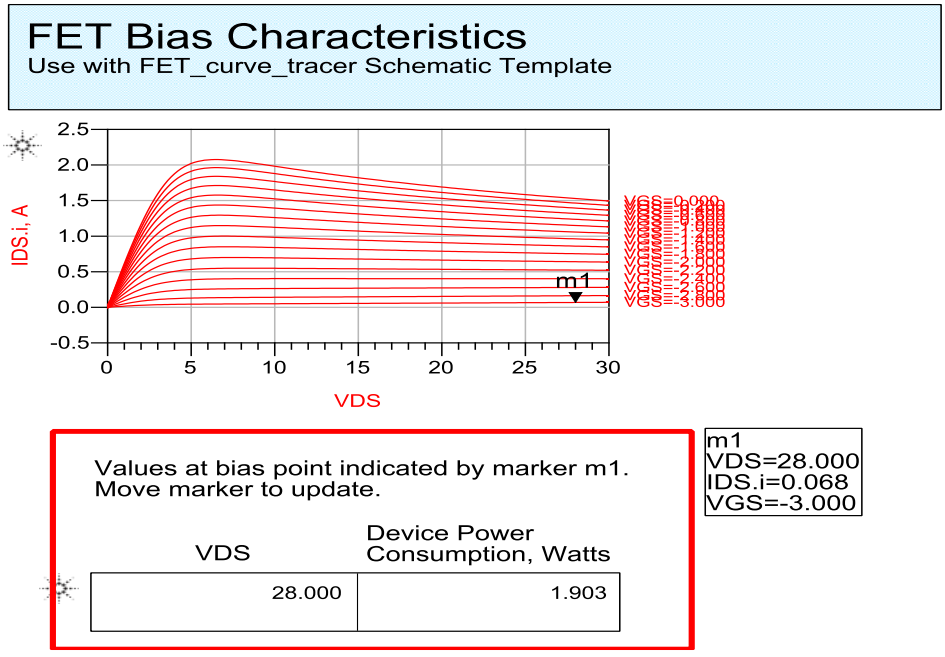

Figure 6.3: DC characteristics of the device and the selected quiescent bias point.

6.2.3 Load-pull and Harmonic Loading Consideration

Load-pull simulations can be done in ADS using HB1Tone load-pull design guide with a nonlinear model of transistor. In this work, a large signal model CGH40010F from Cree is used. Figure 6.4 shows the simulation setup from the design guide. The design shows load-pull contours for output power and PAE as a function of load impedance. The load-pull circuit in Figure 6.4 uses harmonic balance simulation in ADS. This iterative simulation calculates the response of large-signal circuits driven by either single or multiple sources and tries to find a stationary solution for the nonlinear system in the frequency domain.

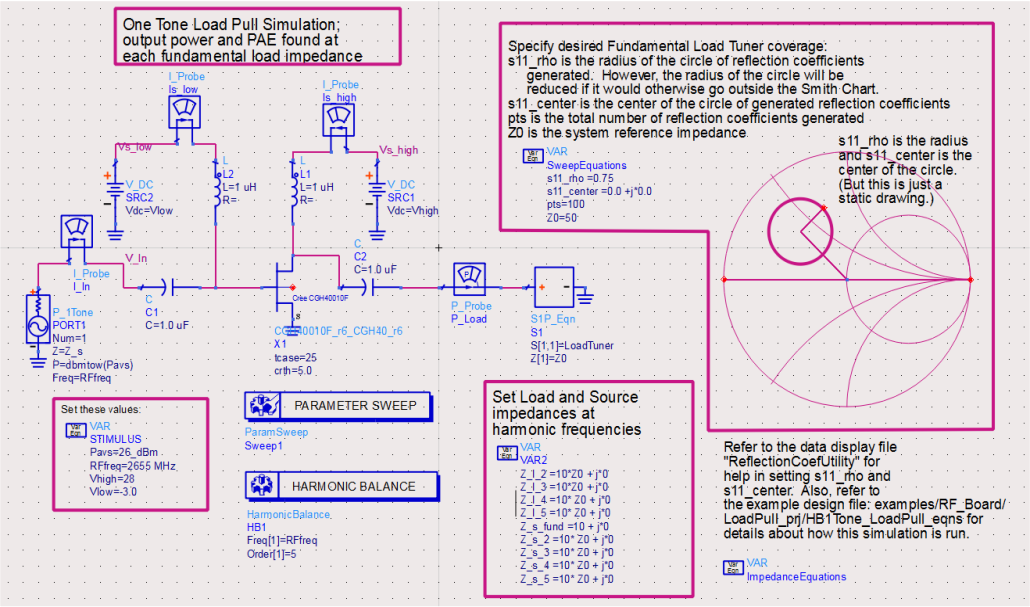

Figure 6.4: Circuit of design guide HB1Tone load-pull for 1-tone analysis.

In Figure 6.5, each contour indicates the set of impedances corresponding to constant output power and PAE [225]. The Figure 6.5 has also shown the result achieved from the HB1Tone load-pull for 1-tone analysis, a source and load reflection coefficients without matching has shown 70.88% maximum PAE of at 41.31 dBm delivered power. This can be a PAE starting point for the final design. However, this performance can be improved by replacement with the active

antenna, which is expected to generate accurate impedances for the load harmonic components. The figure has also shown the input reflection coefficient, input and output impedances of the amplifier load-pull simulation. The input reflection coefficient was generated as a function of the output impedance to maximize the efficiency at a given power [225].

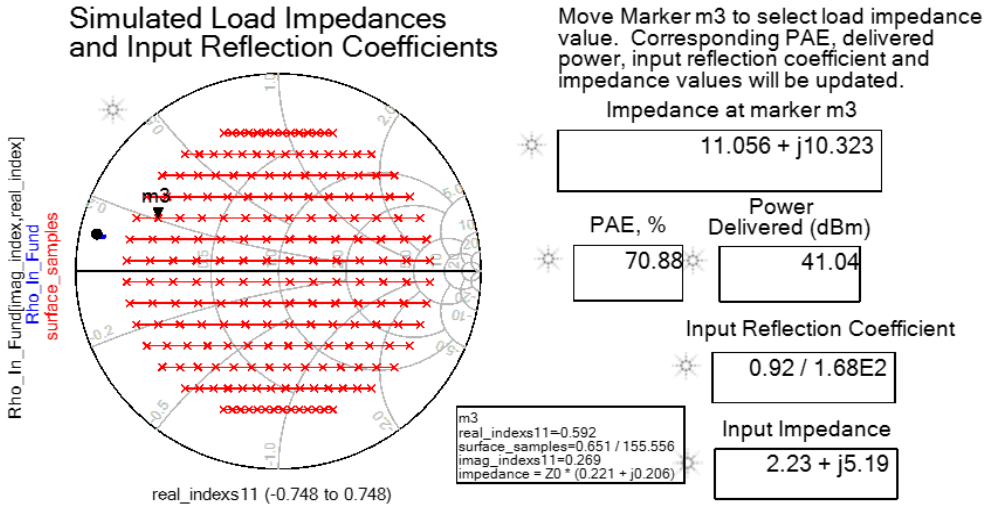

Figure 6.5: Source and load reflection coefficients without matching.

In the case of matching circuit design in power amplifiers, a large signal S-parameters is generally desirable as one of the system most important performance indicators. However, S-parameters measurement is not well explained as expected. Instead, a substitute technique is suggested to derive reflection coefficients of the antenna from measurements of the voltage of the incident wave and reflected wave [226, 227]. In the absence of an output matching circuit, due to the active antenna, only the input reflection coefficient is expected to be taken into account. Input reflection coefficient can be achieved in many number of ways, which one of these ways can be the application of a 2 x 2 simple coupler at the input phase of a class F power amplifier harmonic load-pull [228] design circuit. This circuit was selected from ADS amplifier design guide to

determine the reflection coefficient of large-signal S-parameters of the nonlinear model. Figure 6.6 has depicted a load-pull simulation circuit with a simple coupler for the input matching design. In this circuit, the coupler is connected between a signal generator and the transistor in order to measure the incident voltage at the source and reflected voltage reflected from the transistor. It should be noted that the coupler is not proposed to be a practicable hardware component, but is defined in software as the operation of converting actual current and voltage into equivalent forward and reverse wave components [222, 229]. Then the reflection coefficient of the transistor is derived based on equation (6.8) as:

$$\Gamma = V_{ref} / V_{in} \tag{6.8}$$

The theory of load-pull simulation circuit design is to acquire the optimum load impedance at the fundamental frequency of the amplifier. The class F power amplifier used in the load-pull as a case study with an algorithm to vary the fundamental load impedances are contained in a one-port device as S-parameter data. These are used in the class F power amplifier biasing operation at fundamental frequency to achieve maximum efficiency and output power. These features used in the load-pull are basically part of the ADS software package. Part of the simulation protocol is to:

- Randomly, set a centre point and radius for a circle on Smith chart.
- Set the number of points on the circle (ensuring the circle is completely inside the Smith chart). Each point of the circle provides a specific value of the load impedance.
- Adjust the position of the circle on the Smith chart to generate the optimum load impedance. Furthermore, the source and load impedances at

different harmonic components were assumed to be 50 Ω. These given values are somehow substituted optimum.

Thus, the obtained PAE and P_{out} from this simulation design are not finalised and the design can be used as a starting point when the one-port block is replaced by the antenna which is expected to provide the correct harmonics load impedances. The input reflection coefficients were also simulated as a function of the output load impedances for the maximum power and efficiency. Due to dependence between input reflection coefficient (Γ_{in}) and load reflection coefficient (Γ_{load}) of the two-port device, the advantage of this proposed design approach is that it simplifies the considerations of designing the output matching circuit and the simulation which only aims to obtain the coefficient (Γ_{opt}).

Once the impedance (Z_{opt}) with the satisfying output power and efficiency are obtained, the corresponding Γ_{in} with Z_{opt} values will be calculated so that the input matching circuit is designed accordingly with the aid of the Smith chart. Under the biasing condition mentioned above, the Γ_{in} value was found in the form of magnitude and angle when Z_{opt} was optimised to be (11.056+j*10.323) Ω. With the help of the Smith chart tool, an input matching circuit with two lumped elements was plotted and the coupler at the input stage was replaced with the matching circuit. Discrete components could be used for the matching network because the components have been well enough characterised at the lower microwave communication frequencies.

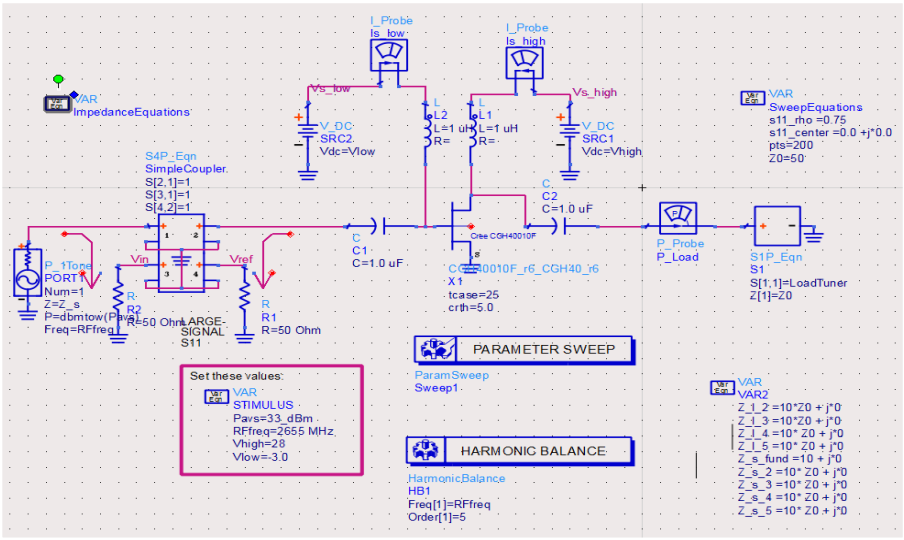

Figure 6.6: Harmonic load-pull simulation circuit with a coupler.

After the introduction of the input matching, the linear gain and return loss of the RFPA were dramatically improved. While, the optimum coefficient (Z_{opt}) was still (11.056+j*10.323) Ω with the same input power level as previously shown in figure 6.5. This process is also expected to improve the power added efficiency as well as the output power of the final design of the power amplifier.

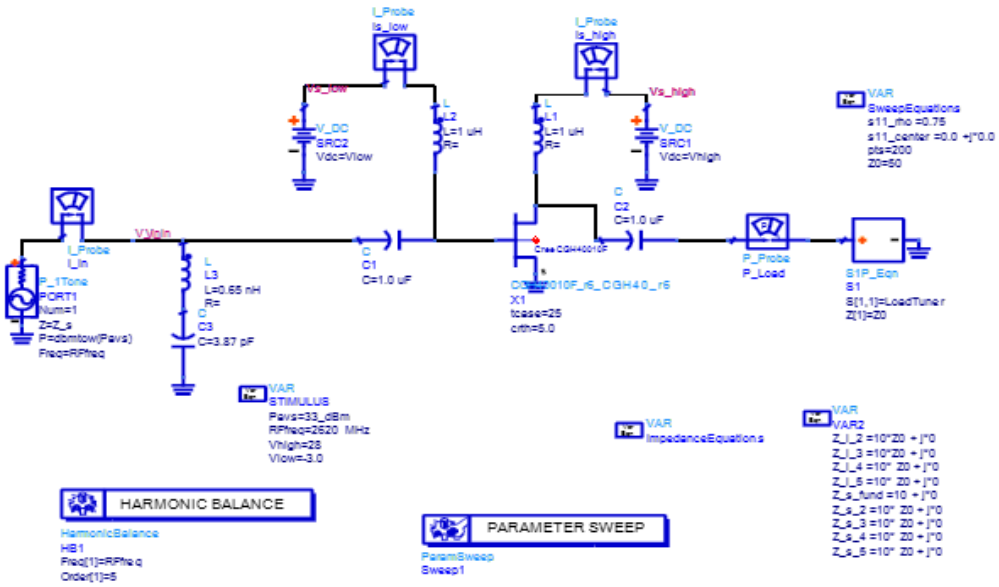

Figure 6.7: Harmonic load-pull simulation circuit with input matching.

Once the Z_{opt} value was set, the micro strip lines were expected to connect the components together.

6.2.4 Wave Shape Circuit and Matching Networks

In this proposed class F design, a multiple-resonant structure [230] in a lumped-element network is adopted. The input network is a low pass structure, while the output is a 5th order low pass L-C structure. However, the low pass network was adopted in this work to provide optimal harmonic terminations for nth harmonic components. The class F structure was also transformed with the use of transmission line depicted in Figure 6.8. The figure is used in describing the design procedure in this technique, how nth harmonics are controlled for proper drain voltage impedance.

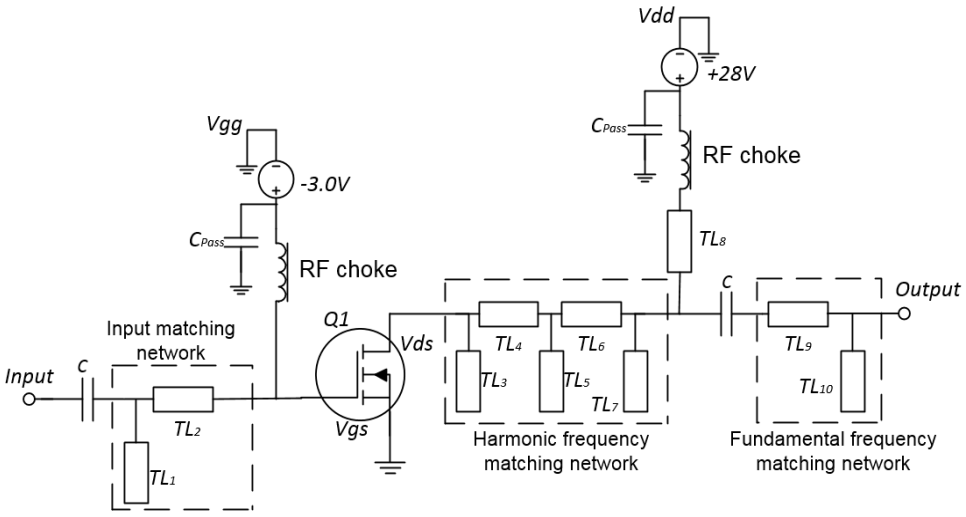

Figure 6.8: Wave shape circuit using a matching method.

To achieve class F operation, the transistor device has to be actively loaded from the input (Z_{in}). While, setting the device to active mode, the device peak voltage and current need to be taken into consideration on delivered power, resistance, supply voltage, when the system is linear, nonlinear, etc. These parameters

determine the required drain load impedance (Z_{DL}) at the fundamental frequency and reactance are at the nth harmonic components [231].

In [220], to determine the drain load impedance (Z_{DL}), transistor drain to source capacitance (C_{DS}) and lead inductance (L_{DS}) were added for proper impedance transformation from device drain impedance (Z_D) to the drain load impedance (Z_{DL}). However, at certain range of frequencies, these elements could add up to the complexity of the circuit. Particularly, with the increasing number of harmonic components, they behave as parasitic elements [231].

A proper output lumped element structure at the output provides the required drain load impedance. The circuit is a *5th* order low-pass L-C ladder structure. The circuit behaves as a load-impedance inverter at the fundamental region and provides a scale with the optimal load-impedance value. The low-pass structure is also provided with multi-resonators for proper higher harmonic components termination [230, 231].

In the *nth* order structure, *3rd* and *5th* harmonic components are odd in nature and are open-circuited, while *2nd* and *4th* behave as even harmonic components are short-circuited at the drain terminal of the transistor. This procedure is referred to as the wave forming a circuit. It is a circuit by which the frequency and amplitude of the harmonics contribute to the shaping of the voltage and current waveforms [231].

There are various types of these circuits with difference in complexity and level of performance in the shaping of the voltage and current waveforms, which also has a great impact on the performance of the power amplifier. Input and output

matching have also been calculated with the use of firefly method. At the output stage, however, the matching has been designed for *3rd* and *5th* as odd harmonic components and the *2nd and 4th* as even harmonics components respectively. Furthermore, the matching is based on the position of *2nd* and *4th* (TL_4, and TL_6) as short circuits, on the way of the *3rd and 5th* harmonic components. The transmission line TL_3, TL_5 and TL_7 transform the harmonic frequency matching network to open circuit [231].

On the other hand, all the transmission lines in the harmonic frequency matching network stage are added to the formation of a short circuit, on the way of the even harmonic components, towards TL_9. TL_8 acts as a quarter-wave ($\pi/2$) to block the RF signal moving back to the source, transforming the impedance to 50 Ω load, ensuring that even harmonic components are shorted and behave as an open circuit to allow the odd harmonic components to infinity [231]. Finally, TL_9 and TL_{10} are designed as the fundamental frequency matching for the optimum load. However, in the end, we need to take into account the matching circuit at high frequencies could lead to circuit complexity [229, 231].

The design of a class F power amplifier is based on the calculated waveform coefficients tabulated in table 1. The circuit was designed and simulated with the use of the Agilent ADS. The transistor model generic GaN-FET has been chosen as a model of nonlinear power transistor suitable use for such power amplifier. The following parameters were used as follows: operating frequency of 2.62 GHz, drain voltage 28 V (dc) and gate voltage -3.0 V (dc). RF4 substrate with the following specifications: substrate thickness (H) 1.6 mm, Permittivity (ε_r) 4.3, conductivity 4.1×10^7 S/m and conductor thickness (T) 0.035 mm. The circuit has

been optimized and the goals have been achieved using the firefly algorithm. Figure 6.8 shows the design circuit connected using a micro strip line with optimal lengths and widths. One-tune swept harmonic balance analysis, with load impedances at harmonic frequencies set at 50 Ω and the optimum load impedance at the fundamental frequency set as 11.056+j10.323 were employed. The output power P_{out} and the power added efficiency characteristics from the active device versus input driving power at 2.655 GHz were presented [225, 231].

Table 6.1*:* The dimensional values for lumped-element and TLs for the class F RFPA design.

Stage	Symbol	Element Value	Distance	Width (mm)	Length (mm)	Transmission Line
Input	C_1	5.61pF	77.8^0	3.08	2.16	TL_1
matching	L_1	0.49nH	9.2^0	-	13.3	TL_2
Wave Shaping	C_1	2.68pF	65.6^0	-	4.34	TL_3
	L_2	3.43nH	48.5^0	-	7.40	TL_4
	C_3	3.77pF	72.1^0	-	3.14	TL_5
	L_4	3.43nH	48.5^0	-	7.40	TL_6
	C_5	2.68pF	65.6^0	-	4.34	TL_7
Output matching	L_1	1.41nH	49.3^0	-	8.64	TL_9
	C_1	2.30pF	37.1^0	-	6.50	TL_{10}
Q-wave	$\lambda/2$	$\pi/2$	90.0^0	-	15.8	TL_8

6.3 Simulation Results and Discussion

At this level of design, linear and nonlinear simulation have been performed using Agilent Technology ADS. The results in Figure 6.9 showing linear simulated results of S-parameter of the amplifier where the flat gain S(2,1) keeps reducing as the frequency increases. The other set of parameters such as return loss S(1,1 and 2,2), leakage or isolation S(1,2) and the gain can be seen in the Figures below.

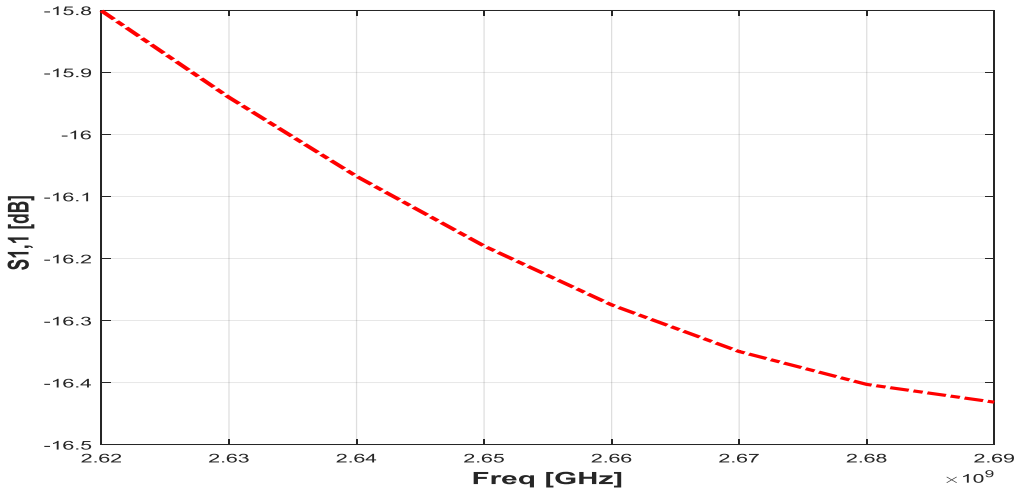
-15.8
-15.9
-16
-16.1
-16.2
-16.3
-16.4
-16.5
S1,1 [dB]
2.62
2.63
2.64
2.65
2.66
2.67
2.68
2.69
Freq [GHz]
×10^9

(a)

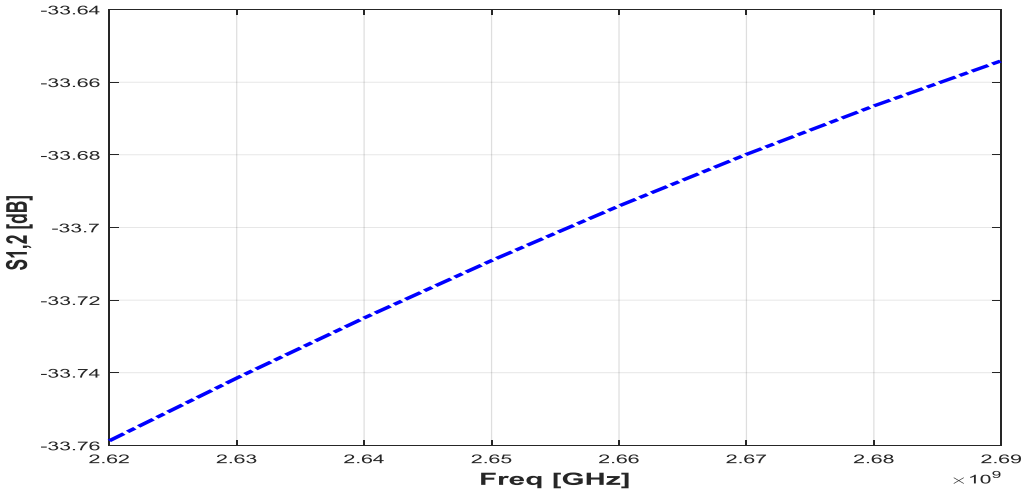
-33.64
-33.66
-33.68
-33.7
-33.72
-33.74
-33.76
S1,2 [dB]
2.62
2.63
2.64
2.65
2.66
2.67
2.68
2.69
Freq [GHz]
×10^9

(b)

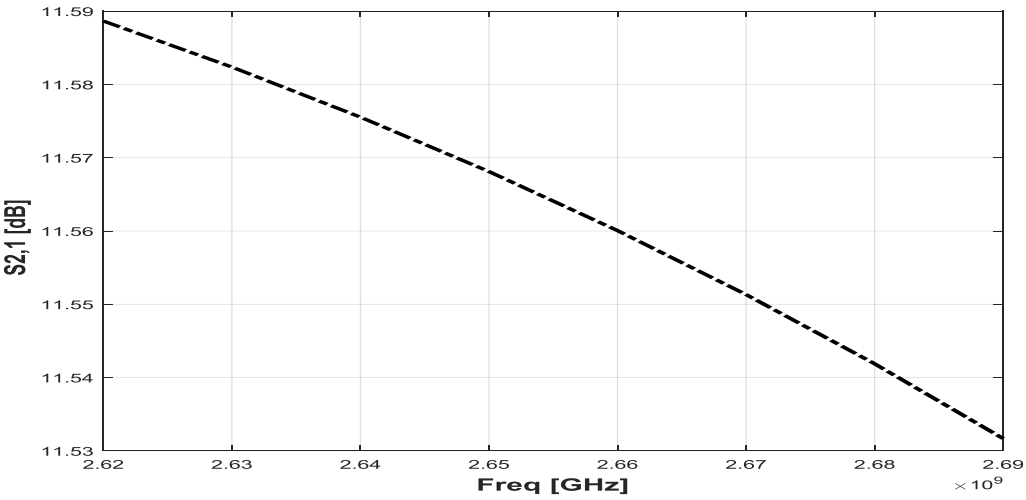
11.59
11.58
11.57
11.56
11.55
11.54
11.53
S2,1 [dB]
2.62
2.63
2.64
2.65
2.66
2.67
2.68
2.69
Freq [GHz]
×10^9

(c)

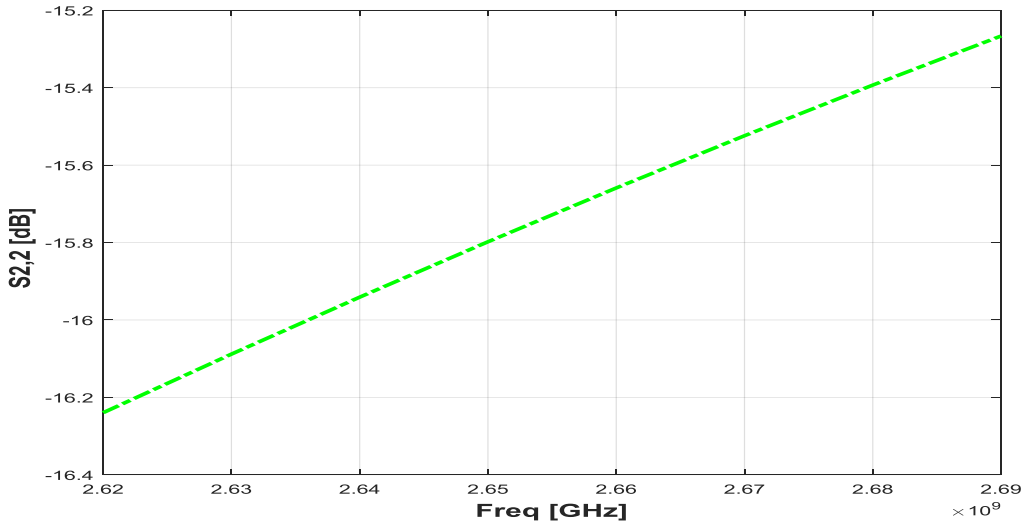

(d)

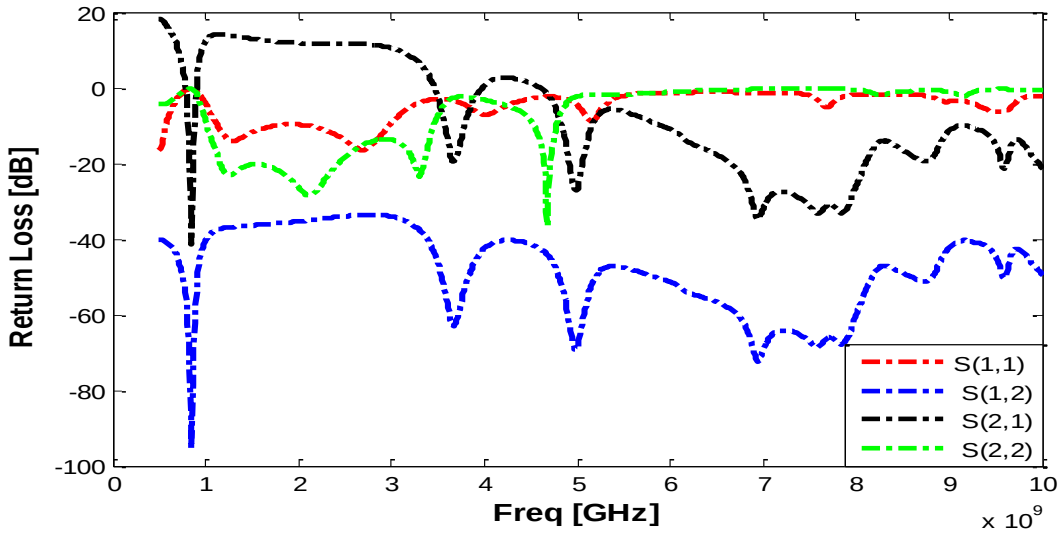

(e)

Figure 6.9: Linear simulation of the class F RFPA. (a) Input return loss: (b) Isolation: (c) Linear power gain: (d) Output return loss: (e) Arrangement of S-parameters using wide range of frequencies to check performance.

As shown, the S-parameters were simulated separately to clearly see the results within the operating frequency which is the region of interest. The S-parameter were employed in order to attain maximum power transfer. The linear simulation results from Figure 6.9 (a) to (d) have demonstrated a good performance in ensuring maximum power is transferred from the input of the RF power amplifier to the output while maintaining the frequency range of 2.62 - 2.69 GHz. Figure

6.9 (c) has also shown the scattering parameters in one figure using wide range of frequency from 0.5 to 10 GHz. This is just to ascertain the performance of the parameters in different frequency region. The performance result of the S-parameters also depend on the application and design parameters. It can be seen that maximum power is transferred in 1 to 3 GHz frequency region.

In the nonlinear characterization of the class F RF power amplifier, Output power and efficiency tests are the most significant performance indicators for the amplifier. Figure 6.10 has shown simulated efficiency versus output power. The class F power amplifier has high efficiency over the range of 79% with the output level of 29 dBm at 1 dB compression point, compare to what was obtained by [217, 220]. The efficiency is also 10.5% higher than what was predicted in the load-pull simulation theory. The cause for the increase in efficiency is due to the transistor device transient response and termination of up to 5^{th} harmonic components.

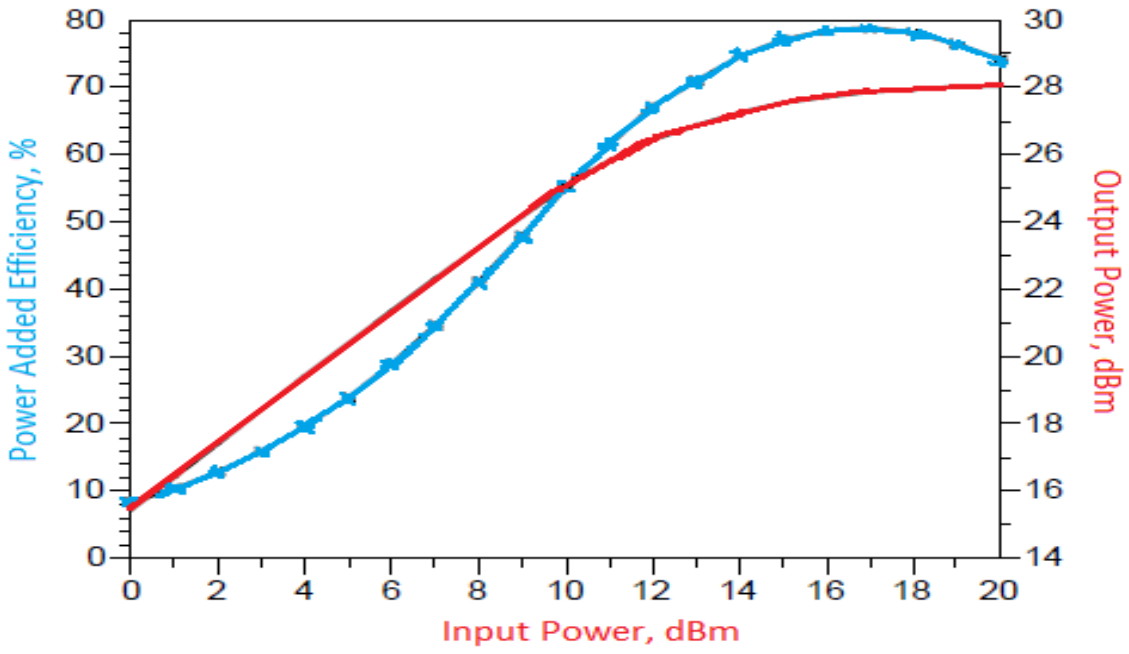

Figure 6.10: Class F RF power amplifier PAE and P_{out}.

Moreover, the class F RF power amplifier simulated output voltage and current results, shown in Figure 6.11 were generated from the drain-source of the device. The fundamental frequency and up to 5th harmonic components were simulated as shown in the Figure above. The nonlinear characteristic of the transistor and nonlinear distortion in the sinusoidal waveform were discovered. However, the distortion is not severe to affect the output signal.

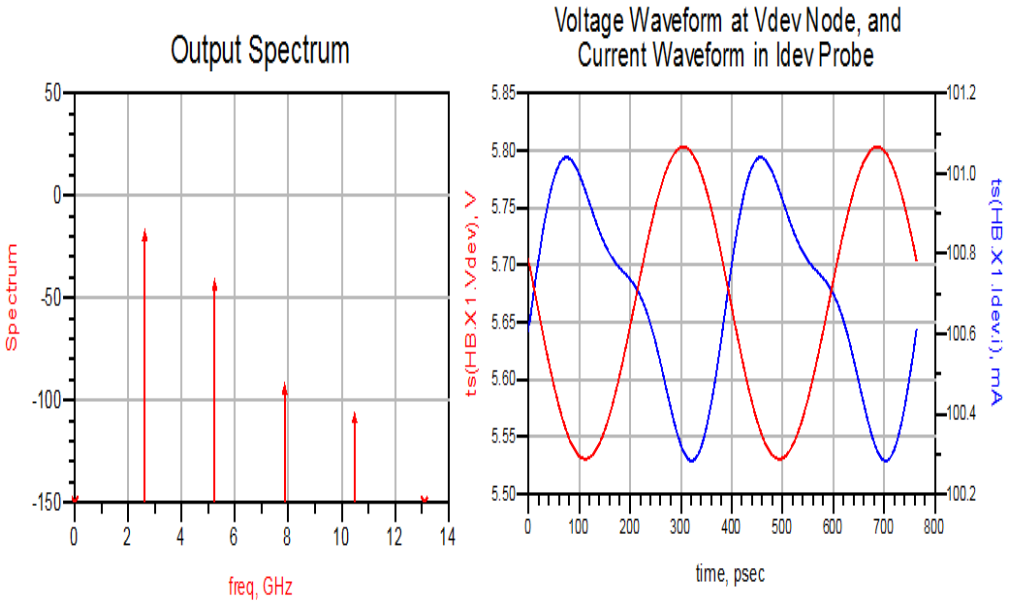

Figure 6.11: Out spectrum, simulated voltage and current waveforms.

6.4 Summarized Conclusion

A simple CAD-oriented approach using a class F power amplifier design to optimise load impedance at the fundamental frequency for the application of the active antenna concept was presented. The design method and procedure were described. Furthermore, one design example at an operating frequency of 2.655 GHz was demonstrated to verify the design principle. It was confirmed that performance could be substantially enhanced in an active integrated antenna by completing the final design of the amplifier using wave shaping to control the harmonic load impedances.

CHAPTER 7

Linearization Techniques and Predistortion Systems with 5G Modulation

7.1 Introduction

A nonlinear RF Power amplifier is faced with difficulties, particularly during amplification to achieving high efficiency and maintain linearity at the same time. There is efficiency improvement when RF power amplifier operates with a small back-off which means reaching the saturation region. However, there are nonlinear distortions at this point of operation which leads to system performance degradation. This implies that efficiency and linearity are essential requirements for system excellent performance. The trade-off between efficiency and linearity usually depends on the particular application. Efficiency has become an important parameter when it comes to handset applications. The battery life span is upgraded to increase the talk-time. In the case of base stations, the most important parameter is linearity. To achieve excellent reception with less error rate in mobile terminals, the downlink signal needs to be extremely linear. Subject to much current research works on efficiency and linearity, solutions are discovered for such constraints. For efficiency problem, efficiency enhancement techniques have successfully been developed, while linearity improvement techniques have been investigated and implemented to add to the body of knowledge [211, 232-234].

To accomplish a highly efficient and linear system in a practical approach, firstly, efficiency must be increased at the expense of linearity. Then afterwards, provide external linearization in order to achieve the linearity requirements. Subsequently, RF power amplifiers linearization is an important task on modern

wireless systems with the aim to satisfy the challenging demands. Several effective linearization techniques have been developed recently and these are classified into three major categories follows [235]:

- Feedback methods.
- Feedforward linearization.
- Predistortion techniques.

However, the linearization techniques classification has been discussed and is debatable in many research works. Several authors' distinct techniques based on the installation of second-order products into a separate set while others retain them within the mentioned techniques. Other methods such as Envelope Elimination and Restoration (EER) and Linear Amplification using Nonlinear Components (LINC) are traditional sets that relate with the efficiency enhancement techniques with characteristics of improving linearity [236].

This chapter presents an overview of the main techniques used in improving the linearity such as the feedback and predistortion methods. The feedback method consists of passive and active RF feedback. The predistortion methods are classified into analogue and digital. The work will also present the concepts of the techniques and highlighting their advantages and drawbacks.

7.2 Feedback Linearization

Feedback is basically one of the simplest and direct forms of feedback system which is based on the idea of comparing the linear input signal with the offset output signal obtained through the feedback chain and correcting the input signal

for linear output signal [237]. A typical instance of the feedback method is given in Figure 7.1.

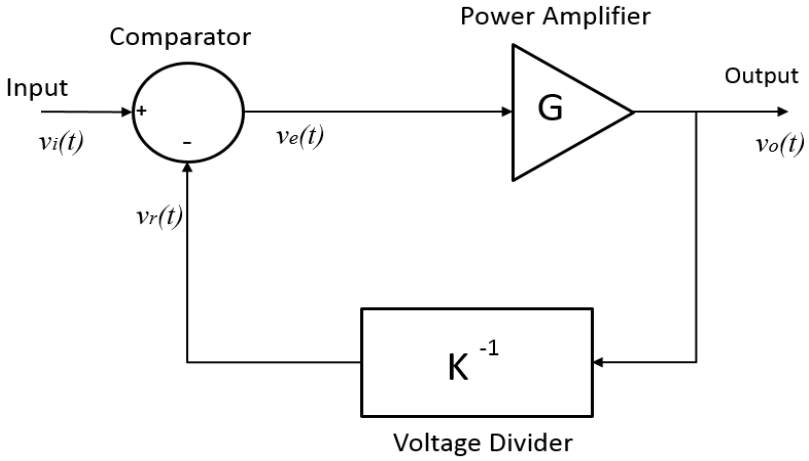

Figure 7.1: General feedback linearization system.

Where $v_i(t)$, $v_r(t)$, $v_e(t)$, $v_o(t)$, are the input signal, reference signal, error signal and the output signal. The feedback system comprises of an amplifier with the instantaneous gain (G), a feedback chain and a comparator. The output signal is fed back with the gain (α) to achieve the reference signal. Input and reference signals are fed into the comparator to produce an error signal which is fed to the amplifier for the overall linear output signal. The overall output signal can be expressed as:

$$v_o(t) = Gv_e(t) \tag{7.1}$$

The output signal is fed to the feedback system to produce attenuated distortion signal $v_r(t)$.

$$v_r(t) = \frac{v_o(t)}{K} \tag{7.2}$$

Then, the error signal $v_e(t)$ is expressed as:

$$v_e(t) = v_i(t) - v_r(t) \tag{7.3}$$

The relationship between the linear input and the linear output signal can be realized through composing the (7.1), (7.2) and (7.3).

$$v_o(t) = \left(\frac{GK}{G+K} \right) v_i(t) \tag{7.4}$$

Applying the gain of the feedback rather than the attenuation ratio, $G_{FB} = 1/K$ and can be written as:

$$v_o(t) = \left(\frac{G}{1+GG_{FB}} \right) v_i(t) \tag{7.5}$$

The connection has proved that using a feedback method to reduce the composite gain produces a more stable amplified output signal. In (7.1), the noise and distortion of the device under test have been included, while combining the first three equations by introducing a new summand $d(t)$ which is expressed as:

$$v_o(t) = Gv_e(t) + d(t) \tag{7.6}$$

Also, composing (7.1), (7.2), and (7.3) results to:

$$v_o(t) = \frac{K(Gv_i(t) + d(t))}{G+K} \tag{7.7}$$

Assuming $G \rangle\rangle K$, then $G + K \approx G$ and (7.7) can be reduced to:

$$v_o(t) = Kv_i(t) + \left(\frac{K}{G} \right) d(t) \tag{7.8}$$

The feedback chain reduces effectively the effect of distortion of the device under test by the factor of K/G, but at the expense of reducing the overall gain. Apart

from being a straightforward method, the feedback technique has the advantage of setting additional feedback in the system, while the sensitivity of the closed-loop gain is negligible to the gain variation. However, in return, the delay appears between the input and feedback signal which reduces the gain and bandwidth which also affects the stability of the system. In this type of compensator, extra caution needs to be taken while designing a linear feedback path, so that it cannot be corrected afterwards [238].

There are many various types of feedback method and they are classified based on active and passive, direct and indirect methods. These methods are RF feedback, envelope or modulation feedback, polar and Cartesian loop feedback [238, 239].

7.2.1 RF Feedback

The RF feedback method is both active and passive components feedback system in which the output signal can be subtracted from the input at the RF frequency level without demodulation of any form. The issue of stability in feedback loops is a bigger concern which limits the system in compensating the individual amplification per phase, rather than the entire transmitter.

In this technique, the active feedback component system includes an auxiliary amplifier in the feedback path for power dissipation reduction in the feedback modules [240].

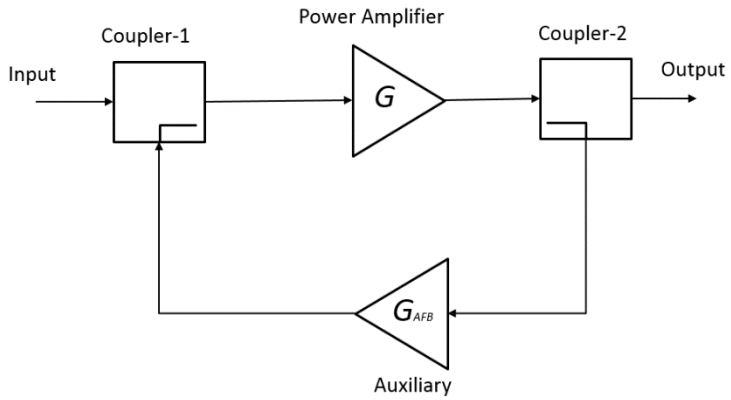

Figure 7.2: Active feedback linearization system.

Figure 7.2 has shown an active feedback linearizer where the auxiliary amplifier operates in a nonlinear manner to improve the intermodulation level by 12 dB and compensate for the nonlinearities of the main amplifier at the expense of the overall gain [240]. In the case of passive feedback component system, a voltage divider is used at the feedback path. This arrangement preserves system stability while compromising the overall gain. The active and passive feedback techniques are primarily meant to improve the broadband performance of the device under test by gain levelling rather than the device harmonic distortion or inter-modulation. However, due to the limitation of the conventional RF feedback methods, many RF feedback techniques have been proposed in the literature to mitigate the existing drawbacks [240, 241].

Distortion feedback is among other techniques aimed at improving the overall gain and overcoming the intermodulation effects that the conventional RF feedback is unable to overcome. Distortion RF feedback is the combination of both RF feedback and feed forward methods. The first section of the distorted output is captured and subtracted from the delayed version of the input RF signal. The resulted error signal is added to the input signal and sent to the power

amplifier. This method is similar to the predistortion method but uses a real-time feedback approach [242, 243].

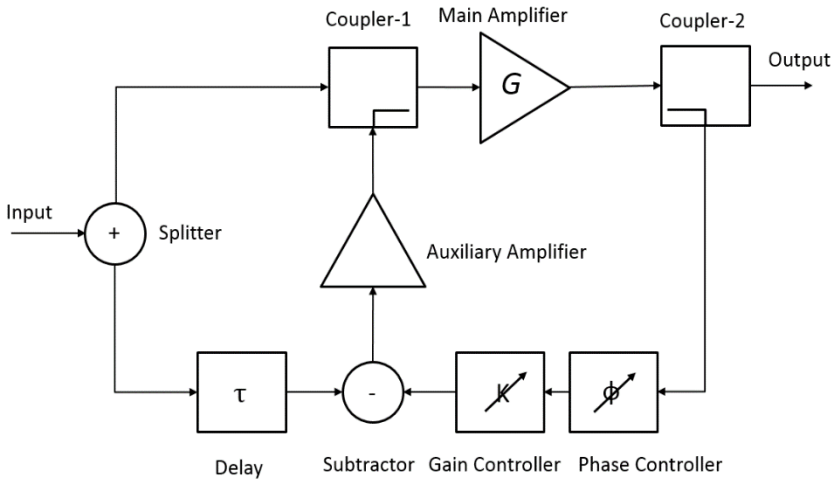

Figure 7.3: Distortion feedback linearization system.

In general terms, the RF feedback technique is more flexible than other techniques. In addition, the RF signal is compared at the input and output of the nonlinear device. Moreover, a feedback linearizer can be implemented in RF, intermediate frequency (IF) or baseband frequency. Consequently, feedback systems at the RF frequencies suffer time delay between the appearance of the power amplifier output signal and the subtraction of the input and reference signals. High delay in feedback system reduces the signal bandwidth and reduces operation stability. Furthermore, stability is difficult to achieve when the signal bandwidth of RF frequency rises to a high level. RF feedbacks can be used in the narrow band than the wideband applications [243].

7.2.2 Envelope Feedback

Envelope feedback known as modulation feedback is an indirect feedback technique used in reducing stability difficulties, inherited from RF feedback

system while using modulation frequencies. A general envelope feedback system is shown in Figure 7.4 below.

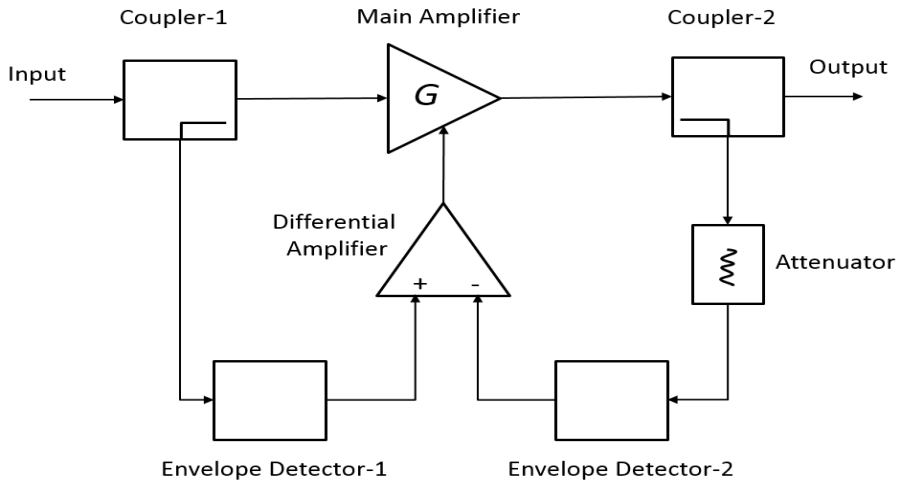

Figure 7.4: General layout of an envelope feedback system.

The feedback system shown in Figure 7.4 uses two similar envelope detectors attached to the input of the differential amplifier and the output of the main amplifier which produces an amplitude error correction signal from the envelopes. When the gain of the main amplifier is controlled by the error signal, the output envelope is forced to reproduce the input envelope to reduce distortion effects. However, this system can only at power saturation level degrade the system performance. Moreover, the phase distortion has been compensated by the non-coherent envelope detection. Hence, the gain of the differential amplifier needs to be set higher to obtain a lower power level and avoid unstable system. In this technique, the differential amplifier has limited the performance of the system due to slow signal processing of the data in high bit rates of megahertz which is not suitable for wideband applications [244].

7.2.3 Polar Loop Feedback

The polar loop feedback is another modulation feedback technique which can perform both amplitude and phase corrections. The amplifier characteristics are corrected in different loops. The polar as shown in Figure 7.5 is not a linearizer, but part of linearization is included in the modulation process. The entirely modulated input signal is set at the IF, the amplifier was used in ER formation to produce the AM transfer response, while on the RF carrier voltage controlled oscillator (VCO) source is locked to the IF signal to produce the PM response. Phase IF modulated and envelope signal are separated. The modulated IF signal is used to achieve phase-modulated carrier by the use of a limiter, while the envelope signal achieves the amplitude modulated carrier.

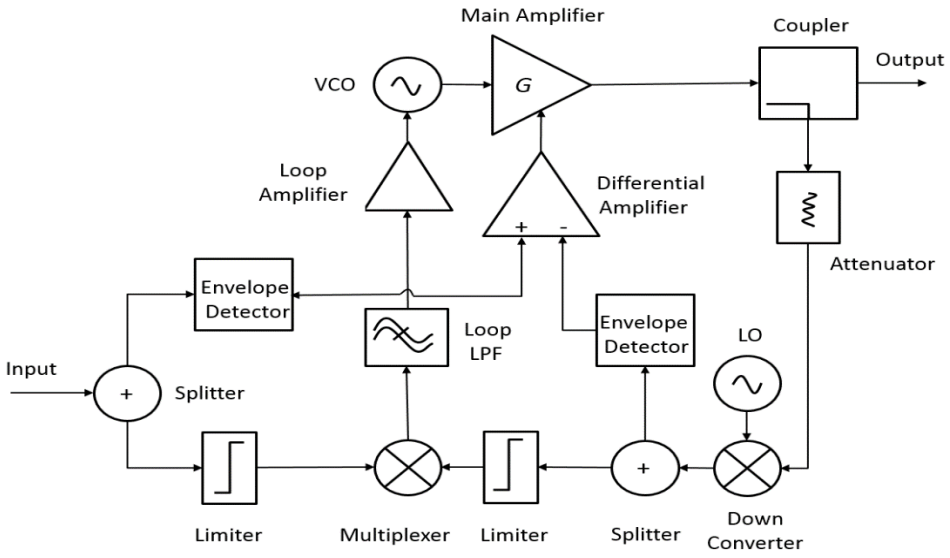

Figure 7.5: Polar-loop feedback system.

The signal is down-converted at the amplifier output, while a control loop produces an error signal to feed the ER envelope modulator through the baseband. The amplitude and phase transfer functions of the nonlinear amplifier are guided to the frequency divider and a phase-locked loop for cancellation. The envelope signal from the feedback loop, on the other hand, is directed to a

differential amplifier for cancellation. The resulting amplitude and phase signals were passed to the input of the power amplifier through the mixer [245]. The polar loop system can be implemented in the RF level. However, the main challenge is the bandwidth requirement for the amplitude and the phase error amplifiers. The modulated signal is split into envelope amplitude and phase components, resulting in a wider bandwidth for the channels, which causes stability limitations. Another disadvantage of the polar loop feedback is the PLL errors are locked due to sharp phase jump and instantaneous power [245].

7.2.4 Cartesian Loop Feedback

Cartesian loop feedback is a widely used correction system in the design of solid-state radio transmitters. It is capable of 30 dB reduction of intermodulation for signal modulation bandwidths lower than 0.1 MHz. Cartesian correction loop is not considered as power amplifier technique, but a transmitter that requires the modulating signal in the baseband as the original source. The recent digital systems have the advantage of having a baseband signal already available in an In-phase and Quadrature (I-Q) format. The resulting I-Q channels can be set to fit the path with bandwidth comparable to the original signal bandwidth [246]. The remaining I and Q signals passed through differential amplifiers and to the vector modulators for the actual RF signal ($S(t)$), where:

$$S(t) = I(t)\cos(\omega_c t) + Q(t)\sin(\omega_c t) \tag{7.9}$$

Where ω_c represents the RF carrier frequency, $S(t)$ is the output signal fed into RF power amplifier exhibiting some distortion. Some part of the output signal is down-converted to restore the distorted I and Q signals which are then compared with the baseband signal. The input differential amplifier gain will guide the loop

into making an output signal looking similar to the original I and Q signals. However, the accuracy of the signal depends on the gain, bandwidth and linearity of the down converter of the demodulators [246].

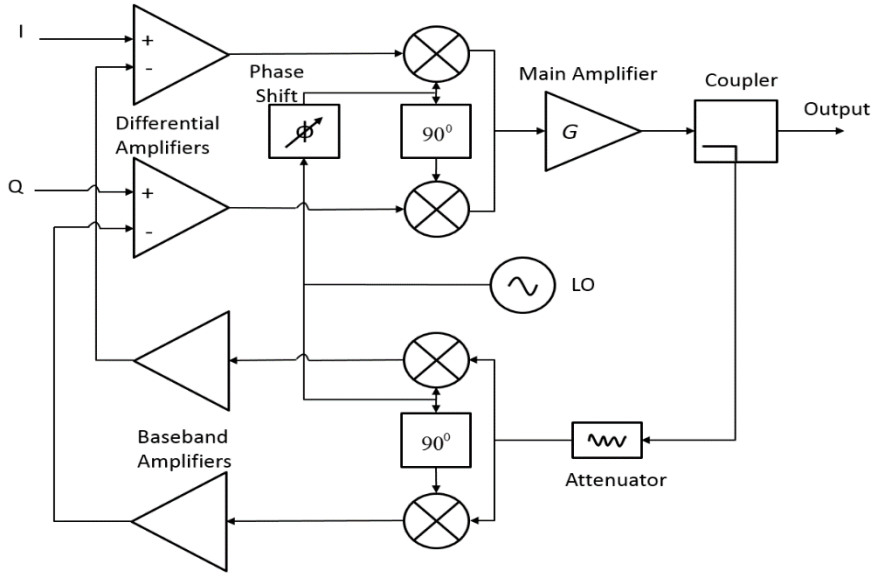

Figure 7.6: Cartesian-loop feedback system.

The Cartesian loop system operation is almost parallel to polar loop operation where the input and output signals are divided into I and Q signals using a broadband phase shifter and a differential amplifier. The phase shifter ensures the relationship between the input and feedback signals to remain constant. However, the temperature and power level change based on the phase shift of the local oscillator and this ultimately affect the stability of the system. In the case of the Cartesian loop in the wideband application, the system will not suffer stability as the overall performance is better than the polar loop system. However, there will be delays in the feedback chain. In addition to that, the Cartesian loop is also easier to implement than the polar loop, based on the availability of I and Q signals from the digital circuit. Another advantage Cartesian loop enjoys other than the polar loop is the regularity of bandwidth and gain in the Q signals

processing paths. This will mitigate the phase shift between the amplifier transfer functions processes [246, 247].

7.3 Feedforward Linearization

Feedforward is a well know RF technique used in the linearization of power amplifiers nonlinearities. The feedforward is centred on compensating a power amplifier nonlinear distortion at the output level, where the distortion components are subtracted from the overall output signal. Hence, through the feedforward chain, the distorted signals are achieved and forward to the output. Figure 7.7 presents a general layout of the feedforward system. The layout is composed of signal cancellation and error cancellation loops. In the signal cancellation loop, the fundamental signal is achieved by removing the intermodulation products. In the error cancellation loop, the linear amplified signal is achieved by deducting the adjacent distortion products from the overall output [248].

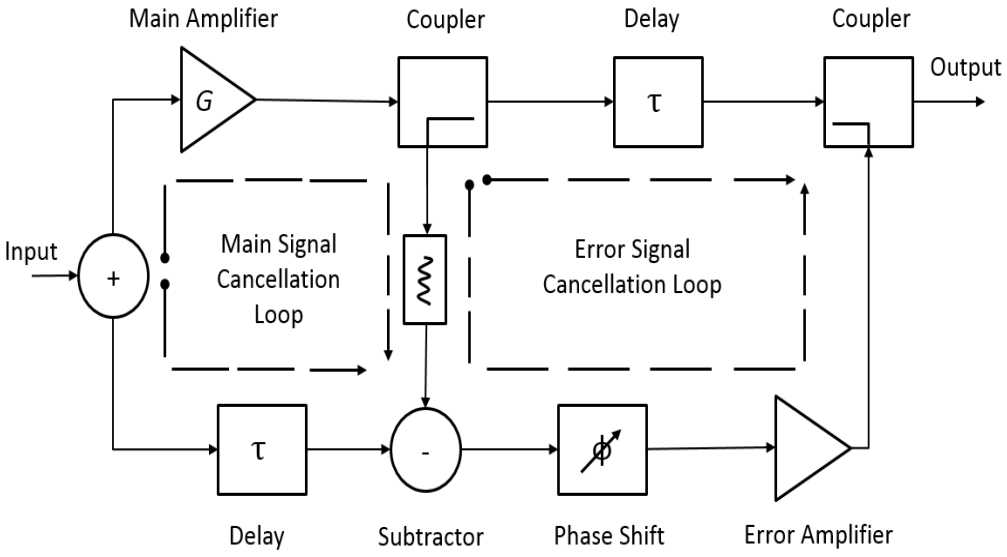

Figure 7.7: General layout of a feedforward system.

The layout also illustrates the input signal is split into the main part and error part. The nonlinear power amplifier amplified the signal at the main part, and the delay

of the amplifier is compensated by a delay line in the error part. In the main part, the distorted signal from a copy version of the original signal of the power amplifier forms an error signal. While the error amplifier amplified the error signal which was deducted from the main amplifier output signal. The deducted signal is referred to as a reference signal and the resulting distortion signal is achieved. The error signal from the error amplifier is used to obtain a suitable level and using the output coupler and phase shifter to add in anti-phase to the main output signal [248].

In general, the feedforward linearization technique provides excellent linearizing performance with unconditional stability and wideband signal capability. The linearization of this technique does not affect the gain of the power amplifier while maintaining phase tracking. However, this technique has some drawbacks such as low efficiency, modifying components characteristics due to heat and ageing, sensitive to circuit elements matching, and the use of a large number of components makes it complex, occupy more size, attract high cost and unsuitable for many applications [248, 249].

7.4 Envelope Elimination and Restoration (EER)

The Envelope Elimination and Restoration (EER) is a linearity and efficiency enhancement method which was proposed by Kahn in [24]. The aim is to split the input signal into two portions, which one potion is composed of amplitude modulation (AM) and the other potion is composed of phase modulation (PM) data. A diagram of EER has shown the separation of AM and PM modulated signals, the formation of envelope information before baseband amplification and formation of limiter before RF amplification [24, 250].

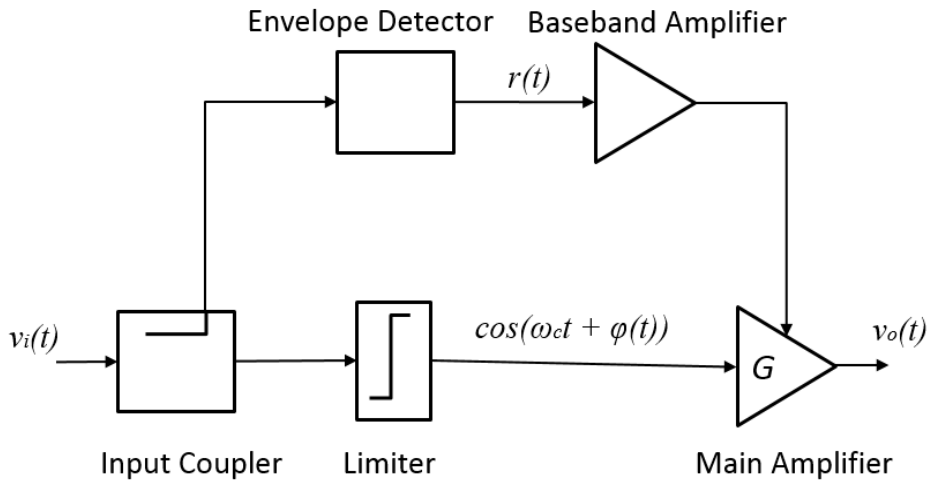

Figure 7.8: Envelope elimination and restoration system.

The general band pass signal is written as follows:

$$v_i(t) = r(t)\cos(\omega_c t + \varphi(t)) \tag{7.10}$$

Where $r(t)$ and $\varphi(t)$ $\varphi(t)$ are the amplitude and phase modulation of the input modulated signal, ω_c represents the carrier frequency which is dispersed from amplitude modulation use by an envelope detector. While the limiter formulated a phase modulation with the constant envelope as shown in the two equations (7.11) and (7.12):

$$r(t) = r_{AM}(t) \tag{7.11}$$

$$\cos(\omega_c t + \varphi(t)) = r_{PM}(t) \tag{7.12}$$

The limiter detects and removes the phase modulation (PM) distortions and the achieved PM signal is amplified by a switch-mode amplifier in order to preserve the information with high efficiency. The amplitude modulation (AM) signal is amplified by the baseband amplifier and modulated by the overall RF amplifier

[251]. In addition, at the overall RF amplification stage, the modulated overall RF signal and restoration of the constant envelope are however obtained by modulating the DC supply of the overall amplifier as illustrated in (7.13).

$$v_o(t) = r_{AM}(t)G(r_{PM}(t)) \tag{7.13}$$

Where G has added the gain of the overall RF amplifier.

The advantage of using EER approach is that high efficiency is achieved by using a switching amplifier at the overall RF amplifier stage, reduction of amplitude and phase modulation distortions and improving the linearity of the system [251]. The EER technique has also many drawbacks in practical implementation. The baseband amplifier consumes a considerable amount of power during amplification of AM modulated signal and hence, affects the overall efficiency of the system. The EER system suffers from intermodulation products due to a large number of nonlinear components such as nonlinear behaviour of envelope modulator. It is sensitive to delay, particularly between the separation of AM and PM paths, amplification of high level AM modulated signal by the overall RF amplifier and limiter adaptation of AM-PM signal [251, 252].

7.5 Linear Amplifier using Nonlinear Component (LINC)

The linear amplifier using a nonlinear component (LINC) is a linear amplification-based technique aimed at achieving compensation at microwave frequencies [253]. In this technique, high efficiency is maintained using switching power amplifiers. The LINC means two separate amplifiers are fed with constant envelope signals to produce a band pass signal. It is a linear input-output relation

where a circuit is composed of nonlinear components [253, 254]. Figure 7.9 illustrates the LINC concept with two high efficient nonlinear amplifiers.

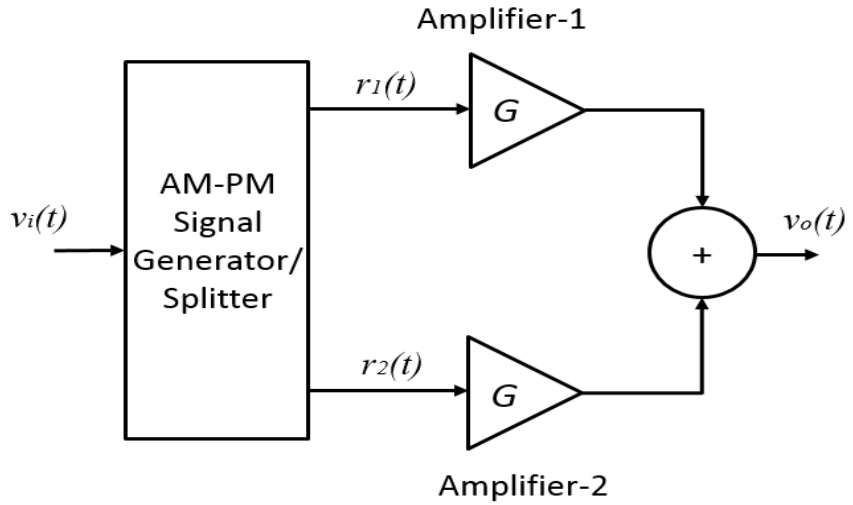

Figure 7.9: Linear amplification using nonlinear components system.

The signal coming from the source is given as:

$$v_i(t) = r(t)\cos(\omega_c t + \varphi(t)) \tag{7.14}$$

Where $r(t)$ and $\varphi(t)$ are the amplitude and phase modulation of the input modulated signal, ω_c represents the carrier frequency. The signal is split into amplitude and phase-modulated signals with constant envelopes. These signals are separated by the signal separation device, an AM-PM modulator [253]. A trigonometric transformation is used to derive the input signal in (7.14) which can be rewritten as:

$$v_i(t) = \frac{r_{\max}}{2}[\cos(\omega_c t + \varphi(t) + \vartheta(t)) + \cos(\omega_c t + \varphi(t) - \vartheta(t))] \tag{7.15}$$

Where r_{max} is the amplitude modulation signal and $\varphi(t)$ is expressed as:

$$\varphi(t) = \cos^{-1}\left(\frac{r(t)}{r_{\max}}\right) \tag{7.16}$$

The achieved equal constant-envelope phase-modulated signals are written as:

$$r_1(t) = r_{\max}\cos(\omega_c t + \varphi(t) + \vartheta(t)) \tag{7.17}$$

$$r_2(t) = r_{\max}\cos(\omega_c t + \varphi(t) - \vartheta(t)) \tag{7.18}$$

The constant-envelope phase modulated signals are amplified by two identical power amplifiers. The signals are combined at the output resulting from the (7.19) written as:

$$v_o(t) = 2r(t)G\cos(\omega_c t + \varphi(t)) \tag{7.19}$$

The output signal illustrated in (7.19) is an indication of linear signals amplified by two similar and highly efficient RF amplifiers. At the output of the amplifiers, the signals contain both AM and PM modulations, which are expected to retain only the phase data of the signal [253].

According to the theory of literature, Linear Amplification using Nonlinear Component is a simple and flexible technique for high efficiency and linearity [253]. Consequently, this technique has practical limitations such as:

- Very sensitive to gain and phase disparity between the two paths.
- The amplifiers must be the same to avoid distortion at the output.
- Signal separation and phase modulation inaccuracy due to uncertainty in providing an exact AM-PM modulator.

- Additional overall system complexity due to the circuit complexity of the modulator.
- Limitations in the overall system bandwidth for the effect of the gain and phase disparity of the two paths. Furthermore, the bandwidth of the generated modulation signals overwhelms ten times the original bandwidth.

7.6 Predistortion Systems

Predistortion is one of the most common and effective linearization methods that are based on adding a nonlinear circuit that exhibits inverse characteristics of the nonlinear device before the nonlinear device so that the combined output is linear. The inverse characteristics are obtained by the inversion of the nonlinear model that can be developed from input-output measurements. In another word, predistortion is based on expanding the input signal to compensate for the nonlinear distortion caused by the amplifier.

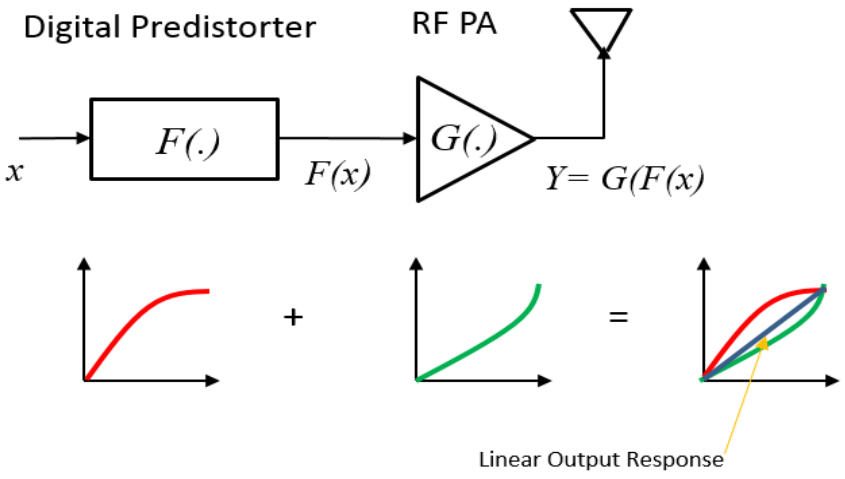

Figure 7.10: Fundamental of predistortion topology.

A predistorter can be built by introducing in the system a nonlinear block earlier to the device. The inverse of the amplifier function is represented by the transfer

function of the nonlinear block. Figure 7.10 has shown a predistorter which producing a linear response due to a cascade of nonlinear blocks in the system [255].

Figure 7.10 has shown a classic predistortion system topology where the AM-AM response of the RF power amplifier is predistorted. On the other hand, the AM-PM response can be corrected by means of introducing for the amplifier a phase to the input signal in the phase shift. Several techniques have been produced for the predistortion algorithms such as RF signal processing, digital processing and baseband frequency. These techniques can, however, be implemented based on the position of the predistortion in the system. It can be processed either in the RF, IF or baseband. Figure 7.11 has shown the three possible ways of implementing predistortion in the transmitter [255].

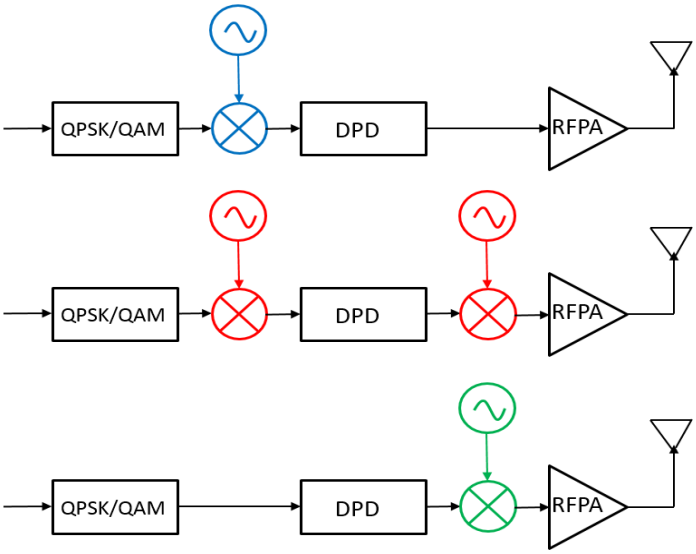

Figure 7.11: RF, IF and BB predistorter positions in RF transmitters.

The RF predistortion technique operates right on the input signal of the RF power amplifier. It is simple to implement on high frequencies but suffers challenges of constraining adaptability and poor performance. It is more active in correcting the

odd-order distortion components [256]. The IF predistortion is simple and more adaptable than the RF predistortion. It operates on the intermediate frequency and different RF frequencies. However, it has its limitation such as operating on narrow bandwidth than RF predistortion and limitation over digital signal processing techniques. Since, IF predistortion lacks high digital sampling frequency capability, it cannot be used efficiently. In the case of baseband predistortion, it is simpler with high adaptability technique than IF and RF predistortion. It operates at the RF to baseband after the signal is down-converted. The predistorted signal will now be passed to the RF power amplifier after it is up-converted to the carrier frequency signal. These classes of predistortion are characterize based on adaptableness towards power amplifier [256].

A good design of digital predistorter depends on a fixed power amplifier behavioural model which can help discover the inverse function of the nonlinearity. The amplitude and phase modulation responses are the nonlinear static function of the power amplifier. In some cases, the AM-AM and AM-PM responses frequency bandwidth independent. But, according to the research facts, the output signal is determined by the previous and current input signal values. Similarly, the preceding values of the input signal diverge on the frequency bandwidth. The digital predistortion can be used for several applications such as the narrowband, wideband and broadband application. For a narrowband system, the key to predistortion solution is to develop a nonlinear system to ensure a fixed transfer function. Whereas, in the broadband systems, the transfer function diverge due to memory effects of the power amplifier. However, way out is to use an adaptive solution for which a feedback device from

the output signal can be used to improve the adaptive predistortion process with the extra robust performance [177].

The digital predistortion system is divided into memory and memoryless. The memory predistorters are implemented by digital solution, while memoryless predistortion can be implemented by digital or analogue solutions. The predistortion methods are divided into analogue and digital predistortion (DPD). Some of these systems are discussed in this section:

7.6.1 Analogue (RF) Predistorter

The different ways the analogue predistortion can be implemented is by the design of multipliers to achieve polynomial nonlinearity or by basic diodes and transistors circuit. The analogue predistorter can be fixed or adaptive which however depends on the system requirement. One of the system requirements is high linearity. It is highly challenging to implement an analogue predistorter with high linearity which can meet all these conditions. To achieve these conditions, a dependable system must be employed to correct the predistorter based on the potential changes in the system. The operation bandwidth suffers from gain and phase flatness of the predistorter and the RF power amplifier in the system. In addition, memory effects also limit the performance of linearization [257]. Figure 7.12 has shown a block diagram of an RF predistorter.

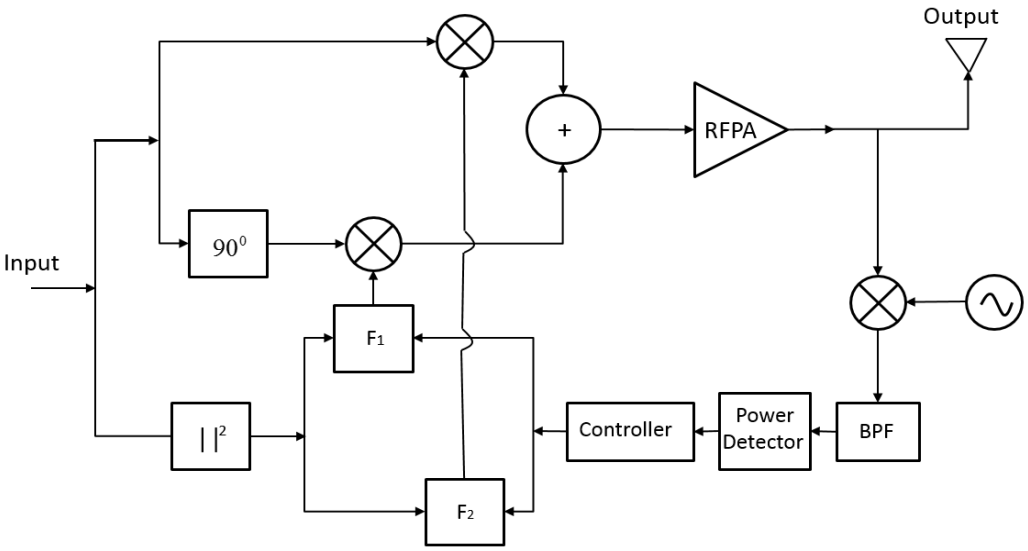

Figure 7.12: Block diagram of an RF predistorter.

From the possible implementation of the RF predistorter figure illustrated above, *F1* and *F2* are the polynomials that define the predistorter. The output signal information which is fed to the feedback system is used by the controller in updating the coefficients of polynomials. The coefficients of *F1* and *F2* are controlled by the squared magnitude of the input signal and power in the adjacent channel of the output spectrum. These polynomials are implemented using analogue circuits and the coefficients are adjusted according to the discharge of the adjacent channel. The polynomials (*F1* and *F2*) will then increase the level of the input signal to the output of the system. The analogue RF predistorter has a simple circuitry, easy to use, cost very low and also consumes very low power. It is capable of managing signal in a broadband system. On the other part, it introduces insertion loss product in the system, its performance moderate in term of linearization and challenging to implement the adaptive version [257].

7.6.2 Digital (IF) Predistorter

IF predistorter is a well-known high-speed digital system, it is flexible and easy to implement by the use of digital devices. It is more stable than the RF predistorter,

which makes it adapt in times of temperature and time oscillation. Subsequently, the predistorter is implemented digitally and friendlier than the analogue predistorter. Figure 7.16 illustrates the possible implementation of a mapping digital predistortion system with a mapping unit at the input. The input *I* and *Q* signals are mapped to produce I' and Q' modulated signals. The transfer function of the mapping unit is defined by the in-phase, quadrature and the gain of the predistorter [258]. The outputs at the mapping system are expressed as follows:

$$I' = G_I(I,Q) \tag{7.20}$$

$$Q' = G_2(Q,I) \tag{7.21}$$

Where *G* stands for gain and represents two-dimensional function (*G1* and G_2). The predistorter consists of a look-up table kept in the system memory. The disadvantage of IF predistorter is that it requires a large amount of memory. It slows down the system due to the size of the memory.

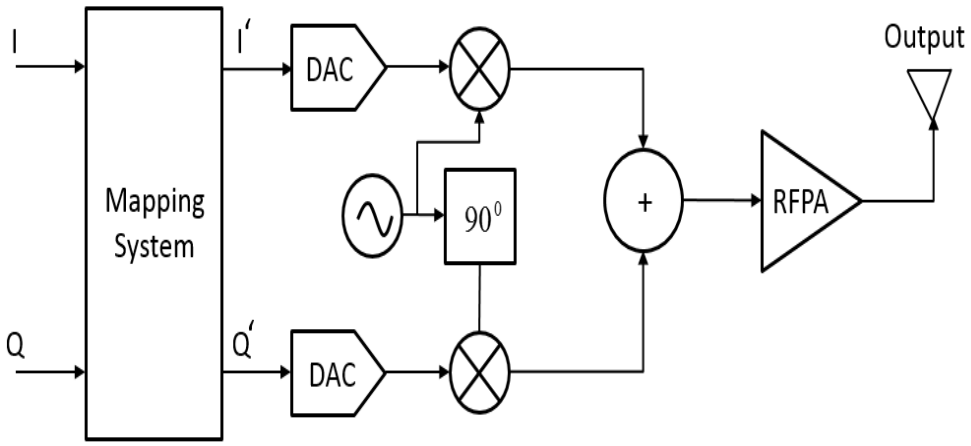

Figure 7.13: Mapping digital predistorter.

Another type of IF digital predistorter is a gain-based system. It is developed to reduce the memory size of the predistorter by interpolation. In this case, the

interpolation unit research for the transitional values that are omitted in the look up table. To organize the values of the look up table, the complex input signal is increased into two by the magnitude of the predistorter [258] as shown in Figure 7.14.

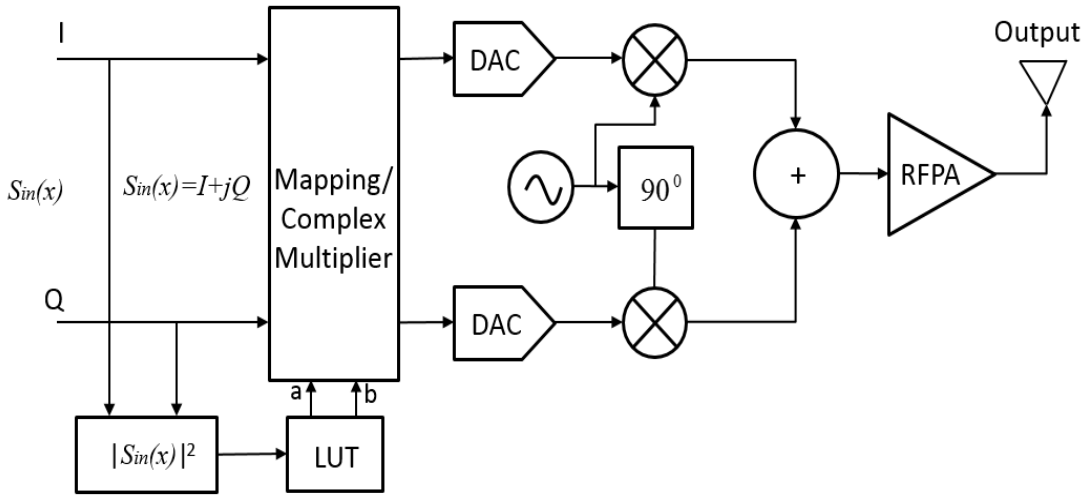

Figure 7.14: Gain-based digital predistorter topology.

This predistorter is again based system where complex mathematical processing in the digital domain is implemented. This means that the samples of the data are constantly changing and hence, introduce limitation on the operating bandwidth. Increase in data sample increases the sampling frequency resulting in more mathematical process and increases power consumption. However, the power consumption can be reduced by the use of power consumption reduction techniques [258].

7.6.3 Baseband Predistorter

Baseband predistortion system is a memoryless type of predistorter that is classified into data and signal predistortion. Data and signal predistorters have been effectively working since discovery over the years. The data predistorters

input signal constellation points are altered before directed to the transmit unit. Consequently, after the pre-distorter, the corrected signal constellation appeared at the output of the power amplifier. This type of predistorter can be implemented based on the position of the shaping filter which are in two types. The first type of shaping filter is an RF band pass filter, positioned subsequent to the RF power amplifier. It is sufficient to compensate for the nonlinearity of a memoryless RF power amplifier. While the second type is more of baseband filter positioned directly subsequent to the predistorter [259]. Figure 7.15 has shown the schematic diagram of the two data pre-distorters. The RF band pass filters with sharp cut-off frequency are hard to achieve. Due to high losses, the structure has become unattractive. The predistortion process is not accurate using the second type of data predistorter, as the correction is useful to only signals that the level of power is shown in the signal constellation [259].

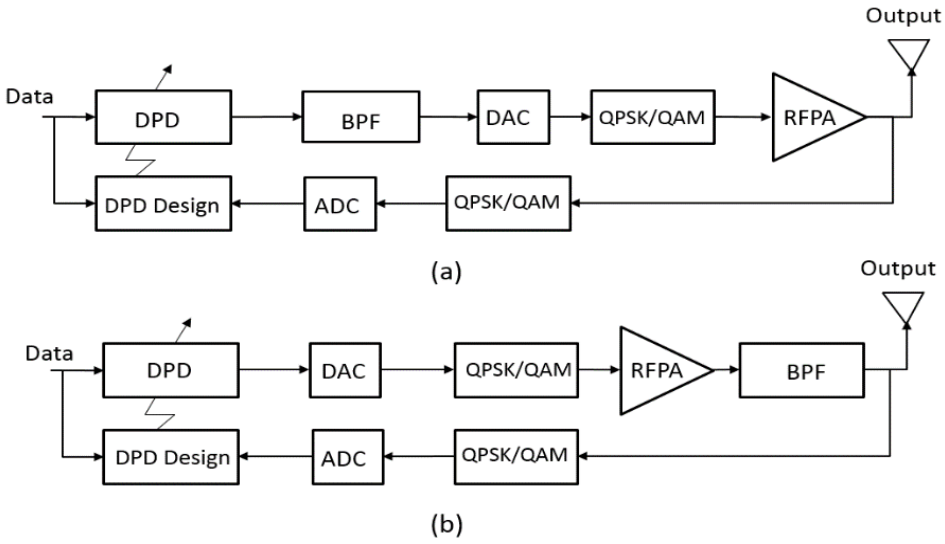

Figure 7.15: Memoryless data predistorters.

Due to the limitation of the data predistorters system, the symbol rate results in correcting only the channel bandwidth data. Whereas the transmitted digital symbols are directly affected by the nonlinearity of the amplitude-modulated

signals. Hence, the use of this system is sufficient to overcome the nonlinearity of the power amplifier. The data predistorters are commonly used in linear modulation such as pulse amplitude modulation (PAM). However, nonlinear modulation applications such as OFDM are not suitable for data predistorter [260].

In the case of memoryless digital signal predistorter, the multicarrier application is used at the baseband of a transmitter for arbitrary input waveforms processing. This system shows a better performance than the data predistorter. Generally, signal predistorter can be used for both linear modulation and nonlinear modulation applications. The memoryless data predistorter and memoryless signal predistorter systems have some common characteristics. But, in the case of the type of signal usage depends on predistorter suitability. For example, a linear modulation such as pulse amplitude modulation system can be corrected using a signal or data predistorter. Whereas, a nonlinear modulation such as orthogonal frequency division multiplexing or a phase modulated signal can be corrected using a memoryless signal predistorter [261].

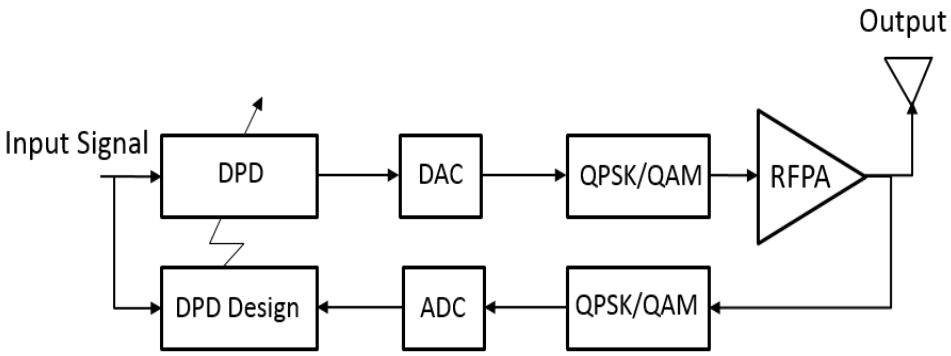

Figure 7.16: A memoryless signal predistorter.

Figure 7.16 is a block diagram of a memoryless digital signal predistortion model. It was extended in 1991 by Sari and Karan after the first signal predistorter was

developed based on look up table for linear modulation application by Saleh. In general, the digital signal predistorters are classified into two methods. The mapping technique, in the form of look-up-tables and polynomial functions which is by means of either polar (magnitude and phase) or Cartesian (in-phase and quadrature). Some of the examples of digital predistorter models are look-up-table, nested look-up-table, Volterra, memory polynomial, envelope memory polynomial, Wiener, Hammerstein, augmented Hammerstein, augmented Wiener and twin-nonlinear-two-box. Several other models have subsequently been investigated and developed for different applications [261, 262].

7.7 Comparison of Different Linearization Techniques

Several linearization techniques have been discussed in this section. It is important to compare from the simplest technique to the most complex pre-distorter technique. Since predistorters are implemented in real systems, linearity and complexity of the technique can be the parameters for comparison. The simplest linearization technique such as power back-off [263] losses efficiency for linearity. Such techniques are not used regularly due to the inefficiency of the device. The RF feedback method [240, 243] perform better with low power applications, but not suitable for high-frequency systems due to the high cost of implementation. Another drawback is the feedback correction algorithm has low correction capability and poor digital implementation. The polar loop feedback [245] and envelope elimination and restoration methods [250] are narrowband applications, simple to implement and have moderate complexity. However, limited by linearization process and stability. Furthermore, the wide bandwidth of the phase detector at the output of the system produces bandwidth noise and unwanted signal. The Cartesian loop [264, 265] method uses the real and

imaginary parts of the baseband data but is not suitable for multicarrier systems. The feedforward is a wideband system with amplitude and phase imbalance of loop circuit elements in which reduces the linearization performance due to mismatched. But, the adaptive feedforward method [248] can be used to correct the mismatch. The disadvantage of adaptive feedforward has high complexity and complex to implement. Since, digital predistortion technique [266] is not an accurate method of compensation, adaptive baseband predistorter [267] is developed to linearize simple and highly complex systems. Similarly, comparing the performance between look up table and polynomial predistortion [268] based models, where the former is known to be the excellent model for linearization using any kind of power amplifier. The disadvantage of this model is due to its large size which causes low convergence speed. Therefore, the polynomial predistortion based model can be used as an optional method considering linearization and complexity of a system. It is suitable for orthogonal frequency division multiplexing application and other multicarrier applications. After the performance comparison of several type of predistortion models discussed in previous section, a Hammerstein predistortion model and the contribution will be discussed in following section. Its performance will be shown in comparison to other models in terms of the size, complexity, reliability, flexibility, stability and adaptability towards other applications.

7.8 Adaptive Hammerstein-Wiener Predistortion Design Approach

The Hammerstein model is an inverse structure of the Wiener system. A predistorter is constructed using a memoryless nonlinear subsystem cascaded with a linear time-invariant filter. Many research works have been developed on Hammerstein predistorter system. However, this research proposes a new

approach using Hammerstein-Wiener system to compensate the memoryless and memory effects of the RFPA.

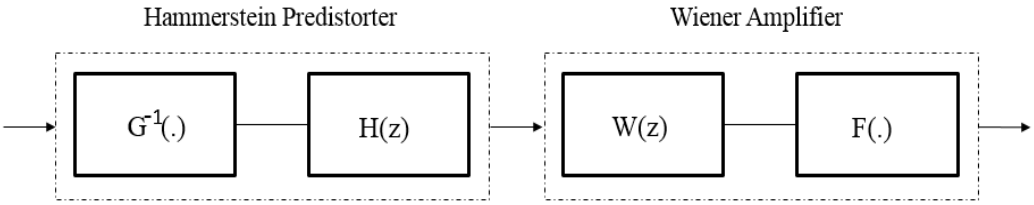

Figure 7.17: A Hammerstein predistortion and power amplifier equivalent model of Wiener system.

Figure 7.17 has shown a block diagram of a Hammerstein predistorter and a Wiener model. Some of the common ways Hammerstein predistorter parameters can be estimated are briefly introduced in this work. Hammerstein predistortion can be approximated by structuring the Wiener system to be an inverse of the Hammerstein. The power amplifier parameters represented by the Wiener model which consist of FIR filter and a nonlinear block are determined using the preferred methods available. The inverse of each block is replaced in the Hammerstein predistortion system. The second way is that the nonlinear block of a power amplifier which contains AM-AM and AM-PM responses is considered to be an inverse of the nonlinear block of the predistorter. The linear and nonlinear blocks of both predistorter and power amplifier can be modelled using adaptive filters. The normalized least means square method can be used in approximating both the linear blocks of predistorter and the power amplifier. In the third case, the predistortion system, as well as the linear block of the power amplifier are approximated. The nonlinear block of the power amplifier is constructed with transfer function and characteristics are obtained from a single tone test. These are the very many ways in which the Hammerstein predistorter can create a

behavioural model of power amplifier such that it can behave like a linear system [269].

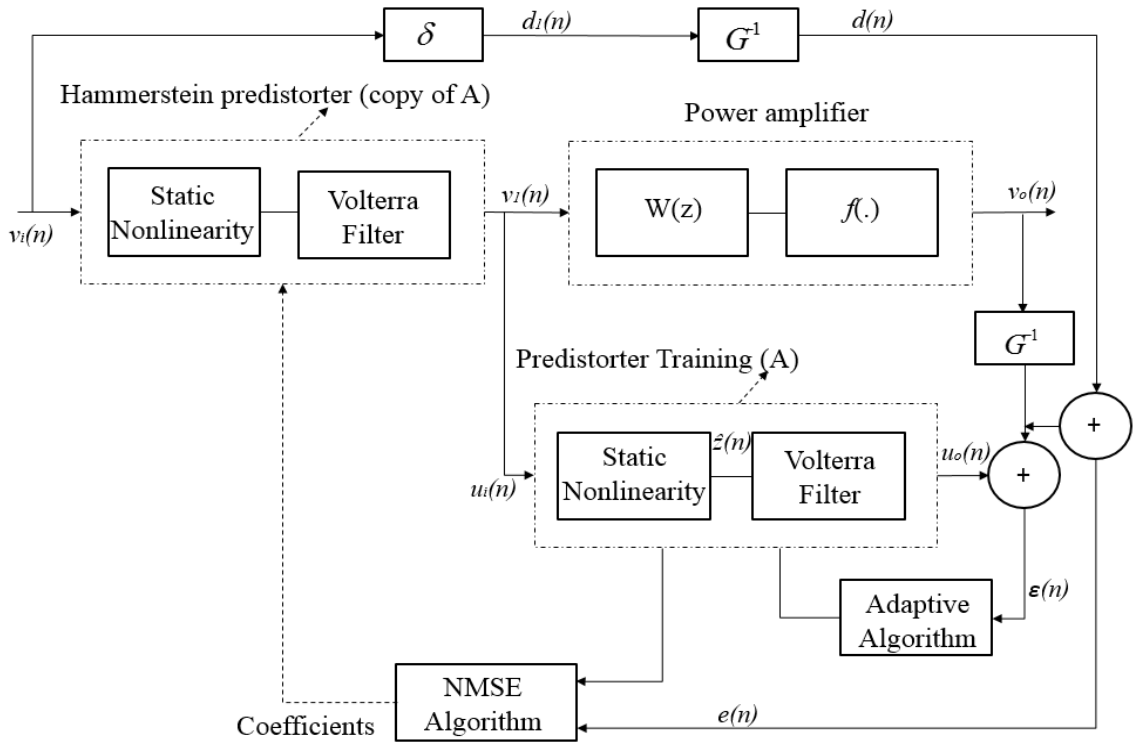

Figure 7.18: Enhanced adaptive Hammerstein-Wiener predistorter approach.

Several predistortion functions have been introduced to obtain the inverse of the power amplifier behavioural model. In this case, the Wiener model has been proposed as the function to provide the behavioural model for adaptive Hammerstein predistorter system with Volterra series as the linear filter. This work design and simulate an adaptive Hammerstein predistortion method using a normalized least mean square error based on indirect learning approach to correct the nonlinearities of the power amplifier. The model applies an indirect learning approach to obtain the predistorter coefficients. The indirect learning method updates the coefficients of the Hammerstein predistorter based on the linearization errors between the input signal of the Hammerstein predistorter and the output signal of the RF power amplifier. This method is used due to its adaptability and structure of the predistorter [269].

Figure 7.18 has shown an enhanced adaptive Hammerstein-Wiener predistorter with the indirect learning-based structure used for identification. The aim of this structure is to achieve a linear power amplifier output ($v_o(n)$) with respect to the predistorter input ($v_i(n)$). Hammerstein predistortion model is designed with a truncated Volterra filter to compensate for the power amplifier nonlinear memoryless and memory effects. The performance of the predistorter improves when harmonic components, intermodulation terms and cross-terms are incorporated in the model. It makes the Hammerstein predistorter correct effectively, the nonlinear distortion effects of the power amplifier. The input signal to the predistorter training system ($v_i(n)$) represents the output signal of the Hammerstein predistorter system ($v_1(n)$), while the output signal of the power amplifier is normalized by the linear gain (G^{-1}). However, the input signal of the power amplifier is the output of the predistorter including the signal from the pre-distorter training sequence. The signals received from the predistorter system are used in extracting the static nonlinearity where $\hat{z}(n)$ can be expressed as:

$$\hat{z}(n)=\sum_{t=0}^{N}\beta_{2t-1}u_i^{2t+1}(n) \tag{7.22}$$

β_{2t-1} are the coefficients of a polynomial describing the static nonlinearity of the nonlinear block. In discrete-time, the second-order Volterra series with finite memory systems is expressed as:

$$u_o(n)=\sum_{t=0}^{M_1-1}h_1(t)\,\hat{z}(n-t)+\sum_{t=0}^{M_1-1}\sum_{r=0}^{M_2-1}h_2(t,r)\,\hat{z}(n-t)\left|\hat{z}(n-r)\right| \tag{7.23}$$

Where M_1 and M_2 represent the memory durations of the first and second-order terms. $h_1(t)$ and $h_1(t, r)$ are the complex Volterra kernels of nonlinear order 1 and 2. The Volterra filter is used for mild nonlinearity. The cross-terms and the second-order of nonlinearity are chosen to reduce the complexity of the algorithm. The series is expressed in vector form as:

$$v_1(n) = H^T Y \tag{7.24}$$

Where $M_1 = M_2 = M$ and

$$Y = [h_1(0),..,h_1(M-1),h_2(0,0),..,h_2(0,M-1),h_2(1,0,..,h_2(1,M-1),.., h_2(M-1,M-1)]^T \tag{7.25}$$

$$H = [v_i(n),\cdots,v_i(n-M+1,v_i(n)|v_i(n)|,\cdots,v_i(n)|v_i(n-M+1)|,\cdots, v_i(n-1)|v_i(n-M+1)|,\cdots,v_i(n-M+1)|v_i(n-M+1)|]^T \tag{7.26}$$

By applying the normalized least mean square method, the filter coefficients can be developed by:

$$Y^{(n+1)} = Y^{(n)} + \mu \frac{e(n) * H}{\in + \|H\|^2} \tag{7.27}$$

Where $e(n)$ is given by:

$$e(n) = v_1(n) - H^T Y \tag{7.28}$$

$e(n)$ is the error terms which is equivalent to zero which means that $vo = Gv_i(n)$, while, the power amplifier nonlinearity is invertible. The error energy $||e(n)||2$ is reduced to converge the algorithm. The aim is to find the parameters of the

predistorter. Once the parameter is found and the characteristics of the power amplifier are not fluctuating, the predistorter training block will be switched off until the predistorter parameter require an update due to shift in power amplifier characteristics.

7.8.1 Verification with OFDM Application

In this section, the proposed digital predistortion technique is verified by simulation. The equivalent model of the Wiener system is used as the amplifier model. The transfer functions are extracted from the proposed balanced amplifier as previously discussed. Estimations algorithms are used to validate the matrix for the coefficients of the amplifier polynomials. Indirect learning architecture is used in order to find the inverse model as explained in the previous section. The Hammerstein model is used as the predistorter model in the IEEE-OFDM transceiver system to verify the amplifier nonlinear behaviour and the performance of the transceiver. The performance of the predistortion is investigated using different modulations in the OFDM system [8]. Performance results of the OFDM transceiver system is illustrated in linearization results, transmitted and received constellation, OFDM complex signal on-time scope frame and the transceiver BER results.

Figure 7.19 shows the IEEE-OFDM transceiver system which was used in the simulation. In the simulation, the amplifier was linearized using the AM-AM and AM-PM transfer functions to generate polynomials in the MATLAB. The extracted AM-AM and AM-PM data are measured in the context of the normalized input voltage as a function of the output voltage. The MATLAB curve fitting generated AM-AM polynomials is expressed as: $a_6 = 33.066$, $a_5 = -85.52$, $a_4 = 82.06$, $a_3 = -$

34.052, a_2 = 2.85, a_1 = 3.21 and a_0 = -0.01. The AM-AM distortion was cancelled as the device reaching a saturation point.

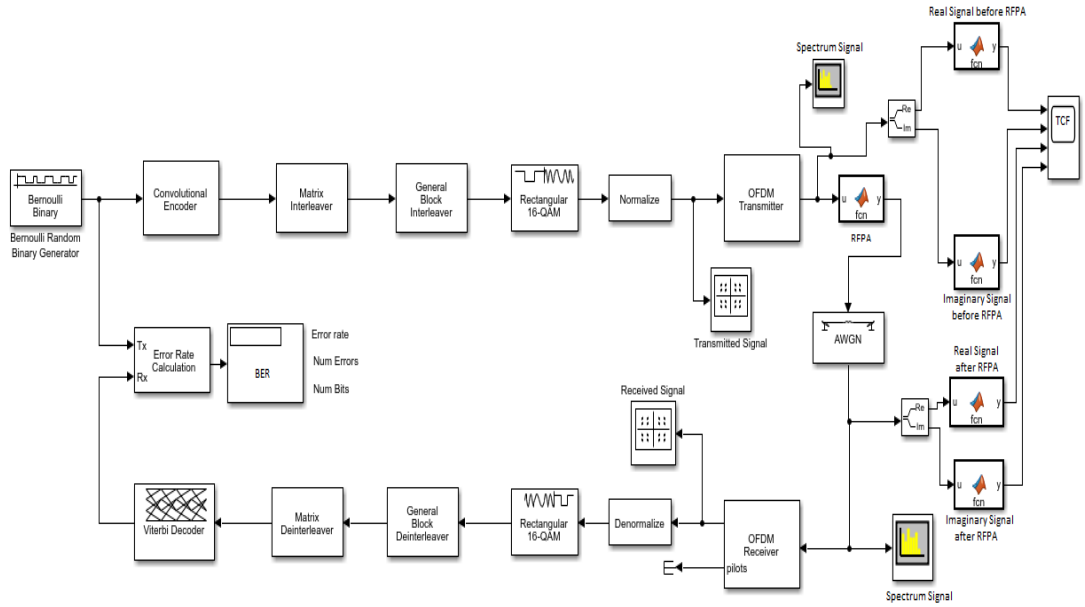

Figure 7.19: Simulated IEEE OFDM transceiver system.

The normalized input voltage as a function of output phase of the amplifier is also considered with the following AM-PM MATLAB fitted coefficients to generate polynomials expressed as: b_6 = 3.5485, b_5 = -5.7836, b_4 = 3.0384, b_3 = -0.8434, b_2 = 0.1826, b_1 = -0.0225 and b_0 = 0.1001. The AM-PM distortion was removed as the device reaching a saturation point. This data will be embedded in the device under test (DUT) of a Simulink transceiver system based on IEEE 802.11a OFDM HiperLAN/2 standard [8]. The variations of AM-AM and AM-PM can be presented in (7.29) and (7.30), expressed by:

$$y(t)=a_2u^5+a_4u^4+a_3u^3+a_2u^2+a_1u+a_0 \tag{7.29}$$

$$z(t)=b_5u^5+b_4u^4+b_3u^3+b_2u^2+b_1u+b_0 \tag{7.30}$$

where $y(t)$ and $z(t)$ are the AM-AM and AM-PM responses of the balanced RF power amplifier [270].

Simple linear formulas are presented for the functions involved in the amplitude and phase nonlinear models of the balanced amplifier as shown in the above equations and fit measured data very well. This model is exported to the memoryless baseband digital predistorter to linearize the DUT at the front-end of the OFDM transceiver system. The multiple-input-single-output (MISO) transceiver system is set to run on a simple linear model with baseband digital predistortion to compensate for the nonlinearity of a balanced power amplifier. In the transmitter, the signal was coded before OFDM. The modulation was normalised as a frame where 16-QAM was chosen for the OFDM system. The signal handed over to OFDM was cyclic prefixed [8].

The OFDM is a complex signal which can be seen in the frequency domain. The OFDM transmitter passed the complex signal to the power amplifier in the form of real and imaginary. The signal from the power amplifier is fitted in order to achieve signal variation. The amplitude of the input voltage of the power amplifier is 3 V. After the amplifier, the signal was handed over to the channel. The noise added to the channel is the AWGN. A magnitude in +ve and -ve polarities are used to re-organise the signal which remains exactly the same. Results have been produced to show the validity of the predistortion algorithms used in the process of transmitting OFDM signal through the proposed balanced RF power amplifier which the measured data was extracted for linearization [271].

The amplifier has been implemented on the OFDM transceiver system. Most figures of merits demonstrated the existence of amplifier distortion in the signal without linearization and several results showing the removal of distortion with the use of linearization technique. The transceiver has undergone several stages of simulation such as transmission without an amplifier, adding RF amplifier to demonstrate the existence of distortion and introduction of linearization technique to remove the amplifier distortion.

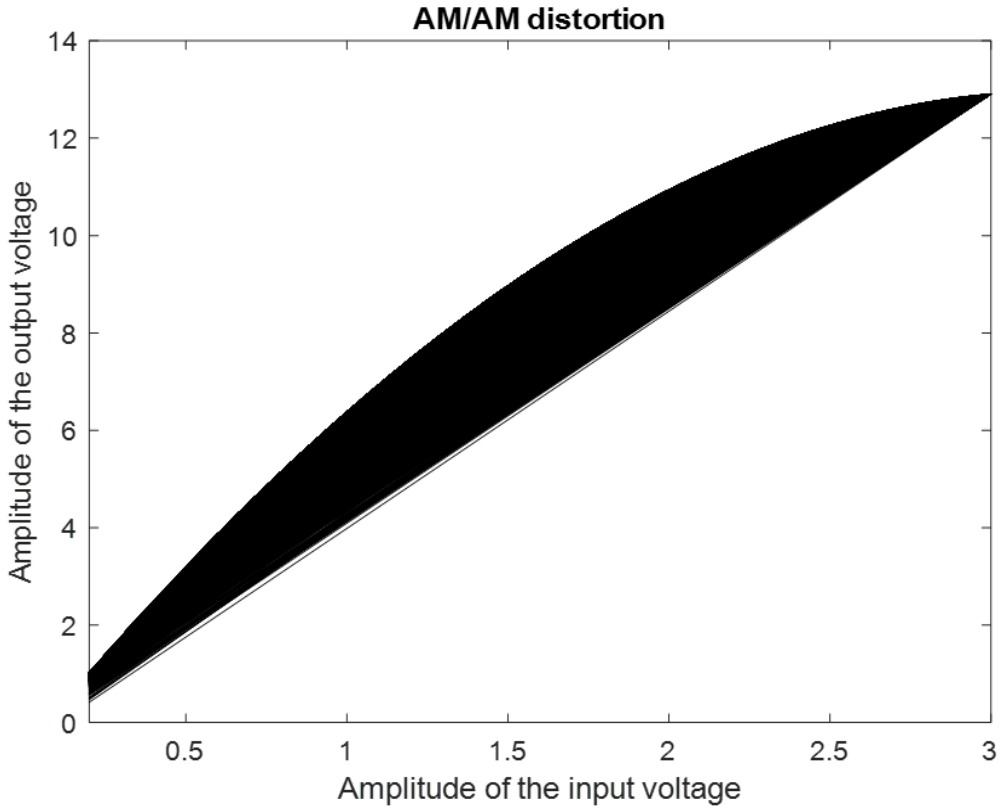

Figure 7.20: AM-AM distortion of the amplifier in the OFDM transceiver system.

In the first stage, the OFDM signal was transmitted to the channel without an amplifier. The signal is expected to be linear with no nonlinear distortion of all kinds. No amount of distortion demonstrated in all the results simulated, unlike when adding the power amplifier in the RF chain. In the case where balanced RF power amplifier is added to the RF front-end of the transmitter, performance

results have shown different ways in which the distortion was described such as display of AM-AM, AM-PM, 16-QAM constellation, bandwidth spectrum signal and OFDM signal in time scope frame.

First of all, Figure 7.20 and 7.21 depict results of AM-AM and AM-PM signal distortions of the amplifier. The responses of the amplifier have shown clearly that the device under taste is without linearizer. The AM-AM characteristics are displayed with thousands of bits which introduced errors because of the magnitude. Errors occurred due to variation of the magnitude. This also depends on the signal-to-noise-ratio (SNR). Hence, the errors can be reduced by increasing the level of SNR and controlling the magnitude.

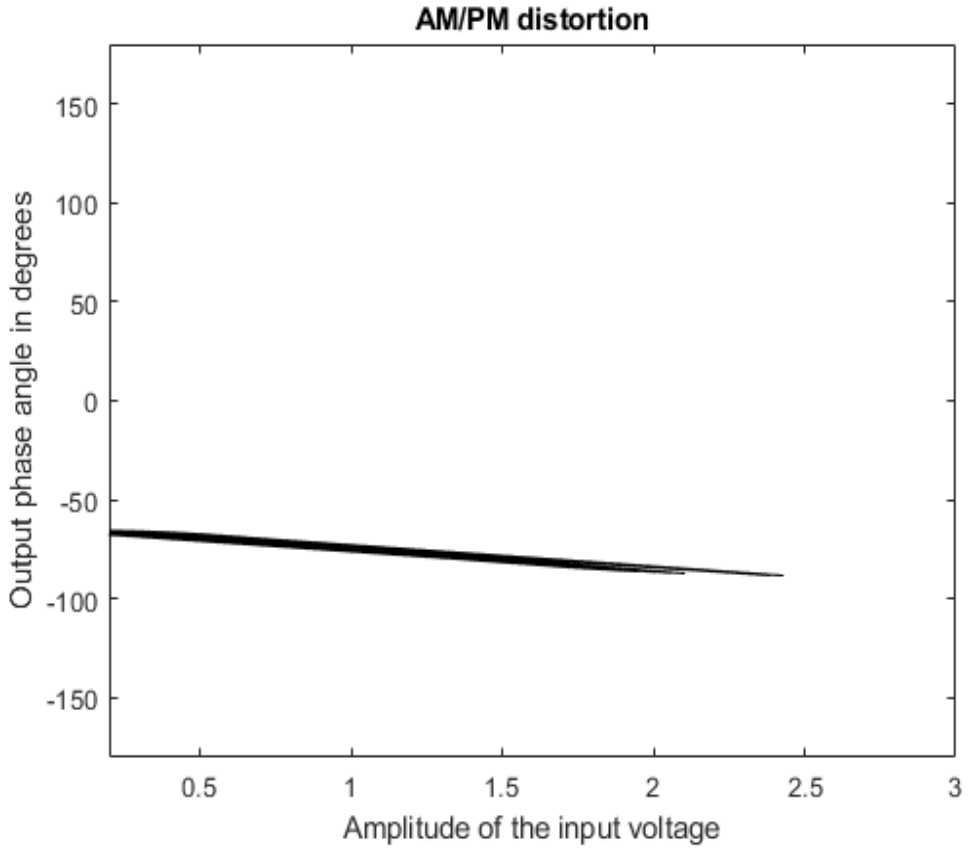

Figure 7.21: AM-PM distortion of the amplifier in the OFDM transceiver system.

Figure 7.22 shows the transmitted signal before the OFDM transmitter and received signal after the AWGN channel. The signal constellations represent the coded 0-15, 16-QAM modulation which at the transmit shows clean bits of a signal without adding noise. The received signal is the signal after demodulation of the OFDM signal which can be seen as similar constellation to the transmitted signal constellation except for the high distortion power amplifier which scattered the signal, at the same time affecting the magnitude and phase of the signal.

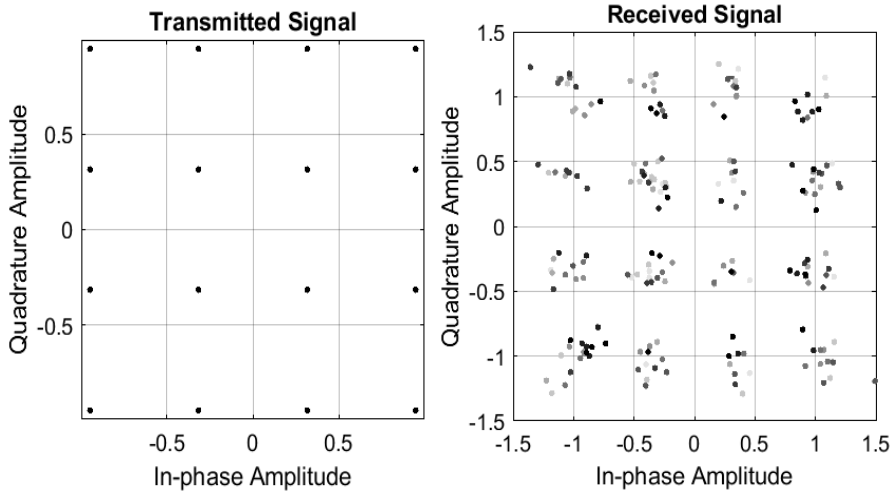

Figure 7.22: OFDM transmitted and received signal constellations without linearization.

Figure 7.23 shows the spectrum analyser figure of merit describing the OFDM frequency domain signal before and after the channel. The bandwidth and sampling frequency used in the OFDM signal are shown. It also shows the bandwidth that was utilised during the transmission.

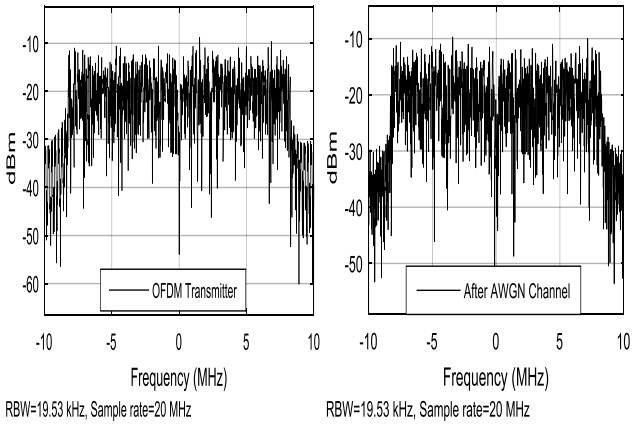

Figure 7.23: Spectrum signal illustrating the bandwidth.

Figure 7.24 shows the time scope figure of merit demonstrating the OFDM complex signal in two forms which are before the power amplifier and after the AWGN channel. Each signal has been displayed with a real and imaginary portion as shown below.

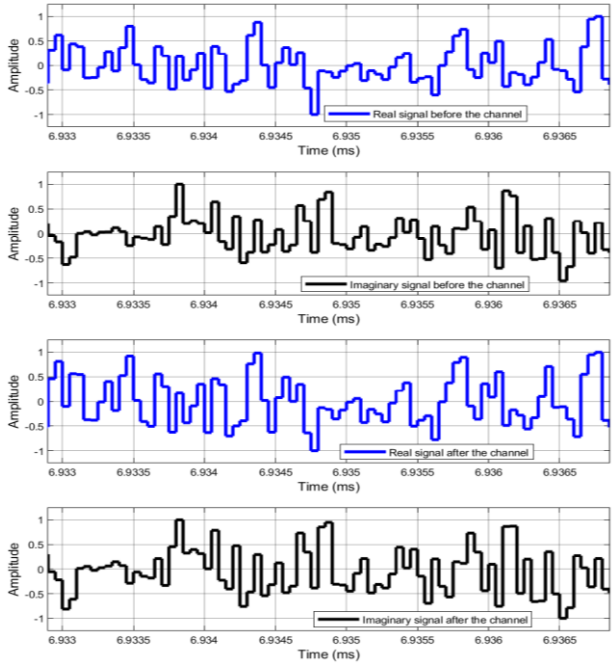

Figure 7.24: OFDM complex signal on-time scope frame before linearization.

In the previous stage, the OFDM signal was transmitted to the channel with the proposed amplifier where results were presented with distortions causing signal

variation in the system. In the next stage, predistortion is introduced to linearize the nonlinearity of the RF power amplifier. In linearization, signal variation does not change the phase, but changing the magnitude and will stay where it is or on the same angle. This implies that the phase distortion is not existing in the signal. To analyse the predistortion, it is assumed that the predistorter is added before the power amplifier, which means adding the phase on the signal to remove the amplitude. The predistorter and the power amplifier can be expressed mathematically as:

$$Pe^{J\phi} + Ae^{J\phi} = 0 \tag{7.31}$$

Where $Pe^{j\varphi}$ is the linearizer and $APe^{j\varphi}$ is the RFPA distortion. The expression can be rewritten as:

$$PA(e^{J\phi_P + J\phi_A}) = 0 \tag{7.32}$$

Then

$$\phi_P + \phi_A = 0 \tag{7.33}$$

To cancel the RFPA distortion, it can be defined as:

$$\phi_P = -\phi_A \tag{7.34}$$

The equations above were added to the angle of the input signal as a means of predistortion to compensate for the nonlinearity of the amplifier. However, performance results have shown different ways in which the distortion of the amplifier was compensated.

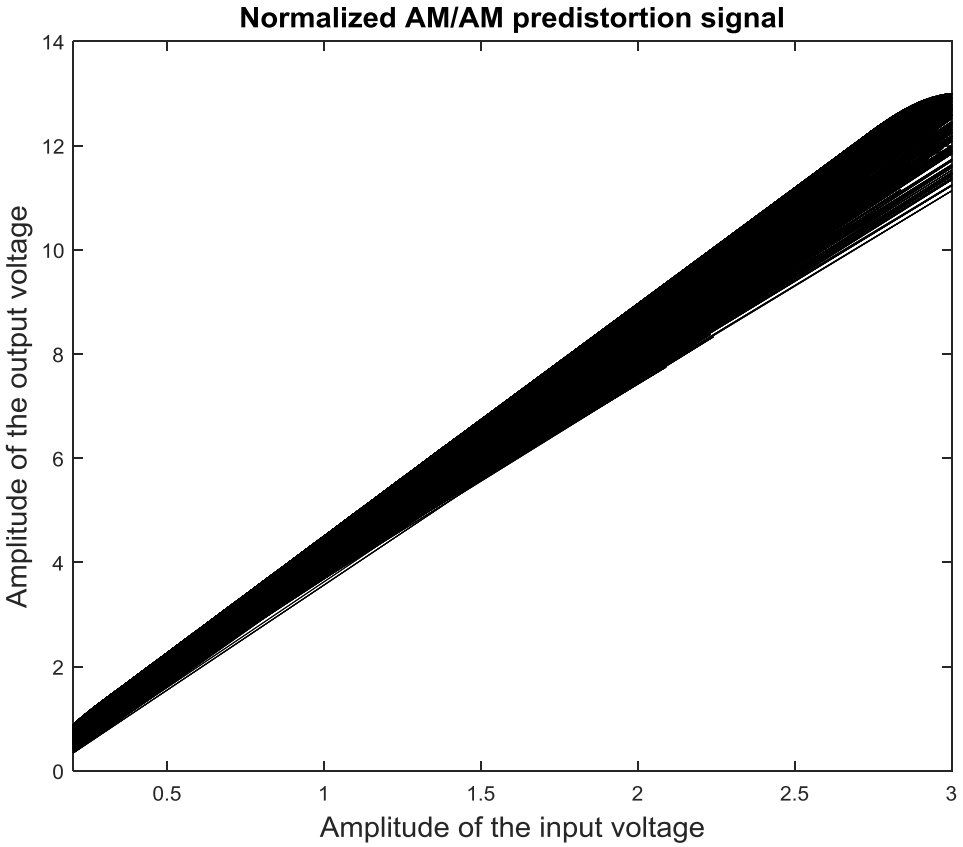

Figure 7.25: Normalized AM-AM amplifier predistorted signal in OFDM transceiver system.

The first result of linearizing the power amplifier is shown in Figure 7.25. The figure shows the normalized AM-AM response of the amplifier signal linearized using the predistortion technique. The responses of the amplifier have shown clearly that the device under taste was responding to linearization. The AM-AM characteristics are displayed with thousands of bits which errors were introduced because of the magnitude. Errors occurred due to variation of the magnitude. However, adapting predistorter reduced the thousands of spikes and linearized the signal.

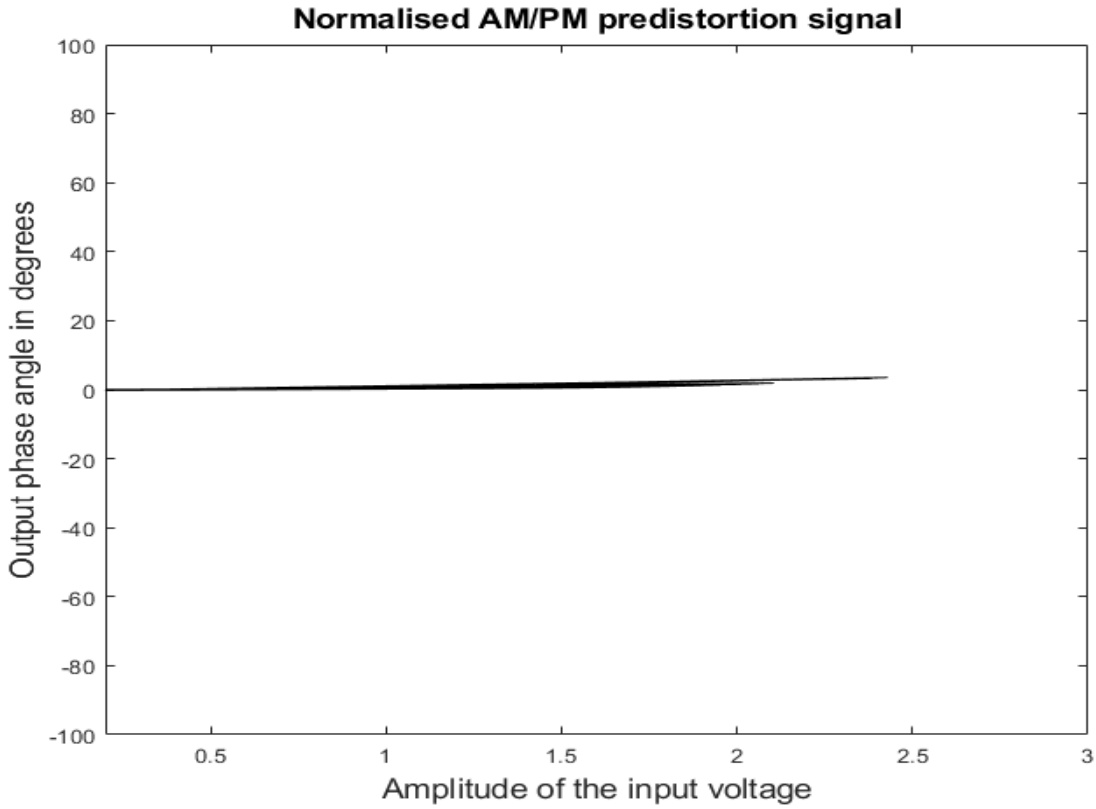

Figure 7.26: Normalized AM-PM amplifier predistorted signal in OFDM transceiver system.

Figure 7.26 shows the normalized AM-PM amplifier predistorted signal. Like mentioned in Figure 7.25 that spikes were generated on the amplitude signal affecting the performance of the predistorter is also experience in AM-PM signal as shown above. The predistortion cannot remove the distortion properly which has also shown no very effective impact on signal. The amplitude and phase of the amplifier were simulated by normalization. AM-AM and AM-PM signals were predistorted by normalizing the polynomials. The performance of the predistorter at the stage of normalizing the polynomials has improved the AM-AM signal of the amplifier.

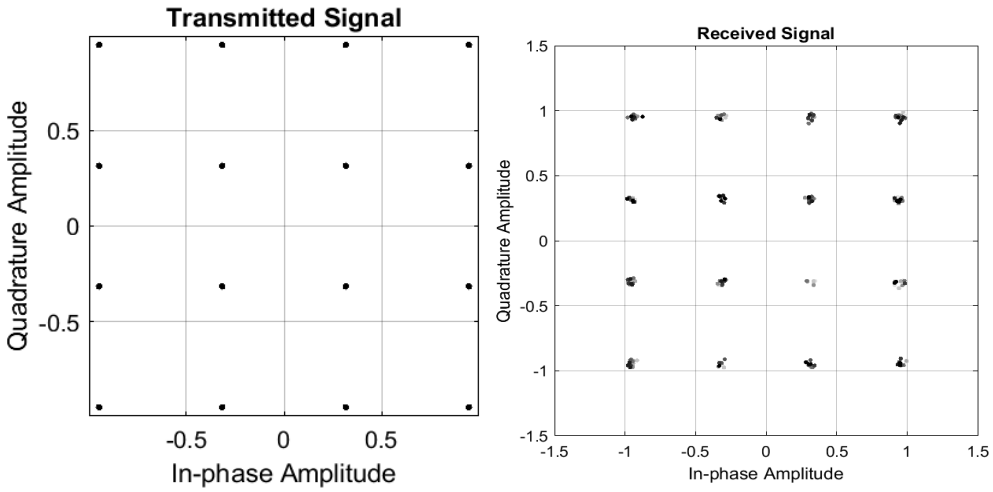

Figure 7.27: OFDM transmitted and received signal constellations after linearization.

Figure 7.27 shows the signal before the OFDM transmitter and received signal after the AWGN channel. The signal constellations represent the coded 0-15 16-QAM modulation which at the transmit shows clean bits of a signal without adding noise. The received signal is the signal after demodulation of the OFDM signal which can be seen as similar constellation to the transmitted signal constellation which in this case predistortion has been used to cancel the high distortion of the power amplifier. Predistorter has made the received signal almost close to the transmit signal.

Figure 7.28 shows the time scope figure of merit demonstrating the OFDM complex signal in two forms which are before the power amplifier and after the AWGN channel. Each signal has been displayed with a real and imaginary portion as shown above. The first signal was obtained before the RF power amplifier and the second was after the channel. The noise added to the signal that passed through the amplifier introduced disturbance.

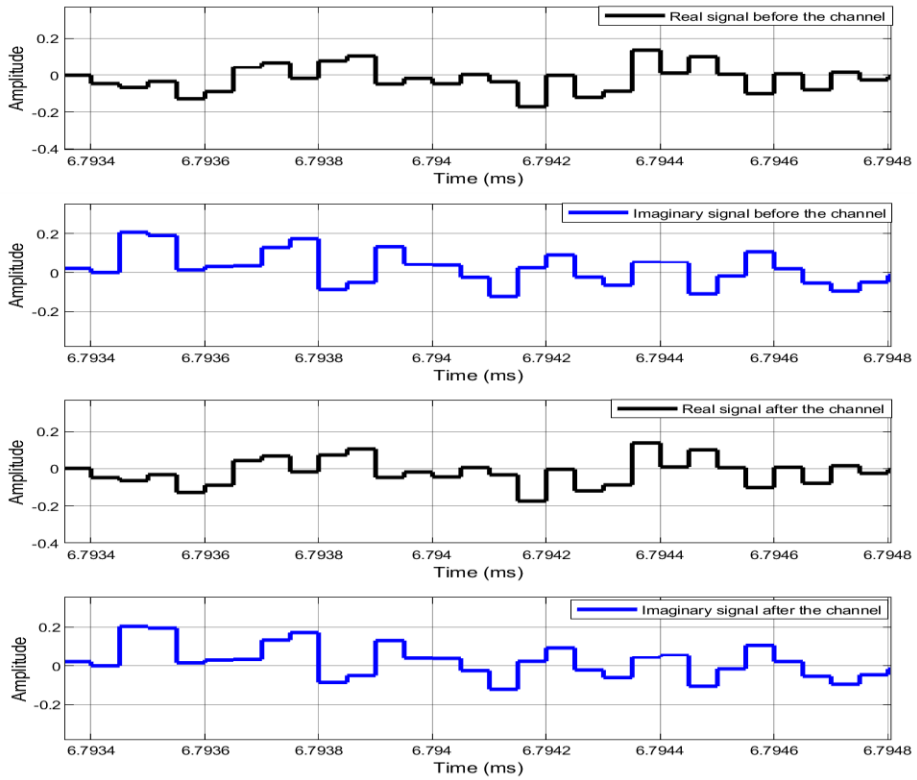

Figure 7.28: OFDM complex signal on-time scope frame after linearization.

Because of the distortion affecting the magnitude in the signal, the imaginary side of the signal after the channel might not follow the imaginary side of the signal before the channel. The predistorter has compensated the high distortion which the signals have demonstrated similarities both on real and imaginary [8].

7.8.2 Verification with 5G Modulation Application

In this section, the f-OFDM 5G modulation transceiver is used in verifying the proposed predistortion in terms of performance in cancelling the distortion of the amplifier. The f-OFDM 5G modulation transceiver is used for the simulation to compare with the existing OFDM system. As it is a well-known fact, filtered-OFDM is one of the simplest techniques with flexible waveform configuration that can ensure better spectral efficiency than OFDM itself [272]. This technique can be used to filter OFDM signal as it can offer in the sub-band a flat passband over the

subcarriers, minimize guard bands with sharp transition band and have enough stopband attenuation [272]. It has very low out-of-band (OOB) emissions and can also apply filtering to the OFDM symbols in the time domain to control the complex orthogonality of the symbols [272-274]. It can be used in multiple-input-multiple-output (MMO) applications as well as providing asynchronous multiple access [275].

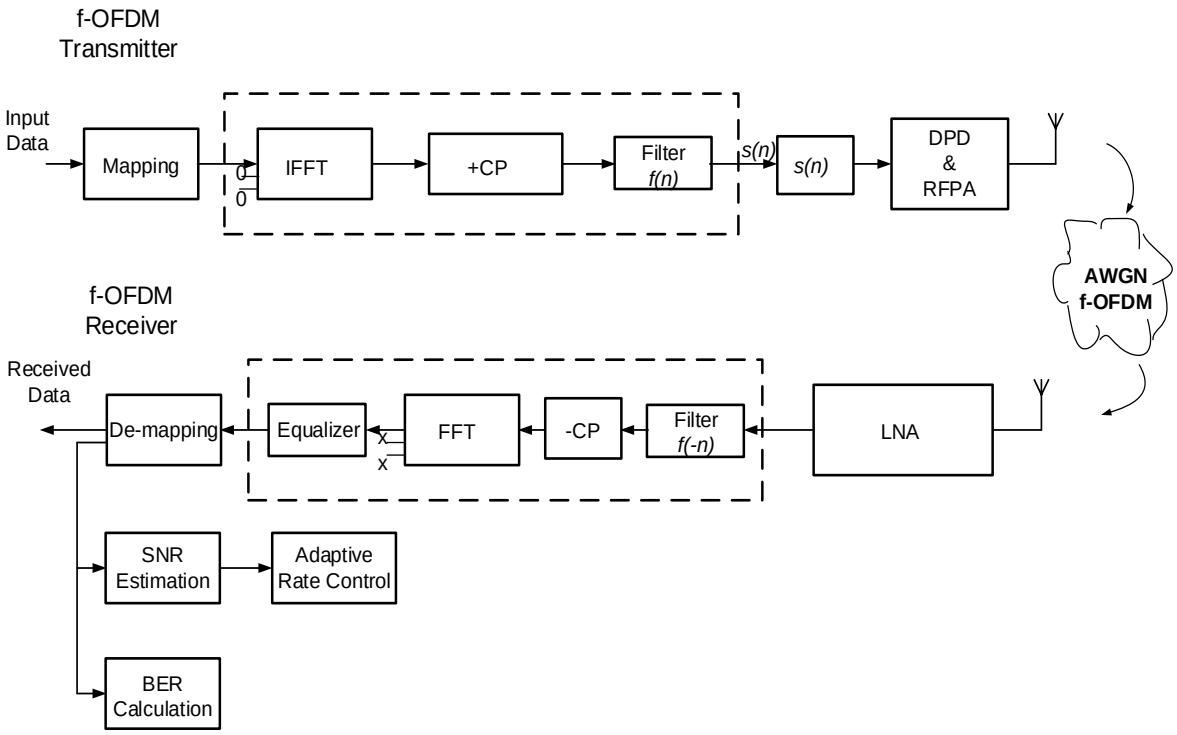

Figure 7.29: Filtered-OFDM transceiver system with added predistortion.

Figure 7.29 shows a block diagram of the proposed filtered-OFDM transceiver structure with power amplifier and predistortion system at the front end. The diagram describes the transmit/receive process with f-OFDM modulation using specific system parameters. The performance of the f-OFDM scheme is evaluated based on specifications. The specifications depend on the preferences which can, however, be adjusted to take an effect on the performance of the system. These parameters are 1024 as the number of FFT points, 50 as the

number of resource blocks, 12 as the number of subcarriers per resource block and 72 as the length of cyclic prefix in samples. The excess bandwidth in subcarriers is 2.5, the length of the filter is 513 in different modulation. On the transmit side, the baseband signals are generated at random in the frequency domain. In the modulation process, the signals are mapped by any of the mapping schemes.

During each symbol period, the transmitter used inverse fast Fourier transform with the cyclic prefix to modulate the signals in the time domain. The OFDM signal then passes through a filter to generate an f-OFDM signal which can be described as the spectrum shaping filtered signal. The spectrum shaping filter is focused on the assigned subcarrier in the frequency domain. The bandwidth of the filter is similar to the entire frequency width of the assigned subcarriers and the length of time used by the filter as a portion of the length of time used by the OFDM symbol.

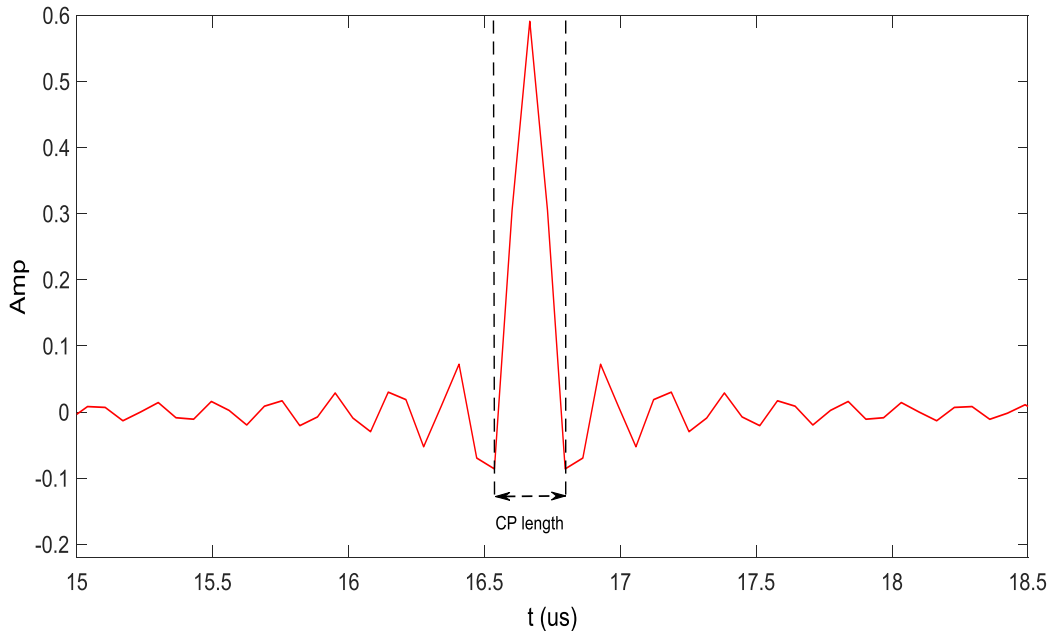

Figure 7.30: Impulse response of the designed filter for f-OFDM with bandwidth equal to 3 RBs.

Figure 7.30 shows the baseband impulse response of the desired filter with the bandwidth equivalent to 3 RBs. It can be seen that the bandwidth of the filter cover certain space in the cyclic prefix (CP) and is proportional to the spectral efficiencies. Hence, the filter energy in the CP reduced the ISI. The ISI continues to reduce with an increase in filter bandwidth within the CP [274]. The assigned bandwidth is splits into several sub-band. However, in this research work, a conventional f-OFDM is adopted to illustrate the impact of predistortion on 5G modulation, where f-OFDM is the case study. Then, the proposed digital predistorter and the power amplifier are connected at the RF front end, respectively. In the end, the signal passes through the channel to the receiver.

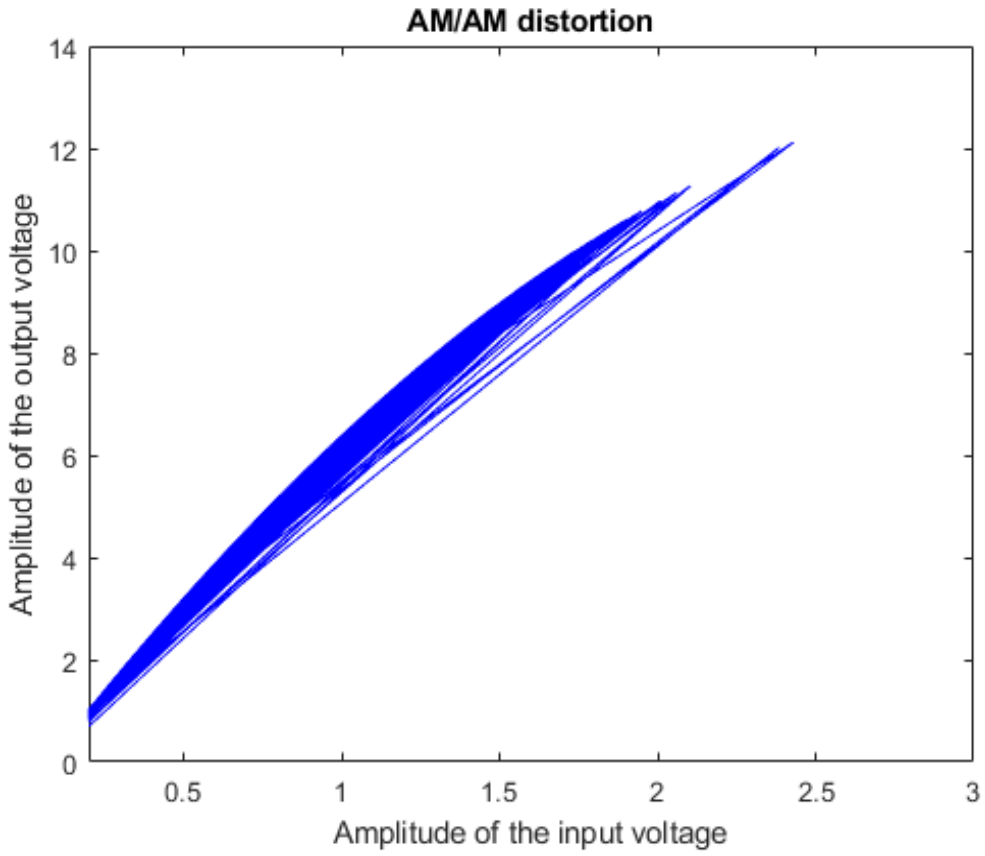

Figure 7.31: AM-AM distortion behaviour of the amplifier in the 5G f-OFDM transceiver system.

At the receiver, the signal from the channel is first passed through the filter which is matched with the transmitter filter. The signal then passed through the OFDM processes, i.e., after removal of cyclic prefix, the signal passed through FFT which demodulate and recover the OFDM transmitted signal. The cyclic prefix is used as a copy of the last portion of the OFDM symbol before the OFDM signal is estimated and equalize by the equalization block.

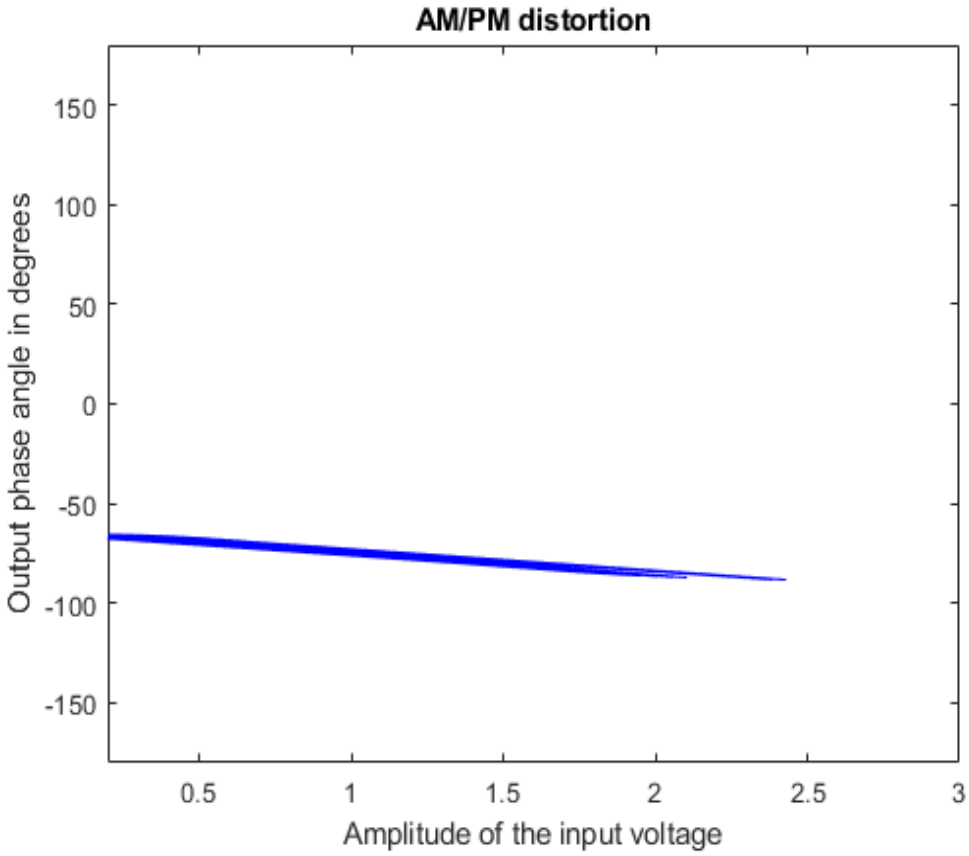

Figure 7.32: AM-PM distortion behaviour of the amplifier in f-OFDM transceiver system.

As a result of simulating the filtered-OFDM transceiver system using our proposed balanced RF power amplifier and the predistorter system, Figure 7.31 and 7.32 demonstrate the results of AM-AM and AM-PM signal distortions of the amplifier with predistortion. The results have shown that the amplifier behaves

nonlinearly in the absence of linearizer. The AM-AM and AM-PM characteristics are displayed with thousands of bits with errors due to magnitude variation. The signal-to-noise-ratio (SNR) needs to be improved to control the magnitude and reduce the errors.

The proposed power amplifier nonlinear behaviour changes at a different frequency and this need to be taken into consideration to ensure that during predistortion, the gain and phase transfer functions of the device are required to change over frequency as well as the input level to fit the changes. However, this amplifier operates on 2.620 to 2.690 GHz frequency in which the proposed predistorter is expected to operate over this bandwidth and above.

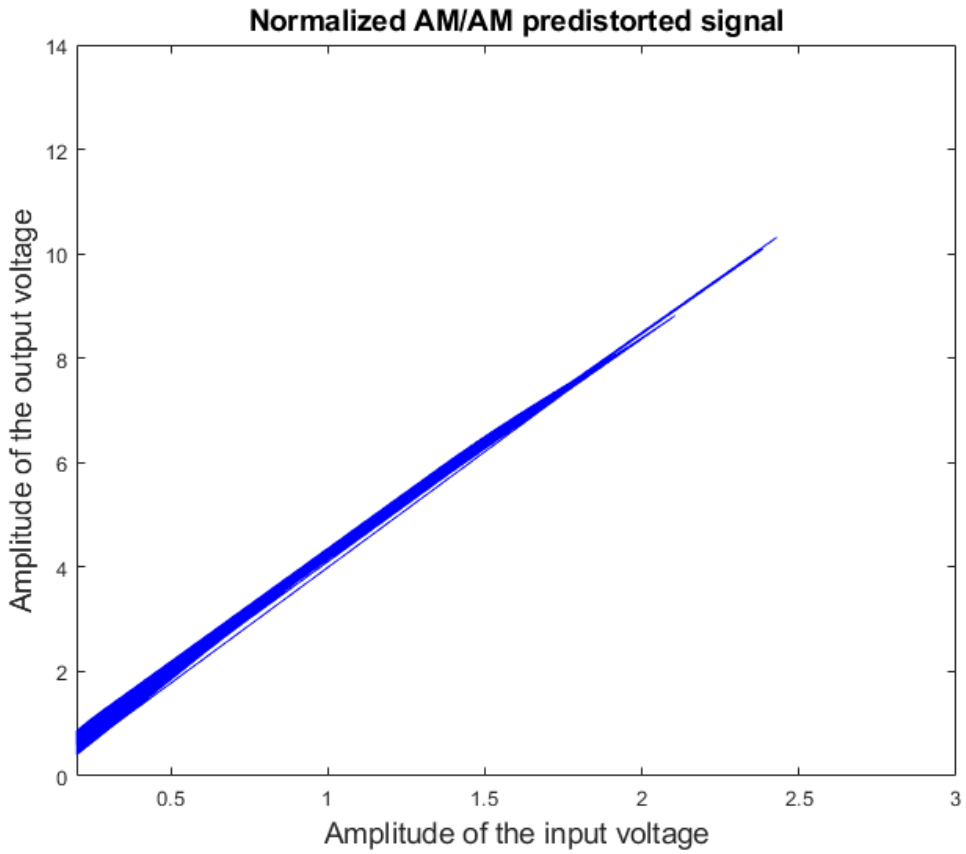

Figure 7.33: AM-AM predistortion performance of the amplifier in f-OFDM transceiver system.

The first result of linearizing the power amplifier distortion in the 5G f-OFDM modulation system is shown in Figure 7.33. The figure shows the normalized AM-AM response of the amplifier signal predistorted using the NLMSE algorithm in adaptive Hammerstein predistorter technique. It is shown clearly that the technique has a significant effect on the amplifier signal distortion. As shown above, the AM-AM characteristics are displayed linearly with thousands of bits as errors appeared due to the magnitude variation in the signal. However, adapting predistorter reduces the thousands of these spikes and linearized the signal.

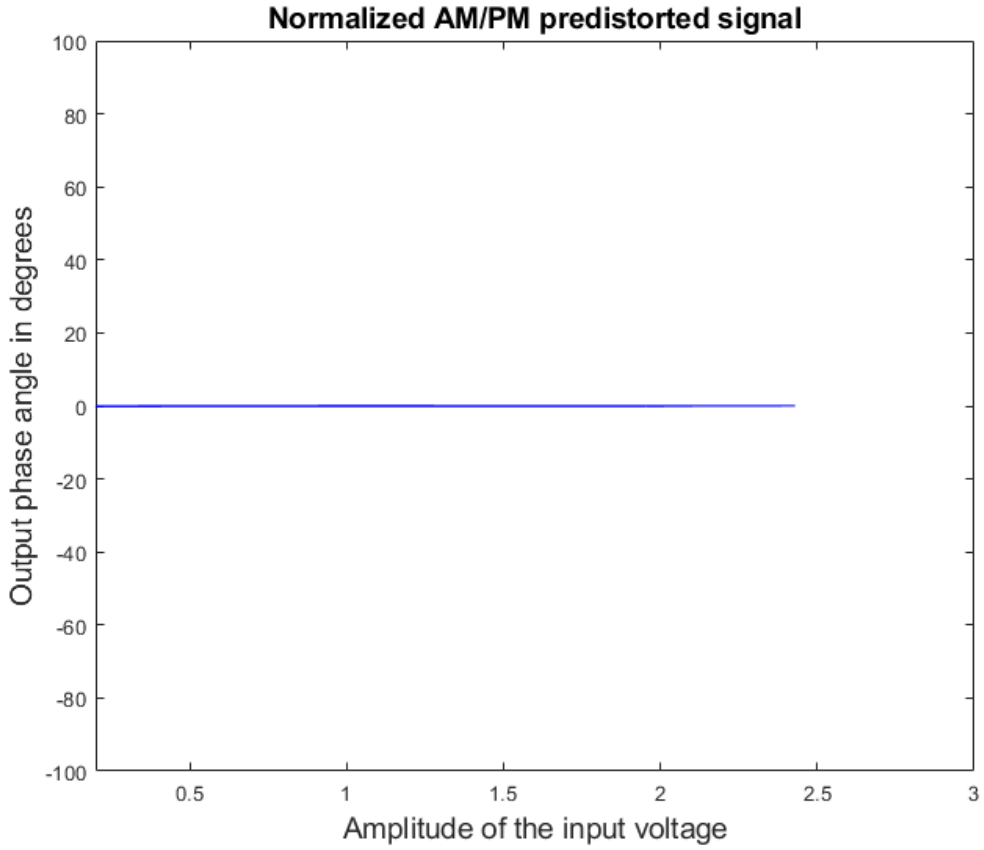

Figure 7.34: AM-PM predistortion performance of the amplifier in f-OFDM transceiver system.

Figure 7.34 shows the normalized AM-PM amplifier predistorted signal. Like mentioned in Figure 7.33 that spikes were generated on the amplitude signal affecting the performance of the predistorter is a moderately different experience in AM-PM signal as shown above. The predistortion cannot remove all the spikes

around the signal in the case of AM-AM which has not also shown a very effective impact on the errors. The amplitude and phase of the amplifier signals are pre-distorted by normalizing the polynomials. The performance of the predistorter has effectively linearized the signals and remove the nonlinearity of the amplifier. This has been proven in the signal SER performance result shown in Figure 7.35. The SER result illustrates the performance of the f-OFDM transceiver system in different modulations with clear proof of the authentic existence of improvement in the signal.

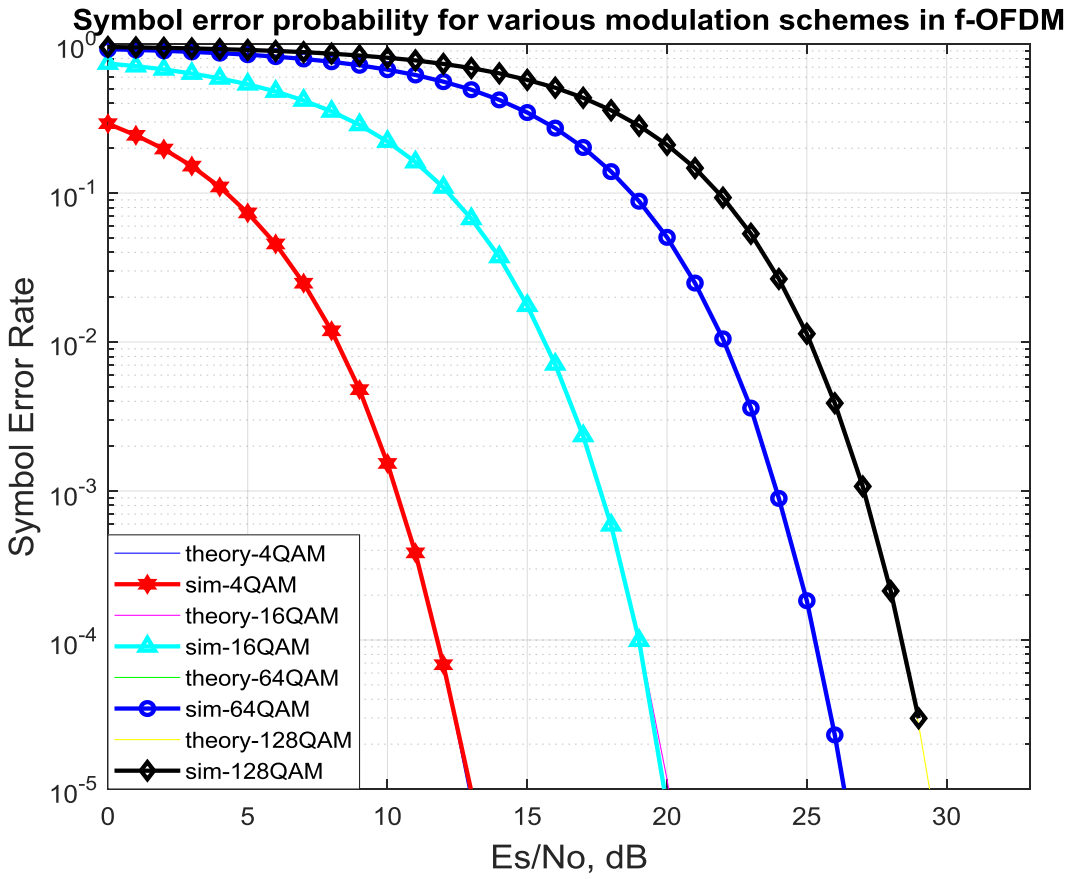

Figure 7.35: SER performance of f-OFDM in AWGN channel for different modulations.

Figure 7.35 has presented simulation result showing the performance of f-OFDM system in terms of symbol error probability in the presence of our proposed balanced RFPA nonlinear distortion. The SER performance curve is shown of the

RFPA output signal in the presence of predistorter. The predistorter has illustrated a good sign of spectral efficiency in the f-OFDM signal. The performance of the signal is received when predistorter is used in the system. The signal presented bits during the transmission which escalated the adjacent channel leakage of the RFPA. The number of errors occurred due to the RF power amplifier nonlinearities which are suppressed by the predistortion model. The simulation is repeated for QPSK, 4-QAM, 16-QAM and 128-QAM. The result presented variation based on modulation. To the best author's knowledge, this work has potentially good spectral efficiency and predistortion performance from adaptive predistorter used in the f-OFDM transceiver system to cancel the distortion and linearize the amplifier signal distortion.

7.8.3 Verification by Experimental Test-bed

The next step is to evaluate the models using measured data from the designed balanced RF power amplifier. The test-bed environment is processed with vector signal generator (RS SMBV100A), a signal analyzer (RS FSG13L), a computer for offline data training (ADS, WinIQsim and IQWizard) and the RFPA prototype. The MATLAB codes for signal processing was used and modelling algorithms (genetic algorithm) was also used in the case of off-line training.

An Agilent ADS2018a was used for the simulation test-bed to authenticate the performance of the predistorter through numerical simulations. The test-bed was simulated in the Agilent advanced design system Ptolemy environment (software platform). The analogue circuits were integrated with the digital circuits, while the power amplifier was simulated using the MRN28394056837 LDMOS Free-scale transistor and the micro strip circuits. The proposed power amplifier is a 15.5 W

MOSFET transistor from Free-scale. The RFPA was initiated by the linear wideband mini circuit pre-amplifier and finally connecting to the vector signal analyzer.

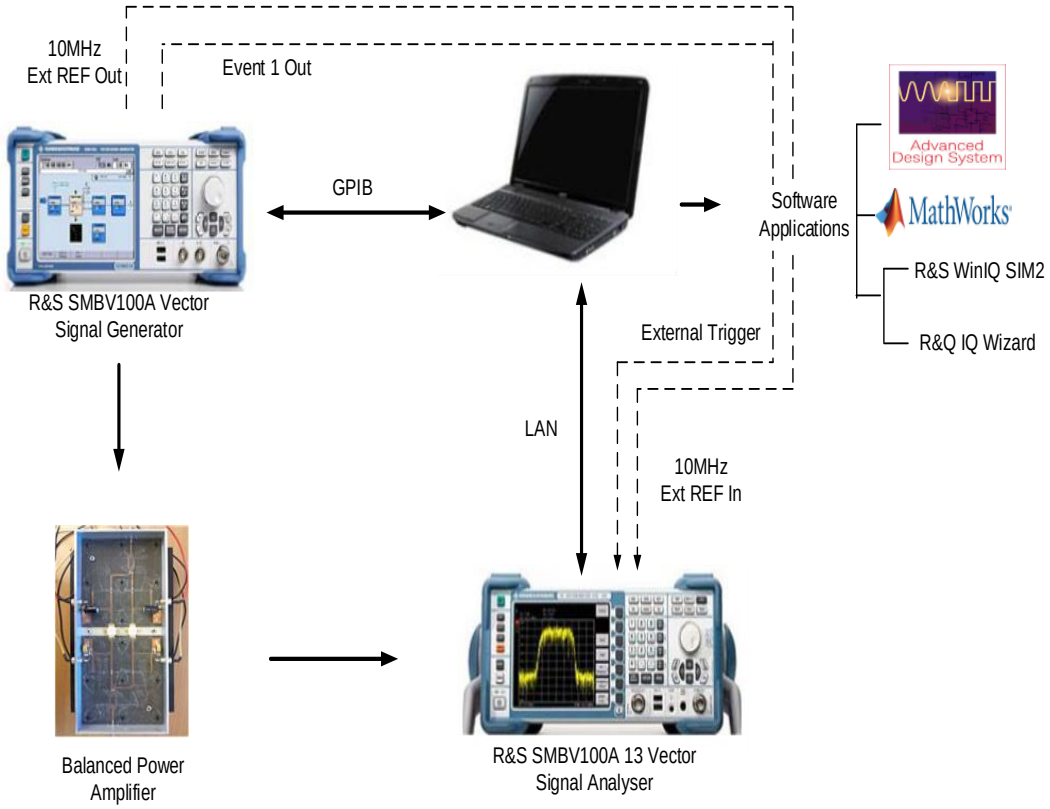

Figure 7.37: Diagram of the ADS simulation test-bed.

Figure 7.37 shows the basic block diagram of the test-bed settings which are listed previously. The importance of using the test-bed settings is to verify the amplitude and phase distortion signal of the power amplifier through measurement such that the RS SMBV100A and RS FSG13L are capable of transmitting and receiving an actual set of data which the data link controls the software routines where the measurement tools are connect to each other. To authenticate the proficiency of the proposed predistorter in the multicarrier systems, the OFDM signal is generated in AWGN channel with 16-QAM modulation scheme at 10MHz bandwidth, covering the data length of 8000 data samples for 4 sampling factor.

The power amplifier is using received 1024-point FFT/IFFT and is driven by an LTE-Advanced signal to feed to the power amplifier. The input signal is generated, while BPSK modulation is used in coding the pilot signal which is transmitted for long and short detection. The test signal is loaded in the simulation software, R&S WinIQsim2. Subsequently, the signal is fed to the transmitter after using the MATLAB compensator to predistort the test signal. The test signal fed into the transmitter and out are processed in MATLAB to ensure corresponding predistorter parameters are updated.

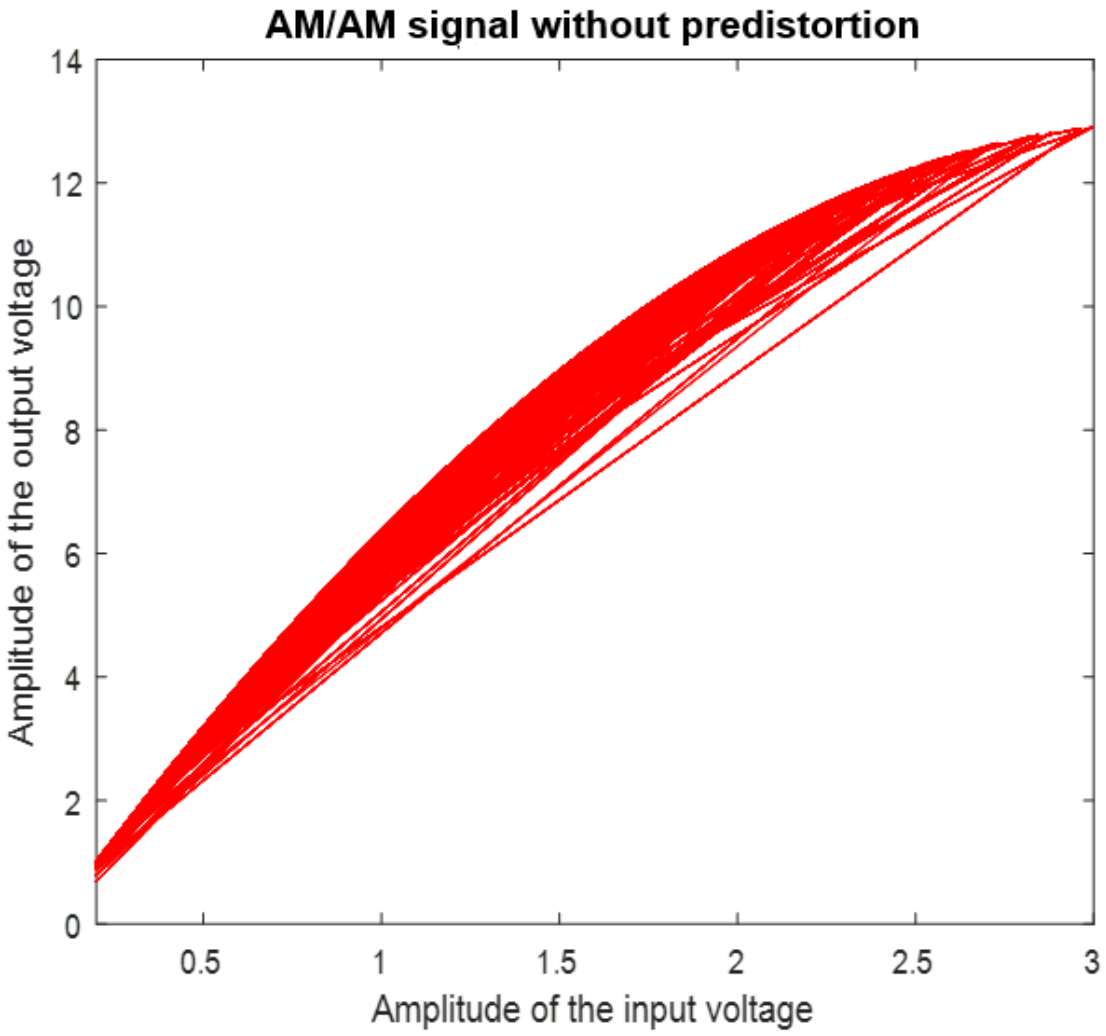

Figure 7.38: AM-AM distortion behaviour of the amplifier in the OFDM transceiver system test-bed.

This data is uploaded to the computer and simulated with ADS to process the response of the signal through BER, constellation and PSD. The performance of the proposed predistorter is evaluated by considering the output signal of the transmitter with and without the predistorter. The transfer function of the RFPA and response of the proposed predistorter are shown in Figure 7.38, 7.39, 7.40 and 7.41.

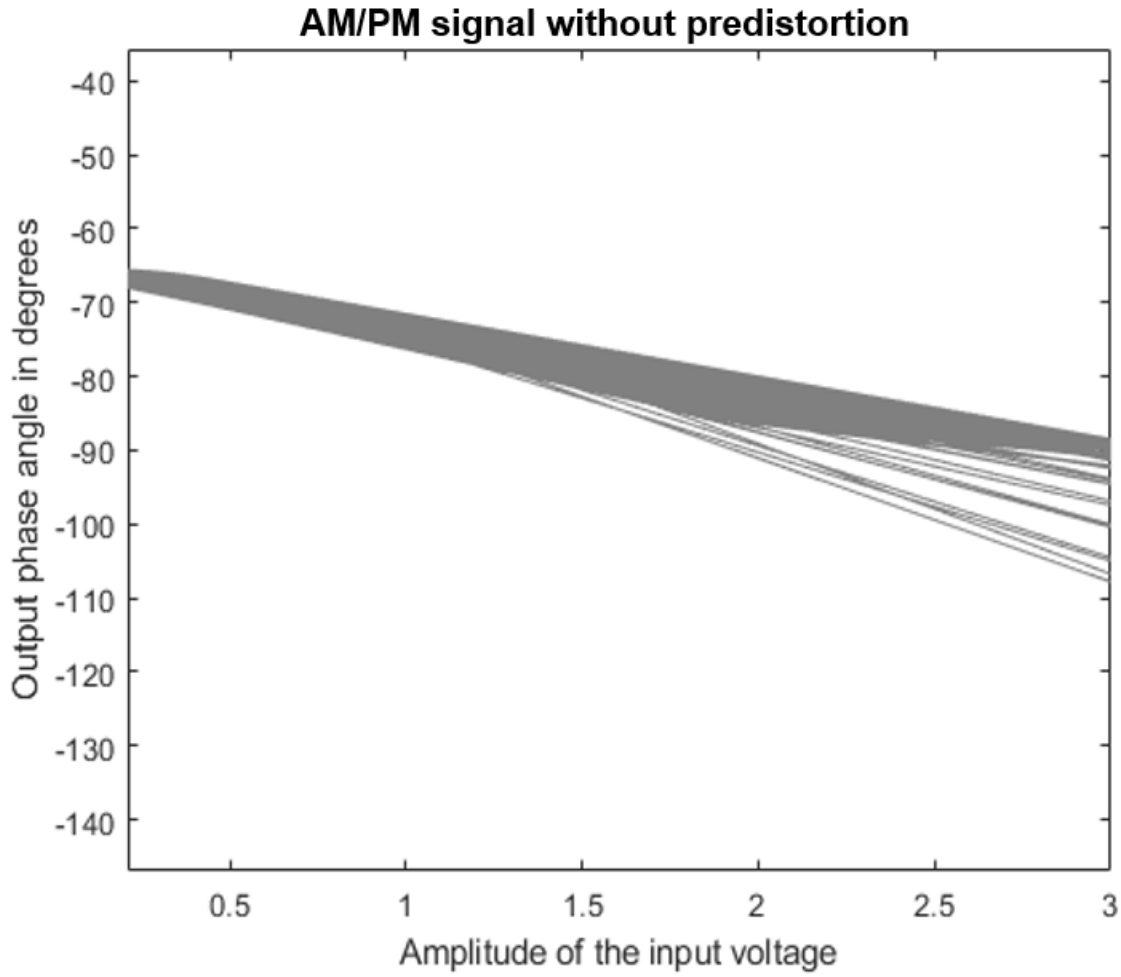

Figure 7.39: AM-PM distortion behaviour of the amplifier in the OFDM transceiver system test-bed.

Figure 7.38 and 7.39 show the AM-AM and AM-PM transfer functions of the proposed balanced RF power amplifier. The response of the amplifier has clearly shown that the distortion from the signal is before linearization. The signal produced thousands of bits which errors were due to the magnitude. The signal-

to-noise-ratio (SNR) plays a major role in this circumstance. Hence, by increasing the level of SNR and controlling the magnitude, the bits can be reduced. In this case, the predistorter cannot compensate for the effect.

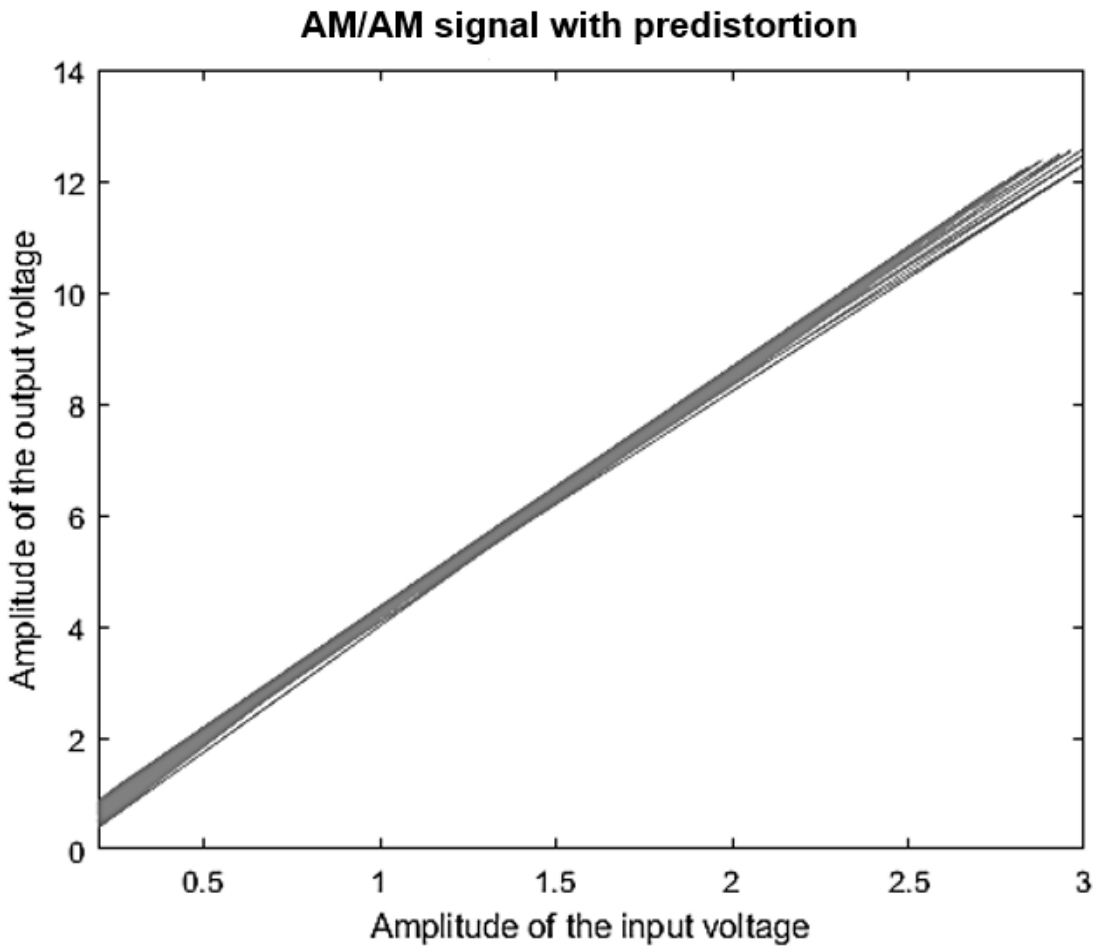

Figure 7.40: Normalized AM-AM amplifier predistorted signal.

Figure 7.40 and 7.41 the result of the proposed predistorter using Wiener-Hammerstein approach to suppress the distortion effect of the amplifier. Figure 7.42 shows the normalized AM-AM predistorted signal which has presented robustness of the algorithm used in cancelling the distortion effects. The signal has shown an effective linearization despite thousands of bits introduced by the signal.

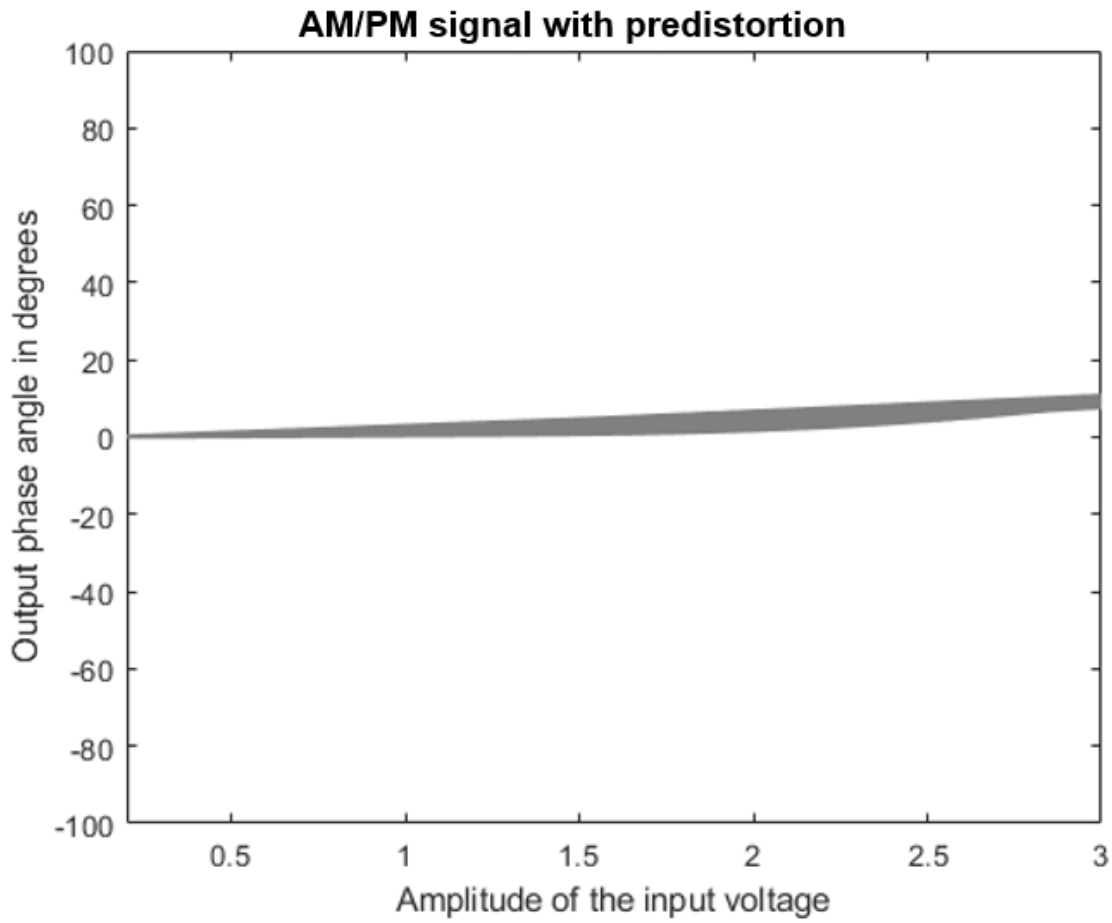

Figure 7.41: Normalized AM-PM amplifier predistorted signal.

Figure 7.41 also shows the normalized AM-PM predistorted signal which has presented robustness of the algorithm used in cancelling the distortion effects. The signal has shown an effective linearization despite thousands of bits introduced by the signal. It can be seen that due to the effect of the predistorter employed, the influence of amplifier distortion has partially reduced for both amplitude and phase signal.

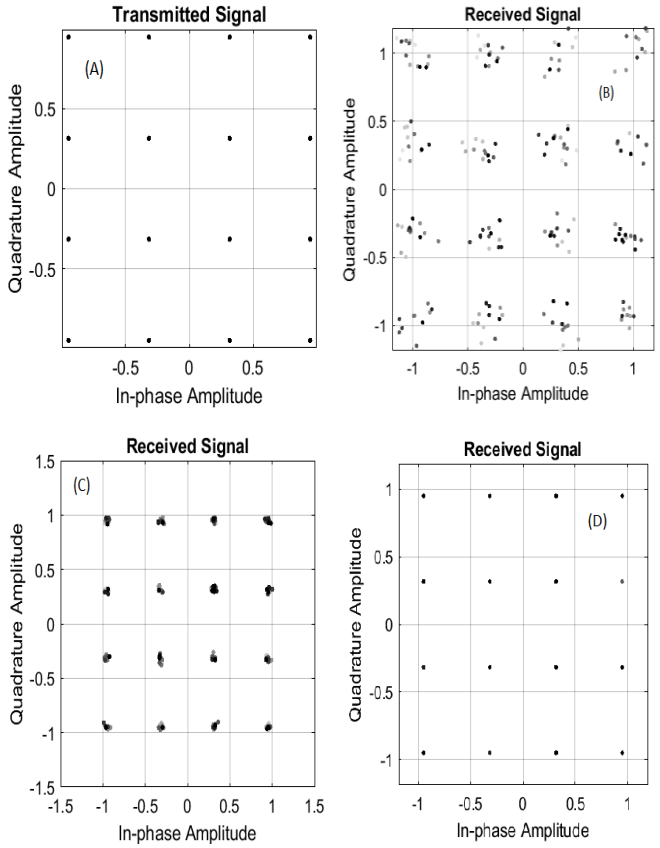

Figure 7.42: Different level constellation. (a) Input signal; (b) RFPA distorted signal; (c) Non-normalized NLMSE compensate signal; (d) Normalized NLMSE compensation signal.

Figure 7.42 shows the constellations of different signals in the OFDM transmitter, where Figure 7.42 (a) is the input signal, (b) is the received signal without predistortion, while (c) and (d) are received signals are the received signals with predistortion effect. The signal constellations represent the coded 0-15, 16-QAM modulation which at the transmit shows clean bits of a signal without adding noise. Figure 7.42 (b) is the amplifier signal received after the channel with distortion. It can be seen that the signal is received without linearization. Figure 7.42 (c) and (d) have shown the predistorted signals using the NLMSE method to achieve a different level of linearization. Figure 7.42 (c) is the signal after demodulation of the OFDM signal which can be seen as linearized, however, not having similar constellation to the transmitted signal. Hence, Figure 7.42 (d) has illustrated a constellation signal which in this case NMSE method has been

normalized, improving the predistortion to cancel the high distortion of the power amplifier. This method has almost made the received signal closely similar to the transmit signal.

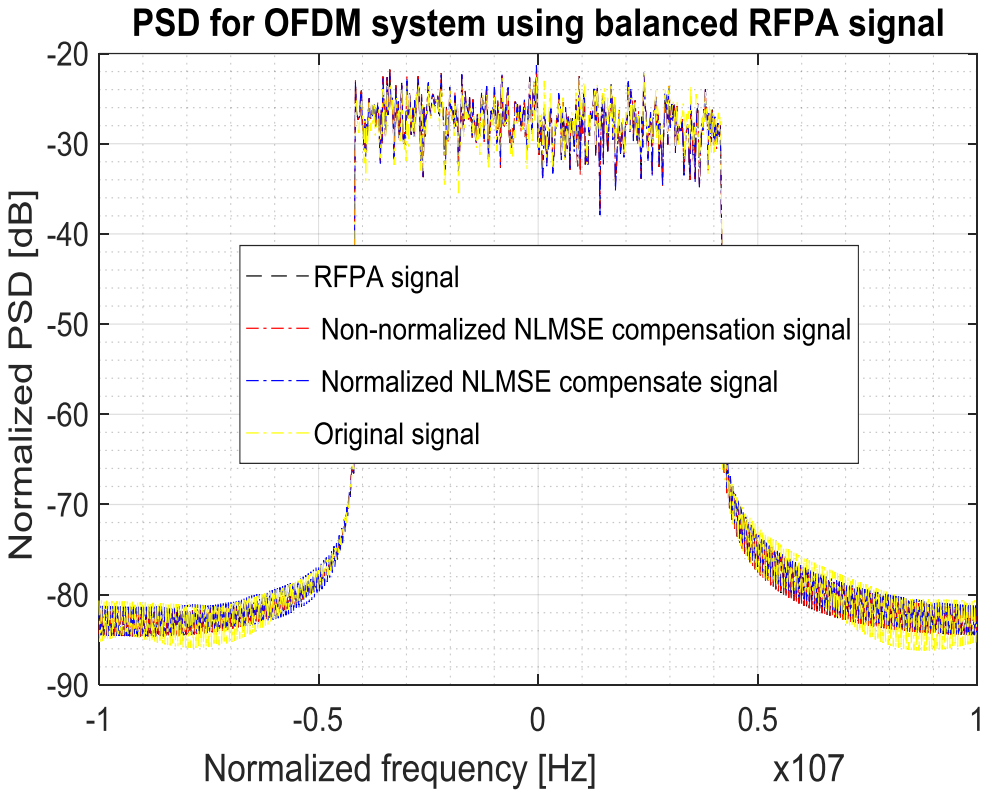

Figure 7.43: PSD comparison in low input saturation level.

Figure 7.43, 7.44, 7.45 and 7.46 also illustrate the performances of predistortion in power spectral density (PSD) and bit error rate (BER) form. In the two figures showing power spectrum densities, the actual transmit signal and the NMSE model is discussed. Figure 7.43 shows an algorithm which has been used in modelling the nonlinearity of the amplifier using the non-normalized and normalized approach at low saturation level. Using the low saturation level at the input limits the model from removing the whole nonlinearities of the amplifier. This implies that nonlinearities still exist in the signal after the AWGN channel.

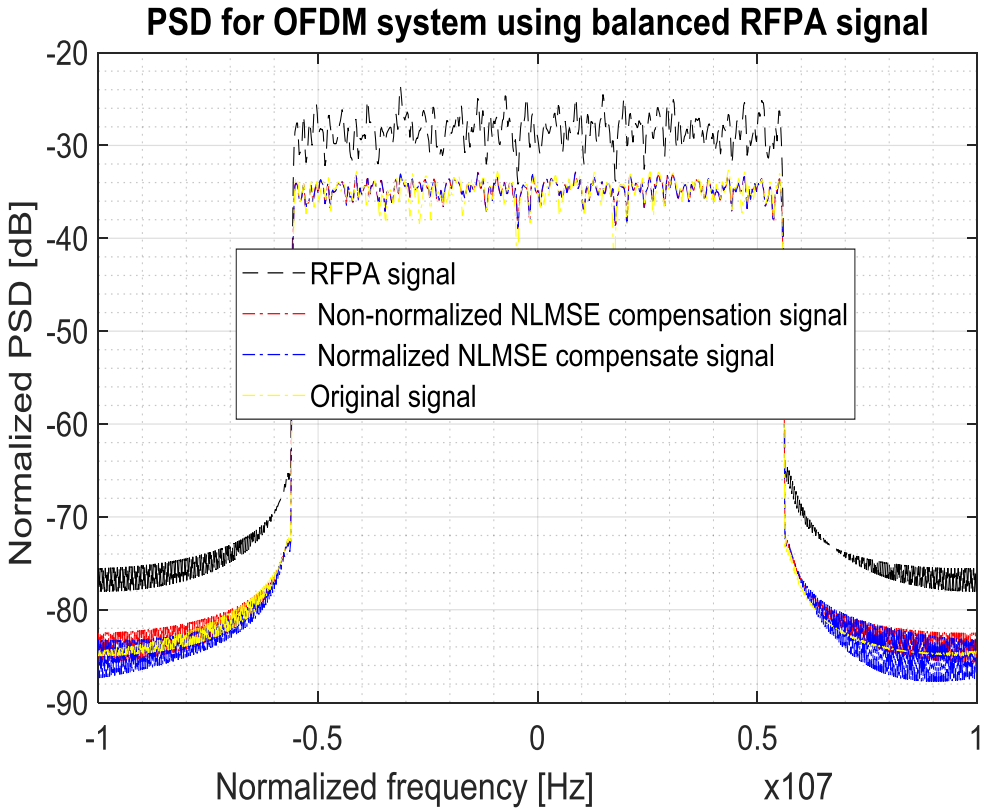

Figure 7.44: Power spectrum density comparison in high input saturation level.

For this reason, the NLMSE approach has been proposed using high input saturation level to accurately model the nonlinearity of the power amplifier. It can be seen in Figure 7.44 that the power amplifier distortion in the signal is quite obvious which is separated from the compensated signal. However, the linearity of the PSD result improves by up to 7 dB while the distortion of the power amplifier remains high before compensation.

Figure 7.45 is the BER result that illustrate performances of the NLMSE approach in the transceiver system using two different types of RFPAs. Different modulations have been used in order to ascertain the level of distortion that can be reduced in the signal. The NLMSE model was set to low input saturation level. IT can be seen the BER level reduction is minimal according to the figure. Hence, the modulations include 4-QAM as the lowest, 16-QAM, 64-QAM and 128-QAM

respectively. Each modulation was demonstrated in the condition, such that first test was simulated with the original signal (without the use of RFPA). The second test was done with the proposed balanced RFPA. While the third test used the class F RFPA to check the signal in the absence of compensation. The non-presence of compensation technique results to high saturation effect which means there is no much improvement in term of BER.

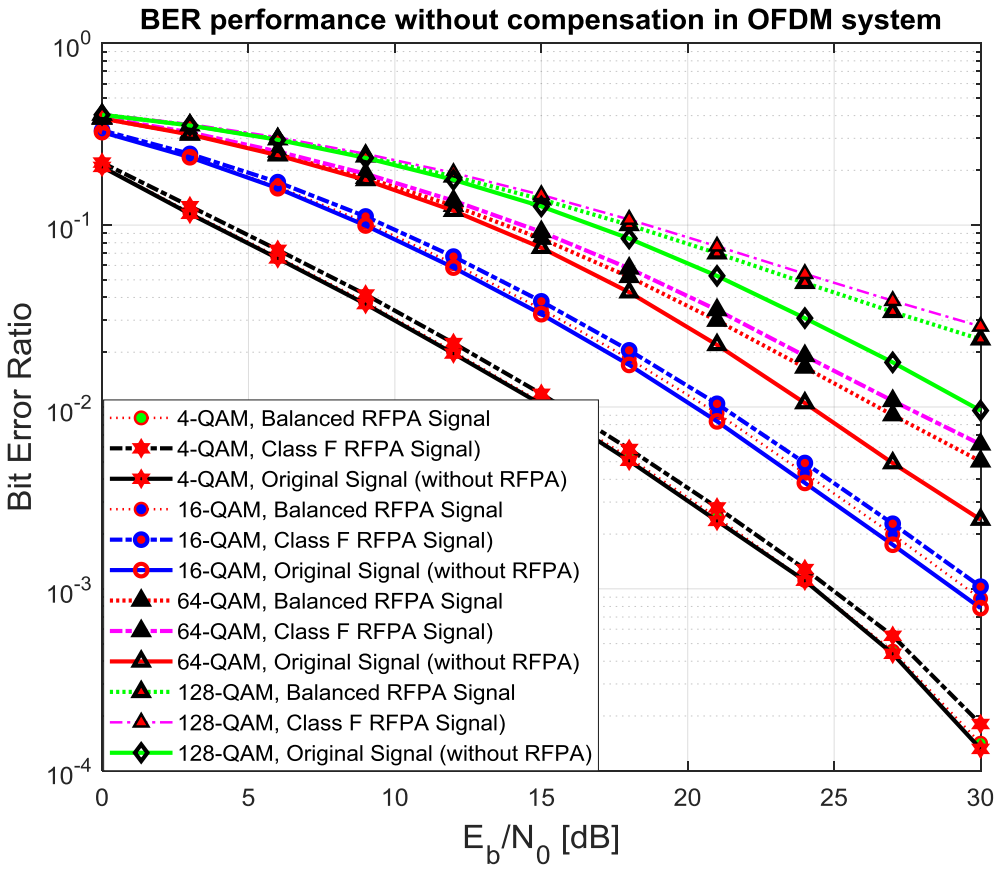

Figure 7.45: BER performance using different modulations without compensation.

In addition, this result illustrated the performance of system without applying the compensation technique to remove the signal distortion of the RFPAs. Since the approach cannot completely remove the BER in this level, the NLMSE is set in high input level saturation level as shown below where the compensation technique is used in order to reduce the saturation level in the higher modulation.

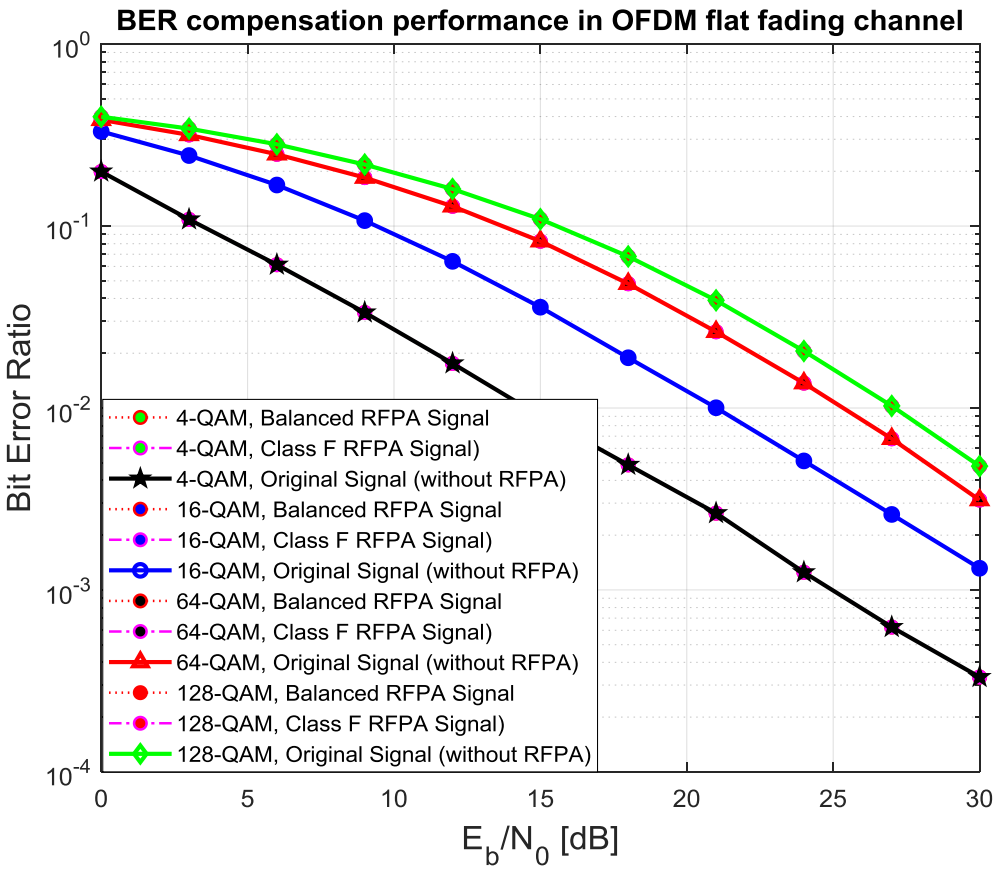

Figure 7.46: BER performance using compensation technique in different modulations.

As shown in Figure 7.46, the BER performance using compensation technique in different modulations of OFDM flat fading channel. The NLMSE approach has been used to reduce the BER. As seen in the figure above, at zero normalised signal-to-noise-ratio, the signals of different modulations are achieved at 0.2 to 0.4 of the bit-error-rate level. This is to say that none of the signal has reach near to the 10^0 level. Consequently, the BER performance has improved significantly. Each modulation has illustrated the results generated in 3-different ways. The modulation was set from 4-QAM to 128-QAM, showing the original signal, compensation with balanced and class F RFPA signals. The result has shown variation in modulation level where the RFPAs distortion effects were compensated accurately similar to the original signal. This implies that the approach has completely reduced the BER to the minimal level based on the

effectiveness of the approach in the system. The results presented in this work, to the best of author's knowledge are a potentially good model and predistortion performance has been effective in high distortion reduction of the amplifier.

7.9 Summarized Conclusion

In this section, the adaptive digital predistortion structure for RF power amplifier linearization has been presented. The normalized least mean square method has been proposed to extract the coefficients for the predistorter. The method optimizes the coefficients using indirect learning architecture. It was assumed that the static nonlinearity is identified where the parameters of the linear dynamic block and the nonlinear system are approximated. The proposed balanced RF power amplifier and the predistorter were verified in MATLAB Simulink OFDM application, 5G modulation application and experimental test-bed. The test of the simulation and the test-bed demonstrate the new algorithm can overcome the nonlinearity and distortion effect of the power amplifier effectively. The absence of a predistorter allows the spectral regrowth to manifest when a non-constant envelope 16-QAM signal was applied to the RFPA. The proposed linearization technique has demonstrated a good performance in a significant reduction of distortion, the bit errors and the memory effects.

CHAPTER 8

Summarized Conclusions and Recommendations for Future Work

8.1 Summary of the Thesis

In wireless communication systems, the design of linear and efficient transmitters for base stations and terminals is a major task. As one of the most important parts of a transmitter, more attention is given to RF power amplifier in search of avenue to improve performance. A common approach for achieving both the high linearity and efficiency is to design a RFPA operating in a nonlinear efficient mode and to provide linearization. Therefore, linearization of power amplifier has become one of the most important subject in wireless communication systems.

In this thesis, research work on the topic of linearization of power amplifier for wireless communication systems has been presented. An advanced adjustable linearisation technique incorporating the digital predistortion method for memoryless nonlinearity compensation and the baseband cancellation method for minimising memory effects was discussed in this research work. The theoretical concept, designs, simulations, practical measurements and performance results were presented.

The research work included the following areas. Firstly, RFPA parameters, classes of amplification, the trade-off between efficiency and linearity, nonlinear analysis and characteristics used to quantify RFPA performances were explained. A study of the origins, types and consequences of memory effect, as well as an overview of the methods used to quantify model and compensate for memory effects were presented. A comparative review of the existing linearization techniques was accomplished by highlighting the advantages and

shortcomings of each method. A digital predistortion is one of the most cost-effective, easily integrated and flexible linearization methods. These were chosen as basis for the development of the proposed technique. As the baseband equalisation technique offers a minimisation of the memory effects in wideband communication systems by digitally processing the input signal without modifying the RF part of the transmitter, the method was implemented as the memory-compensating part of the linearizer. Detailed conclusions to each of the areas of the current research work are presented below:

In chapter 2, the general parameters of RF power amplifiers were introduced with the description of the amplification principle, class of amplification and nonlinear analysis. The main parameters, such as linearity, efficiency, power and gain were defined and the relations between them were discussed. The nonlinear analysis, characterization of power amplifier nonlinearities and phenomena related to nonlinear distortions were discussed. Different types of memory effects of power amplifier, quantifying memory effects and frequency-dependent transfer function were also described.

Chapter 3 presented OFDM as a multicarrier system, its basic principles, advantages and disadvantages. Discussed the nonlinear effects of power amplifier over the OFDM modulated signal and how these nonlinear effects can be estimated. Proved how the nonlinear distortion affects the signal, a simple application over the nonlinear OFDM transmitter with and without saturator was studied and simulated using MATLAB. The OFDM was also compared with 5G modulations such as FQAM-OFDM, FBMC, UFMC and other OFDM families.

Chapter 4 reviewed the different types of methods for RFPA behavioural modelling. The memory effect models and memoryless modelling procedures were carefully studied. Moreover, the parameter estimation algorithms for Wiener and Hammerstein's systems used in RFPA modelling approaches were modified. Finally, the proposed behavioural models based on the Wiener and improved Wiener approaches with an optimal technique for system parameter estimation was presented. Both linear and nonlinear memory effects were considered in the proposed model.

Chapter 5 presented one of the proposed base stations RF power amplifier using a balanced technique. A linear balanced RF power amplifier with high efficiency was designed and implemented. The amplifier was first proposed to improve the power efficiency of LTE base station to work over a given dynamic range.

Chapter 6 presented a class F approach to optimise load impedance at the fundamental frequency for the application of the active antenna concept. The design method and procedure are demonstrated through source/load-pull for high efficiency and optimal load impedance. This is investigating on modelling aspects of active antennas of the class F power amplifier. The work presented a general computer-aided design (CAD) approach to obtain the optimal fundamental load impedance and design the input matching circuits for an active integrated antenna of the transmitting type in order to achieve class F active amplifier antenna operation. The performance of this was considerably improved using an active integrated antenna while shaping a patch radiator to control the harmonic load impedances. The proposed CAD approach was also used as an efficient tool in optimizing the input impedance of the active antenna to achieving harmonic

suppression at the desired operating frequency and harmonics with any given type of transistor.

Chapter 7, the most common methods of linearization used in RF transmitters were reviewed. These techniques were power back-off, feedback linearization, envelope elimination and restoration, linear amplification with nonlinear components, feed forward, and predistortion. In this chapter, look up tables and polynomial based PD were studied. Two different methods of parameter estimation to evaluate the Hammerstein blocks, as well as an enhanced adaptive Hammerstein algorithm were proposed. The proposed balanced RF power amplifier and the predistorter were verified in MATLAB Simulink OFDM application, 5G modulation application and experimental test-bed. The test of the simulation and the test-bed demonstrated that the new algorithm can overcome the nonlinearity and distortion effect of the power amplifier effectively. The absence of a predistorter allowed the spectral regrowth to manifest when a non-constant envelope 16-QAM signal was applied to the RFPA. The proposed linearization technique demonstrated a good performance in a significant reduction of distortion where the BER performance illustrated a compensation effects.

8.2 Conclusions

The main subject of this work is to improve the performance of OFDM transmitter through investigation, design and measurement of a digital predistortion that is able to compensate the dynamic nonlinear distortion of a high power amplifier. To evaluate the compensation performance of the proposed models, a linear 15.5 W balanced RFPA with a gain of 15 dB using an n-channel Si-LDMOS device

and a nonlinear 10 W class F RFPA with up to 18 dB gain with RF power GaN HEMT device were designed. A comprehensive comparative analysis between the linear and nonlinear was shown. The extracted transfer function of the balanced RFPA was used in single tone and two-tone simulations. The 2.620 to 2.690 GHz operating frequency band was used for both RFPAs in the design. The effectiveness of the proposed baseband predistorter on the performance of OFDM transmitter utilizing a nonlinear RFPA with memory effect was observed and discussed. The normalized least mean square method was proposed to extract the coefficients for the predistorter. The method optimizes the coefficients of indirect learning architecture. It was assumed that the static nonlinearity is identified where the parameters of the linear dynamic block and the nonlinear system are approximated. The proposed balanced RF power amplifier and the predistorter were verified in MATLAB Simulink OFDM application, 5G modulation application and experimental test-bed. The test of the simulation and the test-bed demonstrate the new algorithm can overcome the nonlinearity and distortion effect of the power amplifier effectively. The absence of a predistorter allowed the spectral regrowth to manifest when a non-constant envelope 16-QAM signal was applied to the RFPA. The proposed linearization technique demonstrated a good performance in a significant reduction of distortion, the bit errors and the memory effects. The results of the new algorithms on accuracy and adaptation time were compared analytically with previously reported approaches.

8.3 Recommendations for Future Work

Possible directions for the future research work include:

- An extensive study of the different algorithms is proposed to model the nonlinearity of RFPA. The accurate behavioural model based on the

Wiener system with an improved robust technique for parameter estimation has been recommended. The effects of RFPA nonlinear distortion on the OFDM signal is presently under research with the objective to provide new approaches that can accurately compensate for the distortion.

- In chapter 5, we proposed the use of balanced RFPA system for efficiency enhancement and linearity compensation. We still believe that other effective techniques can be put into consideration for examination. Further research recommends using Doherty RFPA application into 3-stage dynamic load modulation system with 5G-LTE frequency for mobile and Satellite RF systems. The RFPA is known for spectral efficiency performance in terms of low leakage and energy consumptions.
- An efficient adaptive predistortion technique based on the Hammerstein model is recommended to compensate for the distortion of the RFPA. Three optimal methods of parameter estimation are suggested with the aim of reducing the complexity of the required filtering. Furthermore, to include the nonlinear memory effects, an adaptive Wiener predistorter approach is proposed where the predistorter will work with 3-stage dynamic load modulation system in OFDM IEEE 802.11ax application.
- The proposed 3-stage dynamic load modulation system and the proposed Wiener predistorter systems will be verified in 5G modulation applications and will also be evaluated with the use of real world signals. The aim is to demonstrate effectiveness in cancelling the nonlinearity and distortion effect of the amplifier.

References

[1] S. Sesia, M. Baker, and I. Toufik, *LTE-the UMTS long term evolution: from theory to practice*: John Wiley & Sons, 2011.

[2] T. S. Rappaport, *Wireless communications: principles and practice* vol. 2: prentice hall PTR New Jersey, 1996.

[3] Y. Ma, D. G. Kuester, J. Coder, and W. Young, "Coexistence analysis of LTE and WLAN systems with heterogenous backoff slot durations," in *Communications (ICC), 2017 IEEE International Conference on*, 2017, pp. 1-7.

[4] L. Nuaymi, *WiMAX: technology for broadband wireless access*: John Wiley & Sons, 2007.

[5] Y. Wu and W. Y. Zou, "Orthogonal frequency division multiplexing: A multi-carrier modulation scheme," *IEEE Transactions on Consumer Electronics,* vol. 41, pp. 392-399, 1995.

[6] A. R. Bahai, B. R. Saltzberg, and M. Ergen, *Multi-carrier digital communications: theory and applications of OFDM*: Springer Science & Business Media, 2004.

[7] S. T. Le, K. J. Blow, V. K. Mezentsev, and S. K. Turitsyn, "Bit error rate estimation methods for QPSK CO-OFDM transmission," *Journal of Lightwave Technology,* vol. 32, pp. 2951-2959, 2014.

[8] B. A. Mohammed, A. S. Hussaini, R. A. Abd-Alhameed, I. M. Danjuma, A. S. Asharaa, I. T. E. Elfergani*, et al.*, "Towards a 15.5W Si-LDMOS Energy Efficient Balanced RF Power Amplifier for 5G-LTE Multi-carrier Applications," *EAI Endorsed Transactions on Creative Technologies,* vol. 5, 2018.

[9] P. Marsch, M. Maternia, M. Panek, A. Yaver, R. Dokuczał, and R. Marcin, "3GPP Mobile Communications: WCDMA and HSPA," *The Telecommunications Handbook: Engineering Guidelines for Fixed, Mobile and Satellite Systems,* pp. 371-416, 2015.

[10] P. Muszynski and H. Holma, "Introduction to WCDMA," *WCDMA for UMTS—Radio Access for Third Generation Mobile Communications,* vol. 3, pp. 43-49, 2004.

[11] T. Jiang, Y. Yang, and Y.-H. Song, "Exponential companding technique for PAPR reduction in OFDM systems," *IEEE Transactions on broadcasting,* vol. 51, pp. 244-248, 2005.

[12] Y.-C. Wang and Z.-Q. Luo, "Optimized iterative clipping and filtering for PAPR reduction of OFDM signals," *IEEE Transactions on Communications,* vol. 59, pp. 33-37, 2011.

[13] F. H. Raab, P. Asbeck, S. Cripps, P. B. Kenington, Z. B. Popovic, N. Pothecary*, et al.*, "Power amplifiers and transmitters for RF and microwave," *Microwave Theory and Techniques, IEEE Transactions on,* vol. 50, pp. 814-826, 2002.

[14] V. K. Garg, *IS-95 CDMA and CDMA2000: Cellular/PCS systems implementation*: Pearson Education, 1999.

[15] M. M. Buddhikot, G. Chandranmenon, S. Han, Y.-W. Lee, S. Miller, and L. Salgarelli, "Design and implementation of a WLAN/CDMA2000 interworking architecture," *IEEE Communications Magazine,* vol. 41, pp. 90-100, 2003.

[16] D. J. Costello, "Fundamentals of Wireless Communication (Tse, D. and Viswanath, P.) [Book review]," *IEEE Transactions on Information Theory,* vol. 55, pp. 919-920, 2009.

[17] A. Hussain, *Advanced RF Engineering for Wireless Systems and Networks*: Wiley, 2004.
[18] S. C. Cripps, *RF Power Amplifiers for Wireless Communications*: Artech House, 2006.
[19] S. C. Cripps, *Advanced Techniques in RF Power Amplifier Design*: Artech House, 2002.
[20] B. A. Mohammed, N. A. Abd-Alhameed, R. A. Hussaini, A.S. Nche, C. Fonkam, M. Elfergani, I.T. E. Rodriguez, J. Abdulmula, E. A. and Elkazmi, E., "Towards a Green Energy RF Power Amplifier for LTE Applications," in *Internet Technologies and Applications (ITA), IEEE*, 2015, pp. 388-392.
[21] W. H. Doherty, "A new high efficiency power amplifier for modulated waves," *Proceedings of the Institute of Radio Engineers,* vol. 24, pp. 1163-1182, 1936.
[22] T. Ni and F. Liu, "A new impedance match method to improve efficiency of LINC with Chireix combiner," *Microwave and Optical Technology Letters,* vol. 52, pp. 1418-1421, 2010.
[23] J. Hur, H. Kim, O. Lee, K.-W. Kim, F. Bien, K. Lim*, et al.*, "A Multilevel Class-D CMOS Power Amplifier for an Out-Phasing Transmitter With a Nonisolated Power Combiner," *IEEE Transactions on Circuits and Systems II: Express Briefs,* vol. 63, pp. 618-622, 2016.
[24] L. R. Kahn, "Single-sideband transmission by envelope elimination and restoration," *Proceedings of the IRE,* vol. 40, pp. 803-806, 1952.
[25] J. Hur, K.-W. Kim, O. Lee, C.-H. Cho, K. Lim, and J. Laskar, "Highly efficient and linear level shifting digital LINC transmitter with a phase offset cancellation," in *Radio and Wireless Symposium, 2009. RWS'09. IEEE*, 2009, pp. 211-214.
[26] P. B. Kenington, *High-linearity RF Amplifier Design*: Artech House, 2000.
[27] T. Niubó-Alemán, Y. Hahn, P. Roblin, J.-P. Teyssier, J. Reynoso-Hernández, V. Chen*, et al.*, "Calibrated Digital Predistortion Using a Vector Network Analyzer as the Receiver," in *2019 93rd ARFTG Microwave Measurement Conference (ARFTG)*, 2019, pp. 1-4.
[28] J. C. Pedro and S. A. Maas, "A comparative overview of microwave and wireless power-amplifier behavioral modeling approaches," *IEEE Transactions on Microwave Theory and Techniques,* vol. 53, pp. 1150-1163, 2005.
[29] J. Vuolevi and T. Rahkonen, *Distortion in RF power amplifiers*: Artech house, 2003.
[30] A. A. Saleh, "Frequency-independent and frequency-dependent nonlinear models of TWT amplifiers," *IEEE Transactions on communications,* vol. 29, pp. 1715-1720, 1981.
[31] M. Schetzen, "The Volterra and Wiener theories of nonlinear systems," 1980.
[32] S. A. Maas, *Nonlinear microwave and RF circuits*: Artech House, 2003.
[33] W. Bosch and G. Gatti, "Measurement and simulation of memory effects in predistortion linearizers," *IEEE Transactions on Microwave Theory and Techniques,* vol. 37, pp. 1885-1890, 1989.
[34] C. Cripps, "RF Power Amplifiers For Wireless Communications Steve," 2006.
[35] H. Bölcskei, "Fundamentals of wireless communication," *Tc,* vol. 1, p. 4.17, 2012.
[36] D. Tse and P. Viswanath, *Fundamentals of wireless communication*: Cambridge university press, 2005.

[37] W. A. Davis and K. K. Agarwal, "Class A Amplifiers," *Radio Frequency Circuit Design,* pp. 122-143, 2001.
[38] M. Albulet, *RF power amplifiers* vol. 2: SciTech Publishing, 2001.
[39] P. B. Kenington, *High linearity RF amplifier design*: Artech House, Inc., 2000.
[40] H. Deguchi, N. Ui, K. Ebihara, K. Inoue, N. Yoshimura, and H. Takahashi, "A 33W GaN HEMT Doherty amplifier with 55% drain efficiency for 2.6 GHz base stations," in *Microwave Symposium Digest, 2009. MTT'09. IEEE MTT-S International*, 2009, pp. 1273-1276.
[41] D. Hu, X. Xie, X. Zhang, and S. Qi, "Research and Design of Class D Amplifier at 1 MHz," in *2018 IEEE 3rd International Conference on Integrated Circuits and Microsystems (ICICM)*, 2018, pp. 29-32.
[42] M. Sakalas, J. Wagner, N. Joram, and F. Ellinger, "Design Approach for a Broadband Class-D Power Amplifier for Low Power Application in a 28 nm Digital CMOS Technology," in *2019 15th Conference on Ph. D Research in Microelectronics and Electronics (PRIME)*, 2019, pp. 157-160.
[43] F. Tamjid, A. Ghahremani, M. Richardson, and A. E. Fathy, "A novel approach to the design of a broadband high efficiency Class-E power amplifier with over 87% bandwidth," in *2017 IEEE Topical Conference on RF/Microwave Power Amplifiers for Radio and Wireless Applications (PAWR)*, 2017, pp. 25-28.
[44] E. Herceg and T. Urbanec, "Comparison of Class C and High Efficiency Class E Amplifiers at 435 MHz," in *2019 29th International Conference Radioelektronika (RADIOELEKTRONIKA)*, 2019, pp. 1-4.
[45] D. Schmelzer and S. I. Long, "A GaN HEMT Class F Amplifier at 2 GHz With $>\, $80% PAE," *IEEE Journal of Solid-State Circuits,* vol. 42, pp. 2130-2136, 2007.
[46] S. M. Wood, R. S. Pengelly, and M. Suto, "A high power, high efficiency UMTS amplifier using a novel Doherty configuration," in *Radio and Wireless Conference, 2003. RAWCON '03. Proceedings*, 2003, pp. 329-332.
[47] A. Hussain, *Advanced RF engineering for wireless systems and networks*: IEEE Press, 2005.
[48] B. Bukvić and M. M. Ilić, "Simple design of a class-J amplifier with predetermined efficiency," *IEEE Microwave and Wireless Components Letters,* vol. 26, pp. 699-701, 2016.
[49] J. F. White, *High Frequency Techniques: An Introduction to RF and Microwave Design and Computer Simulation*: John Wiley & Sons, 2004.
[50] C. S. Aitchison, M. Mbabele, M. R. Moazzam, D. Budimir, and F. Ali, "Improvement of third-order intermodulation product of RF and microwave amplifiers by injection," *IEEE Transactions on Microwave Theory and Techniques,* vol. 49, pp. 1148-1154, 2001.
[51] J. C. Pedro and N. B. De Carvalho, "On the use of multitone techniques for assessing RF components' intermodulation distortion," *IEEE Transactions on Microwave Theory and Techniques,* vol. 47, pp. 2393-2402, 1999.
[52] N. B. Carvalho and J. C. Pedro, "Multi-tone intermodulation distortion performance of 3rd order microwave circuits," in *Microwave Symposium Digest, 1999 IEEE MTT-S International*, 1999, pp. 763-766.
[53] J. Groe, "Polar transmitters for wireless communications," *IEEE Communications Magazine,* vol. 45, 2007.

[54] S.-W. Yoon, "Static and dynamic error vector magnitude behavior of 2.4-GHz power amplifier," *IEEE Transactions on Microwave theory and techniques,* vol. 55, pp. 643-647, 2007.
[55] P. Celka, N. J. Bershad, and J.-M. Vesin, "Stochastic gradient identification of polynomial Wiener systems: Analysis and application," *IEEE transactions on signal processing,* vol. 49, pp. 301-313, 2001.
[56] W. Sansen, "Distortion in elementary transistor circuits," *IEEE Transactions on Circuits and Systems II: Analog and Digital Signal Processing,* vol. 46, pp. 315-325, 1999.
[57] G. Erdogdu, "Linearization of RF Power Amplifıers By Using Memory Polynomial Digital Predistortion Technique," MS Thesis, Department of Electrical and Electronics Engineering, Middle East …, 2012.
[58] Y. Ye, T. Liu, T. Xu, and F. M. Ghannouchi, "Analysis and Decomposition of the Nonlinearities in RF Power Amplifiers," in *Wireless Communications Networking and Mobile Computing (WiCOM), 2010 6th International Conference on*, 2010, pp. 1-4.
[59] D. Bondar, N. Lopez, Z. Popovic, and D. Budimir, "Linearization of high-efficiency power amplifiers using digital baseband predistortion with iterative injection," in *Radio and Wireless Symposium (RWS), 2010 IEEE*, 2010, pp. 148-151.
[60] D. Bondar, D. Budimir, and B. Shelkovnikov, "Minimizing memory effects in OFDM transmitters using adaptive baseband equalization," in *Microwave & Telecommunication Technology, 2008. CriMiCo 2008. 2008 18th International Crimean Conference*, 2008, pp. 272-275.
[61] D. Bondar and D. Budimir, "Digital baseband predistortion of wideband power amplifiers with improved memory effects," in *Radio and Wireless Symposium, 2009. RWS'09. IEEE*, 2009, pp. 284-287.
[62] S. Boumaiza and F. M. Ghannouchi, "Thermal memory effects modeling and compensation in RF power amplifiers and predistortion linearizers," *IEEE Transactions on Microwave Theory and Techniques,* vol. 51, pp. 2427-2433, 2003.
[63] O. Hammi, S. Carichner, B. Vassilakis, and F. M. Ghannouchi, "Novel approach for static nonlinear behavior identification in RF power amplifiers exhibiting memory effects," in *Microwave Symposium Digest, 2008 IEEE MTT-S International*, 2008, pp. 1521-1524.
[64] T. Liu, S. Boumaiza, A. B. Sesay, and F. M. Ghannouchi, "Quantitative measurements of memory effects in wideband RF power amplifiers driven by modulated signals," *IEEE microwave and wireless components letters,* vol. 17, pp. 79-81, 2007.
[65] Y. Yang, J. Yi, B. Kim, Y. Kim, and M. Park, "Measurement and Modeling of Two Tone Transfer Characteristics of High Power Amplifiers," in *Microwave Conference, 2000. 30th European*, 2000, pp. 1-4.
[66] A. V. Oppenheim, *Discrete-time signal processing*: Pearson Education India, 1999.
[67] H. Ku, M. D. McKinley, and J. S. Kenney, "Quantifying memory effects in RF power amplifiers," *IEEE Transactions on Microwave Theory and Techniques,* vol. 50, pp. 2843-2849, 2002.
[68] S.-J. Yi, S. Nam, S.-H. Oh, and J.-H. Han, "Prediction of a CDMA output spectrum based on intermodulation products of two-tone test," *IEEE Transactions on Microwave Theory and Techniques,* vol. 49, pp. 938-946, 2001.

[69] H. R. Chayon and H. Ramiah, "Key challenges and potential applications of LTE-Advanced," in *Systems, Process and Control (ICSPC), 2017 IEEE Conference on*, 2017, pp. 146-150.
[70] B. A. Bjerke, "LTE-advanced and the evolution of LTE deployments," *IEEE Wireless Communications,* vol. 18, 2011.
[71] Z. Ding, Y. Liu, J. Choi, Q. Sun, M. Elkashlan, I. Chih-Lin*, et al.*, "Application of non-orthogonal multiple access in LTE and 5G networks," *IEEE Communications Magazine,* vol. 55, pp. 185-191, 2017.
[72] K. H. Teo, Z. Tao, and J. Zhang, "The mobile broadband WiMAX standard [standards in a nutshell]," *IEEE Signal Processing Magazine,* vol. 24, pp. 144-148, 2007.
[73] W.-F. Alliance, "Wi-Fi Protected Access: Strong, standards-based, interoperable security for today's Wi-Fi networks," *White paper, University of Cape Town,* pp. 492-495, 2003.
[74] J. Tu, Y.-j. Zhang, Z. Zhang, Z.-w. Ye, and Z.-l. Chen, "Performance analysis of vertical handoff in wifi and wimax heterogeneous networks," in *Computer Network and Multimedia Technology, 2009. CNMT 2009. International Symposium on*, 2009, pp. 1-5.
[75] B. A. Sheik, P. Sridevi, and P. R. Raju, "Comparison of inset-fed rectangular and E-shaped antenna arrays for LTE & Wi-Fi applications," in *Signal Processing And Communication Engineering Systems (SPACES), 2018 Conference on*, 2018, pp. 6-11.
[76] D. Laselva, D. Lopez-Perez, M. Rinne, and T. Henttonen, "3GPP LTE-WLAN Aggregation Technologies: Functionalities and Performance Comparison," *IEEE Communications Magazine,* vol. 56, pp. 195-203, 2018.
[77] J. L. Mitchell, "Introduction to digital audio coding and standards," *Journal of Electronic Imaging,* vol. 13, p. 399, 2004.
[78] U. Reimers, *DVB: the family of international standards for digital video broadcasting*: Springer, 2013.
[79] B. H. Chandana, R. Rudheesh, and S. N. Rasool, "Receiver modules for 3G UMTS mobile communications," in *Wireless Communications, Signal Processing and Networking (WiSPNET), 2017 International Conference on*, 2017, pp. 2645-2651.
[80] M. Kassim, R. A. Rahman, M. A. A. Aziz, A. Idris, and M. I. Yusof, "Performance analysis of VoIP over 3G and 4G LTE network," in *Electrical, Electronics and System Engineering (ICEESE), 2017 International Conference on*, 2017, pp. 37-41.
[81] T. S. Rappaport, S. Sun, R. Mayzus, H. Zhao, Y. Azar, K. Wang*, et al.*, "Millimeter wave mobile communications for 5G cellular: It will work!," *IEEE access,* vol. 1, pp. 335-349, 2013.
[82] Y. Xiao and F. Hu, *Cognitive radio networks*: CRC press, 2008.
[83] C. R. Stevenson, G. Chouinard, Z. Lei, W. Hu, S. J. Shellhammer, and W. Caldwell, "IEEE 802.22: The first cognitive radio wireless regional area network standard," *IEEE communications magazine,* vol. 47, pp. 130-138, 2009.
[84] R. Y. Mesleh, H. Haas, S. Sinanovic, C. W. Ahn, and S. Yun, "Spatial modulation," *IEEE Transactions on Vehicular Technology,* vol. 57, pp. 2228-2241, 2008.
[85] A. B. Narasimhamurthy, M. K. Banavar, and C. Tepedelenliouglu, "OFDM systems for wireless communications," *Synthesis Lectures on Algorithms and Software in Engineering,* vol. 2, pp. 1-78, 2010.

[86] R. Prasad, *OFDM for wireless communications systems*: Artech House, 2004.
[87] A. Pavani, D. E. K. Rao, and D. B. P. Rao, "A new OFDM standard for high rate wireless LAN in the 5 GHZ band," *International Journal of Future Generation Communication and Networking,* vol. 4, pp. 57-64, 2011.
[88] K. T. Wong, B. Wang, and J.-C. Chen, "OFDM PAPR reduction by switching null subcarriers and data-subcarriers," *Electronics letters,* vol. 47, pp. 62-63, 2011.
[89] I. Koffman and V. Roman, "Broadband wireless access solutions based on OFDM access in IEEE 802.16," *IEEE communications magazine,* vol. 40, pp. 96-103, 2002.
[90] R. v. Nee and R. Prasad, *OFDM for wireless multimedia communications*: Artech House, Inc., 2000.
[91] D. Rajeswaran, J. A. Sam, and A. K. Nair, "OFDM receiver design and characterization with reduction of PAPR," in *Communication and Electronics Systems (ICCES), 2017 2nd International Conference on*, 2017, pp. 452-457.
[92] M. Windisch and G. Fettweis, "Standard-independent I/Q imbalance compensation in OFDM direct-conversion receivers," in *Proc. 9th Intl. OFDM Workshop (InOWo)*, 2004, pp. 57-61.
[93] V. Sharma, A. Shrivastav, A. Jain, and A. Panday, "BER performance of OFDM-BPSK,-QPSK,-QAM over AWGN channel using forward Error correcting code," *International Journal of Engineering Research and Applications (IJERA),* vol. 2, pp. 1619-1624, 2012.
[94] L. Dewangan, M. Singh, and N. Dewangan, "A Survey of PAPR Reduction Techniques in LTE-OFDM System," *International Journal of Recent Technology and Engineering (IJRTE),* vol. 1, 2012.
[95] J. Faezah and K. Sabira, "Adaptive modulation for OFDM systems," *International Journal of Communication Networks and Information Security (IJCNIS),* vol. 1, 2009.
[96] M. Hiraoka, T. Nagashima, B. Karanov, G. Cincotti, S. Shimizu, T. Murakawa*, et al.*, "Optical serial-to-parallel conversion based on fractional OFDM scheme," in *OptoElectronics and Communications Conference (OECC) held jointly with 2016 International Conference on Photonics in Switching (PS), 2016 21st*, 2016, pp. 1-3.
[97] B. Muquet, Z. Wang, G. B. Giannakis, M. De Courville, and P. Duhamel, "Cyclic prefixing or zero padding for wireless multicarrier transmissions?," *IEEE Transactions on communications,* vol. 50, pp. 2136-2148, 2002.
[98] J. Lee and H.-G. Ryu, "Performance comparison between wavelet-based OFDM system and iFFT-based OFDM system," in *Information and Communication Technology Convergence (ICTC), 2017 International Conference on*, 2017, pp. 957-960.
[99] A. Peled and A. Ruiz, "Frequency domain data transmission using reduced computational complexity algorithms," in *Acoustics, Speech, and Signal Processing, IEEE International Conference on ICASSP'80.*, 1980, pp. 964-967.
[100] N. LaSorte, W. J. Barnes, and H. H. Refai, "The history of orthogonal frequency division multiplexing," in *Global Telecommunications Conference, 2008. IEEE GLOBECOM 2008. IEEE*, 2008, pp. 1-5.
[101] S. B. Weinstein, "The history of orthogonal frequency-division multiplexing [History of Communications]," *IEEE Communications Magazine,* vol. 47, 2009.

[102] A. Pandharipande, "Principles of OFDM," *IEEE potentials,* vol. 21, pp. 16-19, 2002.
[103] H. Xu, L. Zhu, P. Wang, T. Tang, C. Li, and W. Zhao, "The application of orthogonal frequency division multiplexing narrow-band carrier in communication of electric control valve," in *Computer and Communications (ICCC), 2016 2nd IEEE International Conference on*, 2016, pp. 2659-2663.
[104] F. H. Gregorio, *Analysis and compensation of nonlinear power amplifier effects in multi-antenna OFDM systems*: Helsinki University of Technology, 2007.
[105] J. Kim and K. Konstantinou, "Digital predistortion of wideband signals based on power amplifier model with memory," *Electronics Letters,* vol. 37, pp. 1417-1418, 2001.
[106] E. Costa, M. Midrio, and S. Pupolin, "Impact of amplifier nonlinearities on OFDM transmission system performance," *IEEE Communications Letters,* vol. 3, pp. 37-39, 1999.
[107] L. Tianjiu, "Nonlinear characteristics and pre distortion modeling of a non memory RF power amplifier," in *Electronic Measurement & Instruments (ICEMI), 2017 13th IEEE International Conference on*, 2017, pp. 184-187.
[108] B. S. Krongold, "New techniques for multicarrier communication systems," University of Illinois at Urbana-Champaign, 2001.
[109] A. K. NAHAR, "Enhanced PAPR Reduction and Channel Estimation Techniques In Multi-Carrier Wireless Communication System," UNIVERSITI MALAYSIA PAHANG, 2016.
[110] L. Dang, H. Li, and S. Guo, "PAPR reduction in OFDM with active constellation extension and hadamard transform," in *Intelligent Computer Communication and Processing (ICCP), 2017 13th IEEE International Conference on*, 2017, pp. 543-549.
[111] S.-H. Wang, W.-L. Lin, B.-R. Huang, and C.-P. Li, "PAPR reduction in OFDM systems using active constellation extension and subcarrier grouping techniques," *IEEE Communications Letters,* vol. 20, pp. 2378-2381, 2016.
[112] U. I. Butt, *A Study On The Tone-Reservation Technique For Peak-To-Average Power Ratio Reduction In Ofdm Systems*: Universal-Publishers, 2010.
[113] X. Li and L. J. Cimini, "Effects of clipping and filtering on the performance of OFDM," in *Vehicular Technology Conference, 1997, IEEE 47th*, 1997, pp. 1634-1638.
[114] J. Armstrong, "Peak-to-average power reduction for OFDM by repeated clipping and frequency domain filtering," *Electronics letters,* vol. 38, pp. 246-247, 2002.
[115] T. Yunzheng, L. Long, L. Shang, and Z. Zhi, "A survey: Several technologies of non-orthogonal transmission for 5G," *China communications,* vol. 12, pp. 1-15, 2015.
[116] B. Farhang-Boroujeny and H. Moradi, "OFDM inspired waveforms for 5G," *IEEE Communications Surveys & Tutorials,* vol. 18, pp. 2474-2492, 2016.
[117] S. Hong, M. Sagong, C. Lim, S. Cho, K. Cheun, and K. Yang, "Frequency and quadrature-amplitude modulation for downlink cellular OFDMA networks," *IEEE journal on selected areas in communications,* vol. 32, pp. 1256-1267, 2014.

[118] S. Wu, Y. Wang, M. Al-Imari, and M. Nekovee, "Frequency and quadrature amplitude modulation for 5g networks," in *Networks and Communications (EuCNC), 2016 European Conference on*, 2016, pp. 1-5.
[119] N. Maziar, W. Yue, T. Milos, W. Shangbin, Q. Yinan, and A.-I. Mohammed, "Overview of 5G modulation and waveforms candidates," *Journal of Communications and Information Networks,* vol. 1, pp. 44-60, 2016.
[120] Y. Qi and M. Tesanovic, "Fqam-fbmc design and its application to machine type communication," in *Personal, Indoor, and Mobile Radio Communications (PIMRC), 2016 IEEE 27th Annual International Symposium on*, 2016, pp. 1-6.
[121] Y. Wang, W. Liu, M. Jin, S. Jang, and J. M. Kim, "FQAM/FPSK modulation for spatial modulation systems," in *Information and Communication Technology Convergence (ICTC), 2016 International Conference on*, 2016, pp. 511-515.
[122] A. B. Sergienko and S. S. Sylka, "Bit Error Rate of FQAM Transmission in Fast Fading Channel," in *2019 IEEE Conference of Russian Young Researchers in Electrical and Electronic Engineering (EIConRus)*, 2019, pp. 33-38.
[123] G. S. Kishore and H. Rallapalli, "Performance Assessment of M-ary ASK, FSK, PSK, QAM and FQAM in AWGN Channel," in *2019 International Conference on Communication and Signal Processing (ICCSP)*, 2019, pp. 0273-0277.
[124] J. Nadal, C. A. Nour, and A. Baghdadi, "Design and Evaluation of a Novel Short Prototype Filter for FBMC/OQAM Modulation," *IEEE access,* vol. 6, pp. 19610-19625, 2018.
[125] F. Jackisch, "Spectral efficiency gains through the use of FBMC/OQAM for DOCSIS systems," in *Consumer Electronics (ICCE), 2018 IEEE International Conference on*, 2018, pp. 1-4.
[126] B. Saltzberg, "Performance of an efficient parallel data transmission system," *IEEE Transactions on Communication Technology,* vol. 15, pp. 805-811, 1967.
[127] P. Siohan, C. Siclet, and N. Lacaille, "Analysis and design of OFDM/OQAM systems based on filterbank theory," *IEEE transactions on signal processing,* vol. 50, pp. 1170-1183, 2002.
[128] P. Sabeti, H. Saeedi-Sourck, and M. J. Omidi, "Low-complexity CFO correction of frequency-spreading SMT in uplink of multicarrier multiple access networks," in *Electrical Engineering (ICEE), 2015 23rd Iranian Conference on*, 2015, pp. 410-415.
[129] L. Zhan, "Link Level Comparative Study between OFDM and FBMC," in *2019 International Conference on Communications, Information System and Computer Engineering (CISCE)*, 2019, pp. 266-269.
[130] H. Nam, M. Choi, C. Kim, D. Hong, and S. Choi, "A new filter-bank multicarrier system for QAM signal transmission and reception," in *Communications (ICC), 2014 IEEE International Conference on*, 2014, pp. 5227-5232.
[131] F. Schaich, "Filterbank based multi carrier transmission (FBMC)—evolving OFDM: FBMC in the context of WiMAX," in *Wireless Conference (EW), 2010 European*, 2010, pp. 1051-1058.
[132] A. Baki, R. Al Ahsan, and A. Awsaf, "Novel Methods of Filtering For FBMC/UFMC Based 5G Communication Systems," in *2019 7th International Conference on Smart Computing & Communications (ICSCC)*, 2019, pp. 1-4.

[133] Y. Cai, Z. Qin, F. Cui, G. Y. Li, and J. A. McCann, "Modulation and multiple access for 5G networks," *IEEE Communications Surveys & Tutorials,* vol. 20, pp. 629-646, 2018.
[134] D. E. Kebiche, A. Baghaki, X. Zhu, and B. Champagne, "UFMC-based wideband spectrum sensing for cognitive radio systems in non-Gaussian noise," in *Personal, Indoor, and Mobile Radio Communications (PIMRC), 2017 IEEE 28th Annual International Symposium on*, 2017, pp. 1-7.
[135] X. Wang, T. Wild, and F. Schaich, "Filter optimization for carrier-frequency- and timing-offset in universal filtered multi-carrier systems," in *Vehicular Technology Conference (VTC Spring), 2015 IEEE 81st*, 2015, pp. 1-6.
[136] T. Wild, F. Schaich, and Y. Chen, "5G air interface design based on universal filtered (UF-) OFDM," in *Digital Signal Processing (DSP), 2014 19th International Conference on*, 2014, pp. 699-704.
[137] B. Hadjer and B. Abdelhafid, "Comparison & Performance Evaluation of MIMO-FBMC and MIMO-UFMC systems for various equalization techniques," in *2019 International Conference on Networking and Advanced Systems (ICNAS)*, 2019, pp. 1-5.
[138] P. N. Rani and C. S. Rani, "UFMC: The 5G modulation technique," in *Computational Intelligence and Computing Research (ICCIC), 2016 IEEE International Conference on*, 2016, pp. 1-3.
[139] A. Muayyadi and D. Arseno, "Performance analysis of generalized frequency division multiplexing in various pulse-shaping filter for next generation communication systems," in *Wireless and Mobile (APWiMob), 2016 IEEE Asia Pacific Conference on*, 2016, pp. 41-45.
[140] S. Maanasa, V. Ishwarya, N. Hemapriya, and L. Nandita, "Transmit signal characterization of generalized frequency division multiplexing," in *IEEE Region 10 Symposium (TENSYMP), 2017*, 2017, pp. 1-4.
[141] G. Fettweis, M. Krondorf, and S. Bittner, "GFDM-generalized frequency division multiplexing," in *Vehicular Technology Conference, 2009. VTC Spring 2009. IEEE 69th*, 2009, pp. 1-4.
[142] M. Schetzen, "Nonlinear system modeling based on the Wiener theory," *Proceedings of the IEEE,* vol. 69, pp. 1557-1573, 1981.
[143] C. J. Clark, C. P. Silva, A. A. Moulthrop, and M. S. Muha, "Power-amplifier characterization using a two-tone measurement technique," *IEEE transactions on microwave theory and techniques,* vol. 50, pp. 1590-1602, 2002.
[144] L. C. Nunes, P. M. Cabral, and J. C. Pedro, "A physical model of power amplifiers AM/AM and AM/PM distortions and their internal relationship," in *Microwave Symposium Digest (IMS), 2013 IEEE MTT-S International*, 2013, pp. 1-4.
[145] S. Azam, C. Svensson, and Q. Wahab, "Designing of high efficiency power amplifier based on physical model of SiC MESFET in TCAD," in *Applied Sciences & Technology, 2007. IBCAST 2007. International Bhurban Conference on*, 2007, pp. 40-43.
[146] A. Plews, C. Snowden, and M. Howes, "Large-signal design of MMMIC Ka-band power amplifiers based on physical models," in *Microwave Symposium Digest, 1997., IEEE MTT-S International*, 1997, pp. 1729-1732.
[147] D. Guerra, F. Marino, D. Ferry, S. Goodnick, M. Saraniti, and R. Soligo, "Large-signal mm-wave InAlN/GaN HEMT power amplifier characterization through self-consistent harmonic balance/cellular Monte

Carlo device simulation," in *Electron Devices Meeting (IEDM), 2011 IEEE International*, 2011, pp. 34.2. 1-34.2. 4.
[148] J. Peng, S. He, and H. Yuan, "An Interband Time-Delay Compensation Algorithm for Concurrent Dual-Band Power Amplifier Characterization," *IEEE Microwave and Wireless Components Letters,* 2018.
[149] T. R. Cunha, E. G. Lima, and J. C. Pedro, "A polar-oriented Volterra model for power amplifier characterization," in *Microwave Symposium Digest (MTT), 2010 IEEE MTT-S International*, 2010, pp. 556-559.
[150] H. Wang, G.-S. Li, and P.-G. Liu, "Generalization of RF power amplifiers' behavioral model using memory polynomial/Volterra series," in *International Conference on Graphic and Image Processing (ICGIP 2011)*, 2011, p. 82855X.
[151] S. Gupta, A. K. Sahoo, and U. K. Sahoo, "Parameter estimation of Wiener nonlinear model using least mean square (LMS) algorithm," in *Region 10 Conference, TENCON 2017-2017 IEEE*, 2017, pp. 1399-1403.
[152] H. Ku and Y. Park, "Development of Efficient Discrete Model and Error Analysis for Nonlinear RF Power Amplifiers in Wireless Communications," *IEICE transactions on communications,* vol. 93, pp. 2363-2369, 2010.
[153] S. Lim and C. Eun, "Predistorter design for a memory-less nonlinear high power amplifier using the pth-order inverse method for OFDM systems," in *Intelligent Signal Processing and Communication Systems, 2005. ISPACS 2005. Proceedings of 2005 International Symposium on*, 2005, pp. 217-220.
[154] A. S. Sappal, M. S. Patterh, and S. Sharma, "Mathematical modeling of power amplifier with memory effects," *Indian Journal of Science and Technology,* vol. 2, pp. 22-23, 2009.
[155] K. J. Muhonen, M. Kavehrad, and R. Krishnamoorthy, "Look-up table techniques for adaptive digital predistortion: A development and comparison," *IEEE transactions on vehicular technology,* vol. 49, pp. 1995-2002, 2000.
[156] H. Zhi-yong, G. Jian-hua, G. Shu-Jian, and W. Gang, "An improved look-up table predistortion technique for HPA with memory effects in OFDM systems," *IEEE transactions on broadcasting,* vol. 52, pp. 87-91, 2006.
[157] M. Schetzen, *Linear time-invariant systems*: J Wiley-Interscience, 2003.
[158] P. M. Lavrador, J. C. Pedro, and N. B. Carvalho, "A new Volterra series based orthogonal behavioral model for power amplifiers," in *Microwave Conference Proceedings, 2005. APMC 2005. Asia-Pacific Conference Proceedings*, 2005, p. 4 pp.
[159] A. Zhu, J. C. Pedro, and T. R. Cunha, "Pruning the Volterra series for behavioral modeling of power amplifiers using physical knowledge," *IEEE Transactions on Microwave Theory and Techniques,* vol. 55, pp. 813-821, 2007.
[160] P. Śliwiński, A. Marconato, P. Wachel, and G. Birpoutsoukis, "Non-linear system modelling based on constrained Volterra series estimates," *IET Control Theory & Applications,* vol. 11, pp. 2623-2629, 2017.
[161] R. Raich and G. T. Zhou, "On the modeling of memory nonlinear effects of power amplifiers for communication applications," in *Digital Signal Processing Workshop, 2002 and the 2nd Signal Processing Education Workshop. Proceedings of 2002 IEEE 10th*, 2002, pp. 7-10.
[162] J. C. Pedro and N. B. Carvalho, *Intermodulation distortion in microwave and wireless circuits*: Artech House, 2002.

[163] A. Zhu and J. C. Pedro, "Distortion evaluation of RF power amplifiers using dynamic deviation reduction based Volterra series," in *Microwave Symposium, 2007. IEEE/MTT-S International*, 2007, pp. 965-968.
[164] D. D. Silveira and G. Magerl, "Extraction and improvements of a behavioral model based on the Wiener-Bose structure used for baseband Volterra kernels estimation," in *Microwave Symposium, 2007. IEEE/MTT-S International*, 2007.
[165] P. L. Gilabert, D. D. Silveira, G. Montoro, M. E. Gadringer, and E. Bertran, "Heuristic algorithms for power amplifier behavioral modeling," *IEEE Microwave and Wireless Components Letters,* vol. 17, pp. 715-717, 2007.
[166] G. Montoro, P. L. Gilabert, E. Bertran, A. Cesari, and D. D. Silveira, "A new digital predictive predistorter for behavioral power amplifier linearization," *IEEE Microwave and wireless components letters,* vol. 17, pp. 448-450, 2007.
[167] P. N. Landin, K. Barbé, W. Van Moer, M. Isaksson, and P. Händel, "Two novel memory polynomial models for modeling of RF power amplifiers," *International journal of microwave and wireless technologies,* vol. 7, pp. 19-29, 2015.
[168] O. Hammi, A. M. Kedir, and F. M. Ghannouchi, "Nonuniform memory polynomial behavioral model for wireless transmitters and power amplifiers," in *Microwave Conference Proceedings (APMC), 2012 Asia-Pacific*, 2012, pp. 836-838.
[169] O. Hammi, F. M. Ghannouchi, and B. Vassilakis, "A compact envelope-memory polynomial for RF transmitters modeling with application to baseband and RF-digital predistortion," *IEEE Microwave and Wireless Components Letters,* vol. 18, pp. 359-361, 2008.
[170] M. Kozek and N. Jovanovic, "Identification of Hammerstein/Wiener nonlinear systems with extended Kalman filters," in *American Control Conference, 2002. Proceedings of the 2002*, 2002, pp. 969-974.
[171] K. Tiels, M. Schoukens, and J. Schoukens, "Initial estimates for Wiener–Hammerstein models using phase-coupled multisines," *Automatica,* vol. 60, pp. 201-209, 2015.
[172] E.-W. Bai, "An optimal two-stage identification algorithm for Hammerstein–Wiener nonlinear systems," *Automatica,* vol. 34, pp. 333-338, 1998.
[173] H. Ase and T. Katayama, "A subspace-based identification of Wiener–Hammerstein benchmark model," *Control Engineering Practice,* vol. 44, pp. 126-137, 2015.
[174] L. Ding, R. Raich, and G. T. Zhou, "A Hammerstein predistortion linearization design based on the indirect learning architecture," in *Acoustics, Speech, and Signal Processing (ICASSP), 2002 IEEE International Conference on*, 2002, pp. III-2689-III-2692.
[175] O. Hammi, "Augmented twin-nonlinear two-box behavioral models for multicarrier LTE power amplifiers," *The Scientific World Journal,* vol. 2014, 2014.
[176] O. Hammi and F. M. Ghannouchi, "Twin nonlinear two-box models for power amplifiers and transmitters exhibiting memory effects with application to digital predistortion," *IEEE Microwave and Wireless Components Letters,* vol. 19, pp. 530-532, 2009.
[177] C. Quindroit, N. Naraharisetti, P. Roblin, S. Gheitanchi, V. Mauer, and M. Fitton, "2D forward twin nonlinear two-box model for concurrent dual-band digital predistortion," in *Power Amplifiers for Wireless and Radio Applications (PAWR), 2014 IEEE Topical Conference on*, 2014, pp. 1-3.

[178] A. M. Kedir, A. Kwan, O. Hammi, and F. M. Ghannouchi, "Generic bandwidth scalable behavioral models for RF power amplifiers with memory effects," in *RF and Microwave Conference (RFM), 2013 IEEE International*, 2013, pp. 291-294.
[179] O. Hammi and A. Miftah, "Complexity-aware-normalised mean squared error 'CAN'metric for dimension estimation of memory polynomial-based power amplifiers behavioural models," *IET Communications,* vol. 9, pp. 2227-2233, 2015.
[180] A. Wills, T. B. Schön, L. Ljung, and B. Ninness, "Identification of hammerstein–wiener models," *Automatica,* vol. 49, pp. 70-81, 2013.
[181] Y. Tang, "Parameter estimation of Wiener model using differential evolution algorithm," *International Journal of Circuits, Systems and Signal Processing,* vol. 6, pp. 315-323, 2012.
[182] A. Atanasković, N. M. Ilić, and A. Đoric, "Controlled coefficient adaptation in linearization of PA by modified baseband signal," in *Advanced Technologies, Systems and Services in Telecommunications (TELSIKS), 2017 13th International Conference on*, 2017, pp. 355-358.
[183] N. Mizusawa and S. Kusunoki, "Third-and fifth-order baseband component injection for linearization of the power amplifier in a cellular phone," *IEEE transactions on microwave theory and techniques,* vol. 53, pp. 3327-3334, 2005.
[184] A. A. bin Mohd Faudzi and D. Pebrianti, "Simultaneous computation of model order and parameter estimation for system identification based on opposition-based simulated Kalman filter."
[185] C. Cheng, D.-l. Xu, and X.-m. Wang, "Least square smoothing algorithm and gauss decomposition spectral analysis method in spectral gamma ray logging," in *Piezoelectricity, Acoustic Waves, and Device Applications (SPAWDA), 2017 Symposium on*, 2017, pp. 458-462.
[186] M. Amin-Naji, P. Ranjbar-Noiey, and A. Aghagolzadeh, "Multi-focus image fusion using Singular Value Decomposition in DCT domain," in *Machine Vision and Image Processing (MVIP), 2017 10th Iranian Conference on*, 2017, pp. 45-51.
[187] T. Liu, Y. Ye, S. Boumaiza, M. Helaoui, O. Hammi, and F. M. Ghannouchi, "Accurate identification of static nonlinear properties of wideband RF power amplifiers," in *Microwave and Millimeter Wave Technology, 2008. ICMMT 2008. International Conference on*, 2008, pp. 1351-1354.
[188] F. Heese, R. Steinbiss, P. Jax, and P. Vary, "Noise Reduction in the Time Domain Using ARMA Filtering," in *Speech Communication; 12. ITG Symposium; Proceedings of*, 2016, pp. 1-5.
[189] R. Braithwaite, "Digital Predistortion of an RF Power Amplifier Using a Reduced Volterra Series Model With a Memory Polynomial Estimator," *IEEE Transactions on Microwave Theory and Techniques,* vol. 65, pp. 3613-3623, 2017.
[190] L. Ding, G. T. Zhou, D. R. Morgan, Z. Ma, J. S. Kenney, J. Kim*, et al.*, "A robust digital baseband predistorter constructed using memory polynomials," *IEEE Transactions on communications,* vol. 52, pp. 159-165, 2004.
[191] C. Liu, H. Xiao, Q. Wu, and F. Li, "Spectrum design of RF power amplifier for wireless communication systems," *IEEE Transactions on Consumer Electronics,* vol. 48, pp. 72-80, 2002.
[192] F. Zaplata and L. Brancik, "Analysis of nonlinear cell of transmission line model using Volterra series approach," in *Radioelektronika*

(RADIOELEKTRONIKA), 2017 27th International Conference, 2017, pp. 1-4.

[193] A. R. Aghasi, H. Karkhaneh, and A. Ghorbani, "A modified model and linearization method for solid state power amplifier," *Analog Integrated Circuits and Signal Processing,* vol. 51, pp. 81-88, 2007.

[194] S. L. Lacy and D. S. Bernstein, "Identification of FIR Wiener systems with unknown, non-invertible, polynomial non-linearities," *International Journal of Control,* vol. 76, pp. 1500-1507, 2003.

[195] Y. Ye, T. Liu, and F. M. Ghannouchi, "Linear and nonlinear memory effects of RF power amplifiers," in *Microwave Conference, 2008. APMC 2008. Asia-Pacific*, 2008, pp. 1-4.

[196] N. Safari, T. Roste, P. Fedorenko, and J. S. Kenney, "An approximation of Volterra series using delay envelopes, applied to digital predistortion of RF power amplifiers with memory effects," *IEEE Microwave and Wireless Components Letters,* vol. 18, pp. 115-117, 2008.

[197] P. Page, C. Steinbeiser, T. Landon, G. Burgin, R. Hajji, R. Branson*, et al.*, "325W HVHBT Doherty Final and LDMOS Doherty Driver with 30dB Gain and 54% PAE linearized to-55dBc for 2c11 6.5 dB PAR," in *Compound Semiconductor Integrated Circuit Symposium (CSICS), 2011 IEEE*, 2011, pp. 1-4.

[198] A. S. Hussaini, T. Sadeghpour, R. Abd-Alhameed, M. B. Child, N. T. Ali, and J. Rodriguez, "Optimum design of Doherty RFPA for mobile WiMAX base stations," in *International Conference on Mobile Multimedia Communications*, 2010, pp. 700-705.

[199] H. Deguchi, N. Watanabe, A. Kawano, N. Yoshimura, N. Ui, and K. Ebihara, "A 2.6 GHz band 537W peak power GaN HEMT asymmetric Doherty amplifier with 48% drain efficiency at 7dB," in *Microwave Symposium Digest (MTT), 2012 IEEE MTT-S International*, 2012, pp. 1-3.

[200] I. Kim, J. Moon, J. Kim, J. Kim, C. S. Seo, K.-O. Sun*, et al.*, "Envelope injection consideration of high power hybrid EER transmitter for IEEE 802.16 e mobile WiMAX application," in *Microwave Symposium Digest, 2008 IEEE MTT-S International*, 2008, pp. 411-414.

[201] J. Lim, C. Park, J. Koo, H. Cha, Y. Jeong, S.-M. Han*, et al.*, "A balanced power amplifier utilizing the reflected input power," in *Radio-Frequency Integration Technology, 2009. RFIT 2009. IEEE International Symposium on*, 2009, pp. 88-91.

[202] A. Markos, K. Bathich, A. Al Tanany, D. Gruner, and G. Boeck, "Design of a 120 W balanced GaN Doherty power amplifier," in *Microwave Conference (GeMIC), 2011 German*, 2011, pp. 1-4.

[203] B. Mohammed, N. Abduljabbar, A. Hussaini, R. Abd-Alhameed, S. Jones, B. Gwandu*, et al.*, "A Si-LDMOS Doherty Power Amplifier for 2.620–2.690 GHz Applications," *Advanced Science Letters,* vol. 23, pp. 3874-3878, 2017.

[204] A. S. Hussaini, R. Abd-Alhameed, and J. Rodriguez, "Design of energy efficient power amplifier for 4G user terminals," in *Electronics, Circuits, and Systems (ICECS), 2010 17th IEEE International Conference on*, 2010, pp. 611-614.

[205] K. Rawat and F. M. Ghannouchi, "Design methodology for dual-band Doherty power amplifier with performance enhancement using dual-band offset lines," *IEEE Transactions on Industrial Electronics,* vol. 59, pp. 4831-4842, 2012.

[206] R. Quaglia, M. Pirola, and C. Ramella, "Offset lines in Doherty power amplifiers: Analytical demonstration and design," *IEEE Microwave and Wireless Components Letters,* vol. 23, pp. 93-95, 2013.
[207] R. Kshetrimayum, *Electromagnetic Field Theory*, 2012.
[208] H. Sano, N. Ui, and S. Sano, "A 40W GaN HEMT Doherty power amplifier with 48% efficiency for WiMAX applications," in *Compound Semiconductor Integrated Circuit Symposium, 2007. CSIC 2007. IEEE*, 2007, pp. 1-4.
[209] D. Dai, L. Sun, J. Wen, G. Su, and L. Guo, "A 10W broadband power amplifier for base station," in *Microwave and Millimeter Wave Technology (ICMMT), 2012 International Conference on*, 2012, pp. 1-4.
[210] B. Mohammed, A. Hussaini, H. Migdadi, R. Abd-Alhameed, N. Abduljabbar, I. Elfergani*, et al.*, "A 2.62-GHz class-F power amplifier with lumped-element and transmission line network design," in *Internet Technologies and Applications (ITA), 2017*, 2017, pp. 275-279.
[211] B. A. Mohammed, I. M. Danjuma, R. A. Abd-Alhameed, A. S. Hussaini, I. T. Elfergani, and J. Rodriguez, "Design and Simulation of Balanced RF Power Amplifier over Adaptive Digital Pre-distortion for MISO WLAN-OFDM Applications," *Journal of Multidisciplinary Engineering Science and Technology (JMEST),* vol. 4, pp. 8217-8221, 2017.
[212] P. Page, C. Steinbeiser, T. Landon, G. Burgin, R. Hajji, R. Branson*, et al.*, "325W HVHBT Doherty Final and LDMOS Doherty Driver with 30dB Gain and 54% PAE linearized to-55dBc for 2c11 6.5 dB PAR," in *2011 IEEE Compound Semiconductor Integrated Circuit Symposium (CSICS)*, 2011, pp. 1-4.
[213] I. Kim, J. Moon, J. Kim, J. Kim, C. S. Seo, K.-O. Sun*, et al.*, "Envelope injection consideration of high power hybrid EER transmitter for IEEE 802.16 e mobile WiMAX application," in *2008 IEEE MTT-S International Microwave Symposium Digest*, 2008, pp. 411-414.
[214] J. Lim, C. Park, J. Koo, H. Cha, Y. Jeong, S.-M. Han*, et al.*, "A balanced power amplifier utilizing the reflected input power," in *2009 IEEE International Symposium on Radio-Frequency Integration Technology (RFIT)*, 2009, pp. 88-91.
[215] H. Sano, N. Ui, and S. Sano, "A 40W GaN HEMT Doherty power amplifier with 48% efficiency for WiMAX applications," in *2007 IEEE Compound Semiconductor Integrated Circuits Symposium*, 2007, pp. 1-4.
[216] D. Dai, L. Sun, J. Wen, G. Su, and L. Guo, "A 10W broadband power amplifier for base station," in *2012 International Conference on Microwave and Millimeter Wave Technology (ICMMT)*, 2012, pp. 1-4.
[217] R. A. Beltran, "Class-F and inverse class-F power amplifier loading networks design based upon transmission zeros," in *Microwave Symposium (IMS), 2014 IEEE MTT-S International*, 2014, pp. 1-4.
[218] F. H. Raab, "Class-F power amplifiers with maximally flat waveforms," *IEEE Transactions on Microwave Theory and Techniques,* vol. 45, pp. 2007-2012, 1997.
[219] M. Wren and T. J. Brazil, "Experimental class-F power amplifier design using computationally efficient and accurate large-signal pHEMT model," *IEEE transactions on microwave theory and techniques,* vol. 53, pp. 1723-1731, 2005.
[220] R. Beltran and F. H. Raab, "Lumped-element output networks for high-efficiency power amplifiers," in *Microwave Symposium Digest (MTT), 2010 IEEE MTT-S International*, 2010, pp. 324-327.

[221] Y. Chung, C. Y. Hang, S. Cai, Y. Qian, C. P. Wen, K. L. Wang*, et al.*, "AlGaN/GaN HFET power amplifier integrated with microstrip antenna for RF front-end applications," *IEEE Transactions on Microwave Theory and Techniques,* vol. 51, pp. 653-659, 2003.
[222] V. Radisic, Y. Qian, and T. Itoh, "Novel architectures for high-efficiency amplifiers for wireless applications," *IEEE Transactions on Microwave Theory and Techniques,* vol. 46, pp. 1901-1909, 1998.
[223] F. H. Raab, "Class-E, class-C, and class-F power amplifiers based upon a finite number of harmonics," *IEEE Transactions on Microwave Theory and Techniques,* vol. 49, pp. 1462-1468, 2001.
[224] Y.-S. Lee, M.-W. Lee, and Y.-H. Jeong, "High-efficiency class-F GaN HEMT amplifier with simple parasitic-compensation circuit," *IEEE Microwave and Wireless Components Letters,* vol. 18, pp. 55-57, 2008.
[225] B. Mohammed, A. Hussaini, R. Abd-Alhameed, N. Abduljabbar, H. Obeidat, I. Elfergani*, et al.*, "A load-pull approach to design an optimum load impedance and matching network for class-F RF power amplifier," in *Internet Technologies and Applications (ITA), 2017*, 2017, pp. 280-283.
[226] I. T. Elfergani, R. A. Abd-Alhameed, N. T. Ali, A. Alhaddad, C. H. See, and E. Cabongomuqueba, "A novel dual band tunable balanced handset antenna for WLAN application," in *Electronics, Circuits and Systems (ICECS), 2011 18th IEEE International Conference on*, 2011, pp. 516-519.
[227] N. Al Khanbashi, N. Al Sindi, S. Al-Araji, N. Ali, Z. Chaloupka, V. Yenamandra*, et al.*, "Real time evaluation of RF fingerprints in wireless LAN localization systems," in *Positioning Navigation and Communication (WPNC), 2013 10th Workshop on*, 2013, pp. 1-6.
[228] P. Colantonio, F. Giannini, E. Limiti, and V. Teppati, "An approach to harmonic load-and source-pull measurements for high-efficiency PA design," *IEEE Transactions on Microwave theory and Techniques,* vol. 52, pp. 191-198, 2004.
[229] A. Ismail, A. Younis, N. Abduljabbar, B. Mohammed, and R. Abd-Alhameed, "A 2.45-GHz class-F power amplifier for CDMA systems," in *Internet Technologies and Applications (ITA), 2015*, 2015, pp. 428-433.
[230] M. Akkul, M. Roberts, V. Walker, and W. Bosch, "High efficiency power amplifier input/output circuit topologies for base station and WLAN applications," in *Microwave Symposium Digest, 2004 IEEE MTT-S International*, 2004, pp. 843-846.
[231] B. Mohammed, R. Abd-Alhameed, N. Abduljabbar, I. Danjuma, I. Elfergani, A. Hussaini*, et al.*, "A CAD-oriented technique to design an optimum load impedance with multi-coupler network for class-F power amplifier," 2017.
[232] P. J. Green, "Peak-to-average power ratio and power amplifier back-off requirements in wireless transmissions," in *Region 10 Conference, TENCON 2017-2017 IEEE*, 2017, pp. 630-633.
[233] E. Bertran and G. Montoro, "Performance analysis of power amplifier back-off levels in UWB transmitters," *IEEE Transactions on Consumer Electronics,* vol. 53, 2007.
[234] N. Deltimple, L. Leyssenne, E. Kerhervé, Y. Deval, and D. Belot, "Dynamic biasing techniques for RF power amplifier linearity and efficiency improvement," in *IC Design and Technology (ICICDT), 2010 IEEE International Conference on*, 2010, pp. 232-235.
[235] P. B. Kenington, "Methods linearize RF transmitters and power amps," *Microwaves and RF,* vol. 38, pp. 79-89, 1999.

[236] M. D. Nair, R. Giofrè, L. Piazzon, and P. Colantonio, "A comparative study on digital predistortion techniques for Doherty amplifier for LTE applications," in *Integrated Nonlinear Microwave and Millimetre-wave Circuits (INMMiC), 2014 International Workshop on*, 2014, pp. 1-3.
[237] H. K. Khalil, "Noninear systems," *Prentice-Hall, New Jersey,* vol. 2, pp. 5-1, 1996.
[238] J. Kim, C. Park, J. Moon, and B. Kim, "Analysis of adaptive digital feedback linearization techniques," *IEEE Transactions on Circuits and Systems I: Regular Papers,* vol. 57, pp. 345-354, 2010.
[239] J. Kim, Y. Y. Woo, J. Moon, and B. Kim, "A new wideband adaptive digital predistortion technique employing feedback linearization," *IEEE Transactions on Microwave Theory and Techniques,* vol. 56, pp. 385-392, 2008.
[240] A. Prata, D. C. Ribeiro, P. M. Cruz, A. S. Oliveira, and N. B. Carvalho, "RF Subsampling Feedback Loop Technique for Concurrent Dual-Band PA Linearization," *IEEE Transactions on Microwave Theory and Techniques,* vol. 64, pp. 4174-4182, 2016.
[241] A. Kheirkhahi, P. Naghshtabrizi, and L. E. Larson, "Stability analysis of RF power amplifier envelope feedback," *IEEE Transactions on Circuits and Systems II: Express Briefs,* vol. 58, pp. 852-856, 2011.
[242] X. Wang, J. Sturm, N. Yan, X. Tan, and H. Min, "0.6–3-GHz wideband receiver RF front-end with a feedforward noise and distortion cancellation resistive-feedback LNA," *IEEE Transactions on Microwave theory and techniques,* vol. 60, pp. 387-392, 2012.
[243] I.-W. Park, J.-O. Kim, M.-H. Oh, and W. Yang, "Realization of stabilization using feed-forward and feedback controller composition method for a mobile robot," *International Journal of Control, Automation and Systems,* vol. 13, pp. 1201-1211, 2015.
[244] S. Sharma, N. G. Constantin, and Y. Soliman, "Positive envelope feedback for linearity improvement in RFIC PAs," in *Radioelektronika (RADIOELEKTRONIKA), 2017 27th International Conference*, 2017, pp. 1-5.
[245] D. Rozenblit, T. Sowlati, and M. Damgaard, "Polar loop radio frequency (RF) transmitter having increased dynamic range amplitude control," ed: Google Patents, 2010.
[246] A. Gimeno-Martin, J. M. Pardo-Martin, and F. J. Ortega-Gonzalez, "An adaptive phase alignment algorithm for cartesian feedback loops [applications corner]," *IEEE Signal Processing Magazine,* vol. 27, 2010.
[247] A. V. Kosykh, S. A. Zavyalov, R. R. Fakhrutdinov, K. V. Murasov, and R. A. Wolf, "Influence of LO quadrature formation accuracy on signal spectrum in cartesian loop transmission paths," in *Dynamics of Systems, Mechanisms and Machines (Dynamics), 2017*, 2017, pp. 1-4.
[248] K. A. Gallagher, R. M. Narayanan, G. J. Mazzaro, and K. D. Sherbondy, "Linearization of a harmonic radar transmitter by feed-forward filter reflection," in *Radar Conference, 2014 IEEE*, 2014, pp. 1363-1368.
[249] K. A. Gallagher, G. J. Mazzaro, R. M. Narayanan, K. D. Sherbondy, and A. F. Martone, "Automated cancellation of harmonics using feed-forward filter reflection for radar transmitter linearization," in *Radar Sensor Technology XVIII*, 2014, p. 907703.
[250] Y.-K. Cho, C. Kim, and B. H. Park, "Envelope Elimination and Restoration Transmitter for Efficiency and Linearity Improvement of Power Amplifier,"

The Journal of Korean Institute of Electromagnetic Engineering and Science, vol. 26, pp. 292-299, 2015.

[251] M. Alon, S. Singer, and S. Spiegel, "Power efficiency analysis of envelope elimination and restoration technique in different topologies," in *Electrical and Electronics Engineers in Israel, 2008. IEEEI 2008. IEEE 25th Convention of*, 2008, pp. 805-809.

[252] D. Tena-Ramos, F. J. Ortega-González, and M. Patiño-Gómez, "Hybrid Envelope Elimination and Restoration Technique for Enhancing the Linearity of Switchmode Envelope Amplifiers," *IEEE Microwave and Wireless Components Letters,* vol. 27, pp. 186-188, 2017.

[253] H. Chireix, "High power outphasing modulation," *Proceedings of the Institute of Radio Engineers,* vol. 23, pp. 1370-1392, 1935.

[254] A. Simões, M. Castanheira, M. Gomes, R. Dinis, and V. Silva, "Ring-Type Magnitude Modulation for LINC: A Pragmatic Approach to the Efficiency Challenge," *IEEE Transactions on Communications,* vol. 65, pp. 3302-3315, 2017.

[255] Z. Dunn, M. Yeary, C. Fulton, and N. Goodman, "Memory polynomial model for digital predistortion of broadband solid-state radar amplifiers," in *Radar Conference (RadarCon), 2015 IEEE*, 2015, pp. 1482-1486.

[256] M. S. Hashmi, Z. S. Rogojan, and F. M. Ghannouchi, "A flexible dual-inflection point RF predistortion linearizer for microwave power amplifiers," *Progress In Electromagnetics Research,* vol. 13, pp. 1-18, 2010.

[257] X. Zhang, S. Saha, R. Zhu, T. Liu, and D. Shen, "Analog pre-distortion circuit for radio over fiber transmission," *IEEE Photonics Technology Letters,* vol. 28, pp. 2541-2544, 2016.

[258] S. Boumaiza, J. Li, M. Jaidane-Saidane, and F. M. Ghannouchi, "Adaptive digital/RF predistortion using a nonuniform LUT indexing function with built-in dependence on the amplifier nonlinearity," *IEEE Transactions on Microwave Theory and Techniques,* vol. 52, pp. 2670-2677, 2004.

[259] Y. Zhang, L. Li, S. Xiao, M. Bi, Y. Yu, and W. Hu, "Wideband Over-the-Air RF Self-Interference Cancellation by an EML-Based Optical System With Baseband Predistortion," *IEEE Photonics Journal,* vol. 9, pp. 1-9, 2017.

[260] R. Piazza, R. B. S. Mysore, and B. Ottersten, "Multicarrier LUT-based data predistortion for non-linear satellite channels," in *Communications (ICC), 2014 IEEE International Conference on*, 2014, pp. 4319-4324.

[261] B. F. Beidas, "Adaptive digital signal predistortion for nonlinear communication systems using successive methods," *IEEE Transactions on Communications,* vol. 64, pp. 2166-2175, 2016.

[262] T. Xin, Z. Yongfeng, and L. Liang, "Baseband signal predistortion based compensation technique for broadband I/Q modulation impairments in vector signal generators," in *Electronic Measurement & Instruments (ICEMI), 2015 12th IEEE International Conference on*, 2015, pp. 993-998.

[263] J. L. Dawson and T. H. Lee, *Feedback linearization of RF power amplifiers*: Springer Science & Business Media, 2007.

[264] J. Li, R. Shu, and Q. J. Gu, "A fully-integrated cartesian feedback loop transmitter in 65nm CMOS," in *Microwave Symposium (IMS), 2017 IEEE MTT-S International*, 2017, pp. 103-106.

[265] A. Abuelhaija, K. Solbach, and A. Buck, "Power amplifier for magnetic resonance imaging using unconventional Cartesian feedback loop," in *Microwave Conference (GeMiC), 2015 German*, 2015, pp. 119-122.

[266] Z. Liu and Y. Li, "A digital predistortion method for multi-band aggregation," in *Communication Technology (ICCT), 2017 IEEE 17th International Conference on*, 2017, pp. 343-349.
[267] K. M. Prasad and H. Suresh, "An efficient adaptive digital predistortion framework to achieve optimal linearization of power amplifier," in *Electrical, Electronics, and Optimization Techniques (ICEEOT), International Conference on*, 2016, pp. 2095-2101.
[268] S. Zhalehpour, J. Lin, and L. Rusch, "SiP IQ modulator Linearization by memory polynomial pre-distortion model," in *Photonics Conference (IPC), 2017 IEEE*, 2017, pp. 317-318.
[269] N. Dawar, T. Sharma, R. Darraji, and F. M. Ghannouchi, "Linearisation of radio frequency power amplifiers exhibiting memory effects using direct learning-based adaptive digital predistoriton," *IET Communications,* vol. 10, pp. 950-954, 2016.
[270] B. A. Mohammed, N. A. Abduljabbar, M. A. G. Al-Sadoon, K. Hameed, A. S. Hussaini, S. M. R. Jones*, et al.*, "A 15.5 W Si-LDMOS Balanced Power Amplifier with 53% Ultimate PAE for High Speed LTE," in *International Conference on Wireless and Satellite Systems*, 2016, pp. 193-201.
[271] S.-C. Jung, O. Hammi, and F. M. Ghannouchi, "Design optimization and DPD linearization of GaN-based unsymmetrical Doherty power amplifiers for 3G multicarrier applications," *IEEE Transactions on Microwave Theory and Techniques,* vol. 57, pp. 2105-2113, 2009.
[272] F. A. De Figueiredo, X. Jiao, W. Liu, R. Mennes, I. Jabandžić, and I. Moerman, "A Spectrum Sharing Framework for Intelligent Next Generation Wireless Networks," *IEEE Access,* vol. 6, pp. 60704-60735, 2018.
[273] X. Zhang, M. Jia, L. Chen, J. Ma, and J. Qiu, "Filtered-OFDM-enabler for flexible waveform in the 5th generation cellular networks," in *2015 IEEE Global Communications Conference (GLOBECOM)*, 2015, pp. 1-6.
[274] J. Abdoli, M. Jia, and J. Ma, "Filtered OFDM: A new waveform for future wireless systems," in *2015 IEEE 16th International Workshop on Signal Processing Advances in Wireless Communications (SPAWC)*, 2015, pp. 66-70.
[275] H. Chen, J. Hua, F. Li, F. Chen, and D. Wang, "Interference Analysis in the Asynchronous f-OFDM Systems," *IEEE Transactions on Communications,* vol. 67, pp. 3580-3596, 2019.

Author's Publication Record

Journals:

1. **B. A. Mohammed**, A. S. Hussaini, I. M. Danjuma, Y. I. Abdulraheem, R. A. Abd-Alhameed, G. Oguntala, N. N. Eya and F. El-megri, "Distortion level approximation of Linear and Nonlinear RF Power Amplifier over OFDM System," in International Journal of Engineering and Science (IJES), vol. 7, issue 11, 2018, pp. 58-69.

2. **B. A. Mohammed**, A. S. Hussaini, R. A. Abd-Alhameed, I. M. Danjuma, A. S. Asharaa, I. T. E. Elfergani and J. Rodriguez, "Towards A 15.5W Si- LDMOS Energy Efficient Balanced RF Power Amplifier for 5G-LTE Multi-carrier Applications," in EAI Endorsed Transactions on Creative Technologies (EAI-EU), vol. 5, issue 15, 2018.

3. **B. A. Mohammed**, I. M. Danjuma, R. A. Abd-Alhameed, N. A. Abduljabbar, A. S. Hussaini, and I. T. E. Elfergani, "A Dynamic Imbalanced Load Modulation Approach To Design and Implement an Energy-Efficient RF Power Amplifier," in International Journal of Engineering and Science (IJES), vol. 7, issue 4, 2018, pp. 53-58.

4. **B. A. Mohammed**, I. M. Danjuma, R. A. Abd-Alhameed, A. S. Hussaini, I.T. E. Elfergani and J. Rodriguez, "Design and Simulation of Balanced RF Power Amplifier over Adaptive Digital Pre-distortion for MISO WLAN-OFDM Applications," in Journal of Multidisciplinary Engineering Science and Technology (JMEST), vol. 4, issue 9, 2017, pp. 8217-8221.

5. **B. A. Mohammed**, N. A. Abduljabbar, A. S. Hussaini, R. A. Abd-Alhameed, S.M.R. Jones, B. A. L. Gwandu and J. Rodriguez, "A Si-LDMOS Doherty Power Amplifier for 2.620-2.690 GHz Applications," *Advanced Science Letters,* vol. 23, pp. 3874-3878, May, 2017.

Conferences and Workshops:

1. **B. A. Mohammed**, R. A. Abd-Alhameed, N. A. Abduljabbar, I. M. Danjuma, I. T. E. Elfergani, A. S. Hussaini and J. Rodriguez, "A CAD-Oriented Technique to Design an Optimum Load Impedance with Multi-coupler Network for Class-F Power Amplifier," in Loughborough Antenna and Propagation Conference (LAPC-2017), IET, IEEE, 2018.

2. **B. A. Mohammed**, A. S. Hussaini, H. Migdadi, R. A. Abd-Alhameed, N. A. Abduljabbar, I.T. E. Elfergani, J. Rodriguez, C. Nche, M. Fonkam, and B. M. Mustapha, "A 2.62-GHz Class-F Power Amplifier with Lumped-Element and Transmission Line Network Design," in *Internet Technologies and Applications (ITA), IEEE*, 2017, Wales, UK, pp. 275-279.

3. **B. A. Mohammed**, A. S. Hussaini, R. A. Abd-Alhameed, N. A. Aduljabbar, H. A. Obeidat, I.T. E. Elfergani, J. Rodriguez, C. Nche, M. Fonkam, and B. M. Mustapha, "A Load-Pull Approach to Design an Optimum Load Impedance and Matching Network for Class-F RF Power Amplifier," in *Internet*

Technologies and Applications (ITA), IEEE, 2017, Wales, UK, pp. 280-283.

4. **B. A. Mohammed**, N. A. Abduljabbar, M. A. G. Al-Sadoon, K. Hameed, A. S. Hussaini, S. M. R. Jones, F. El-megri, R. W. Clark and R. A. Abd-Alhameed, “A 15.5W Si-LDMOS Balanced Power Amplifier With 53% Ultimate PAE for Applications,” 8th EAI International Conference on Wireless and Satellite Systems (WiSATS), Cardiff, Great Britain, September, 9-20, 2016, pp. 193-201.

5. **B. A. Mohammed**, N. A. Abduljabbar, R. A. Abd-Alhameed, A. S. Hussaini, C. Nche, M.Fonkam, I.T. E. Elfergani, J. Rodriguez, E. A. Abdulmula, and E. Elkazmi, "Towards a Green Energy RF Power Amplifier for LTE Applications," in *Internet Technologies and Applications (ITA), IEEE*, Nov, 2015, Wales, UK, pp. 388-392.

6. **B. A. Mohammed**, R. A. Abd-Alhameed, K. O. O. Anoh, R. Asif and T. Sadeghpour, “Energy Efficient Power Amplifier Design over Nonlinear Crosstalk of MISO Wireless MAN-OFDM Transceiver,” Festival of Radio Science (URSI), Manchester, UK, December 2014.

Book Chapters:

1. J. Rodriguez, R. A. Abd-Alhameed, Issa Elfergani, A. S. Hussaini, **B. A. Mohammed**, “Fundamentals of 5G Mobile Networks,” Wiley, 2015,

Co-authored Journals:

1. I. M. Danjuma, **B. A. Mohammed**, N. N. Eya, G. A. Oguntala, H. A. Obeidat, R. A. Abd-Alhameed and J. M. Noras, "Design of a Taper Slot Low Profile Vivaldi Antenna for Ultra-Wideband Microwave Breast Imaging Applications,"in Journal of Multidisciplinary Engineering Science and Technology (JMEST), vol. 7, issue 5, 2018, pp. 32-37.

2. I. M. Danjuma, F. Abdulssalam, **B. A. Mohammed**, E. N. Eya, R. A. Abd-Alhameed and J. M. Noras, "Microwave Imaging Using Arrays of Vivaldi Antenna for Breast Cancer Applications," in Journal of Multidisciplinary Engineering Science and Technology (JMEST), vol. 4, issue 8, 2017, pp. 7972-7976.

3. Y. I. Abdulraheem, A. S. Abdullah, H. J. Mohammed, **B. A. Mohammed** and R. A. Abd-Alhameed, “Design of Radiation Pattern-Reconfigurable 60-GHz Antenna for 5G Applications,” Journal of Telecommunications, ISNN 2042-8839, vol. 27, Issue 2, 2014.

Co-authored Conferences:

1. I. Ahmad, R. Asif, R. A. Abd-Alhameed, H. Alhassan, F. Elmegri, J. M. Noras, C. H. See, H. Obidat, W. Shuaieb, J. C. Riberio, K. Hameed, A. Al-abdullah,

A. Ali, M. Bin melha, M. Al-Khambashi, H. Migdadi, M. B. Child, M. A. G. Al-Sadoon, F. M. Abdussalam, I. M. Dunjuma, A. Saleh, G. Oguntala, N. N. Eya, **B. A. Mohammed**, N. Abduljabbar, G. T. A. El Sanousi, J. Kosha, S. J. Shepherd, A. Mirza, S. M. R. Jones, I. T. E. Elfergani, J Roderguez, A. S. Hussaini, R. Qahwaji, P. S. Excell, and N. J. McEwan, in "Current Technologies and Location Based Services," Proceedings of the Seventh International Conference on Internet Technologies and Applications (ITA 17), Fifth EERT Workshop, EERT Wrexham Glyndŵr University, North Wales, UK, 2017, pp. 299-304.

2. N. A. Abduljabbar, **B. A. Mohammed**, R. A. Abd-Alhameed, Y. Fun Hu and Costa Kyriacou, "Optimization-Based Class-F Power Amplifier for GSM Systems," Meet the industry International Conference, Bradford, UK, 13 April, 2016.

3. N. A. Abduljabbar, **B. A. Mohammed**, R. A. Abd-Alhameed, C. H. See, K. M. Younus, A. T. Younis and A. A. Ismail, "A 850-MHz Class-F Power Amplifier for GSM Systems," Festival of Radio Science (URSI), Manchester, UK, December 2015.

4. A. Abduljabbar, **B. A. Mohammed**, R. A. Abd-Alhameed, M. A. Bomhara, A. A. Jasim A. T. Younis and A. A. Ismail, "Optimum Design of Class-F Power Amplifier for GSM Systems," Festival of Radio Science (URSI), Manchester, UK, December 2015.

5. A. A. Ismail, A. T. Younis, N. A Abduljabbar, **B. A. Mohammed** and R. A. Abd-Alhameed,"A 2.45-GHz Class-F Power Amplifier for CDMA Systems," in *Internet Technologies and Applications (ITA), IEEE*, Nov, 2015, Wales, UK, pp. 428-433.

6. K. O. O. Anoh, R. A. Abd-Alhameed, **B. A. Mohammed** and S. M. R. Jones, "A Modification of MATLAB Based DWT-Algorithm for Digital Signal Processing," Festival of Radio Science (URSI), Manchester, UK, December 2014.

EAI Endorsed Transactions
On Creative Technologies
Research Article EAI.EU

Towards a 15.5W Si-LDMOS Energy Efficient Balanced RF Power Amplifier for 5G-LTE Multi-carrier Applications

B. A. Mohammed[1,2,*], A. S. Hussaini[4,5], R. A. Abd-Alhameed[1,3], I. M. Danjuma[1], A. S. Asharaa[1], I. T. E. Elfergani[5], and J. Rodriguez[5,6]

[1]School of Engineering, Design and Technology, University of Bradford, Bradford, BD7 1DP, UK
[2]National Space Research and Development Agency, Abuja, Nigeria
[3]Depart. of Communication and Informatics Eng., Basra University College of Science and Technology, Basra 61004, Iraq
[4]School of Information Technology and Computing, American University Yola, Adamawa, Nigeria
[5]Instituto de Telecomunicacoes, Aveiro, Portugal
[6]University of South Wales, UK

Abstract

In this paper, a 15.5W Si-LDMOS balanced RF power amplifier has been designed using 2.620-2.690GHz frequency band to improve efficiency and linearity for 5G-LTE mobile applications. The amplifier was designed and simulated using large signal Si-LDMOS transistor model to achieve 53% PAE, 41dBm P_{out}, 14 dB gain at P_{1dB} saturation point. The proposed balanced RF power amplifier was fabricated and measurement results for phase variation of the signal between the carriers have been the main focus. At 1dB compression point power added efficiency increased to 81.5% with 19.5 gain at the P_{out}. The AM-AM and AM-PM measured data of the balanced RF power amplifier was extracted from the MATLAB fitting tool to produce polynomials. The polynomials were used in the proposed pre-distortion technique to compensate for the nonlinearities of the balanced power amplifier. A simple linear model was designed for behavioural modelling of the memory-less baseband digital pre-distorter. A Simulink IEEE 802.11a OFDM Transceiver system was used to demonstrate validity of the proposed pre-distorter. To the best of authors' knowledge, this study presented excellent results of pre-distortion system that compensated the nonlinearity behaviour of the balanced RF power amplifier using the Simulink version R2011a.

Keywords: Balanced Power Amplifier (BPA); Linearity; Power Added Efficiency (PAE); Long Term Evolution (LTE); Digital Pre-distortion (DPD).

Received on 08 December 2017, accepted on 05 April 2018, published on 10 April 2018

Copyright © 2018 B. A. Mohammed *et al.*, licensed to EAI. This is an open-access article distributed under the terms of the Creative Commons Attribution licence (http://creativecommons.org/licenses/by/3.0/), which permits unlimited use, distribution and reproduction in any medium so long as the original work is properly cited.

doi: 10.4108/eai.10-4-2018.155858

1. Introduction

In modern communication systems, frequency division multiplexing (OFDM) transceiver systems, such as long-term evolution (LTE), wideband code division multiple access (WCDMA), IEEE 802.11a OFDM Transceiver system and numerous IEEE wireless communication systems that adopt highly-efficient modulation schemes to enhance the spectral efficiency and increase multiple spectral user channels for more wide range of data and voice services [1, 2]. These systems are highly sensitive to nonlinear distortion effects in the transmission path, due to their non-constant envelope. Such systems produce high peak-to-average-power-ratio (PAPR). Therefore, the source of the nonlinear distortion effects of the transceiver configuration is associated with the RF power amplifier and this research focuses on the design and modelling of highly energy efficient balanced RF power amplifier with high linearity [1-3].

*Corresponding author. Email: m.b.abubakar1@student.bradford.ac.uk

RF power amplifier is an important device not only in wireless communication systems but also in TV transmission, radar systems and RF heating with the amplitude of radio frequency signal increase to high value [4, 5]. Spectral efficiency and linearity are the main elements deriving the design of power amplifier. The most challenging aspect of power amplifier concept is achieving excellent efficiency with linearity [6]. Though, the design of power amplifier has to be accomplished in accordance to the system specifications, such as operating frequency, bandwidth, output power, gain, linearity, efficiency and return loss [7]. According to [8, 9], linearity is required to sustain information for error-free transmission. Efficiency reduces power consumption and improves battery lifespan at the mobile station [5, 10].

The effect of spectral re-growth in power amplifiers has become a major concern in communication systems engineering [11]. This phenomenon causes the apparent presence of nonlinearities in the frequency band which leads to transmission power loss and adjacent channel interference [3]. To reduce the effect of nonlinearity and achieve state-of-the-art system, a power amplifier must be designed carefully to increase high data rate and spectral efficiency for high-speed broadband services. The optimization of these technologies produces higher data rate and higher spectral efficiency from 20MHz signal bandwidth, with a downlink data rates of 100Mbps, and an uplink rate of 50Mbps is obtainable [5, 12].

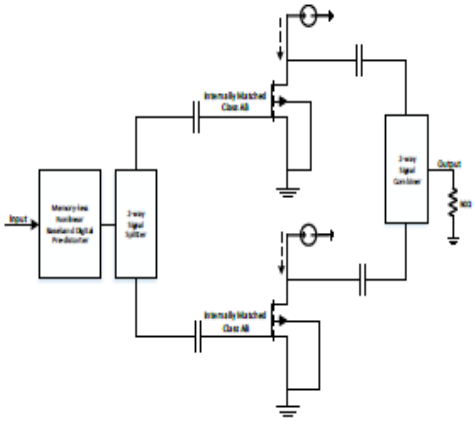

Figure 1. Balanced RF power amplifier architecture

This work discusses the design of a balanced RF power amplifier. The amplitude-to-amplitude and amplitude-to-phase characteristics (AM-AM/AM-PM) of the amplifier used in the modelling of nonlinearities of wireless metropolitan area network IEEE 802.11a OFDM transceiver using Simulink version R2011a configuration is presented. The aim of this study is to design and implement a 5G power amplifier that can have increase in power added efficiency and respond to high linearity. This is in view of the demand to reduce power amplifier energy consumption and the need for increase in battery life span. The objectives of this study is to design the proposed balanced RF power amplifier and implement the prototype. The design simulation and prototype measurement will be performed and compare. Amplitude and phase raw data of the proposed balanced amplifier will be extracted and converted to polynomial for linearization. A pre-distortion technique is proposed for cancellation of the proposed balanced RF power amplifier. Section 2 presents Power Amplifier Linearity, Efficiency and Output Power Requirement. The subsection 2.1 explains the Trade-off between linearity and efficiency. Section 3 describes in detail the circuit design architecture of the balanced RF power amplifier and the proposed system, while 3.1 discusses the circuit analysis of balanced RF power amplifier. Section 4 explains the design and simulation of a balanced RF power amplifier, while 4.1 presents simulation results and discussion. The design was implemented. A prototype for the balanced RF power amplifier has been shown. AM-AM and AM-PM measurement was conducted and is presented in section 4.1 respectively. Section 6 discusses the Linearization of balanced RF power amplifier Using Adaptive DPD. The section also covers the extraction and modelling of AM-AM and AM-PM polynomials in the pre-distorter. The work based on results from simulations and measurements discusses a potential technique to improve the efficiency in wide range linearity. Finally, the paper is concluded with the discussion in Section 7.

2. Power Amplifier Linearity, Efficiency and Output Power Requirement

The 5G-LTE multicarrier systems require a more linear radio frequency amplification and higher efficiency. A balanced power amplifier is employed to provide a multicarrier signal, while putting linearity, efficiency and output power into consideration. The IEEE 802.11a standard for information technology and wireless communication systems have not identify the minimum requirement for the power amplifier intermodulation distortion. However, stated the maximum allowable intermodulation distortion in the system level requirement. These include the adjacent channel power ratio (ACPR), error vector magnitude (EVM) and envelope spectral mask (ESM).

The ACPR is the ratio between the total power transferred to the main channel and the signal power transferred to the adjacent channel. The multicarrier transmitter signal passing through the power amplifier is characterized using a complex RF band. The RF band is overwhelmed by the RF PA nonlinearity called spectral regrowth. This type of power amplifier nonlinearity is measured using the adjacent channel power ratio. There are two ways in which ACPR is measured. The first way is by defining 10*log of the ratio of the total p_{out} to the adjacent channel power expressed by.

$$ACPR_{dBc} = P_{im3} + 10\log\left[\frac{C^3}{A+B}\right] \qquad (1)$$

where P_{in}^3 is the third order intermodulation distortion, C is the number of carriers or the main channel, A is the upper adjacent channel and B is the lower adjacent channel. The measurement of the total output power and the adjacent channel power are calculated in logarithmic ratio. The second is based on the ratio of the specific output power in a less significant bandwidth around the centre of the carrier to the adjacent channel power. The smaller bandwidth is equal to the bandwidth of the adjacent channel signal, having an equivalent bandwidth of the main channel. The spectral mask is identified by the IEEE 802.11a standard as a metric for passing or failing signal at the output of the power amplifier [13]. The spectral mask provides facts about the dispersal of the modulated channel spectral energy. The test is through if the RF spectrum is within the stipulated limit defined by the mask, while the test fails if the energy level is not beyond the mask limit.

The error vector magnitude (EVM) also estimates the properties of deficiency in the communication system constellation. The error vector *(E(c))* is the variation between the actual transmitted constellation point *(AT(c))* and the ideal constellation point *(I(c))*. The error vector magnitude (EVM) can be expressed in RMS form by.

$$EVM_{rms} = \sqrt{\frac{\frac{1}{N}\sum_{c=1}^{N}|E(c)|^2}{\frac{1}{N}\sum_{c=1}^{N}|I(c)|^2}}. \quad (2)$$

where N is the total number of constellation points defining the level of modulation. The N is used for EVM calculation. $I(c)$ is the c^{th} number of normalised constellation points and $E(c)$ can be expressed by.

$$E(c)=x(c)-y(c). \quad (3)$$

where $x(c)$ is the measured normalised symbol. The rms value of the error vector magnitude is calculated by taking the average value of all the frames. In the measurement, it is recommended by the IEEE 802.11a for WLAN standard to take a large number of transmitted frames of at least 20 frames [13]. The computation of error vector magnitude for the IEEE 802.11a, WLAN standard is expressed in [13] by.

$$EVM_{rms} = \frac{\sum_{a=1}^{N_f}\left(\sqrt{\frac{\sum_{v=1}^{L_p}(\sum_{n=1}^{52}\{(I-I_0)^2+(Q-Q_0)^2\})}{52L_p\cdot P_a}}\right)}{N_f} \quad (4)$$

let I, I_0, Q and Q_0 sequentially be expressed as: $[I(a,v,n), I_0(a,v,n), Q(a,v,n)$ and $Q_0(a,v,n)]$, where N_f is the frame number, L_p is the packet data length, P_a is the average power of the constellation diagram and n is the OFDM symbol subcarrier. EVM can also be achieved in percentage by using the rms value. In the system level, it is very important figure of merit to evaluate the precision of the OFDM signal. The $EVM_{\%}$ can be expressed by.

$$EVM_{\%} = \frac{\sqrt{\frac{1}{N}\sum_{a=0}^{N_r-1}I_{er}(a)^2+Q_{er}(a)^2}}{N_r}\times 100\%. \quad (5)$$

where N is the number of symbols, N_r is the normalized reference of the EVM, a is the symbol index, while

$$I_{error} = I_{reference} - I_{measured}$$

$$Q_{error} = Q_{reference} - Q_{measured}$$

The EVM can as well be measured in decibel (dB) as expressed below.

$$EVM_{dB} = 10\log_{10}\left[\frac{P_{error}}{P_{reference}}\right]. \quad (6)$$

Where P_{error} stands for the error vector power, and $P_{reference}$ is the reference constellation point power for both single and multiple carrier modulation. It is the average power of the reference constellation. In the IEEE 802.11 standard for LTE, the adjacent channel power ratio (ACPR), envelope spectral mask (ESM) and error vector magnitude (EVM) are demanding as expressed in the existing standard.

2.1. The trade-off between Linearity and Efficiency

The aim of realizing energy efficient power amplifier with excellent linearity is to have a system with high efficiency over a magnificent range of input power. The most challenging task in RF power amplifier design is to obtain high efficiency with a wide range of linearity [14, 15]. However, achieving high efficiency with a wide range of linearity at the same time is a difficult task, except with advent of linearization and efficiency enhancement approaches. At low-level output power, high efficiency can be achieved if the efficiency enhancement method in the linear operation region of RF power amplifier is adopted. Maximum efficiency can, however, be realised once the output power of RF power amplifier reaches almost the maximum saturation level, which is the 1dB compression point. This leads to serious intermodulation distortion where efficiency drastically decreases with the decrease in output power.

However, the RF power amplifier must be in linear mode at the whole dynamic range of time to maintain the level of efficiency. The peak power range can escalate to 8-10dB output power back-off. This is applicable for cascade amplifiers. It is a significant challenge for traditional single-stage RF power amplifier due to the effect of the peak-to-average-power ratio (PAPR) that operates on high output power back-off. RF power amplifiers operating on lager

output power back-off end off with a very low efficiency. A study in [12] has shown that low efficiency must be reduced to conform to the standard or will otherwise affect the operation of other applications.

However, RF power amplifier design has continued to be a challenging task when trying to satisfy this linearity-efficiency and power requirement trade-off. Previous studies have shown that there is no breakthrough in the trade-off. To optimise linearity-efficiency trade-off, more investigation is required on various power amplifier architectures.

3. Balanced RF Power Amplifier Circuit Design Architecture

Figure 1 has shown the balanced RF power amplifier architecture. The balanced power amplifier is a cascaded system with two transistor device opposite to each other. The two amplifiers share the same input and output. They have parallel output power capability, but different in the biasing circuit. The two amplifiers are operating in class-AB with the first one in first carrier stage and the second one in second carrier stage respectively. At this point, the first carrier stage is referred to the first amplifier, while the second carrier stage refers to the second amplifier. The signal from the input is divided equally using a 3dB signal splitter. The splitter is designed with 90^0 phase difference and same amplitude, to drive the two cascaded class-AB amplifiers. The output of both amplifiers are connected to a combiner which collects the amplifiers signals to the final stage of amplification [16, 17].

The balanced RF power amplifier attains high efficiency as a result of output power back-off over the traditional single stage amplifier. Hence, the multicarrier applications are affected by nonlinear distortion due to peak to average power ratio (PAPR), which the efficiency of the power amplifier can be enhanced by the used of efficiency enhancement and linearization techniques.

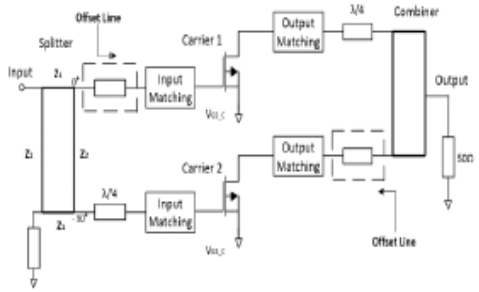

Figure 2. Proposed schematic diagram of the balanced RF power amplifier with offset lines

Figure 2 has shown a proposed balanced RF power amplifier with two amplifiers parallel to each other having equal output power capability. The two amplifiers have the same bias point which means they are both carrier amplifier stage operating in class AB mode. The phase difference between the two amplifiers is 90^0 phase shift. A special signal splitter was separately designed for the input. A coupler was also designed for the output. Independent measurements were taken in term of operational bandwidth and frequency response for both the splitter and the output coupler. In the design, no mode was chosen to behave as the carrier amplifier. Both class-AB modes operate at the same time and capable of improving the efficiency. Resonator circuits are applied to the input of the first carrier and output of the second carrier. These acts as the summing circuits which act as a phase difference signal compensator. The circuits constructively supplement the signal from the two amplifiers to the output load. The quarter-wave transmission line similarly applied to the input of the second carrier and the output of the first carrier. According to the study, the proposed balanced RF power amplifier design complexity increases and equally improve the efficiency with a wide range of linearity which will be discussed in the next section.

3.1. Balanced Power Amplifier Circuit Analysis

This section derives and demonstrates the equation that runs the relationship between input current (I_{in}) and input voltage (V_{in}) to the output current (I_{out}) and output voltage (V_{out}) in the transmission line, showing how the frequency dependent impedance of the material present the attenuation and distortion of the high-frequency signal as expressed in matrix form [14, 18].

$$\begin{bmatrix} V_{in} \\ I_{in} \end{bmatrix} = \begin{bmatrix} \cosh \pi/2 & z_o \sinh \pi/2 \\ 1/z_o \sinh \pi/2 & \cosh \pi/2 \end{bmatrix} \begin{bmatrix} V_{out} \\ I_{out} \end{bmatrix} \quad (7)$$

The source impedance $Z_{in} = V_{in}/I_{in}$, Z_o is the characteristic impedance of the transmission line, while Z_L is the load impedance given as $Z_L = V_{out}/I_{out}$. Hence, the source impedance Z_{in} can be expressed by.

$$Z_{in} = \frac{Z_L \cos \pi/2 + jZ_o \sin \pi/2}{j(Z_L/Z_o)\sin \pi/2 + \cos \pi/2}. \quad (8)$$

From the wave equation to the relationship between voltage and current, quarter wave transmission line source Z_{in} can be defined by.

$$Z_{in} = \frac{V(-l)}{I(-l)} = Z_o \left[\frac{V_o^+ (e^{j\beta} + \Pi e^{-j\beta})}{V_o^+ (e^{j\beta} - \Pi e^{-j\beta})} \right]. \quad (9)$$

This can be expressed by the impedance function in by expanding the (9) while giving a common source impedance for both voltage and current.

$$Z_{in} = Z_o \left[\frac{\left[e^{j\beta l} + \left(\frac{Z_L - Z_o}{Z_L + Z_o} \right) e^{-j\beta l} \right]}{e^{j\beta l} - \left(\frac{Z_L - Z_o}{Z_L + Z_o} \right) e^{-j\beta l}} \right]. \quad (10)$$

This equation can be expanded by.

$$Z_{in} = Z_o \left[\frac{Z_L \left(e^{j\beta l} + e^{-j\beta l} \right) + Z_o \left(e^{j\beta l} - e^{-j\beta l} \right)}{Z_o \left(e^{j\beta l} + e^{-j\beta l} \right) + Z_o \left(e^{j\beta l} - e^{-j\beta l} \right)} \right]. \quad (11)$$

and this can be extended in sine waveform by.

$$Z_{in} = Z_o \left[\frac{Z_L (\cos \beta l) + j Z_o (\sin \beta l)}{Z_o (\cos \beta l) + Z_L (\sin \beta l)} \right]. \quad (12)$$

Finally, the impedance Z_{in}, looking into the transmission line is given by.

$$Z_{in} = Z_o \left[\frac{Z_L + j Z_o \tan(\beta l)}{Z_o + j Z_L \tan(\beta l)} \right]. \quad (13)$$

The two-stage balanced RF power amplifier is shown in figure 2 with the quarter wavelength at the output of the first carrier and the input of the second carrier amplifier respectively. These act as the basis for the impedance to stay low when the two carriers are on the active stage.

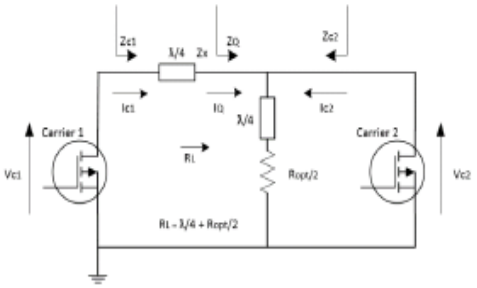

Figure 3. Current and voltage analysis diagram for balanced power amplifier

Figure 3 shows a balanced RF power amplifier analysis diagram which will be used for the current and voltage analysis. The phase output current of the first carrier (I_{c1}) leads the phase output current of the second carrier (I_{c2}) by 90^0. This implies that the phase difference of the splitter is separating the two amplifiers by 90^0 phase shift. Nevertheless, the operating principle of the balanced amplifier two-stage load modulation can be derived by splitting the level of input signal to high-level drive. In this mode, first carrier (I_{c1}) and second carrier (I_{c2}) are set to be turned on and there will be current flow through the circuit. When the balanced amplifier is in ON state, the current envelope can be expressed by.

$$I_{c1} = \frac{I_{max}}{3}(1 + x). \quad (14)$$

$$I_{c2} = \frac{I_{max}}{3}(x + 1). \quad (15)$$

At high-level drive, the x component will have a value of 1, where the two carrier amplifiers will turn on. The effective impedance (Z_Q) will have to pull influence on both carriers at the load as expressed below.

$$Z_Q = R_L \left[1 + \frac{I_{c2}}{I_Q} \right]. \quad (16)$$

and

$$Z_{c2} = R_L \left[1 + \frac{I_Q}{I_{c1}} \right]. \quad (17)$$

where the resistive impedance of the quarter wavelength increases, the two carrier amplifiers acts as load modulation. The quarter wavelength transmission line input, output transformation and the characteristic impedance can be expressed by.

$$Z_{c1} = \frac{Z_x^2}{Z_Q}. \quad (18)$$

The output impedance can be substituted to the effective impedance (Z_Q) and can be seen by both amplifiers. The output impedance is written as.

$$Z_{c1} = \frac{Z_x^2}{\left[R_L \left(1 + \frac{I_{c2}}{I_Q} \right) \right]}. \quad (19)$$

The effective output voltage (V_{c1}) of first carrier amplifier is expressed by.

$$V_{c1} = Z_{c1} \times I_{c1} = I_{c1} \times \left[\frac{Z_x^2}{R_L \left(1 + \frac{I_{c2}}{I_Q} \right)} \right]. \quad (20)$$

Since $I_Q = V_{c1}/Z_x$ then output voltage becomes.

$$V_{c1} = \frac{I_{c1} \times Z_x^2}{R_L\left(1 + \frac{I_{c2} \times Z_x}{V_{c1}}\right)}. \quad (21)$$

I_{c1} *and* I_{c2} have been substituted into Z_{c1} to become.

$$V_{c1} = \left(\frac{Z_x}{2R_L}\right)\left(I_{max}\right)\left(Z_x(1+x)\right) - 2R_L x^2 + R_L x. \quad (22)$$

But $R_L = R_{opt}/2$. Hence the output voltage will be.

$$V_{c1} = \left(\frac{Z_x}{R_{opt}}\right) \left(I_{max}\right)\left(Z_x(1+x) - 2\frac{R_{opt}}{2}x^2 + \frac{R_{opt}}{2}x\right). \quad (23)$$

Then $Z_x = R_{opt}$

$$V_{c1} = R_{opt} + I_{max}\left(-x^2 + \frac{x}{2}\right). \quad (24)$$

Finally, the mathematical illustration has shown that the output voltage maintains the stability at a high stage when the two carriers remain in the active stage. The output voltage increases negligibly.

4. BPA Design and Simulation

The balanced RF power amplifier has been designed and discussed in this paper, using two transistor models for high data rate, providing efficiency with a dynamic range of linearity. Dynamic load adaptation is conveyed by the use of transmission line impedance inverter of 50Ω quarter wavelength. In the design of this amplifier, there are stages that are followed to achieve high-level performance [19, 20]. The first stage of the design is DC circuit design and simulation. Simulation of the DC circuit determines the bias point and bias network. This is in accordance with the class of operation and power requirement. The bias condition set drain-source voltage (Vds) = 28V, drain-source current (Ids) = 422mA and gate-source voltage (Vgs) = 2.7V. The bias network is designed based on class-AB carrier. The DC simulation results also indicate the class of operation. The main purpose of good biasing is to prevent signal reflection. The DC quiescent current is obtained to prevent signal distortion [5]. The radio frequency signal is prevented from going back to the DC source. For the matching network, this transistor requires no matching process, as indicated in the datasheet of the component, input and output impedance are internally matched. The 21mm length of microstrip line are connected using line-calc from Agilent advanced design system simulator (ADS) with RT 5880 substrates, parameters; Er = 2.2, H = 0.508mm, zo = ohms, T = 3um and TanD = 0.017. The 50Ω impedance of 90^0 open and a short circuit is incorporated to the right angle of the RF blocking transmission lines. A class-AB power amplifier element values have been positioned using tune tool of the ADS simulator for best performance of the proposed system.

Linear and nonlinear simulation was performed for class-AB design. The design and simulation process for class-AB amplifier is necessary in order to prepare the single stage class-AB design into a multiple stage balanced power amplifier. The linear simulation has shown a good flat gain, where the S_{11} is almost 14dB, the return loss, S_{11} and S_{22} are also satisfactory. The nonlinear single tone simulation result of class-AB amplifier was achieved. However, it also produced up to 29% PAE at 39dBm P_{1dB}. A 3dB 2-ways 90^0 hybrid splitter was designed using 100Ω impedance for optimum matching. This is to achieve 90^0 phase difference between the first carrier class-AB and the second carrier class-AB amplifier. For a two-stage balanced PA, the first carrier and second carrier bias points are in the same mode, the input-output matching circuitry and the output impedances are similar as well. For the two-way splitter, various simulation tests were performed such as isolation response over the operating bandwidth, phase difference across port 1-2 and 1-3, and insertion loss response of the splitter [3]. From the 3dB splitter, the insertion loss achieved is reasonably low due to the high return loss, the phase difference of two signals are parallel to each other by 100Ω, which means they are separated by 90^0 and have equal magnitude, and the isolation between 2 and 3, which results to -48.56dB at 2.655GHz centre frequency. Consequently, these results represent a response to protect the amplifier with all the instruments connected to it and allow measurement with reasonable accuracy. At the output of the two-stage amplifier is a combiner coupling the first carrier and second carrier amplifiers signal to the output of the balanced amplifier [3, 21].

Table 1: Performance comparison with selected work based on power amplifiers

Device	Freq [MHz]	PAE [%]	P_{out} [dBm]	Gain [dB]	Reference
LDMOS	2655	51	41	14.6	Balanced
LDMOS	2655	29	39	15	Class-AB
LDMOS	2140	54	48.77	30	[4]
GHEMT	2655	37.14	41.18	12.78	[10]
GHEMT	2125	33.4	34.9	7.7	[11]
GHEMT	2500	48	46	13.4	[13]
LDMOS	1900	50	40	14.5	[14]

Table 1 shows the performance of the current work compared a few selected PA's reported in the literature, taking account of operating frequency, output power, efficiency and gain. In [4] a power amplifier consist of up to 54% PAE at 2.14GHz

operating frequency is presented. The design presented a two-stage line-up of Doherty amplifiers, consisting of a High Voltage HBT Doherty final design cascaded with a 20W LDMOS Doherty driver, exhibiting up to 325W (55dBm) power to improve the gain to 30dB. In the case of [10] a high power hybrid envelope elimination and restoration transmitter were designed using gallium arsenide high electron mobility transistor (GaN-HEMT) at 2.655GHz operating frequency. The design introduced a conventional hybrid switching amplifier with up to 71.2% PAE. However, the efficiency of H-EER transmitter reduced to 37.04% at 41.18dBm P_{out}. In [11] a conventional balanced amplifier with 90° branch line hybrid coupler (BLHC) was used to achieve power matching rather than maximum high gain. The impedance matching is not excellent and there is inherent out-of-phase characteristic cause from the properties of 90^0 BLHC. To improve the performance and correct the high signal reflection, an auxiliary amplifier was added to the conventional balanced amplifier design, only to increase the PAE to 33.4%. The design for [22] used up to 250W output power at saturation to achieve 60% drain efficiency. The final 40W GaN-HEMT Doherty power amplifier design used a digital pre-distorter to enhance linearity, as a result, experienced a reduction in PAE to 48%. Finally, in [14] a 10W, Si-LDMOS transistor power amplifier was presented with 50% PAE, 14.5dB gain achieved at 41.8dBm saturation within 1.8 to 2.0GHz operating frequency. The drawback of [14] is that heat sink is used due to excessive heating produced by the amplifier, which extensively affects the general performance of the system.

However, the current work presents a simplified balanced amplifier using Si-LDMOS transistor, while achieving up to 53% PAE, 14dB gain at 41dBm P_{1dB}. This design is matched perfectly due to the internal input and output matching network in the transistor device. There is no evidence of leakage or signal reflection from the first stage of the design to the design of balanced amplifier. Another advantage of this design is for its simplicity, requires no auxiliary amplifier or additional cascade Doherty device to improve the efficiency. Additional circuit accounts for extra power consumption, but have negligible impact to the overall efficiency of the amplifier [3].

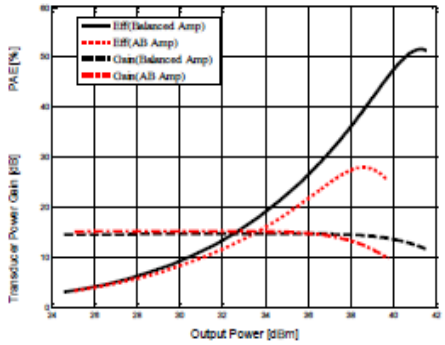

Figure 4. Simulated results of the proposed balanced RF power amplifier and conventional class AB showing PAE and gain characterization

4.1. Simulation Results and Discussion

The proposed balanced amplifier consisting of two similar class-AB amplifiers tested and simulation results are discussed. The results have shown the signal waveforms for best of performance and hence the best choice for LTE base station applications. Figure 4 shows the results of the balanced amplifier in comparison with the conventional class-AB amplifier. This indicates good performance from the balanced amplifier, achieving up to 53% PAE with 14dB gain at 41dBm P_{1dB}, as against the conventional class-AB amplifier with 29% PAE, 39dBm P_{out} and 15dB gain.

These results presented above is based on the linear simulation was conducted for the nonlinear simulation. The results obtained are the gain compression for 1dB compression point. The gain compression result is flat as expected, excellent input and output return loss was also achieved as shown in figure 4 The flat gain, S(2, 1) is almost 14 dB, the return loss, S(1, 1) and S(2, 2) was also achieved at 1 dB compression point. The results have shown quite a few kinds of signal waveforms to characterize the best of performance and the best choice for 2.620-2.690 GHz applications.

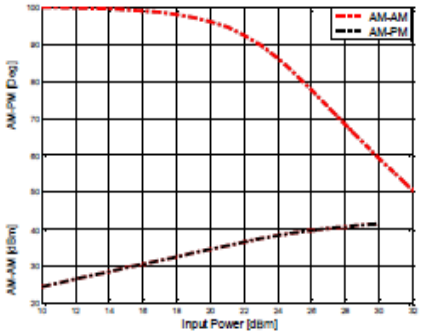

Figure 5. AM-AM and AM-PM characterization of the balanced RF power amplifier

In the one-tone nonlinear simulation test, the obtained AM-AM and AM-PM characterization parameters are shown in figure 5. These are very important parameters in the characterization of PA and demonstrate that AM-AM distortion appears in a nonlinear PA, while the AM-PM distortion appears in MOSFET PA's and produces memory effects.

5. Implementation of Balanced RF Power Amplifier

5.1. Circuit Design Layout

The balanced power amplifier was designed and implemented using ADS software with RF field effect Si-LDMOS 15.5W transistor at 2.620-2.690GHz frequency band. The final stage circuit of the amplifier is fabricated with RT 5880 substrates,

H=0.5mm and relative permittivity of 2.2. Figure 6 shows the layout of the balanced RF power amplifier. In order to experimentally verify the proposed power amplifier circuit topology, the agilent advanced design system generated microstrip layout was used. The layout was exported as Gerber files from ADS and it was milled on a printed circuit board known as PCB. Note that metal pads have been added in the layout as ground plane and power supply connection in the layout. Further, the amplifier has been subjected to following mechanical engineering:

- The length of the cooling ribs was cut to fit the card
- Holes for the transistor was milled out
- A total number of 44 screw holes were threaded into the board
- 4 for the transistors
- 36 for in and outsides of the board
- 4 for each SMA connectors

The screws were tried to be positioned so that they would have minimal impact on scattering field from the lines. At the same time, it was necessary to place multiple screws relatively close to the transistor in order to provide a good signal ground at this point. The same procedure was done with screws at each SMA connector. The components were fitted on the finished circuit board.

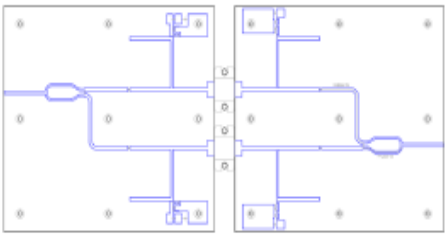

Figure 6. Design layout of balanced RF power amplifier

5.2. Circuit Prototype

The balanced RF power amplifier circuit is fabricated with RT 5880 substrates, H=0.5mm and relative permittivity of 2.2. The RT/duroid 5880 high-frequency laminate from Rogers Corporation is used. The substrate material is good for microstrip and strip-line applications. Because of the uniform dielectric constant over a wide range of frequency and the low dissipation factor of RT/duroid 5880, it extends its usefulness compared to FR-4 substrate in high-frequency Ku-band and above. The Line-Calc application from ADS is able to calculate the width and the length of microstrip line given the characteristics impedance and electrical distance or vice versa at 2.655GHz. Some important characteristics of RT/duroid 5880 such as dielectric constant, the height of board and conductivity are defined in ADS Line-Calc.

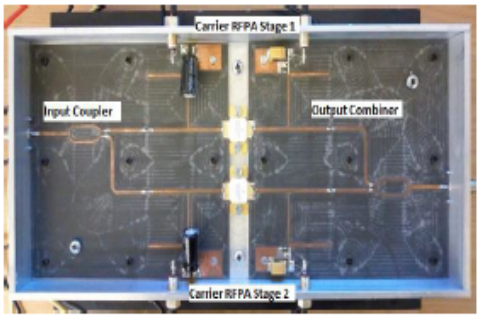

Figure 7. A prototype of the two-stage balanced RF power amplifier Fabricated with FR-4 substrate

While verifying the impedances in schematic and layout, the Gerber files are created from the layout and the circuit is milled on the RT/duroid 5880 board. During the RF operation, heat generation of the transistor would be one of the biggest problems causing performance degradation. Therefore, the transistor has to be mounted right on a heat sink in order to diffuse generated heat. In this project, a large piece of aluminium plate will be used as a heat sink and the skeleton to support the PA. The transistor is mounted on the aluminium plate with thermal paste glued in between in order to maximize heat transfer. The PA consists of two parts, the input board and the output board. SMA connectors are inserted at the input and output terminals. Banana plugs must be used for power connection as required by the competition rules. Vias are created by putting wire through drilled holes or inserting long copper tape through cut slits as connection bridges between the top and bottom ground planes. Vias should cover as much area as possible on the PA in order to provide the same reference level between the top and bottom ground planes. Components are then soldered on the board. 300pF capacitors are used as coupling capacitors at the input and output board. 1pF/1000pF/33pF capacitors are used as a decoupling capacitor in the gate bias. 1pF/1000pF/33pF/ capacitors are put in parallel and used as decoupling capacitors in drain bias.

5.3. Measurement

The design of the proposed balanced RF power amplifier circuit has undergone simulation test and measurement was performed on the fabricated circuit. The measurement result is focussed on the phase variation of the power amplifier using various frequency band to report the differences at some points. The measurement includes determining the linearity of the amplifier by means of looking at the power from the input to the power to the output and also discuss improvement achieved from the measured PAE.

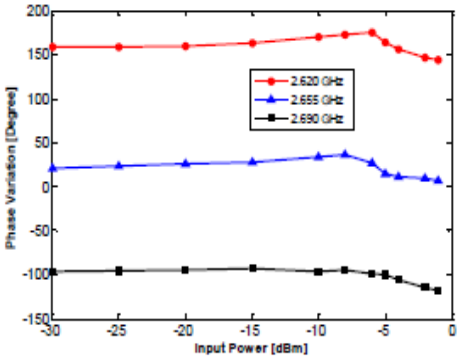

Figure 8. Phase variation of the proposed balanced RF power amplifier

Figure 8 shows the phase variation of the proposed balanced RF power amplifier which was derived as a function of the input power level. The result shows a range of frequency band used which is within the LTE mobile frequency level. The phases of the amplifier path are almost fixed along with bias condition throughout the range of the power used in the amplifier. There is no record of phase variation between the first carrier and second carrier in the low or high power region. The reason behind this development is because the balanced amplifier consists of same class-AB amplifiers in both carriers.

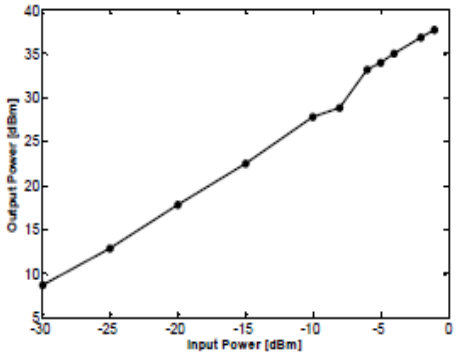

Figure 9. Output versus the input power of the balanced RF power amplifier

Nevertheless, the result shows power derive has increased at the output level when compared with that of input as the phase variation through both carriers path is almost close. It is anticipated a small drop at the full drive and both signals will look equal and disappear. The power that has been used between the input and the output of the amplifier is shown in figure 9. It represents the evaluation of the phase variation of the signal. And this clearly shows how much power has been derived through the amplifier. Up to 37dBm output power has been accomplished at the linear region of the proposed balanced RF power amplifier.

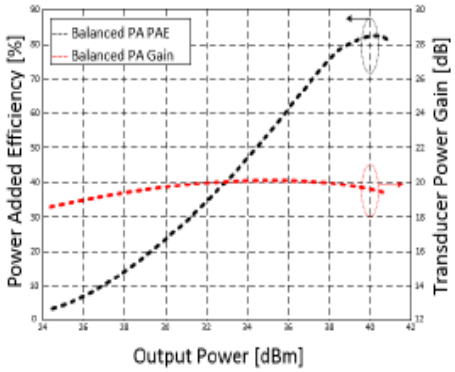

Figure 10. Measured results of the proposed balanced RF power amplifier with improved power added efficiency and gain

Figure 10 shows the performance of proposed balanced RF power amplifier through measured PAE and gain. The same frequency range of 2.620-2.690 GHz has been used for the simulation as well as the measurement. 1dB compression point of the amplifier was used to obtain up to 40dBm of the output power because of the two cascaded class-AB amplifiers working actively at the same time. However, the balanced amplifier output saturation power (P_{sat}) point reached up to 40.90dBm. The power added efficiency of the balanced amplifier at 40dBm and 40.90dBm were 83% and 81.5% respectively. While the gain of the amplifier reached up to 20dB which was reduced to 19.5dB before saturation point. Increase in gain and PAE improves the linearity of the amplifier. This is attributed to the input and output offset lines used in the design and fabrication. This performance shows that the design and fabrication of the proposed balanced RF power amplifier has achieved a substantial improvement in this class of power amplifiers.

6. Linearization of Balanced RF Power Amplifier Using Adaptive DPD

In this section, the balanced RF power amplifier was linearized using the AM-AM and AM-PM transfer functions to generate polynomials in the MATLAB. The extracted AM-AM and AM-PM data are measured in the context of the normalized input voltage as a function of the output voltage. The MATLAB curve fitting generated AM-AM polynomials is expressed as: $a_6 = 33.066$, $a_5 = -85.52$, $a_4 = 82.06$, $a_3 = -34.052$, $a_2 = 2.85$, $a_1 = 3.21$ and $a_0 = -0.01$. The AM-AM distortion is effected by the device reaching a saturation point. The normalized input voltage as a function of output phase of the balanced amplifier is also considered with the following AM-PM MATLAB fitted coefficients to generate polynomials expressed as: $b_6 = 3.5485$, $b_5 = -5.7836$, $b_4 = 3.0384$, $b_3 = -0.8434$, $b_2 = 0.1826$, $b_1 = -0.0225$ and $b_0 = 0.1001$. The AM-PM distortion is effected by the device reaching a saturation point. This data will be embedded in the device under test (DUT) of a simulink transceiver system

based on IEEE 802.11a OFDM HiperLAN/2 standard. The variations of AM-AM and AM-PM can be presented in (25) and (26), expressed by:

$$y(t) = a_5u^5 + a_4u^4 + a_3u^3 + a_2u^2 + a_1u + a_o \quad (25)$$

$$z(t) = b_5u^5 + b_4u^4 + b_3u^3 + bu^2 + b_1u + ab_o \quad (26)$$

Where y(t) and z(t) are the AM-AM and AM-PM responses of the balanced RF power amplifier [17].

Simple linear formulas are presented for the functions involved in the amplitude and phase nonlinear models of the balanced amplifier as shown in the above equations and fit measured data very well. This model is exported to the memory-less baseband digital pre-distorter to linearize the DUT at the front-end of the OFDM transceiver system. The multiple-input-single-output (MISO) transceiver system is set to run on a simple linear model with baseband digital pre-distortion to compensate for the nonlinearity of a balanced power amplifier. In the transmitter, the signal was coded before OFDM. The modulation was normalised as a frame where 16-QAM was chosen for the OFDM system. The signal handed over to OFDM was cyclic prefixed. The OFDM as complex signal can be seen in frequency domain. The OFDM transmitter passed the complex signal to the power amplifier in the form of real and imaginary. The signal from the power amplifier is fitted in order to achieve signal variation. The amplitude of the input voltage of the power amplifier is 3volts. After the amplifier, the signal was handed over to the channel. The noise added to the channel is the Additive White Gaussian Noise (AWGN). A magnitude in +ve and -ve polarities is used to re-organise the signal which remain exactly the same. Results have been produced to show the validity of the pre-distortion algorithms used in the process of transmitting OFDM signal through the proposed balanced RF power amplifier which the measured data was extracted for linearization [23].

The amplifier has been implemented on OFDM transceiver system. Most figures of merits demonstrated the existence of amplifier distortion in the signal without linearization and several results showing removal of distortion with the use of linearization technique. The transceiver has undergo several stages of simulation such as transmission without amplifier, adding RF amplifier to demonstrate the existence of distortion and introduction of linearization technique to remove the amplifier distortion.

In the first stage, OFDM signal was transmitted to the channel without amplifier. The signal is expected to be linear with no nonlinear distortion of all kinds. No amount of distortion demonstrated in all the results simulated, unlike when adding the power amplifier in the RF chain. In the case where balanced RF power amplifier is added to the RF front-end of the transmitter, performance results have shown different ways in which the distortion was described such as display of AM-AM, AM-PM, 16-QAM constellation, bandwidth spectrum signal and OFDM signal in time scope frame.

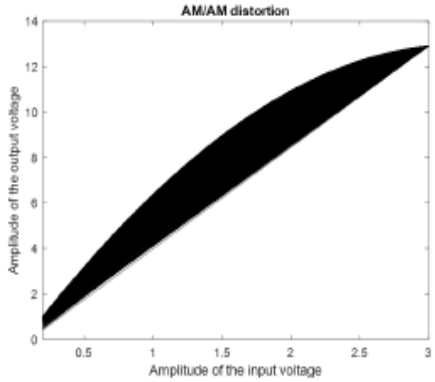

Figure 11. AM-AM distortion of the proposed balanced RF power amplifier

First of all, figure 11 and 12 depict results of AM-AM and AM-PM signal distortions of the proposed balanced RF power amplifier. The responses of the amplifier has shown clearly that the device under taste is without linearizer. The AM-AM characteristics are displayed with thousands of bits which errors were introduced because of the magnitude. Errors occurred due to variation of the magnitude. This also depends on the signal-to-noise-ratio (SNR). Hence, the errors can be reduced by increasing the level of SNR and controlling the magnitude.

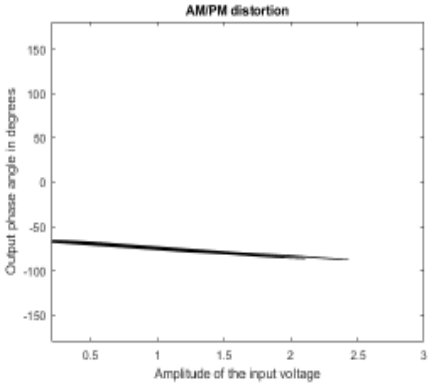

Figure 12. AM-PM distortion of the proposed balanced RF power amplifier

Figure 13 shows the transmitted signal before OFDM transmitter and received signal after AWGN channel. The signal constellations represent the coded 0-15 16-QAM modulation which at the transmit shows clean bits of signal without adding noise. The received signal is the signal after demodulation of the OFDM signal which can be seen as similar constellation to the transmitted signal constellation except the high distortion power amplifier which scattered the signal, at the same time affecting the magnitude and phase of the signal.

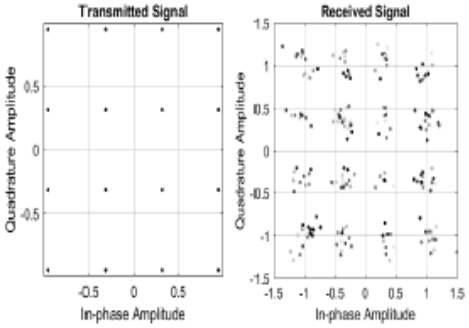

Figure 13. OFDM transmitted and received signal constellations without linearization

Figure 14 shows the spectrum analyser figure of merit describing the OFDM frequency domain signal before and after the channel. The bandwidth and the sampling frequency used in OFDM signal shown. It shows the bandwidth that has been utilised during the transmission.

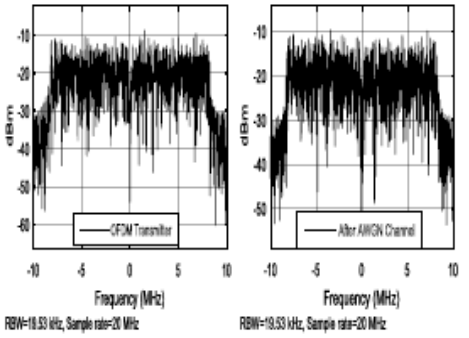

Figure 14. Spectrum signal illustrating the bandwidth

Figure 15 shows the time scope figure of merit demonstrating the OFDM complex signal in two forms which is before the power amplifier and after the AWGN channel. Each signal has been displayed with real and imaginary potion as shown below.

The first signal was obtained before the RF power amplifier and the second was after the channel. The noise added to the signal that passed through the amplifier introduced disturbance. Because of the distortion affecting the magnitude in the signal, the imaginary side of the signal after the channel is not following the imaginary side of the signal before the channel. Without distortion, the two signals are expected to demonstrate similarities. Even with increase in SNR will not make a major impact in the signal due to the distortion. This has been proven in the BER performance of the receiver side as shown in figure 22.

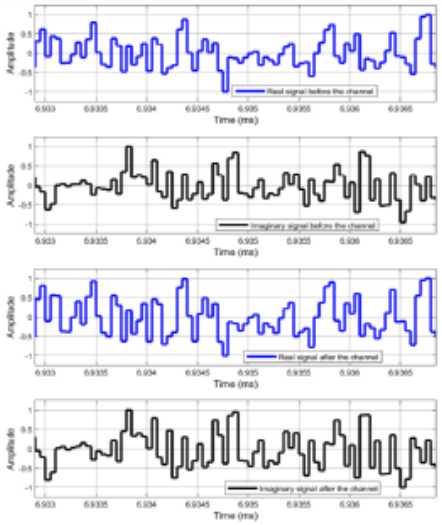

Figure 15. OFDM complex signal on time scope frame before linearization

The OFDM transceiver shows the BER performance of the signal received when the balanced RF power amplifier is used in the system. As shown in figure 22, the BER displayed number of bits received and the number of errors. Number of errors occurred base on amplifier distortion. However, change in SNR will change the configuration. This will affect the magnitude due to signal variation. This is to say the symbol is moving in and how to recover it is only by adapting the pre-distorter.

In the previous stage, OFDM signal was transmitted to the channel with our proposed balanced RF power amplifier where results were presented with distortions causing signal variation in the system. In the next stage, pre-distortion is introduced to linearize the nonlinearity of the RF power amplifier. In linearization, signal variation does not change the phase, but changing the magnitude and will stay where it is or on the same angle. This implies that the phase distortion is not existing in the signal. To analyse the pre-distortion, it is assume that the pre-distorter is added before the power amplifier, which means adding the phase on the signal to remove the amplitude. The pre-distorter and the power amplifier can be expressed mathematically as:

$$Pe^{J\phi} + Ae^{J\phi} = 0. \quad (27)$$

where $Pe^{J\phi}$ is the linearizer and $Ae^{J\phi}$ is the PA distortion. The expression can be rewritten as:

$$PA(e^{J\phi_P + J\phi_A}) = 0. \quad (28)$$

Then

$$\phi_P + \phi_A = 0. \quad (29)$$

To cancel the RFPA distortion, we can say that

$$\phi_P = -\phi_A. \tag{30}$$

From the equations above, to compensate for the nonlinearity of the balanced RF power amplifier, a pre-distorter is added to add to the angle of the input signal. However, performance results have shown different ways in which the distortion of the power amplifier was compensated.

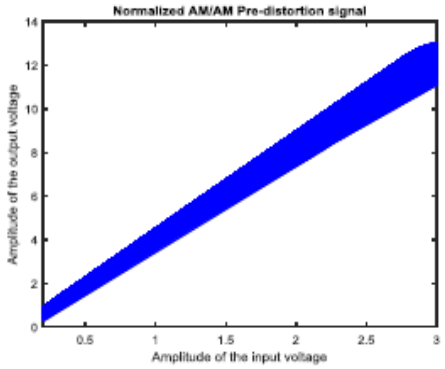

Figure 16. Normalized AM-AM balanced RF power amplifier pre-distorted signal

First result on linearizing the power amplifier is shown in figure 16. Figure 16 shows the normalized AM-AM response of the balanced RF power amplifier signal linearized using the pre-distortion technique. The responses of the amplifier has shown clearly that the device under taste was responding to linearization. The AM-AM characteristics are displayed with thousands of bits which errors were introduced because of the magnitude. Errors occurred due to variation of the magnitude. However, adapting pre-distorter reduced the thousands spikes and linearized the signal.

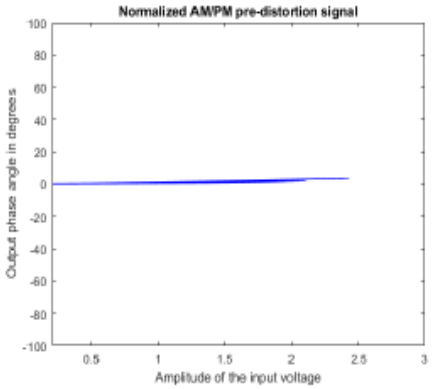

Figure 17. Normalized AM-PM balanced RF power amplifier pre-distorted signal

Figure 17 shows the normalized AM-PM balanced RF power amplifier pre-distorted signal. The performance of the pre-distorter towards figure 16 and 17 was illustrated respectively. Because of the spikes on the amplitude signal which affected the performance of the pre-distorter and cannot remove the distortion properly which has also shown not very effective impact on BER. The amplitude and phase of the amplifier were simulated by de-normalization. AM-AM and AM-PM signals were pre-distorted by not normalizing the polynomials. The performance of the pre-distorter without normalization of polynomials has improved the AM-AM signal of the amplifier.

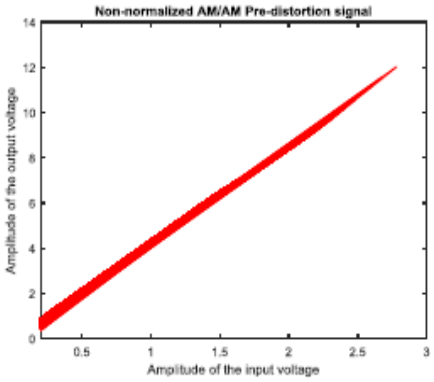

Figure 18. Non-normalized AM-AM balanced RF power amplifier Pre-distorted signal

Figure 18 shows the non-normalized AM-AM balanced amplifier pre-distorted signal. The performance of the pre-distorter towards the results has improved. The spikes have been reduced, the distortion was properly reduced and the BER has improved at the receiver end.

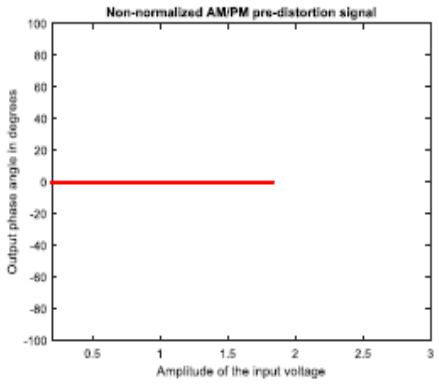

Figure 19. Non-normalized AM-PM balanced RF power amplifier pre-distorted signal

Figure 19 shows the non-normalized AM-PM balanced amplifier pre-distorted signal. The performance of the pre-distorter towards the results has improved more than the normalized AM-PM pre-distorted signal. The pre-distorter produced better linearization even before reaching 3 Volts at the input voltage than the one in figure 17 which is the normalized pre-distortion. However, the pre-distorter ensures no BER at the receiver end.

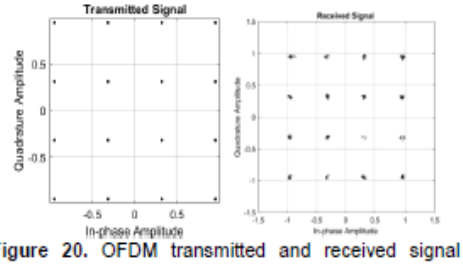

Figure 20. OFDM transmitted and received signal constellations after linearization

Figure 20 shows the transmitted signal before OFDM transmitter and received signal after AWGN channel. The signal constellations represent the coded 0-15 16-QAM modulation which at the transmit shows clean bits of signal without adding noise. The received signal is the signal after demodulation of the OFDM signal which can be seen as similar constellation to the transmitted signal constellation which in this case pre-distortion has been used to cancel the high distortion of the power amplifier. Pre-distorter gas made the receive signal almost close to the transmit signal.

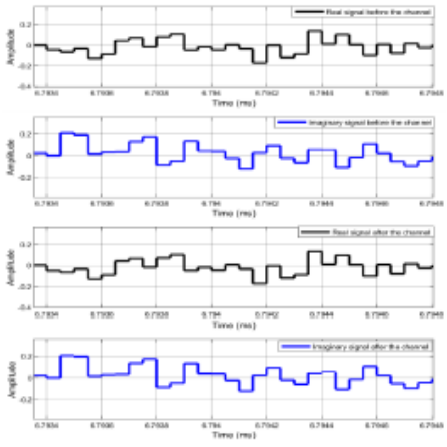

Figure 21. OFDM complex signal on time scope frame after linearization

Figure 21 shows the time scope figure of merit demonstrating the OFDM complex signal in two forms which is before the power amplifier and after the AWGN channel. Each signal has been displayed with real and imaginary potion as shown above. The first signal was obtained before the RF power amplifier and the second was after the channel. The noise added to the signal that passed through the amplifier introduced disturbance. Because of the distortion affecting the magnitude in the signal, the imaginary side of the signal after the channel might not follow the imaginary side of the signal before the channel. The pre-distorter has compensated the high distortion which the signals have demonstrated similarities both on real and imaginary. This has been proven in the BER performance of the receiver side as shown in figure 23. This study has been compared with some other works that was done before and were referenced accordingly. The study has relatively try to understand the knowledge of other works and improve based on facts of findings and practical experiments.

Figures 22 and 23 are the BER results that illustrated performances of the transceiver system when balanced RF power amplifier was connected and when pre-distorter was applied to the system. Both of them has practically displayed a clear proof of authenticity existence of these particular devices in action.

The OFDM transceiver shows the BER performance of the signal received when the balanced RF power amplifier is used in the system. As shown in figure 23, the BER displayed number of bits received without the number of errors. Number of errors occurred base on amplifier distortion. In this case, the errors have been removed by the pre-distorter.

The results presented in this work, to the best of author's knowledge are potentially good efficiency and pre-distortion performance of the balanced RF power amplifier and adaptive pre-distorter used in the Simulink transceiver system based on IEEE 802.11a OFDM HiperLAN/2 standard to cancel the distortion and linearize the OFDM baseband signal.

7. Conclusion

In this study, the balanced RF power amplifier was designed and implemented. A 2.620-2.690GHz frequency band on large signal Si-LDMOS transistor model to achieve 53% PAE, 41dBm P_{out}, 14 dB gain at P_{1dB} saturation point. The proposed balanced RF power amplifier was fabricated and measurement results for phase variation of the signal between the carriers have been the main focus. At 1dB compression point power added efficiency increased to 81.5% with 19.5 gain at the P_{out}. The AM-AM and AM-PM measured data of the balanced RF power amplifier was extracted from the MATLAB fitting tool to produce polynomials. The polynomials were used in the proposed pre-distortion technique to compensate for the nonlinearities of the balanced power amplifier. A simple linear model was designed for behavioural modelling of the memory-less baseband digital pre-distorter. A Simulink IEEE 802.11a OFDM Transceiver system was used to demonstrate validity of the proposed pre-distorter. This study presented excellent results of pre-distortion system that compensated the nonlinearity behaviour of the balanced RF power amplifier using the Simulink version R2011a.

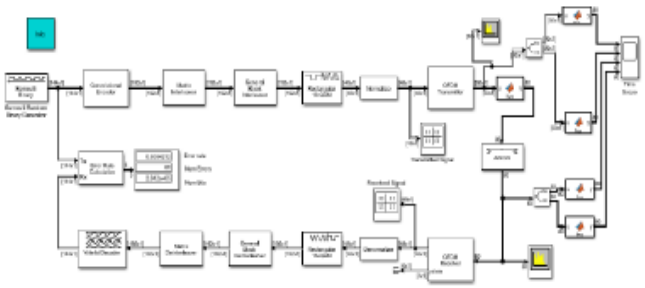

Figure 22. OFDM transceiver illustrating BER performance before linearization

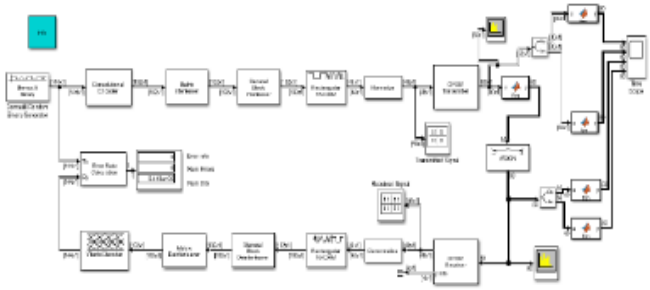

Figure 23. OFDM transceiver illustrating BER performance after linearization

Acknowledgements.

This work is carried out under the grant of the Fundacão para a Ciência e a Tecnologia (FCT - Portugal), with the reference number: SFRH / BPD / 95110 / 2013. This work has received funding from the European Union's Horizon 2020 research and innovation programme under grant agreement H2020-MSCA-ITN-2016 SECRET-722424.

References

[1] M. Helaoui, S. Boumaiza, A. Ghazel, and F. M. Ghannouchi, "Low-IF 5 GHz WLAN linearized transmitter using baseband digital predistorter," in *Electronics, Circuits and Systems, 2003. ICECS 2003. Proceedings of the 2003 10th IEEE International Conference on*, 2003, pp. 260-263 Vol.1.

[2] F. H. Raab, P. Asbeck, S. Cripps, P. B. Kenington, Z. B. Popovic, N. Pothecary, *et al.*, "Power amplifiers and transmitters for RF and microwave," *Microwave Theory and Techniques, IEEE Transactions on*, vol. 50, pp. 814-826, 2002.

[3] B. A. Mohammed, N. A. Abduljabbar, R. A. Abd-Alhameed, A. S. Hussaini, C. Nche, M. Fonkam, *et al.*, "Towards a green energy RF power amplifier for LTE applications," in *Internet Technologies and Applications (ITA), 2015*, 2015, pp. 388-392.

[4] P. Page, C. Steinbeiser, T. Landon, G. Burgin, R. Hajji, R. Branson, *et al.*, "325W HVHBT Doherty Final and LDMOS Doherty Driver with 30dB Gain and 54% PAE linearized to-55dBc for 2c11 6.5 dB PAR," in *Compound Semiconductor Integrated Circuit Symposium (CSICS), 2011 IEEE*, 2011, pp. 1-4.

[5] A. S. Hussaini, T. Sadeghpour, R. Abd-Alhameed, M. B. Child, N. T. Ali, and J. Rodriguez, "Optimum Design of Doherty RFPA for Mobile WiMAX Base Stations," in *Mobile Multimedia Communications*, 2012, pp. 700-705.

[6] H. Deguchi, N. Ui, K. Ebihara, K. Inoue, N. Yoshimura, and H. Takahashi, "A 33W GaN HEMT Doherty amplifier with 55% drain efficiency for 2.6 GHz base stations," in *Microwave Symposium Digest, 2009. MTT'09. IEEE MTT-S International*, 2009, pp. 1273-1276.

[7] Z. Wang, "Demystifying Envelope Tracking: Use for High-Efficiency Power Amplifiers for 4G and Beyond," *Microwave Magazine, IEEE*, vol. 16, pp. 106-129, 2015.

[8] H. Deguchi, N. Watanabe, A. Kawano, N. Yoshimura, N. Ui, and K. Ebihara, "A 2.6 GHz band 537W peak power GaN HEMT asymmetric Doherty amplifier with 48% drain efficiency at 7dB," in *Microwave Symposium Digest (MTT), 2012 IEEE MTT-S International*, 2012, pp. 1-3.

[9] A. A. Ismail, A. T. Younis, N. A. Abduljabbar, B. A. Mohammed, and R. A. Abd-Alhameed, "A 2.45-GHz class-F power amplifier for CDMA systems," in *Internet Technologies and Applications (ITA), 2015*, 2015, pp. 428-433.

[10] K. Ildu, M. Junghwan, K. Jangheon, K. Jungjoon, S. Cheol Soo, S. Kae-Oh, *et al.*, "Envelope injection consideration of high power hybrid EER transmitter for

IEEE 802.16e mobile WiMAX application," in *Microwave Symposium Digest, 2008 IEEE MTT-S International*, 2008, pp. 411-414.

[11] L. Jongsik, P. Chunseon, K. Jakyung, C. Hyeonwon, J. Yongchae, H. Sang-Min, *et al.*, "A balanced power amplifier utilizing the reflected input power," in *Radio-Frequency Integration Technology, 2009. RFIT 2009. IEEE International Symposium on*, 2009, pp. 88-91.

[12] A. Markos, K. Bathich, A. Tanany, D. Gruner, and G. Boeck, "Design of a 120 W balanced GaN Doherty power amplifier," in *Microwave Conference (GeMIC), 2011 German*, 2011, pp. 1-4.

[13] P. Celka, N. J. Bershad, and J.-M. Vesin, "Stochastic gradient identification of polynomial Wiener systems: Analysis and application," *IEEE transactions on signal processing*, vol. 49, pp. 301-313, 2001.

[14] S. C. Cripps, *Advanced Techniques in RF Power Amplifier Design*: Artech House, 2002.

[15] F. H. Raab, "An Introduction to Class-F Power Amplifier RF Design," vol. 19, pp. 79-84, May 1996.

[16] A. S. Hussaini, R. Abd-Alhameed, and J. Rodriguez, "Design of energy efficient power amplifier for 4G user terminals," in *Electronics, Circuits, and Systems (ICECS), 2010 17th IEEE International Conference on*, 2010, pp. 611-614.

[17] B. Mohammed, N. Abduljabbar, M. Al-Sadoon, K. Hameed, A. Hussaini, S. Jones, *et al.*, "A 15.5 W Si-LDMOS Balanced Power Amplifier with 53% Ultimate PAE for High Speed LTE," in *International Conference on Wireless and Satellite Systems*, 2016, pp. 193-201.

[18] R. Kshetrimayum, *Electromagnetic Field Theory*, 2012.

[19] H. Sano, N. Ui, and S. Sano, "A 40W GaN HEMT Doherty power amplifier with 48% efficiency for WiMAX applications," in *Compound Semiconductor Integrated Circuit Symposium, 2007. CSIC 2007. IEEE*, 2007, pp. 1-4.

[20] D. Dai, L. Sun, J. Wen, G. Su, and L. Guo, "A 10W broadband power amplifier for base station," in *Microwave and Millimeter Wave Technology (ICMMT), 2012 International Conference on*, 2012, pp. 1-4.

[21] S. Kim, J. Moon, J. Lee, Y. Park, D. Minn, and B. Kim, "Mitigating Phase Variation of Peaking Amplifier Using Offset Line," *Microwave and Wireless Components Letters, IEEE*, vol. PP, pp. 1-3, 2016.

[22] A. Z. Markos, D. Gruner, K. Bathich, and G. Boeck, "A 2 W GaAs doherty amplifier for 5.5-5.6 GHz applications," in *Microwave Radar and Wireless Communications (MIKON), 2010 18th International Conference on*, 2010, pp. 1-4.

[23] S.-C. Jung, O. Hammi, and F. M. Ghannouchi, "Design optimization and DPD linearization of GaN-based unsymmetrical Doherty power amplifiers for 3G multicarrier applications," *IEEE Transactions on Microwave Theory and Techniques*, vol. 57, pp. 2105-2113, 2009.

Journal of Multidisciplinary Engineering Science and Technology (JMEST)
ISSN: 2458-9403
Vol. 4 Issue 9, September - 2017

Design and Simulation of Balanced RF Power Amplifier over Adaptive Digital Pre-distortion for MISO WLAN-OFDM Applications

Buhari A. Mohammed, Isah M. Danjuma, Raed A. Abd-Alhameed
School of Engineering, Design and Technology, University of Bradford, UK
Email: m.b.abubakar1@student.bradford.ac.uk

Abubakar S. Hussaini, Isa T. E. Elfergani Jonathan Rodriguez
Instituto de Telecomunições, Aveiro, Portugal, Universidade de Aveiro, Portugal

***Abstract*-This paper presents a design and simulation of energy efficient power amplifier for Multiple-Input-Single-Output (MISO) Wireless Local Area Network (WLAN) Orthogonal Frequency Division Multiplexing (OFDM) applications, operating with lateral MOSFET transistor device between 2.620 to 2.690 GHz frequency bands. The power added efficiency reach up to 52 percent at 41dBm p_{out}. The amplitude and phase modulation coefficients are extracted from single tone test. However, new model has been proposed to extend Saleh model, in which the polynomials are modelled using adaptive digital pre-distortion system in WLAN-OFDM IEEE 802.11a physical layer transmitter. The performance of the adaptive digital pre-distorter using the modified Saleh model characterize and compensate the effect of nonlinearity of the power amplifier. This technique is considered useful in improving performance for the mobile communication applications.**

Keywords—balanced power amplifier; multiple input single output; orthorgonal frequency division multiplex; adaptive digital pre-distortion.

I. INTRODUCTION

The greatest challenge facing RF power amplifier devices in wireless communication systems is lack of persistent linearity in the presence of high efficiency. Power amplifier is the most energy consuming device in the transmission system, which more than 52% of the power is converted to a wasted heat energy. This condition progressively affects other devices in the transmitter and however, results to system performance reduction. A technique needs to be employed for dynamic amplification. The technique is to counter balance the cost of energy consumption from base station and improve long battery life of the mobile equipment [1].

Adaptive digital pre-distortion can be one of the most commonly used linearization technique. It is simple to apply and one of the most cost effective. Like other pre-distortion systems, adaptive pre-distortion use inverse parameters to characterize and compensate the nonlinearity and the memory effects of nonlinear power amplifier. The effect of harmonic components and intermodulation distortion in power amplifier is a foremost apprehension for communication systems engineering [1]. The effects result to apparent presence of nonlinearity on the frequency band. These however, lead to power loss and adjacent channel interference. To mitigate these effects of nonlinearity and achieve state of the art system, it is obligatory to prudently design and implement the power amplifier for high speed data rate and spectral efficiency. A healthier power amplifier design is an exceptional candidate for technologies such as multiple-input-multiple-output (MIMO), wireless land area network (WLAN), orthogonal frequency division multiplexing (OFDM), spatial modulation transmitters and several more 5G applications. The features of such systems embrace high speed data rate, wider bandwidth and higher spectral efficiency [2, 3].

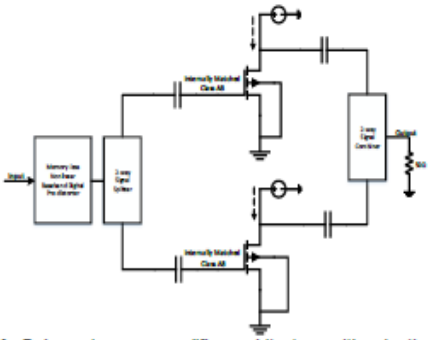

Fig. 1. *Balanced power amplifier architecture with adaptive digital pre-distortion at the baseband.*

This paper presents a discussion on the design of balanced RF power amplifier, the effect of nonlinearity and impact of adaptive digital pre-distorter in transmission system. Section II presents balanced power amplifier circuit design and performance results. Section III discusses adapting modified Saleh model for adaptive digital pre-distortion. Section IV presents conclusion of the paper.

II. BALANCED POWER AMPLIFIER CIRCUIT DESIGN AND PERFORMANCE RESULTS

The balanced power amplifier was designed using an Agilent advanced design system (ADS) software

with a free-scale n-channel enhancement mode lateral MOSFET MRF826060HSR3 transistor model, 2.620GHz to 2.690GHz frequency band. Figure 1 has shown 2 a cascaded class-AB power amplifiers. These circuit represent two amplifiers with gate source voltage to make it a balanced linear system. The two power amplifiers are connected together via a splitter at the baseband and a combiner at the output. The splitter at the baseband splits the signal into two at 90° phase shift to feed the amplifiers. The combiner at the output, combines the signal from the two transistors at 90° un-phase shift. A full wave signal is produced at the output [3].

In the design of balanced power amplifier, there are significant stages of design that are expected to observe:

A. Design of DC and Bias Circuits

DC circuit design can be done using Agilent advanced design system simulator. The DC simulation circuit is designed to define bias point and bias network. This is require in order to select the amplifier class of operation and power to be consumed by the device. The drain source voltage (VDS) is set to 28 volts, while the gate source voltage (VGS) is 2.4 volts respectively. This means that the bias condition has been set at the voltage source. However, these values have been recommended in the data sheet by the manufacturer. The design was simulated and drain source current (IDS) was achieved at 45mA as shown in figure 2. The DC quiescent current was achieved to prevent signal distortion [4, 5].

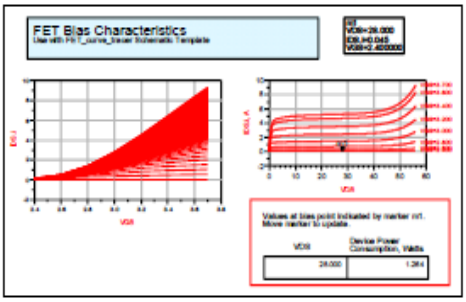

Fig. 2. *DC IV curve simulation result.*

Like the main purpose of DC simulation is to specify the class of operation and the DC quiescent current is to prevent signal distortion. Bias circuit was also designed based on class-AB carrier. A good biasing prevents signal reflection and distortions. In addition to setting the bias network component values, linecalc from ADS simulator is to determine the length of micro-strip transmission lines required in the design. However, the lateral MOSFET MRF826060HSR3 transistor require no matching process, as the input and output impedances are internally matched in the device. The following RT 5880 substrate specifications have been applied to achieve 21mm length of micro-strip line: H = 0.508mm, Er = 2.2, T = 3um, TanD = 0.017 and zo = 50 Ω [4].

B. Final Stage Power Amplifier Design

The design of power amplifier involves quite a few steps of design in order to ensure effective performance on the final device. It is however, important to note that optimization is applied in all stages of the design. In the bias circuit design a DC-feed (inductors) is provided in the drain and gate of the bias circuit to bias the transistor. This allows the DC current to pass through to the transistor, while the RF signal was blocked from passing to the DC bias. A lumped element was configured in the input and output of the amplifier, which acted as a DC-blocking capacitor. These elements blocked the DC voltage from the DC source to the RF line [4, 6].

In this work, input and output matching network have not been considered. The lateral LDMOS transistor is configured with internal matching network. To attain dynamic load variation, a quarter wavelength transmission line with 50 Ω impedance inverter was provided and a final class-AB power amplifier was designed. A 3dB quadrature coupler and a combiner was used in connecting the two class-AB amplifiers to provide a balanced power amplifier.

A balanced power amplifier linear simulation was conducted using Agilent advanced design system simulator (ADS) and result was obtained from 2.620 to 2.690GHz frequency band. The results have shown a good flat gain (S2,1) and outstanding return loss ((S1,1) and (S2,2)).

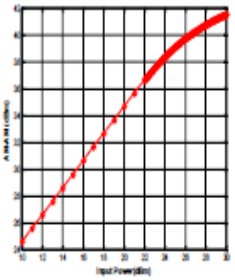

Fig. 3. *AM-AM response.*

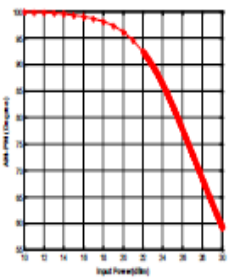

Fig. 4. *AM-PM response.*

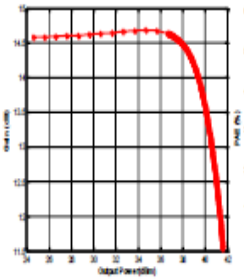

Fig. 5. *Power gain.*

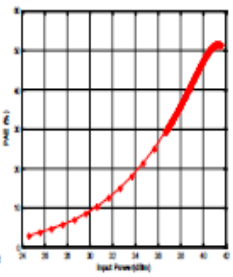

Fig. 6. *Power added efficiency.*

The balanced power amplifier nonlinear simulation was performed. The results were achieved based on single tone simulation and the following are the tests

performed, such as AM-AM, AM-PM, transducer power gain, output power and power added efficiency. Figure 3 and 4 represent amplitude and phase modulation responses [7, 8]. AM-AM characterization has demonstrated a variation of the input power versus the output power. The 40dBm output power is obtained at the safety region of 1dB compression point of the amplifier. While the AM-PM has shown the variation of phase from 100 degrees, decreasing at 1dB compression point. Figure 5 depicts a transducer power gain with a satisfactory gain of 14dB at 36dBm P_{out}. Figure 6 illustrates power added efficiency versus output power. The balanced power amplifier PAE goes up to 52% over the range of 41dBm P_{out}. The results demonstrated a significant upgrade by achieving such range of PAE in the design of the balanced power amplifiers [9, 10].

III. Adapting Modified Saleh Model for Adaptive Digital Pre-distortion in MISO WLAN-OFDM Transceiver

The balanced power amplifier designed for MISO WLAN-OFDM application using adaptive digital pre-distortion due to nonlinear distortions is presented. The amplitude and phase modulation distortions being the coefficients extracted from single tone simulations are characterize using MATLAB software platform. Curve fitting tool in MATLAB converts the amplitude and phase modulation coefficients to generate polynomials. The polynomials are used in developing the modified Saleh model algorithm for the adaptive digital pre-distortion system [8, 9].

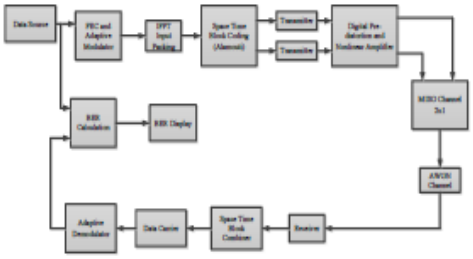

Fig. 7. *MISO WLAN-OFDM Transceiver.*

Figure 7 demonstrated the Simulink structure of wireless local area network IEEE 802.16 OFDM transceiver system configuration with coding support and BPSK, QPSK, 16-QAM or 64-QAM modulations. The transmitter is configured with space time block coding (STBC) for diversity. The STBC used Alamouti code at the downlink. However, this work focus on the digital pre-distortion and nonlinear amplifier block component of the transmitter [11]. The digital pre-distortion and nonlinear amplifier block consist of a circuit system. The subsystem model consists of several existing models such as Cubic Polynomial, Hyperbolic Tangent, Saleh Model, Ghorbani Model and Rapp Model [9, 12].

In Saleh model nonlinearity subsystem, a signal has been multiplied by a gain factor before splitting to magnitude and angle components. The magnitude component is consist of the amplitude and phase respectively. AM-AM represents the amplitude, while AM-PM is the phase of the polynomials in Saleh model as shown in equation 1 and 2 [12].

$$AM-AM^{u}=\frac{\alpha u}{1+\beta u^{2}} \tag{1}$$

$$AM-PM^{u}=\frac{\alpha u^{2}}{1+\beta u^{2}} \tag{2}$$

To improve this model, a simple algorithm for linear equation was developed to characterize the AM-AM and AM-PM polynomials of the balanced power amplifier as shown is equation 3 and 4. It is applied in the adaptive digital pre-distortion to linearize the signal and compensate for the nonlinear distortion produced by the power amplifier [8].

$$x(t)=a_6v^6+a_5v^5+a_4v^4+a_3v^3+a_2v^2+av+a_0 \tag{3}$$

$$y(t)=b_6u^6+b_5u^5+b_4u^4+b_3u^3+b_2u^2+bu+b_0 \tag{4}$$

$$x(t)=am-am \tag{5}$$

$$y(t)=am-pm \tag{6}$$

To implement the transfer functions, the extracted data was measured in the environment of normalized input voltage against the output voltage of the balanced power amplifier. Figure 8 has shown the extracted data based on amplitude modulation, plotted with the following curve fittings: a_6 = 33.066, a_5 = -85.52, a_4 = 82.06, a_3 = -34.052, a_2 = 2.85, a_1 = 3.21 and a_0 = -0.01. The AM-AM characterization was effected by the device reaching a saturation point.

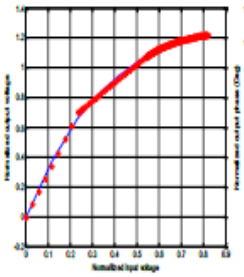

Fig. 8. *Normalized amplitude.*

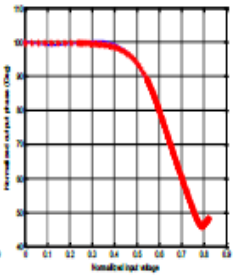

Fig. 9. *Normalized phase.*

The normalized input voltage versus output phase of the balanced amplifier was also considered in figure 9, plotted with the following curve fittings: b_6 = 3.5485, b_5 = -5.7836, b_4 = 3.0384, b_3 = -0.8434, b_2 = 0.1826, b_1 = -0.0225 and b_0 = 0.1001. The AM-PM characterization was effected by the device reaching a saturation point. Now, an accurate model by modified Saleh was developed to compensate for the nonlinear distortion and memory effect of the power amplifier. However, the adaptive digital pre-distortion algorithm was developed respectively. To evaluate the

performance of the pre-distorter, the balanced power amplifier was designed. The implemented balanced power amplifier in the context of amplitude and phase measured data was imported in a Simulink, developed based on IEEE 802.16 MISO WLAN-OFDM transceiver system.

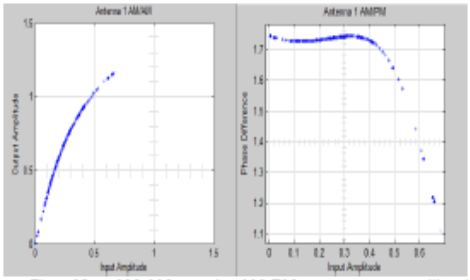

Fig. 10. *AM-AM and AM-PM responses without linearization.*

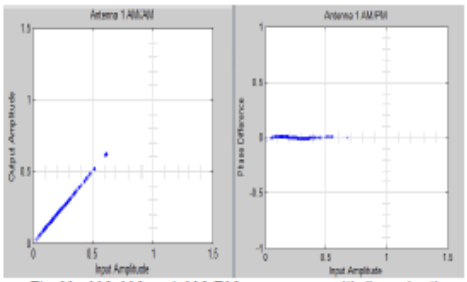

Fig. 11. *AM-AM and AM-PM responses with linearization.*

The memoryless nonlinearity performance of the modified Saleh model has been evaluated. Performance results of the transmitter is shown in figure 10 and 11. Figure 10 illustrates the amplitude and phase signals of the balanced power amplifier, reproduced by the transceiver system, without linearization. While figure 11 illustrates the amplitude and phase signals, linearized by the adaptive digital pre-distorter. Hence, the transceiver system was set to run on modified Saleh model with digital pre-distortion to compensate the nonlinearity of the balanced power amplifier.

Figure 12 illustrates the transceiver channel constellation for 16 and 64 QAM modulations. This is as a result bit error cancelation by the performance of the transceiver system. Gain vector of the MISO was increased, which triggers the adaptive rate control to set high the modulation from 16QAM to 64QAM. Signal to noise ratio was also increased from 21dB to 30dB to improve the constellation and remove the noise factor.

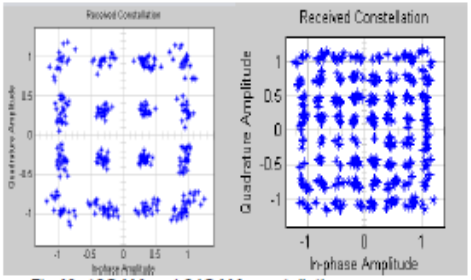

Fig. 12. *16QAM and 64QAM constellations.*

IV. CONCLUSION

The balanced RF power amplifier was designed using Freescale N-Channel enhancement mode lateral MOSFET transistor. Linear and nonlinear simulation were performed with ADS simulator and performance result was obtained with acceptable power added efficiency of 52% for 41dBm output power at 1compression point. This paper conducts research on the effect of nonlinearity on Saleh model and the impact of digital pre-distortion. AM-AM and AM-PM characterizations were used on MATLAB to generate polynomials to model the balanced amplifier spectral re-growth using modified Saleh model. The memoryless nonlinearity has been compensated by the use of digital pre-distortion mechanism. This has proven that the simple linear by modified Saleh mode used in MATLAB Simulink, developed based on IEEE 802.16 MISO WLAN-OFDM transceiver system is capable of correcting nonlinear distortion and memory effects of the balanced power amplifier.

ACKNOWLEDGMENT

This work was supported partially by Yorkshire Innovation Fund, IETG Ltd. Contract, Research Development Project (RDP) and the European Union's Horizon 2020 research and innovation programme under grant agreement H2020-MSCA-ITN-2016 SECRET-722424.

REFERENCES

[1] S. C. Cripps, RF Power Amplifiers for Wireless Communications, Norwood, MA: Artech House, 2006.

[2] P. B. Kenington, High-Linearity RF Amplifier Design, Norwood, MA: Artech House, 2000.

[3] M. Albulet, RF Power Amplifiers(196) Atlanta, GA: Noble Publisher Corporation, 2001.

[4] B. A. Mohammed, N. A. Abduljabbar, A. S. Hussaini, I. Elfergani, R. Adb-Alhameed, S. M. R. Jones, "A Si-LDMOS Doherty Power Amplifier for 2.620-2.690 GHz Applications," vol. 23, pp. 3874-3878, 1 May 2017.

[5] F. H. Raab, P. Asbeck, S. Cripps, P. B. Kenington, Z. B. Popovic, N. Pothecary, J.F. Sevic and N.O. Sokal "Power amplifiers and transmitters for RF and microwave", IEEE Transactions on Microwave Theory and Techniques, Vol. 50, No 3, PP. 814 – 826, March, 2002.

[6] A. S. Hussaini, B. A. L. Gwandu, R. Abd-Alhameed, and J. Rodriguez, "Design of power efficient power amplifier for B3G base stations," in Electronics and Telecommunications (ISETC), 2010 9th International Symposium on, 2010, pp. 89-92.

[7] A. S. Hussaini, I. T. E. Elfergani, J. Rodriguez, and R. A. Abd-Alhameed, "Efficient multi-stage load modulation radio frequency power amplifier for green radio frequency front end," Science, Measurement & Technology, IET, vol. 6, pp. 117-124, 2012.

[8] S. A. Bassam, M. Helaoui, and F. M. Ghannouchi, "Crossover Digital Predistorter for the Compensation of Crosstalk and Nonlinearity in MIMO Transmitters,"IEEE Transactions on Microwave Theory and Techniques, vol. 57, pp. 1119-1128, 2009.

[9] S. A. Bassam, M. Helaoui, and F. M. Ghannouchi, "BER performance assessment of linearized MIMO transmitters in presence of RF crosstalk,"2010 IEEE in Radio and Wireless Symposium (RWS), 2010, pp. 33-36.

[10] T. M. Nguyen, J. Yoh, C. H. Lee, H. T. Tran, and D. M. Johnson, "Modeling of HPA and HPA linearization through a predistorter: Global Broadcasting Service applications," IEEE Transactions on Broadcasting, vol. 49, pp. 132-141, 2003.

[11] J. L. Dawson and T. H. Lee, Feedback Linearization Of RF Power Amplifiers: Kluwer, 2004.

[12] A. A. M. Saleh, "Frequency-Independent and Frequency-Dependent Nonlinear Models of TWT Amplifiers," IEEE Transactions on Communications, vol. 29, pp. 1715-1720, 1981.

A 2.62-GHz Class-F Power Amplifier with Lumped-Element and Transmission Line Network Design

B. A. Mohammed[1], A. S. Hussaini[123], H. Migdadi[1,5], R. Abd-Alhameed[1], N. A. Abduljabbar[1], I.T.E. Elfergani[2], J. Rodriguez[2], C. Nche[3], M. Fonkam[3] and B. M. Mustapha[4]
[1]School of Electrical Engineering and Computer Science, University of Bradford, Bradford,BD7 1DP, UK
[2]Instituto de Telecomunicacoes, Aveiro, Portugal
[3]School of InformationTechnology & Computing, American University Yola, Adamawa, Nigeria
[4]Department of Electrical & Electronics Engineering, University of Maiduguri, Nigeria
[5]Faculty of Engineering, American University of Madaba, Jordan
m.b.abubakar1@student.bradford.ac.uk

***Abstract*—A 2.62-GHz class-F power amplifier with independent analogous method, lumped-element network design is presented. The amplifier is designed using CGH40010 GaN HEMT transistor device with 5th order low pass structure at the lumped-element output network. A transmission line networks has been used in transformation of both input and output of the amplifier. Optimum fundamental impedance matching networks and optimization are applied at the frequencies of interest to controlling the even and odd harmonics, to allow fundamental frequency deliver to the load. The power amplifier achieves 81.5% peak efficiency at 18.1dBm output power.**

Keywords—Power Amplifiers, Class F, ACPR, PAPR.

I. INTRODUCTION

Power amplifiers (Pas) are continuously faced with challenges from linearity and efficiency. Rapid growth of several efficiency enhancement and linearization techniques has been in the increase over the years. These techniques provide high efficiency and linear amplification for today's modern communication systems, as they increase talk time, reduce power consumption, heat dissipation and massive increase in reliability. However, those communication systems are non-constant time envelope systems such as Wideband Code Division Multiple Access (WCDMA) and the very best Orthogonal Frequency Division Multiplexing (OFDM). They are most commonly used multicarrier high modulation techniques that are capable of providing high speed data rate. In the same vein, the use of such modulations result to high peak to average power ratio (PAPR) and adjacent channel interference ratio (ACPR) [1].

Class-F amplifiers regulate the existence of even and odd harmonics of the drain-source voltage and drain current waveform with the use of transmission line network. The output power uses the harmonic resonators to shape the drain current and voltage waveform. The drain voltage waveform comprises of one or more odd harmonics and in the order of a square wave, while the current waveform comprises even harmonics and in the order of a half sine wave. The odd harmonics are open to produce square wave as the voltage waveform, even harmonics remain short to produce current wave.

The use of lumped-element network at the input and output of class-F power amplifier has become essential part of analogue technique. It has been pointed out in [2] that before now, lumped element network has been applied in vacuum tube class-F power amplifiers for high frequency operation. The vacuum tube amplifiers refer to as traveling-wave-tube amplifiers use a fluctuating trap to connect with the fundamental-frequency parallel-tuned circuit, making correction harder [2]. Now, [3] came with idea to implement a 15W power amplifier design at 1.8 GHz by using the Filtronic Compound Semiconductors Limited PHEMT power process to validate the lumped-element network techniques. In his proposed class-F input network, he used low pass structure, terminating with a shunt resonator at the fundamental frequency, acting as impedance inverter to short the 2nd and 4th harmonic frequencies [3].

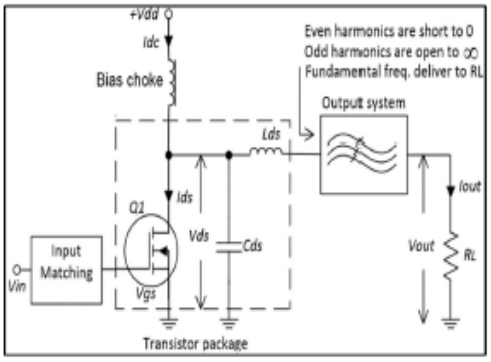

Figure 1: Generic Power amplifier circuit.

In addition to [3] contribution to the body of knowledge, [4, 5] came with the improved idea of load-coupling topology to complement the earlier concept. This approach is adopted to reduce the series inductance in the output network and the effect of passive component parasitic on the performance of switched-mode power amplifiers. Moreover, [6] proposed the use of lumped-element network in the presence of analogue technique. The technique allows the use of lower frequencies

978-1-5090-4815-1/17/$31.00 ©2017 IEEE

where the lumped-element network becomes frequency-adaptive.

Similarly, this paper has essentially propose the use of analogue technique, lumped-element networks in the input and outputs of class-F power amplifier in the presence of low pass multi-resonator ladder structures. It is aims at considering the prospective of the novel output-circuit concept proposed in [6] by comparing its performance theoretically with this load networks. This network tolerates comparatively more convenient tuning effort that takes care of fundamental-frequency and n^{th} harmonic components [7]. Moreover, this technique can be applied at RF and high frequencies. The circuit behaves as an impedance inverter at the fundamental and contributes to scale the optimum load impedance value, which is necessary for maximum power, to a possible impedance value. This network should be terminated with a shunt parallel resonator in order to obtain proper terminations at higher harmonics [7].

The new technique is verified with a simulations operating at 2.620 GHz with a 10-W output power and 81.5% efficiency [1]. The design uses a T and L lumped-element network and a shunt LC series resonator to have control over second harmonic component. The input and output fundamental frequency impedances are also matched using LC lumped elements networks. Theoretical analysis of class-F power amplifier is presented in Section II. The amplifier design including wave shaping and matching networks are described in section III. Design simulation and results are explained in IV.

II. CLASS-F POWER AMPLIFIER THEORY

The class-F RF power amplifier circuit is one among several non-linear circuits, considered as high efficiency achiever [8]. High efficiency provides long battery life period with marginal dc power consumption. However, there are several things that are required to be in place to attain high efficiency. One of them is the use of harmonic termination at the output of nonlinear amplifiers, which was originally introduced by J. V. Tyler [2]. In this respect, the class-F amplifier harmonics are characterize as low impedances representing even harmonic components, while high impedances are the odd harmonics components [7].

The schematic diagram of generic power amplifier shown in figure 1 is a typical example of class-F power amplifier network. The amplifier uses an active GaN HEMT transistor device which is controlled by its input source (V_{in}) and the bias network as the dc current source. The dc voltage source from the drain ($+V_{DD}$) supplied the dc drain current (I_{dc}). The output system which represents the load impedance network provides the even harmonic frequencies shorted to zero, odd harmonic frequencies open to infinity and fundamental frequency delivered to the load (R_l) [7].

Figure 2 demonstrates the ideal time domain voltage and current waveforms of a class-F power amplifier. The class-F power amplifier attains higher efficiency with the adoption of proper harmonic frequency terminations at the output.

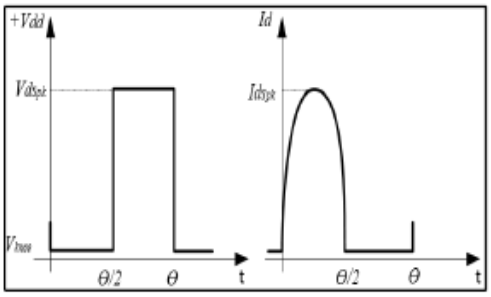

Figure 2: Class-F PA ideal time-domain drain voltage and current waveforms.

The odd harmonics are open to produce square wave and even harmonics remain shorted to produce current wave respectively. The drain current and voltage ideal waveforms of the class-F power amplifier are analytically discussed and as expressed by the form:

$$V(\beta)=+V_{dd}+CV_1\cos\beta-DV_1\sin\beta+.....+.... \quad (1)$$

and

$$I(\beta)=I_{dc}+CI_1\cos\beta-DI_1\sin\beta+.....+.... \quad (2)$$

where β equals to the first harmonic frequency (ω) of the waveform at a period of time (t). The first harmonic frequency remain as $sin\beta$ when $CV_1=0$ and $DV_1=1$. The amplifier output current (I_{av}) is the half sine wave with maximum amplitude expressed as:

$$I_{av}=\frac{1}{\pi}.I_{pk} \quad (3)$$

where I_{pk} is the peak current. Thus, the dc power supply from the drain is presented as:

$$P_{dc}=V_{dd}.I_{dc}=\frac{V_{dd}.I_{pk}}{\pi} \quad (4)$$

where V_{dd} and I_{dc} are the magnitudes of the dc voltage and current. The RF output power at the first harmonic frequency is expressed as:

$$P_{out}=V_{dd}.I_{dc}=\frac{4.V_{dd}.I_{pk}}{\pi\sqrt{2}.2\sqrt{2}}=\frac{V_{dd}.I_{dc}}{\pi} \quad (5)$$

Thus, the maximum efficiency for class-F amplifier is achieved using (5) and (4) as expressed in (6):

$$\eta=\frac{P_{out}}{P_{dc}}=\frac{\frac{V_{dd}.I_{dc}}{\pi}}{\frac{V_{dd}.I_{pk}}{\pi}} \quad (6)$$

And then, the power added efficiency can be written as:

$$PAE=\frac{P_{out}-P_{in}}{P_{dc}} \quad (7)$$

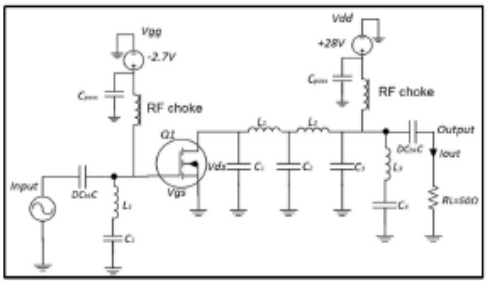

Figure 3: Class-F PA input and output lumped element network.

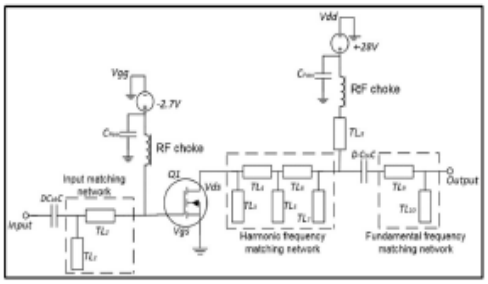

Figure 4: Wave shape circuit using matching method.

If the power added efficiency is in the increase, then, power dissipation and harmonic power will be drastically reduced. Hence, the cause of power dissipation and harmonic power is due to heat from the transistor device. The transistor makes the harmonic power larger than zero when intersection between drain voltage and current occur. This action reduces the class-F amplifier power added efficiency from 100% to less than 90%. Furthermore, efficiency of this grade can only be achieved, based on the number of harmonics controlled in the network [9].

III. AMPLIFIER DESIGN WITH WAVE SHAPE CIRCUIT AND MATCHING NETWORKS

The most interesting key aspect of class-F amplifier design is the architecture of wave formation circuit and the control of harmonic frequencies. Proper terminations of the n^{th} harmonic frequencies at the drain of the transistor device permits sufficient passage of drain current. Thus, the drain current is produced in the form of half sinusoidal waveform, controlling the even harmonic components by short-circuits. The square voltage waveform controls the odd harmonic components by open-circuit, respectively. This, in turn, improves the efficiency of the amplifier and of course reduces transistor heat dissipation.

In this proposed class-F design, a multiple-resonant structure [3], a lumped-element network is adopted as depicted in figure 3. The input networks is a low pass structure, while the output is a 5^{th} order low pass L-C structure. However, the low pass network was adapted in this work to provide optimal harmonic terminations for n^{th} harmonic components. The class-F structure was also transformed with the use of transmission line depicted in figure 4. Furthermore, the depicted figure 3 and 4 are used in describing the design procedure in this technique, how n^{th} harmonics are controlled for proper drain voltage impedance.

Now, to achieve class-F operation, the transistor device has to be actively loaded from the input, (Z_{in}). While, setting the device to active mode, we need to take into consideration the device peak voltage and current, on delivered power, resistance, supply voltage, when system is linear/nonlinear, etc. These parameters, however, determine the required drain load impedance (Z_{VD}) at the fundamental frequency and reactance are at the n^{th} harmonic components.

In [6], to determine the drain load impedance (Z_{VD}), transistor drain to source capacitance (C_{DS}) and lead inductance (L_{DS}) were added for proper impedance transformation from device drain impedance (Z_D) to the drain load impedance (Z_{VD}). However, at certain range frequencies, these elements could add up to the complexity of the circuit. Particularly, with the increase number of harmonic components, they behave as parasitic elements.

A proper output lumped element structure at the output provide the required drain load impedance. The circuit is a 5^{th} order low-pass L-C ladder structure as shown in figure 3. The circuit behaves as a load-impedance inverter at the fundamental region and provides a scale the optimal load-impedance value. The low-pass structure is also provided with multi-resonators for proper higher harmonic components termination [3].

In the n^{th} order structure, 3^{rd} and 5^{th} harmonic components are odd in nature and are open circuited, while 2^{nd} and 4^{th} behave as even harmonic components are short circuited at the drain terminal of the transistor. This procedure is referred to as wave forming circuit. It is a circuit by which the frequency and amplitude of the harmonic contribute in the shaping of the voltage and current waveforms.

There are various types of these circuits with variety in complexity and level of performance in the shaping of the voltage and current waveforms, which also has great impact on the performance of the power amplifier. Input and output matching have also been calculated with the use of firefly method. At the output stage, however, the matching has been design for 5^{th} and 3^{rd} as odd harmonic components and the 4^{th} and 2^{nd} as even harmonics components respectively. Furthermore, the matching is based on the position of 4^{th} and 2^{nd} (TL_4, and TL6) as short circuits, on the way of the 5^{th} and 3^{rd} harmonic components. The transmission line TL_3, TL_5 and TL_7 transform the harmonic frequency matching network to open circuit.

On the other hand, all the transmission lines in harmonic frequency matching network stage, add to formation of short circuit, on the way of the even harmonic components, towards TL_9. TL_8 acts as a quarter wave ($\pi/2$) to block the RF signal moving back to the source, transforming the impedance to 50Ω load, ensuring that even harmonic components are shorted, and, at the same time behaves as an

open circuit to allow the odd harmonic components to infinity. Finally, TL_9 and TL_{10} are design as the fundamental frequency matching for optimum load. However, at the end, we need to take into account the matching circuit at high frequencies could lead to circuit complexity [10, 11].

The design of class-F power amplifier is based on the calculated waveform coefficients tabulated in the table 1. The circuit was design and simulated with the use of Agilent Advanced Design System. The transistor model generic GaN FET has been chosen as a model of non-linear power transistor suitable use for such power amplifier. The following parameters are used: operating frequency 2.62 GHz, drain voltage 28V (dc) and gate voltage -2.7V (dc). RF4 substrate with the following specifications: substrate thickness (H) 1.6mm, Permittivity (ε_r) 4.3, conductivity 4.1×10^7 S/m and conductor thickness (T) 0.035mm. The circuit has been optimized and the goals have been achieved using firefly algorithm.

Table 5: The dimensional values for lumped-elements and TLs used in Figure 3 and 4.

Stage	Symbol	Element Value	Distance	Width (mm)	Length (mm)	Transmission Line
Input matching	C_1	5.61 pF	77.8°	3.08	2.16	TL_1
	L_1	0.49 nH	9.2°	-	13.3	TL_2
Wave shaping	C_2	2.68 pF	65.6°	-	4.34	TL_3
	L_2	3.43 nH	48.5°	-	7.40	TL_4
	C_3	3.77 pF	72.1°	-	3.14	TL_5
	L_4	3.43 nH	48.5°	-	7.40	TL_6
	C_5	2.68 pF	65.6°	-	4.34	TL_7
Output matching	L_1	1.41 pF	49.3°	-	8.64	TL_9
	C_1	2.30 nH	37.1°	-	6.50	TL_{10}
Quarter-wave	$\lambda/4$	$\pi/2$	90.0°	-	15.8	TL_8

IV. Simulation and Results

At this level of design, linear and nonlinear simulation has been performed using Agilent ADS. Results from linear simulation has shown the amplifier flat gain S(2,1) keeps reducing as the frequency increases. This is depicted in figure 5, along with the return loss S(1,1 and 2,2) and leakage S(1,2) from the output.

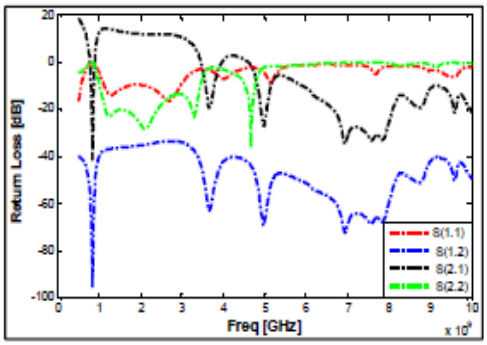

Figure 5: Linear simulation: Return loss (S11 and S22), gain (S21) and Isolation (S12).

In the case of nonlinear simulation, the voltage and current are shown in figure 6b, the fundamental frequency and up to 5th harmonic component has been shown in figure 6a. Output power and efficiency tests are the most significant performance indicators for class-F power amplifier. Figure 7 has shown simulated efficiency versus output power. The class-F power amplifier has high efficiency over the range of 81% with the output level of 18.1dBm, compare to what was obtained by [6]. The efficiency is also 10.5% higher than what was predicted in the theory. The cause for the increase in efficiency is due to the transistor device transient response and termination of up to 5th harmonic components.

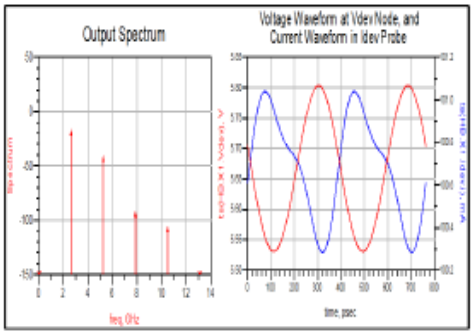

Figure 6: Out spectrum (a), simulated voltage and current waveforms (b).

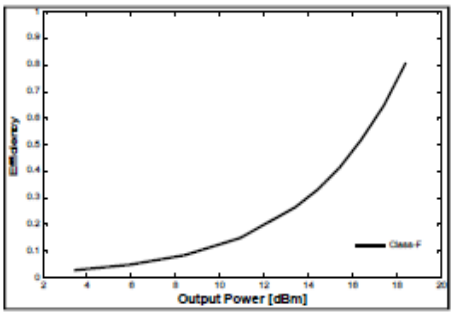

Figure 7: Simulated efficiency versus output power.

V. Conclusion

The design of class-F power amplifier has been presented using technique from [6] to improve efficiency. The analogue technique, lumped-element networks (filter and matching technique) in the input and outputs of class-F power amplifier are used in controlling up 5th coefficients of even and odd harmonic components. A 2.620 GHz operating frequency was used on CGH40010F GaN HEMT transistor to achieve 10.5% efficiency higher than what was predicted in the theory. The selection of this technique has strongly contributes on the stability, gain distortion reduction and improvement in wide dynamic range of the power amplifier.

REFERENCES

[1] B. A. Mohammed, N. A. Abduljabbar, A. S. Hussaini, I. Elfergani, R. Abd-Alhameed, S. M. R. Jones, *et al.*, "A Si-LDMOS Doherty Power Amplifier for 2.620–2.690 GHz Applications," vol. 23, pp. 3874-3878, 1 May 2017 2017.

[2] V. J. Tyler and T. Australia, *A New High-efficiency High-power Amplifier*: Telecom Australia.

[3] M. Akkul, M. Roberts, V. Walker, and W. Bosch, "High efficiency power amplifier input/output circuit topologies for base station and WLAN applications," in *2004 IEEE MTT-S International Microwave Symposium Digest (IEEE Cat. No.04CH37535)*, 2004, pp. 843-846 Vol.2.

[4] R. Negra and W. Bachtold, "Lumped-element load-network design for class-E power amplifiers," *IEEE Transactions on Microwave Theory and Techniques*, vol. 54, pp. 2684-2690, 2006.

[5] R. Negra and W. Bachtold, "BiCMOS MMIC class-E power amplifier for 5 to 6 GHz wireless communication systems," in *2005 European Microwave Conference*, 2005, p. 4 pp.

[6] R. Beltran and F. H. Raab, "Lumped-element output networks for high-efficiency power amplifiers," in *2010 IEEE MTT-S International Microwave Symposium*, 2010, pp. 1-1.

[7] F. H. Raab, "Class-E, Class-C, and Class-F power amplifiers based upon a finite number of harmonics," *IEEE Transactions on Microwave Theory and Techniques*, vol. 49, pp. 1462-1468, 2001.

[8] T. Sadeghpour, R. A. Alhameed, N. T. Ali, I. T. E. Elfergani, Y. Dama, and O. O. Anoh, "Linear and nonlinear crosstalk in MIMO OFDM transceivers," in *2011 18th IEEE International Conference on Electronics, Circuits, and Systems*, 2011, pp. 504-507.

[9] Y. S. Lee, M. W. Lee, and Y. H. Jeong, "High-Efficiency Class-F GaN HEMT Amplifier With Simple Parasitic-Compensation Circuit," *IEEE Microwave and Wireless Components Letters*, vol. 18, pp. 55-57, 2008.

[10] A. A. Ismail, A. T. Younis, N. A. Abduljabbar, B. A. Mohammed, and R. A. Abd-Alhameed, "A 2.45-GHz class-F power amplifier for CDMA systems," in *2015 Internet Technologies and Applications (ITA)*, 2015, pp. 428-433.

[11] O. O. Anoh, N. T. Ali, R. Abd-Alhameed, S. M. R. Jones, and Y. A. S. Dama, "On the performance of DWT and WPT modulation for multicarrier systems," in *2012 IEEE 17th International Workshop on Computer Aided Modeling and Design of Communication Links and Networks (CAMAD)*, 2012, pp. 348-352.